

ADA 058474

14  
AFFDL-TR-78-53

LEVEL

2

6  
EXPERIMENTAL MEASUREMENT OF  
PARACHUTE CANOPY STRESS DURING INFLATION.

AU No. \_\_\_\_\_  
DDC FILE COPY

10  
PEGGY M. WAGNER  
RECOVERY AND CREW STATION BRANCH  
VEHICLE EQUIPMENT DIVISION

MAY 1978

12 185 p.

DDC  
SEP 12 1978  
F

9  
TECHNICAL REPORT AFFDL-TR-78-53  
Final Report 1 Jul 1975 - 30 Dec 1976

16 6065

17 46

Approved for public release; distribution unlimited.

38 10 11 336

AIR FORCE FLIGHT DYNAMICS LABORATORY  
AIR FORCE WRIGHT AERONAUTICAL LABORATORIES  
AIR FORCE SYSTEMS COMMAND  
WRIGHT-PATTERSON AIR FORCE BASE, OHIO 45433

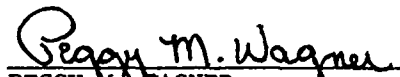
012 070


NOTICE

When Government drawings, specifications, or other data are used for any purpose other than in connection with a definitely related Government procurement operation, the United States Government thereby incurs no responsibility nor any obligation whatsoever; and the fact that the government may have formulated, furnished, or in any way supplied the said drawings, specifications, or other data, is not to be regarded by implication or otherwise as in any manner licensing the holder or any other person or corporation, or conveying any rights or permission to manufacture, use, or sell any patented invention that may in any way be related thereto.


This report has been reviewed by the Information Office (OI) and is releasable to the National Technical Information Service (NTIS). At NTIS, it will be available to the general public, including foreign nations.

This technical report has been reviewed and is approved for publication.

  
PEGGY M. WAGNER  
Project Engineer/Scientist

  
RICHARD J. DOBBEK  
Group Leader, Recovery  
Systems Dynamic Analysis Group

FOR THE COMMANDER

  
AMBROSE B. NUTT  
Chief, Vehicle Equipment  
Division

"If your address has changed, if you wish to be removed from our mailing list, or if the addressee is no longer employed by your organization please notify AFFDL/FER, W-PAFB, OH 45433 to help us maintain a current mailing list".

Copies of this report should not be returned unless return is required by security considerations, contractual obligations, or notice on a specific document.

UNCLASSIFIED

SECURITY CLASSIFICATION OF THIS PAGE (When Data Entered)

REPORT DOCUMENTATION PAGE		READ INSTRUCTIONS BEFORE COMPLETING FORM
1. REPORT NUMBER AFFDL-TR-78-53	2. GOVT ACCESSION NO.	3. RECIPIENT'S CATALOG NUMBER
4. TITLE (and Subtitle) Experimental Measurement of Parachute Canopy Stress During Inflation		5. TYPE OF REPORT & PERIOD COVERED Final July 1975 to December 1976
		6. PERFORMING ORG. REPORT NUMBER
7. AUTHOR(s) Peggy M. Wagner		8. CONTRACT OR GRANT NUMBER(s)
9. PERFORMING ORGANIZATION NAME AND ADDRESS Air Force Flight Dynamics Laboratory/ FER Wright-Patterson AFB, Ohio 45433		10. PROGRAM ELEMENT, PROJECT, TASK AREA & WORK UNIT NUMBERS 60650602
11. CONTROLLING OFFICE NAME AND ADDRESS		12. REPORT DATE May 1978
		13. NUMBER OF PAGES 183
14. MONITORING AGENCY NAME & ADDRESS (if different from Controlling Office)		15. SECURITY CLASS. (of this report) Unclassified
		15a. DECLASSIFICATION/DOWNGRADING SCHEDULE
16. DISTRIBUTION STATEMENT (of this Report) Approved for Public Release; Distribution Unlimited		
17. DISTRIBUTION STATEMENT (of the abstract entered in Block 20, if different from Report)		
18. SUPPLEMENTARY NOTES		
19. KEY WORDS (Continue on reverse side if necessary and identify by block number) Omega Sensors Opening Dynamics Ring Slot Parachute Stress Measurement		
20. ABSTRACT (Continue on reverse side if necessary and identify by block number) The Omega sensor was developed for measuring stress in textile and other flexible materials by the Department of Aerospace Engineering and Mechanics of the University of Minnesota and sponsored by the Air Force Flight Dynamics Laboratory. Two studies were conducted by the University which indicated that the circumferential stresses of inflated parachute canopies indicated by Omega sensors agreed with theoretically predicted stresses and also that the stresses measured by an Omega sensor were not affected by dynamic loading.		

DD FORM 1473 1 JAN 73 EDITION OF 1 NOV 65 IS OBSOLETE


UNCLASSIFIED

SECURITY CLASSIFICATION OF THIS PAGE (When Data Entered)

UNCLASSIFIED

SECURITY CLASSIFICATION OF THIS PAGE(When Data Entered)

612  
→ This particular study deals with an in-house test program, designed to measure the circumferential stresses of a model (five foot nominal diameter) ringslot parachute during inflation and at steady state using modified Omega sensors. Slight modifications to the original Omega sensor had to be made due to complications of the tabs tearing during preliminary testing. Five sensors were attached strategically to the canopy of a ringslot parachute and put through a series of low speed wind tunnel tests. The results are presented in detail and provide for the first time actual measurement of circumferential stresses on the surface of a model ringslot parachute. These results, however, can only present the general trend shown in the parachute's stress distribution and not actual stress values due to the inability to calibrate the sensors while attached to the canopy.



UNCLASSIFIED

SECURITY CLASSIFICATION OF THIS PAGE(When Data Entered)

FOREWORD

This Technical Report was prepared by the Recovery and Crew Station Branch, Air Force Flight Dynamics Laboratory, Wright-Patterson Air Force Base, Ohio. This study was initiated under Project 6065, "Recovery Systems Performance and Similarity," Task 606506, "Canopy Stress Measurement." The work covered in this report was initiated in July, 1975, and completed in December, 1976. This report was submitted in January 1978.

All efforts were accomplished in-house by or under the direction of Peggy M. Wagner. Experimental testing was performed at the Air Force Flight Dynamics Laboratory Vertical Wind Tunnel Test Facility.

The author wishes to express her appreciation to Mr. Eric L. Keck of the Recovery and Crew Station Branch for his participation in the performance of the experimental investigations during the wind tunnel tests.

ACQUISITION	DATE	BY	INITIALS
6065	1978	...	...
DISPATCH/PROJECT CODES		SPL. CODE	
A			

## TABLE OF CONTENTS

<u>Section</u>	<u>Title</u>	<u>Page</u>
I	Introduction	1
II	Test Articles	3
	1. Ringslot Parachute Model	3
	2. OMEGA Sensor	7
III	Instrumentation	17
IV	Test Procedure	19
V	Results	27
VI	Conclusions and Recommendations	35
	Appendix A Fill Strip Tests	39
	Appendix B Stress Vs. Non-Dimensional Time	59
	Appendix C Area Growth Plots	159
	Appendix D Force Plots	167
	References	181

## LIST OF ILLUSTRATIONS

<u>Figure</u>	<u>Title</u>	<u>Page</u>
1	Parachute Gore Warp and Fill Orientation	4
2	OMEGA Sensors Orientation on Canopy	5
3	OMEGA Sensor on Gore Centerline	6
4	Original OMEGA Sensor	8
5	Original OMEGA Sensor with Tabs	10
6	Modified OMEGA Sensor	11
7	OMEGA Sensor and Wire Orientation on Canopy	12
8	OMEGA Sensor Calibration Curve	14
9	Varying Plates Widths Placed Three (3) Inches from Sensor	15
10	Fixed Plate Widths at Varying Locations	16
11	Circuitry for Recording OMEGA Sensor Output	18
12	Vertical Wind Tunnel	20
13	Schematic of Deployment Test Arrangement	21
14	Photo of Test Arrangement in VWT	22
15-18	Deployment Process	24
19	Oscillograph Record	28
A-1	Fill Strip Specimen	40
A-2	Schematic of Fill Strip Test Arrangement	41
A-3	Range of Outputs	43
A-4	Two (2) Inch Plates at Varying Distances	44
A-5	One and One Half (1 1/2) Inch Plates at Varying Locations	45

LIST OF ILLUSTRATIONS (CONTINUED)

<u>Figure</u>	<u>Title</u>	<u>Page</u>
A-6	One (1) Inch Plates at Varying Locations	46
A-7	One-Half (1/2) Inch Plates at Varying Locations	47
A-8	One-Fourth (1/4) Inch Plates at Varying Locations	48
A-9	Varying Plates Widths Placed One-Half (1/2) Inches From Sensor	49
A-10	Ideal Stress Distribution	54
A-11	Actual Stress Distribution	55

LIST OF TABLES

<u>Table</u>	<u>Title</u>	
I	Mean and Standard Deviations of Steady State Tests	30
II	Tabulated Stress Data	31
III	Tabulated Stress Data Per Test Condition	32
IV	Mean and Standard Deviation Over Tests	33



SECTION I  
INTRODUCTION

The earliest studies of canopy stresses have been summarized by Jones in 1923 (Reference 1). Since that time, various analytical methods of calculating canopy stresses have been proposed (References 2-9). These analytical studies of parachute stresses were primarily concerned with the steady-state phase, during which the drag of the parachute equals the suspended weight. Newer studies pursue numerical solutions for cloth stresses during the period of canopy inflation (References 10-20). The great disadvantages of all theoretical attempts of determining canopy stresses is that the actual stress distribution across the canopy is still unknown. These attempts have not been experimentally confirmed primarily due to the nonavailability of a stress sensing method or device which would yield accurate results.

Direct measurement of canopy stresses utilizing a stress sensing device has been recently attempted (References 21-25). One such study was conducted by the University of Minnesota, in which an omega sensor was developed and tested. This sensor measures stress values at the point of application on the canopy.

This report documents the experimental results of measurements of the canopy stresses by an omega sensor across a model ringslot parachute during steady-state and during opening under infinite mass conditions in a series of wind tunnel tests.

The objective of this report was to obtain empirical stress measurement values.

## SECTION II

### TEST ARTICLES

#### 1. Ringslot Parachute Model

The investigation was performed on a five (5) foot nominal diameter ringslot parachute model. The model parachute was fabricated with thirty-two (32) gores and with 16 percent geometric porosity. The cloth material used in the fabrication of the canopy was of block construction with the fill and warp threads oriented as shown in Figure 1. The gores were constructed with ten (10) cloth rings and four (4) vertical ribbons per gore. The gores were formed by cutting slots out of a solid piece of cloth by means of a hot knife, thus creating the rings and ribbons of the chute. The parachute contained thirty-two (32) suspension lines five (5) feet in length. The suspension lines were continuous over the canopy and terminated in four (4) loops which were required for the suspension of the model in the vertical wind tunnel. The lines were sewn to the canopy radial seams by zig-zag stitches. The parachute contained no pocket bands.

Five (5) Omega sensors were attached to the canopy at  $S^* = 0.20, 0.39, 0.58, 0.77,$  and  $0.96$  as shown in Figure 2. These sensor locations correspond to the middle of every other ring on gores 8, 15, 19, 28, and 32.

Each Omega sensor has three electrical leads which were routed across the canopy to the three nearest suspension lines (Figure 3).

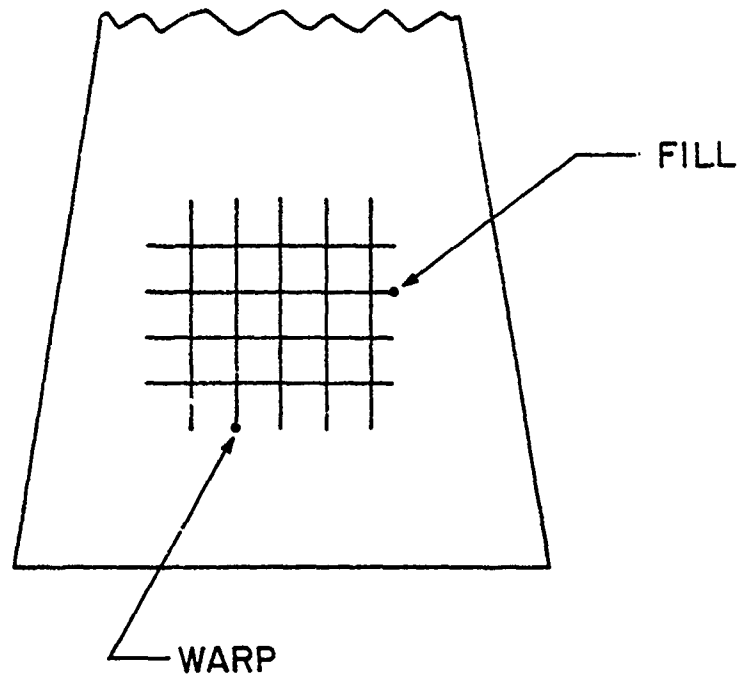


Figure 1. Parachute Gore Warp and Fill Orientation.

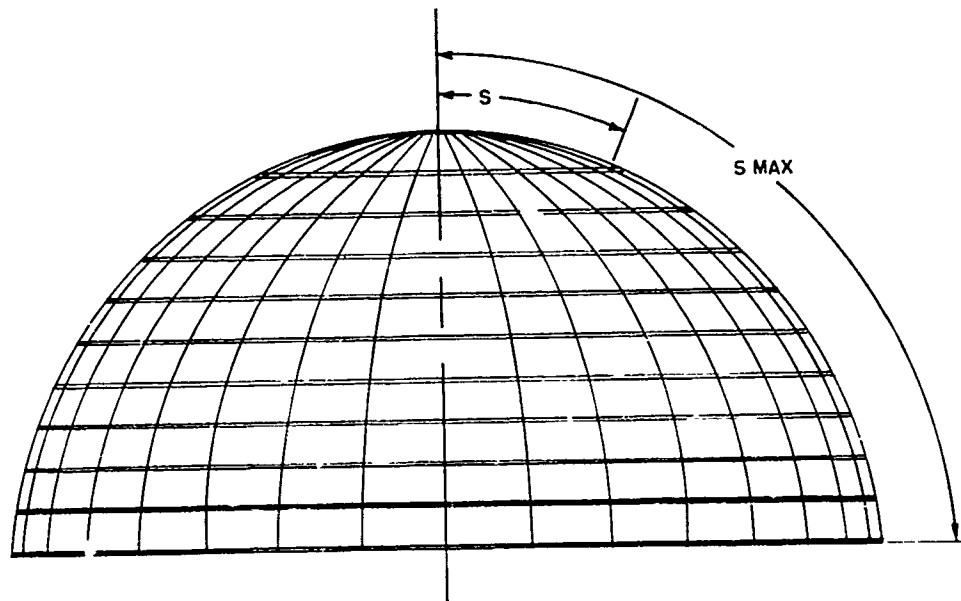
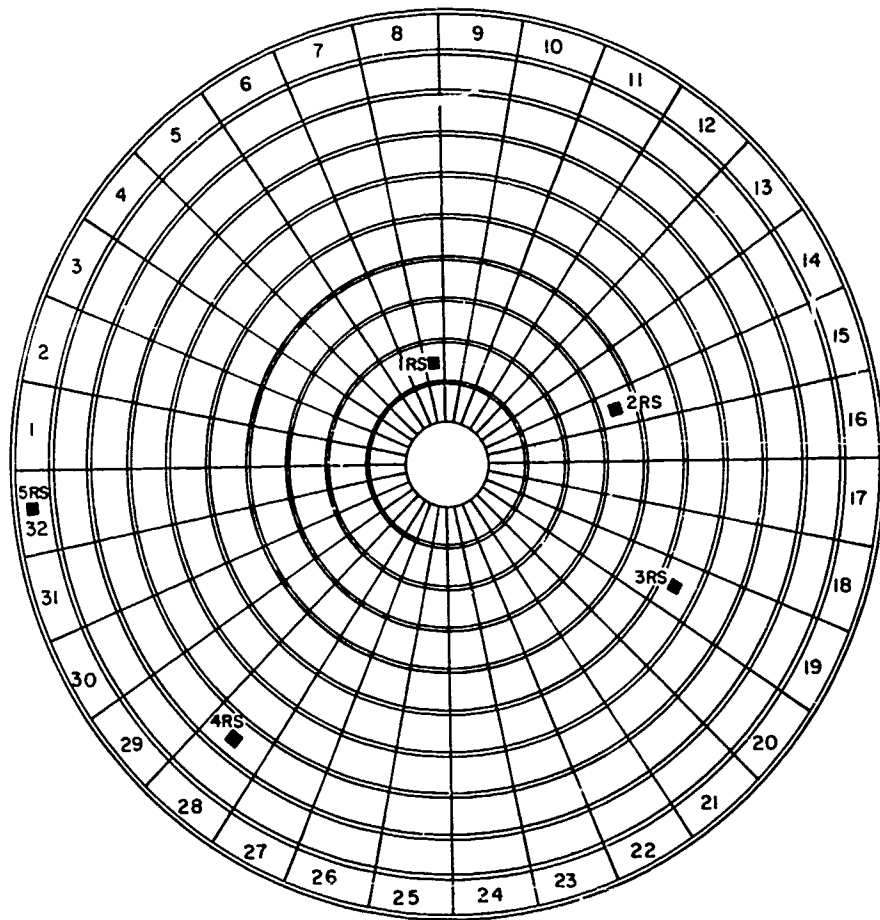


Figure 2. Omega Sensors Orientation on Canopy.

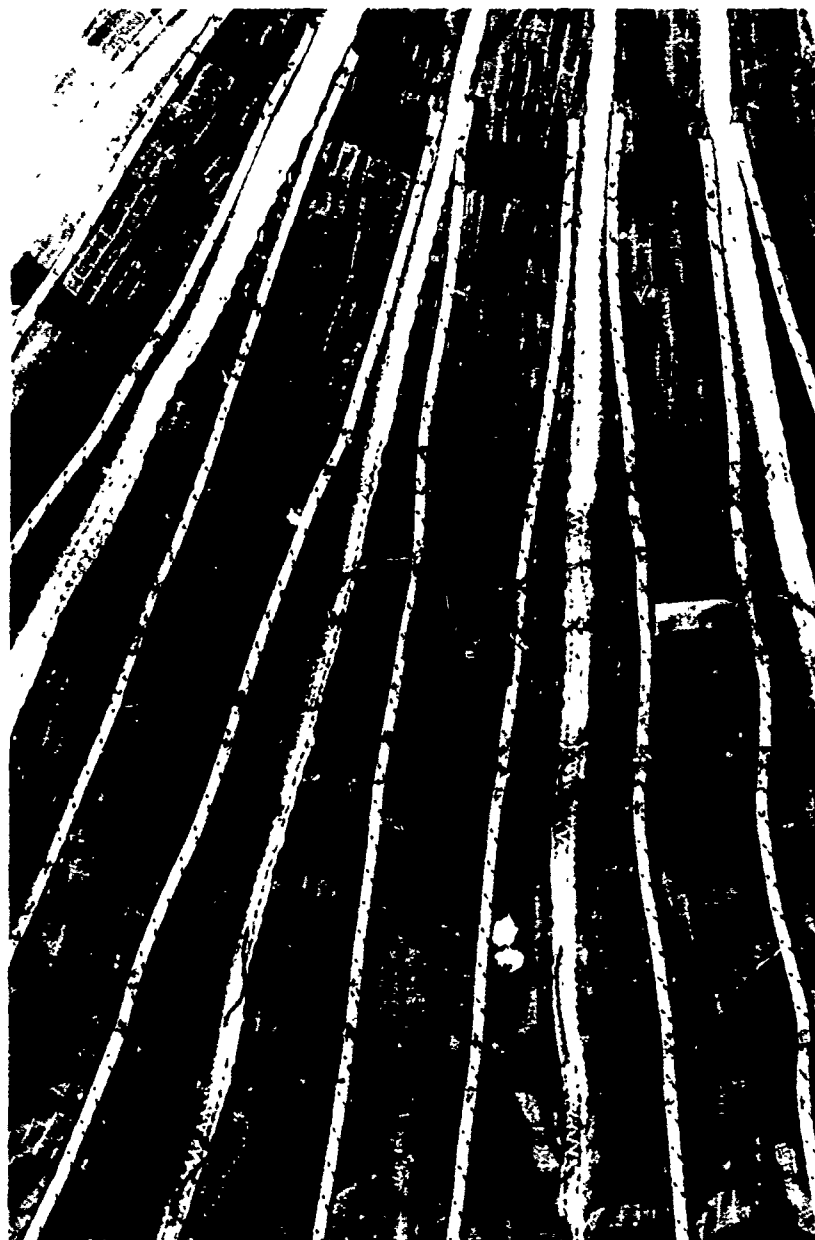


Figure 3. Omega Sensor on Gores Centerline.

The wires then weave in and out of the suspension lines until they reach the four loops where they are connected to cables leading to the oscilloscope. The weaving of the wires was done to minimize the probability of the wires breaking when the lines were pulled taut.

The type of wire used as the electrical leads from the Omega sensor caused difficulties to the test program due to inner breaking of the wires when the suspension lines were pulled taut. When breakage was detected, these plastic covered wires were replaced with teflon coated wires with a higher strength insulation.

## 2. OMEGA Sensor

The Omega sensor was developed for measuring stress in textile and other flexible materials. In earlier studies, it was found that circumferential stresses indicated by Omega sensors of inflated parachute canopies agreed with theoretically predicted stresses (Reference 21) and therefore, the sensor was useful in measuring the canopy stresses under steady state conditions. It was also determined that the stresses indicated by the Omega sensor were not affected by dynamic loading and therefore were useful for stress measurement during a parachute deployment, inflation, and descent (Reference 27).

The original Omega sensor of Reference 21 is shown in Figure 4. Modifications to the original sensor design were necessary due to complications of the tabs tearing during preliminary testing. While statically loading an Omega sensor, the tabs, which were bonded to the inside of the curved beam, were tearing along the edge of the

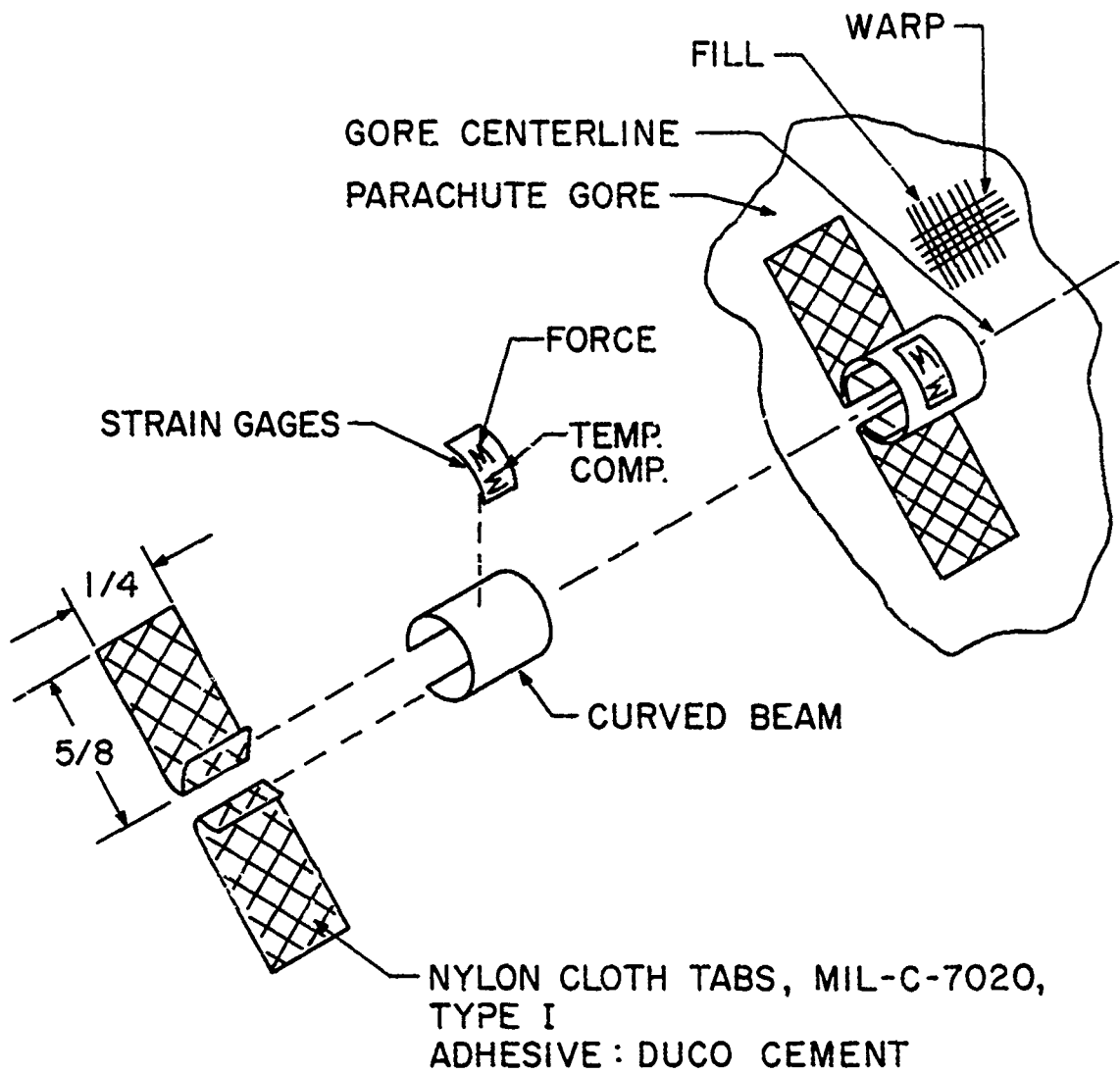


Figure 4. Original Omega Sensor.



slot (Figure 5). Tearing occurred several times to different sensors and it became apparent that the tear began at the sharp corner of the slot and continued along the slot's edge. The cause seemed to be due to the sharp corner and the adhesive used in bonding the tabs to the sensor and the canopy. The adhesive had caused the tabs to become rigid and brittle. The sharp corner and the adhesive resulted in the tabs becoming susceptible to damage.

To correct this, all the sensors were removed from the canopy and their tabs detached. The sharp edges along the slot were filed smooth and the corners blunted. New cloth tabs were attached to the sensor identical to the original ones.

A clear silicone glue and seal adhesive made by General Electric was used to bond the new tabs to the sensor and to the parachute canopy. This adhesive proved to be sufficient as a flexible hinge, as was needed. Figure 6 shows the modifications made to the sensor which were needed to meet this program's requirements.

A small slit was cut in the cloth just beneath the slot in the Omega sensor to minimize possible cloth stress bypassing the sensor (Figure 7). The slit was .3 inches long and 0.5 inches wide and was cut by a hot knife.

Each Omega sensor was individually calibrated off the canopy cloth. The calibration of the sensors consisted of rigidly clamping one sensor tab, while the other cloth tab was loaded with varying weights (static loading). The actual stress applied to the cloth tab was the total load of the weights and the clamp divided by the

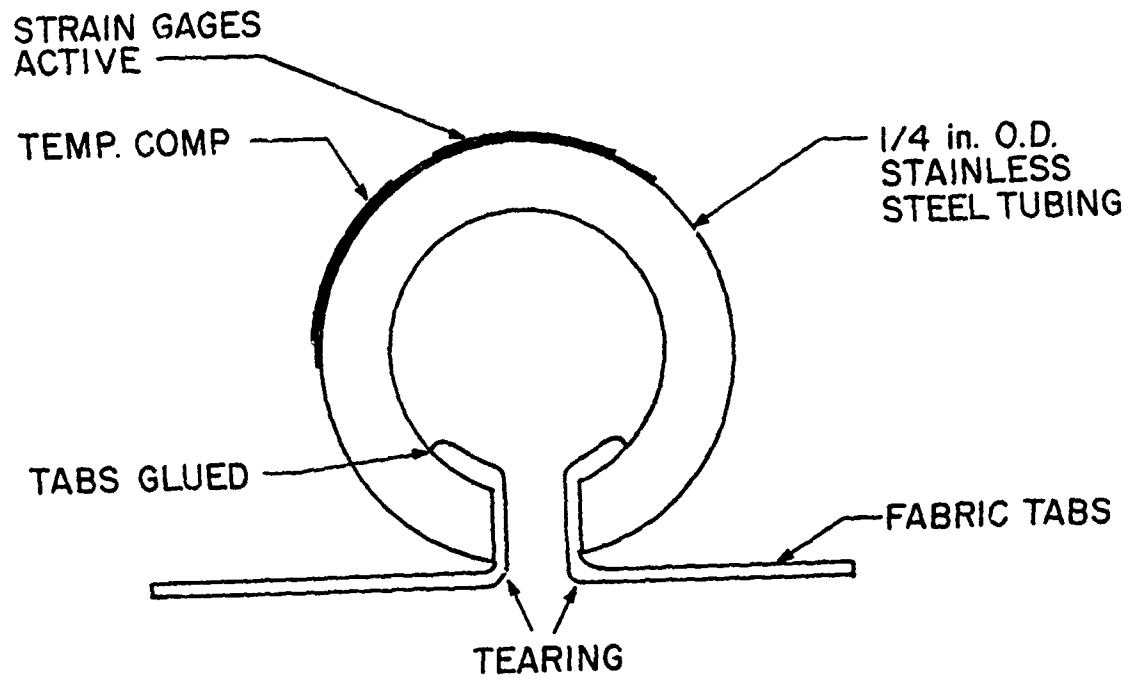


Figure 5. Original Omega Sensors with Tabs.

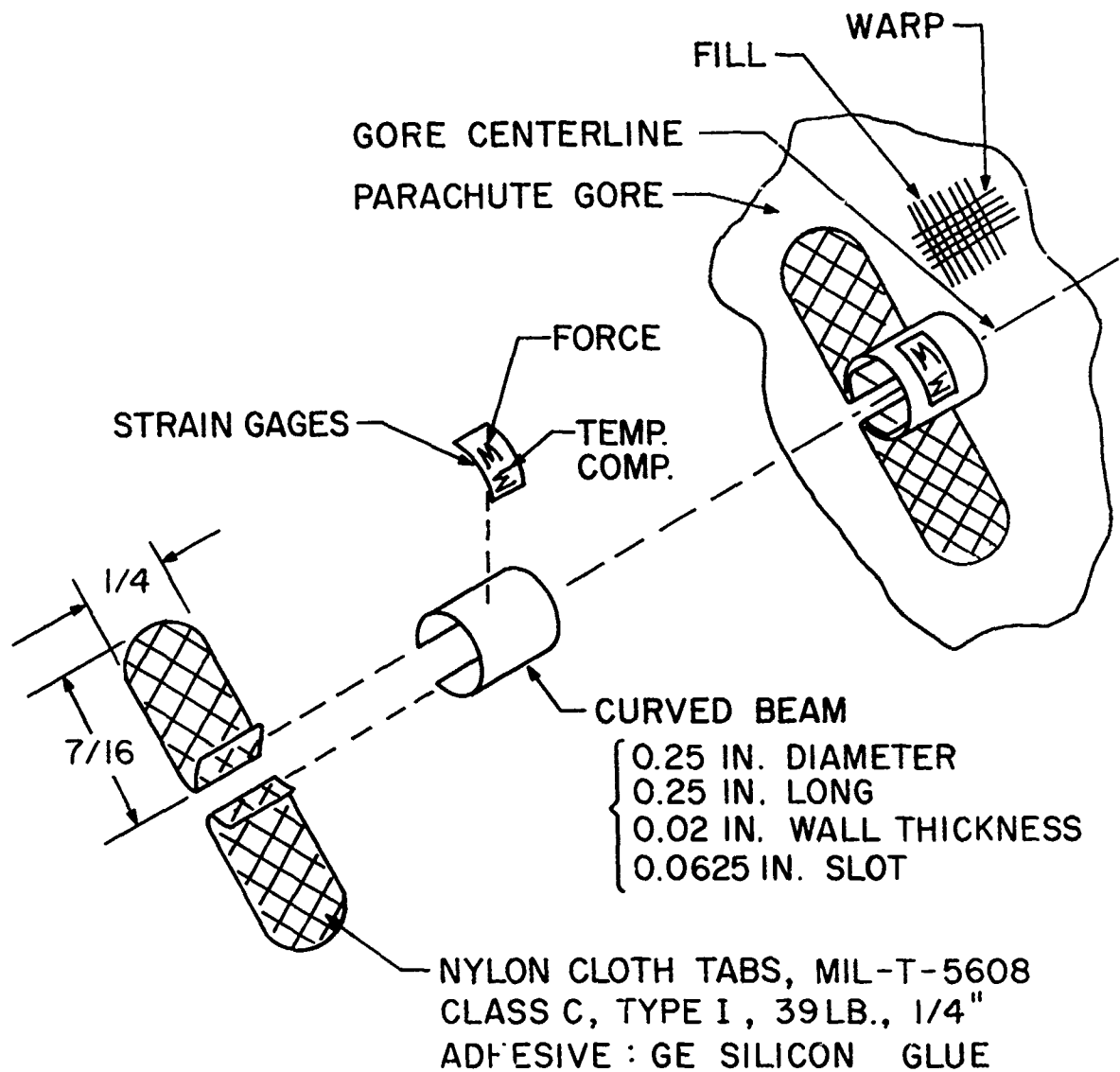


Figure 6. Modified Omega Sensor.



Figure 7. Omega Sensor and Wire Orientation on Canopy.

width of the clamp (.25 inches). Each sensor exhibited a linear calibration curve. These off the canopy calibrations agreed with the University of Minnesota's off the canopy calibrations. The represented calibration's curves, applied stress versus galvanometer deflection, are presented in Figure 8.

A calibration program of the Omega sensors on the canopy was attempted to determine if any damage had occurred when mounting the sensors to the canopy and also to determine if any stress concentrations existed. However, no satisfactory technique could be reached for obtaining reliable on the canopy calibrations. The results obtained from the on the canopy calibrations did not agree with our off the canopy calibrations or the University of Minnesota's on and off the canopy calibrations. A test program, as described in Appendix A, was then conducted to test the effects of clamp width and clamp distance from the sensor on the calibration process. The results are shown in Figure 9 and Figure 10. Figure 9 shows for a fixed distance away from the Omega sensor, the sensitivity increases from the smallest clamp to the largest clamp. Figure 10 shows for a fixed clamp width, the closer the clamp gets to the sensor, the more sensitive the sensor is. The effects of clamp width and of distance from clamp to sensor must be taken into consideration when making calibrations. These effects are explained more completely in Appendix A.

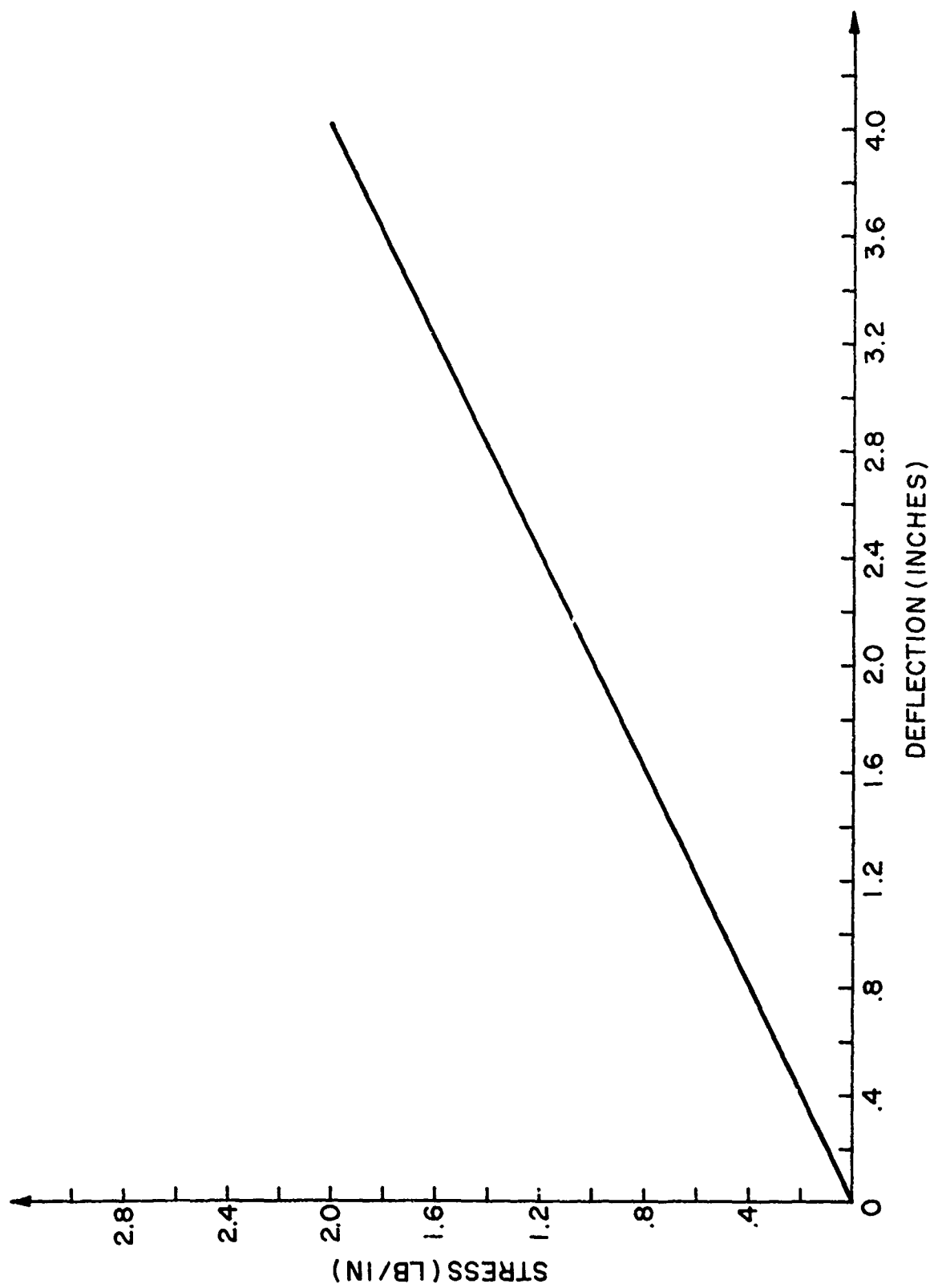


Figure 8. Omega Sensor Calibration Curve.

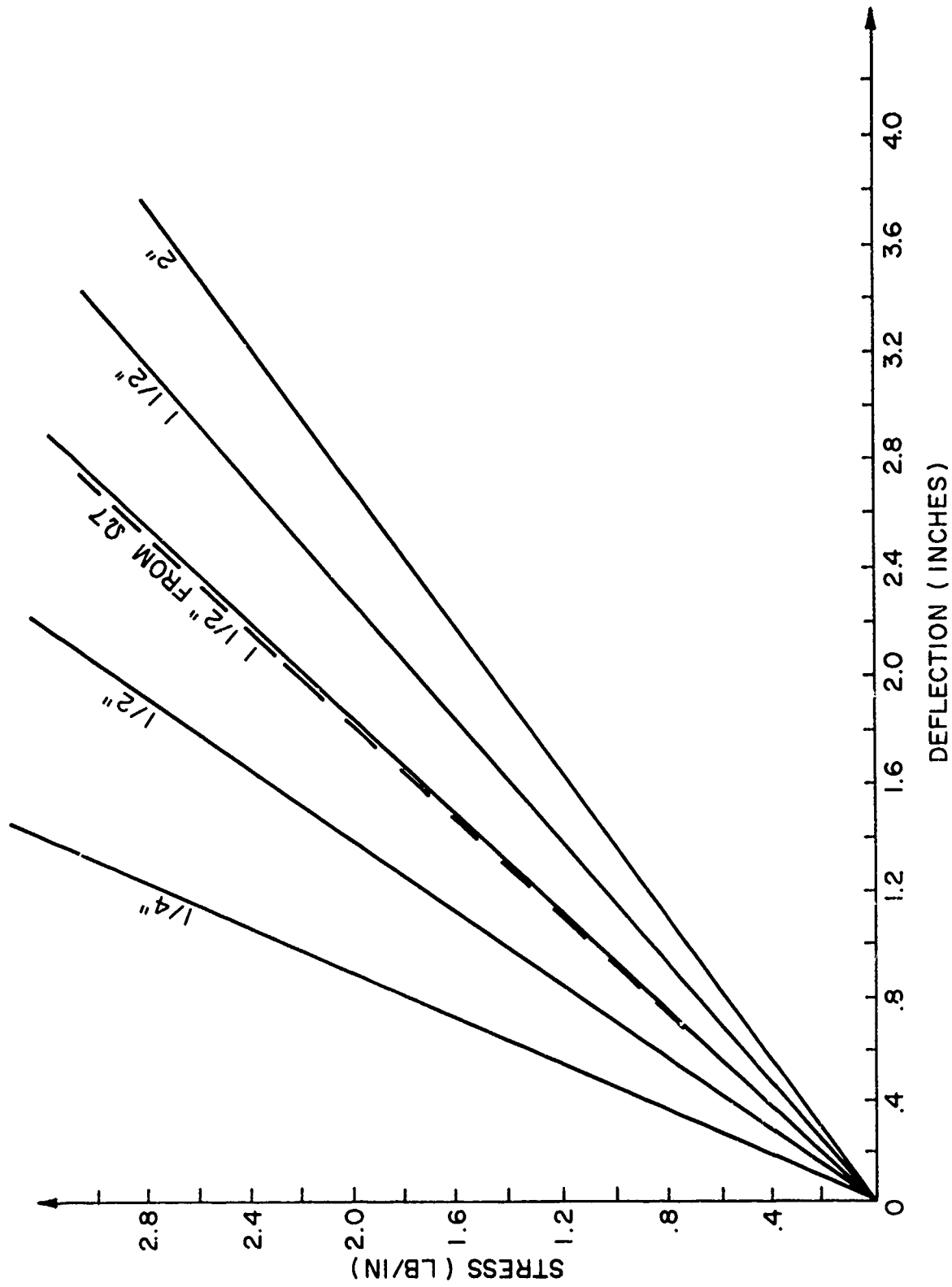


Figure 9. Varying Plates Widths Placed 3" From Sensor.

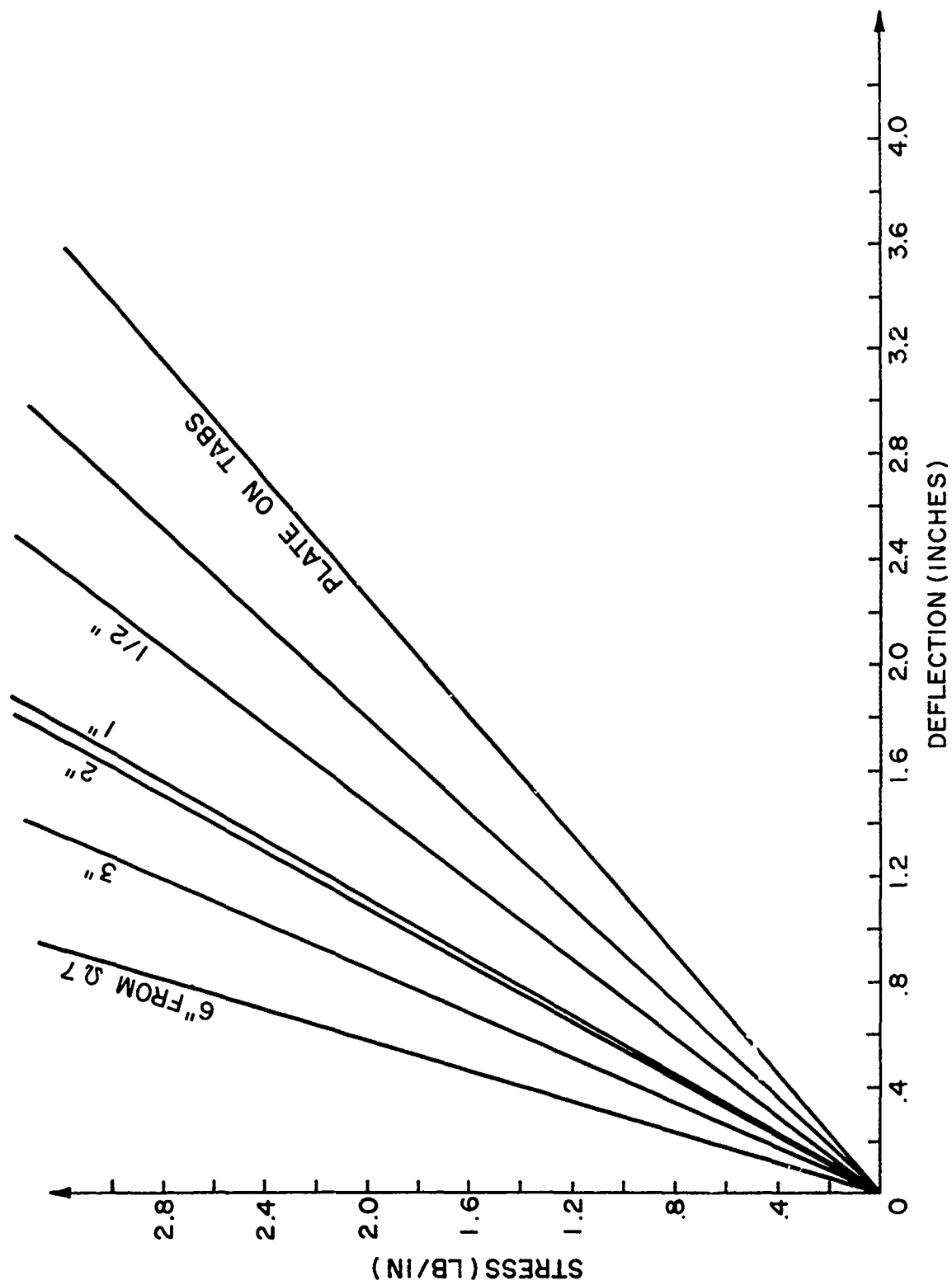


Figure 10. Fixed Plate Width at Varying Locations.



SECTION III  
INSTRUMENTATION

The complete deployment process was photographed by two high-speed cameras at 200 frames per second. One camera was located along the centerline of the chute looking into the opening canopy. The second camera was positioned so it recorded from the side of the parachute. From the photographic coverage, full open, projected diameters and projected canopy areas were obtained. The circuitry used for recording the Omega sensor output is shown in Figure 11.

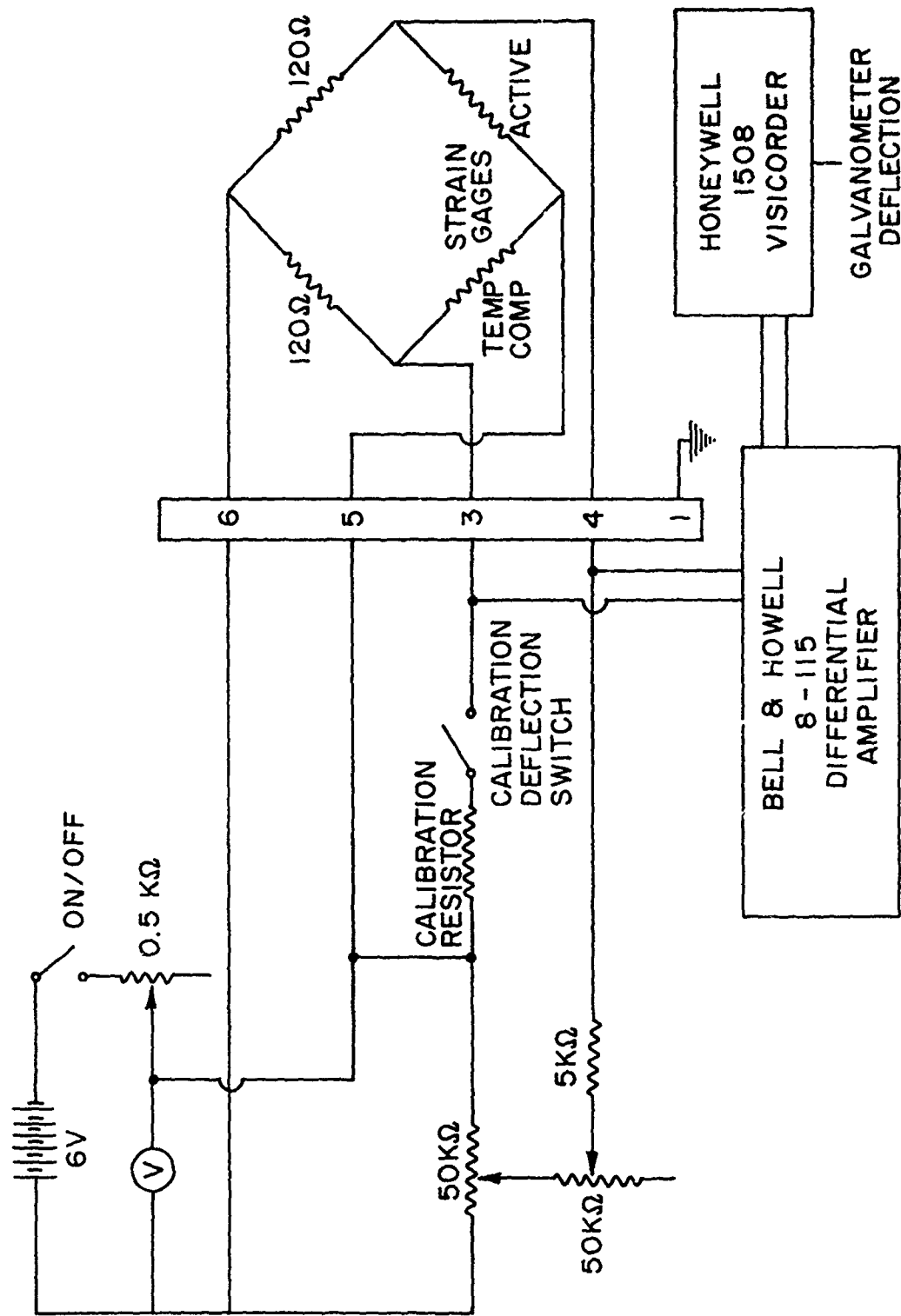


Figure 11. Circuitry for Recording Omega Sensor Output.

SECTION IV  
TEST PROCEDURE

All experimental investigations were performed in the 12-ft low-speed Vertical Wind Tunnel of the Air Force Flight Dynamics Laboratory at Wright-Patterson Air Force Base, Ohio, Figure 12.

A schematic presentation and a test section installation photograph of the test arrangement used for deployment of the model parachute is shown in Figures 13 and 14, respectively. The rod (Figure 13) on which the model parachute was mounted is part of the added mass test fixture (Reference 28) of the wind tunnel. The confluence points of the parachute suspension lines were attached to the force cell of the test fixture and used to measure and record the loads of the chute during inflation. The rod of the fixture helped to restrain the chute from excessive oscillatory movement.

The parachute deployment release mechanism consisted of a burn wire arrangement shown in Figure 13. The burn wire mechanism was comprised of a power supply and an attachment housing a thin wire. The burn wire attachment was located on the rod, six inches above the vent of the chute. An elastic cord extended down from a guide wire with a string and two pins, a foot apart, attached to it. The elastic cord was pulled taut and at that place hooked to the thin wire attachment by the first pin on the string. The second pin was then placed into the strap of the plastic constraint clamping it together.

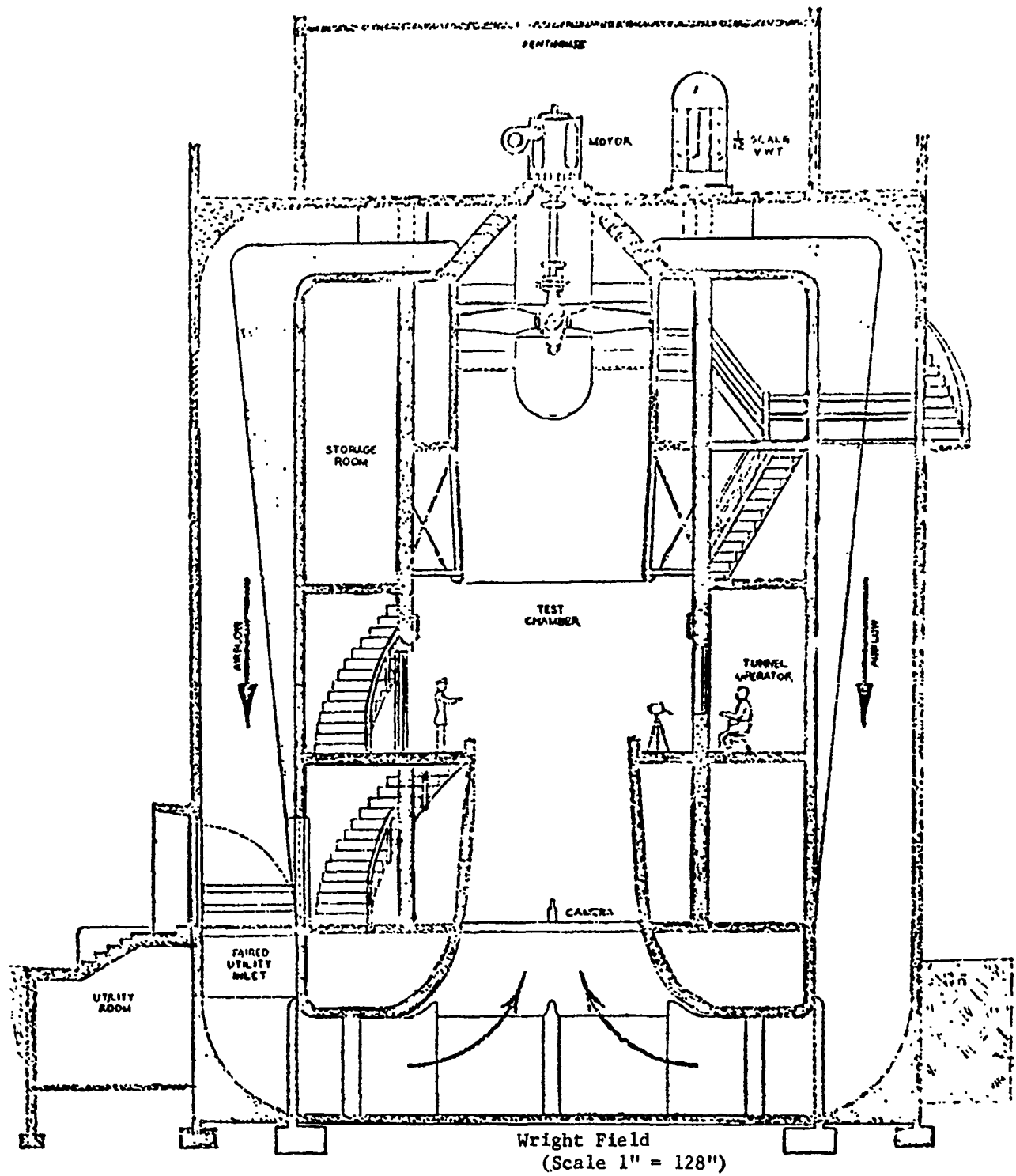


Figure 12. Vertical Wind Tunnel

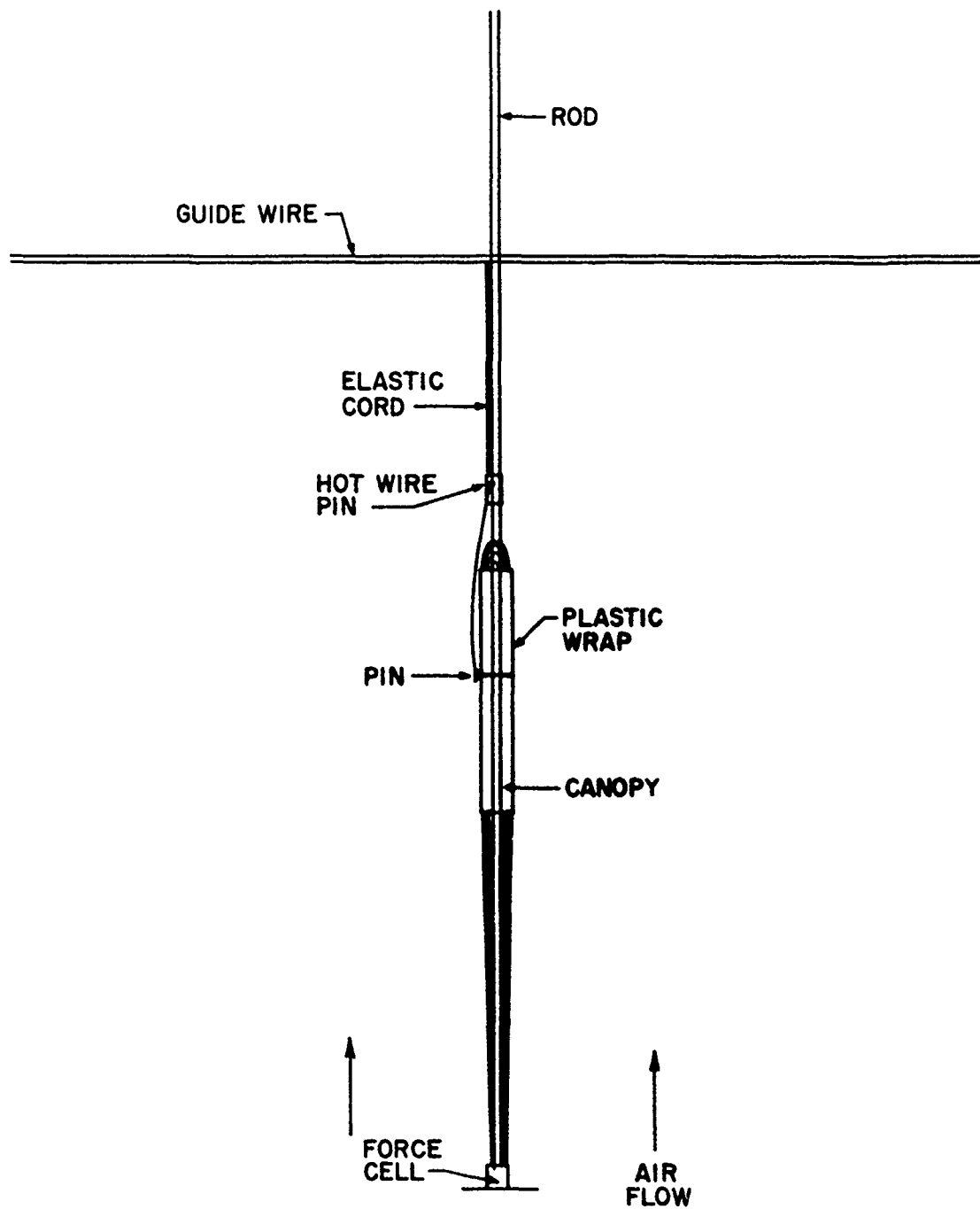


Figure 13. Schematic of Deployment Test Arrangement.

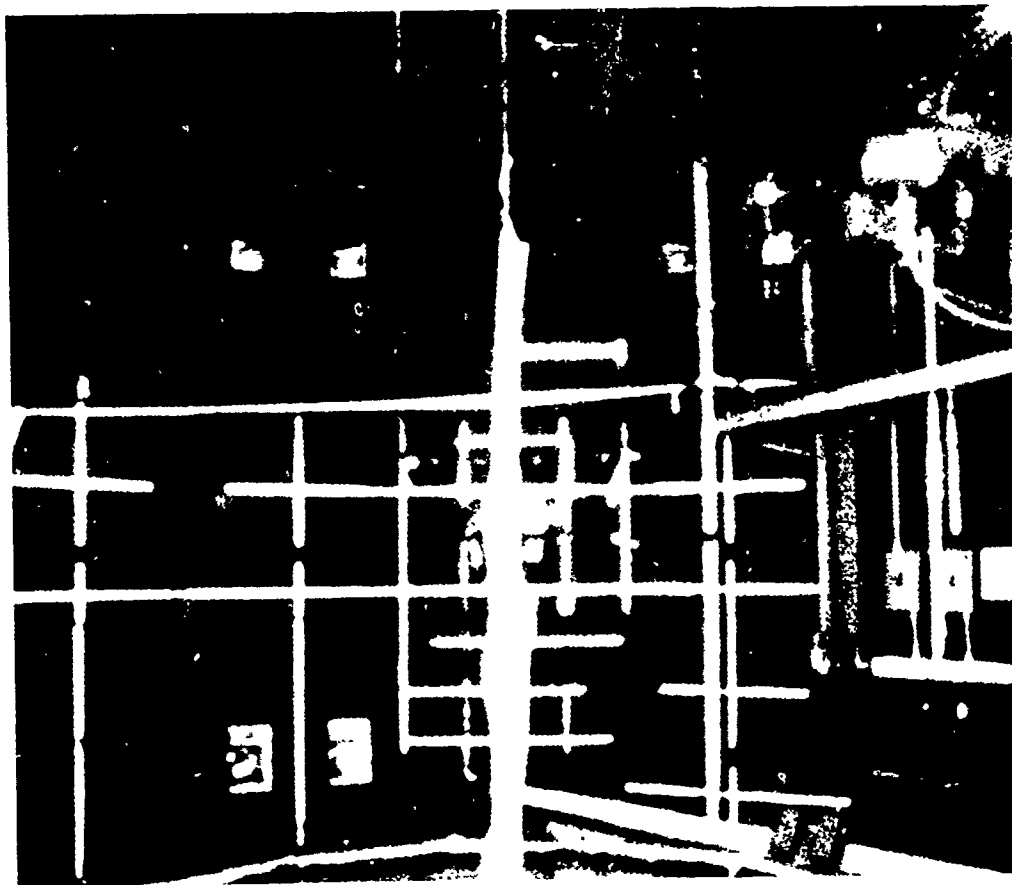


Figure 14. Test Arrangement in Vertical Wind Tunnel.

The test began by setting the particular tunnel velocity needed for the test. Next, the deployment process began by activating the electronic timer which started the cameras and recording instruments and then after a short interim period (1.5 sec) the activation of the burn wire mechanism took place. This consisted of exciting the power supply which sent current to the wire attachment on the rod, burning the wire in two. This released the first pin which was immediately pulled upward by the taut elastic cord, likewise pulling the second pin from the strap clamping the chute, giving it freedom to be carried away by the air flow. The chute is then free to inflate (Figures 15-18).

The canopy stresses and the total force values were measured and recorded during thirty-eight (38) different deployment tests. Eight (8) of these tests were ruined due to camera malfunctions or visicorder malfunctions. At least four separate tests were conducted for each test condition. The tests were conducted at test conditions of  $q$  (dynamic pressure - inches of water) = 0.4, 0.8, 1.2, 1.6, and 2.0.

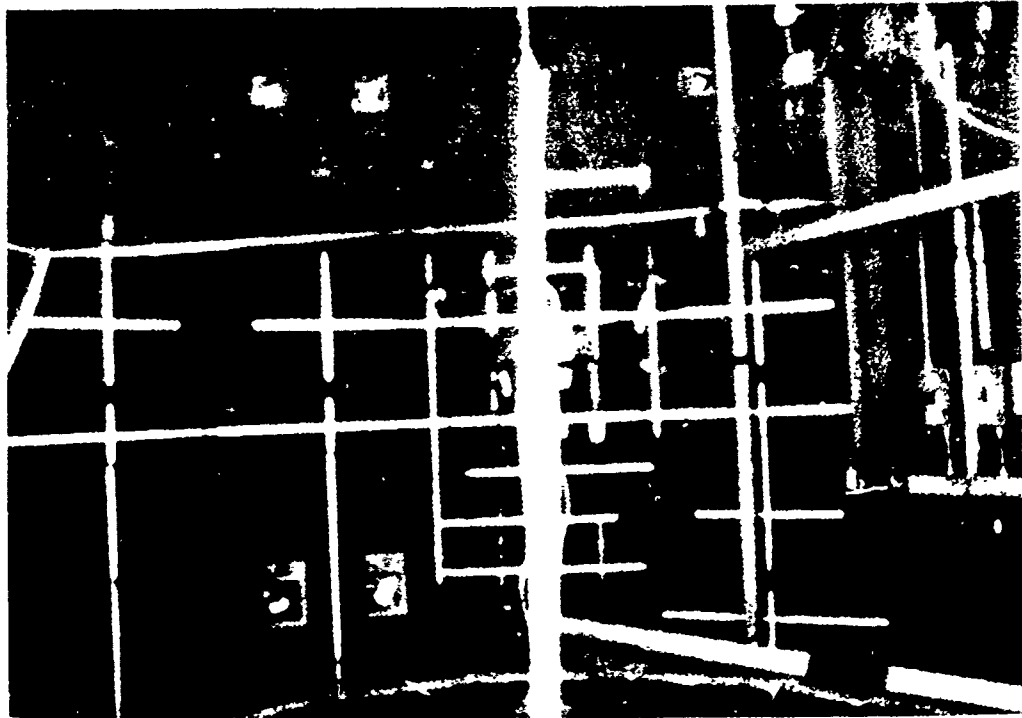


Figure 15. Plastic Constraint Releasing

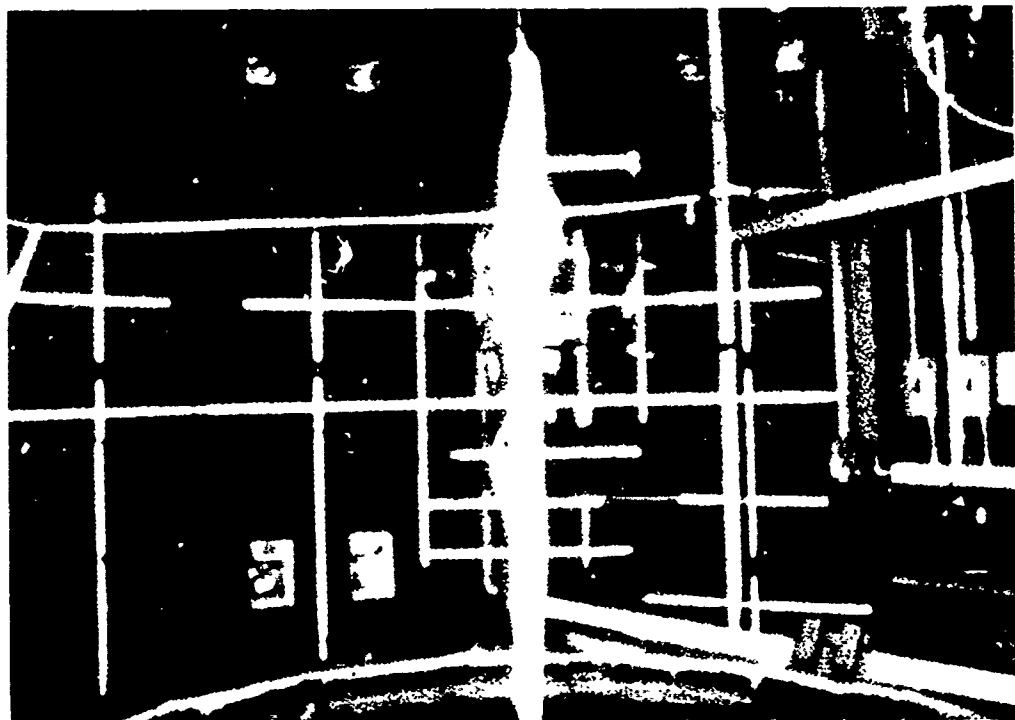


Figure 16. Beginning of Inflation.



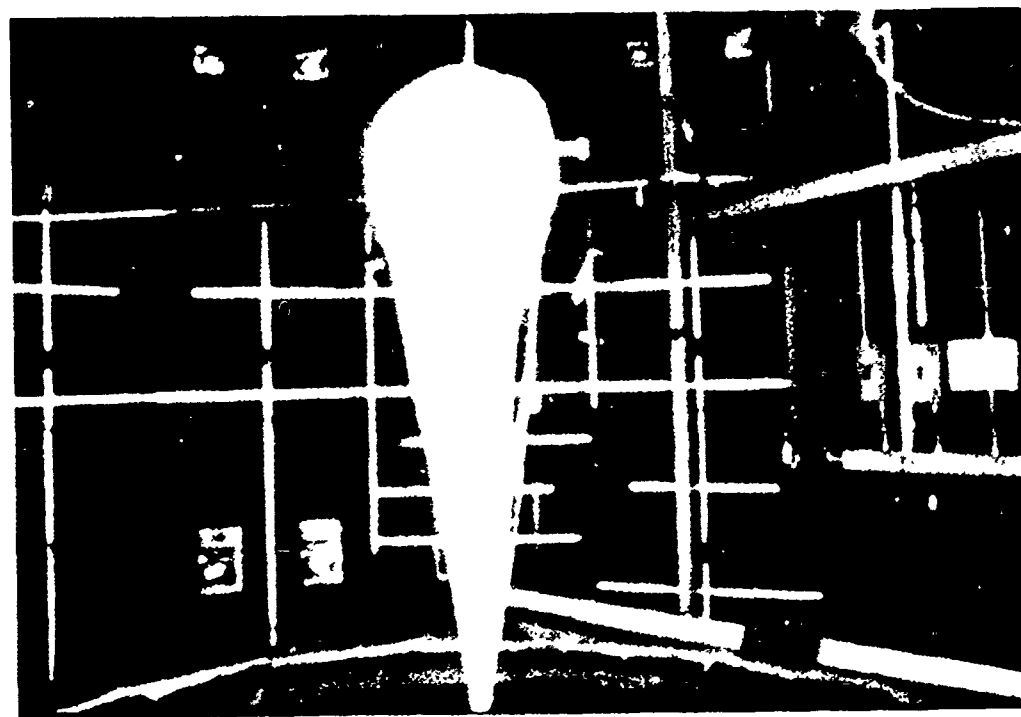


Figure 17. Intermediate Inflation State

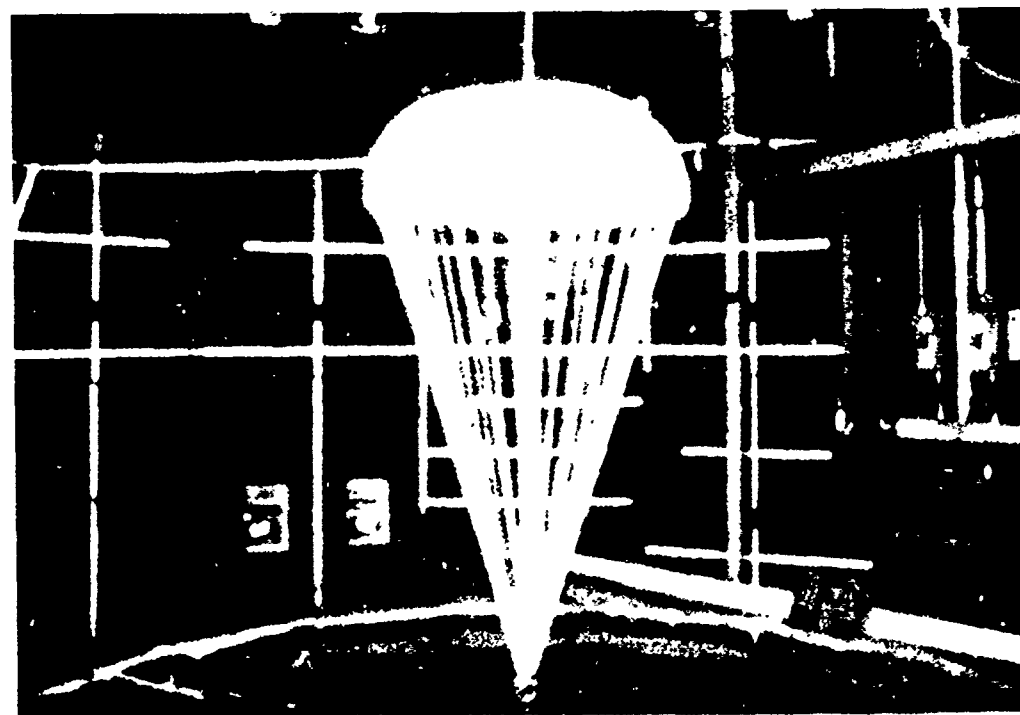


Figure 18. Fully Inflated State.

## SECTION V

### RESULTS

#### 1. Canopy Stress Measurement

A reproduction of an actual oscillograph record obtained from the deployment tests is shown in Figure 19. The oscillograph record represents the registration obtained on a five (5) foot nominal diameter ringslot model parachute during a test run conducted at a deployment condition of 84 ft/sec. The relationship between "q" and velocity (ft/sec) is  $V(\text{fps}) = 66.119 \sqrt{q \text{ (in. H}_2\text{O)}}$ . The start on the oscillograph record represents the point of time at which the plastic wrap is released and the deployment process begins.

As the oscillograph recording illustrates, some stress fluctuations occurred during the unsteady period (canopy inflation) due to the unsteady movement of the canopy material. During the steady state period (canopy fully inflated) the stress also fluctuated due to the flow conditions. The determination of mean steady state values was not obtained at the end of the deployment process due to the actual steady state conditions not being reached immediately after canopy inflation, but several seconds later. To avoid lead breakage and other damages to the Omega sensors, especially at high deployment velocities, the wind tunnel was shut down immediately after canopy filling was complete. Steady state values were obtained from a test program in which readings were taken for at least five (5) seconds per test and at least two tests per test condition performed. The reproducibility of the two measurements made at any one

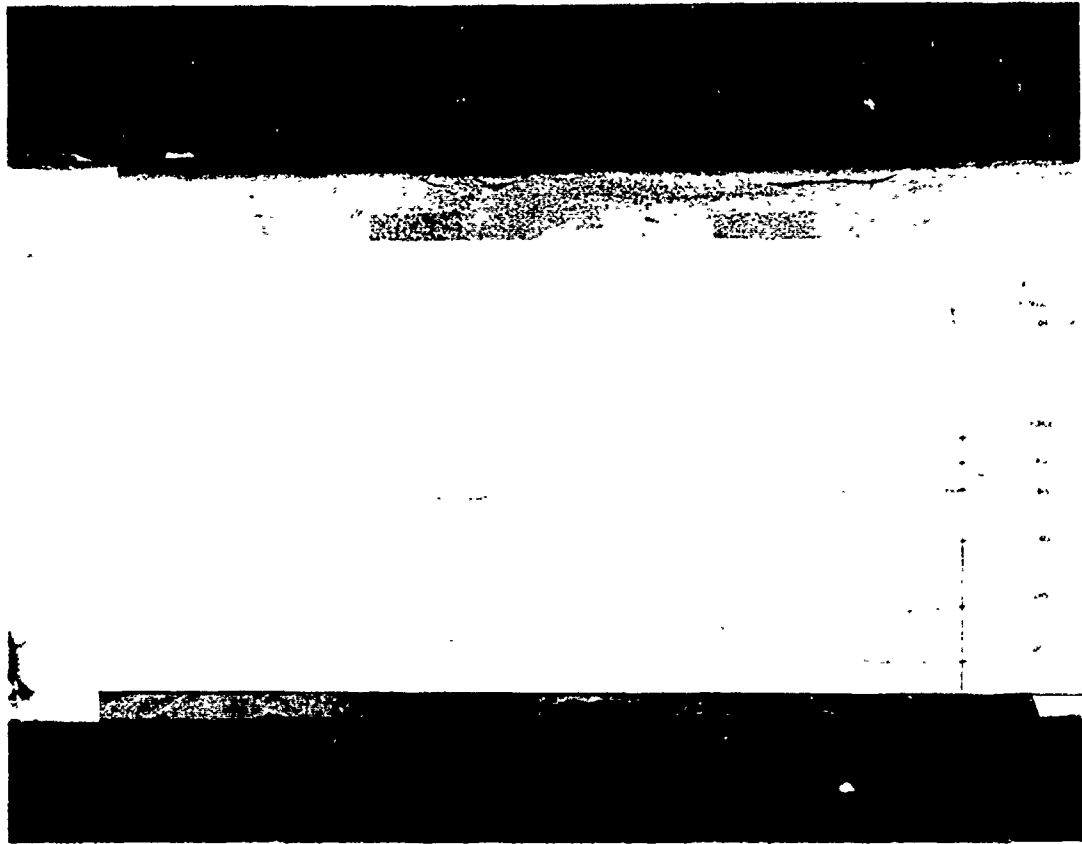


Figure 19. Oscillograph Record.

test condition were very good. The steady state mean values are presented in Table I.

From oscillograph records like the one shown, and from the sensors calibration curves, the stress in the canopy was obtained. These measured stresses on the surface of the canopy were plotted as a function of nondimensionalized time  $t/t_{FO} = T$  in Appendix B. For comparative purposes, the stress values at each location on the canopy were also nondimensionalized  $\sigma/\sigma_{FMAX} = \sigma M$ . This was essential owing to the off the canopy calibrations, instead of on the canopy calibration of the sensors as was needed, and therefore prevents the presenting of untrue stress magnitudes.

A compilation of all maximum nondimensioned stress values, nondimensionalized time of the maximum stresses, maximum force and the actual time of this force are presented in Table II. Table II represents the collection of all the stress measurement information for each of the five (5) sensor locations on the ringslot canopy, for the five (5) deployment speed conditions,  $q$ . A condensed version of Table II is presented in Table III where the mean and standard deviations are computed for the individual deployment velocities. According to Table III, the general stress trends at the different deployment velocities were equivalent and are therefore summarized in Table IV. In general, the stress peak occurs slightly prior to the time at which the canopy reaches its fully inflated shape for the first time. The last peak in the skirt area occurs at almost exactly the time at which the canopy is fully inflated. The peak

TABLE 1  
 MEAN AND STANDARD DEVIATIONS OF STEADY STATE TESTS

q	MEAN					STANDARD DEVIATION					F S.D.	
	S <sub>1RS</sub>	S <sub>2RS</sub>	S <sub>3RS</sub>	S <sub>4RS</sub>	S <sub>5RS</sub>	F <sub>Mean</sub>	S <sub>1RS</sub>	S <sub>2RS</sub>	S <sub>3RS</sub>	S <sub>4RS</sub>		S <sub>5RS</sub>
.4	.0865	.0196	.0284	.0177	-.0051	11.1671	.0267	.0109	.0198	.0135	.0128	1.4395
.8	.0639	.0182	.0648	.0139	.0139	28.3641	.0313	.01999	.0240	.0201	.0229	3.3872
1.2	.1603	.0221	.1231	.0686	.0382	45.5592	.0402	.0144	.0267	.0196	.0318	4.4333
1.6	.1844	.0134	.1684	.0847	.048	61.567	.0446	.014	.0298	.0204	.0336	5.1999
2.0	.2048	.0046	.1978	.0994	.0515	77.8823	.0445	.0146	.0303	.0195	.0303	5.7712

TABLE II  
TABULATED STRESS DATA

Q	F <sub>MAX</sub>	T <sub>FMAX</sub>	S <sub>1RS</sub>	T <sub>1RS</sub>	S <sub>2RS</sub>	T <sub>2RS</sub>	S <sub>3RS</sub>	T <sub>3RS</sub>	S <sub>4RS</sub>	T <sub>4RS</sub>	S <sub>5RS</sub>	T <sub>5RS</sub>
.4	32.29	.9562	1.407	.608	3.0	.683	3.659	.6352	3.2	.9244	1.033	.9631
.4	30.613	.8811	1.50	.435	2.3571	.3916	3.2631	.3524	1.636	.2194	1.02	.8854
.4	30.6129	1.026	1.1587	.4092			1.082	1.048			1.0	1.0258
.8	59.9677	.9365	3.4285	.4645	3.2083	.4428	1.163	.9073			1.279	.9509
.8	61.2258	.9823	2.0897	.4808	1.3438	.3751			2.0277	.6057	1.1666	.9711
.8	59.54	1.023	2.111	.5848								
.8	62.064	.8565	2.989	.514	2.329	.5822			1.2842	1.045	1.054	.9418
.8	61.6452	.9804	1.6154	1.097	1.3261	.435			1.0405	.9742	2.023	.9130
1.2	85.129	.9052	1.9697	.8622					1.0963	1.043		
1.2	86.8064	.9888	1.6391	.4985	1.514	.5379			1.7143	.4193		
1.2	88.4839	1.021	2.4296	.5637	4.6487	.580			1.229	.5229	1.243	1.0475
1.2	132.5161	.9412	1.7944	.497	1.1311	.9562			1.0416	.9261	1.0679	.9562
1.2	87.6452	.9335	1.7917	.3166	6.066	.3815			1.108	.8942		
1.2	84.2903	.909	1.4205	.4108	2.857	.7342			1.976	.944		
1.2	82.1935	1.0	2.103	.4337	1.2414	1.007			1.6053	.9852	1.35	.9485
1.2	84.2903	.7654	2.0769	.3744	1.2456	.3994	1.7083	.7874			1.0	.7654
1.2	84.2903	1.007	3.8433	.446	6.5294	.3446	1.375	.9931				
1.6	109.877	.9878	2.234	.3831	3.368	.625			1.0676	.9678		
1.6	112.387	.9702	1.682	.4291	1.1064	.9794	1.784	.5036	1.0952	1.007	1.324	.9887
1.6	103.7613	.9773	2.254	.4546	2.826	.7197			1.568	.6288	1.009	.9849
1.6	112.8064	.9821	2.849	.5208	1.569	.3944	1.033	1.004				
1.6	109.032	1.009	3.6296	.4821	1.698	.4374	1.9157	.7322				
2.0	130.0	1.043	1.766	.4981	2.163	.4368			1.4118	1.0806	1.042	1.0524
2.0	129.5806	.9969	2.1613	.4747	3.359	.4826					1.383	1.013
2.0	129.5806	.8667	2.707	.3294	3.479	.3194						
2.0	119.5161	.9397	2.887	.4657	1.814	.6456			4.02	.2941	1.088	.67
2.0	135.032	.9863	2.1619	.5176	2.3396	.4981			1.571	.9375	1.633	.6152
2.0	137.129	.9432	2.725	.8434	2.255	.3067	1.141	.9278				

TABLE III  
TABULATED STRESS DATA PER TEST CONDITION

q	F <sub>MAX</sub> Mean	F <sub>MAX</sub> S.D.	T <sub>FMAX</sub> Mean	T <sub>FMAX</sub> S.D.	S <sub>1RS</sub> Mean	S <sub>1RS</sub> S.D.	T <sub>1RS</sub> Mean	T <sub>1RS</sub> S.D.	S <sub>2RS</sub> Mean	S <sub>2RS</sub> S.D.	T <sub>2RS</sub> Mean	T <sub>2RS</sub> S.D.
.4	31.17	.97	.95	.07	1.36	.18	.48	.11	2.68	.45	.54	.21
.8	60.89	1.09	.96	.06	2.20	.57	.63	.27	2.05	.90	.46	.09
1.2	90.63	15.83	.94	.08	2.16	.75	.49	.16	3.40	2.28	.60	.25
1.6	109.45	3.88	.99	.01	2.53	.74	.45	.05	2.11	.94	.64	.24
2.0	130.14	6.10	.96	.06	2.4	.44	.53	.16	2.57	.68	.45	.13

q	S <sub>3RS</sub> Mean	S <sub>3RS</sub> S.D.	T <sub>3RS</sub> Mean	T <sub>3RS</sub> S.D.	S <sub>4RS</sub> Mean	S <sub>4RS</sub> S.D.	T <sub>4RS</sub> Mean	T <sub>4RS</sub> S.D.	S <sub>5RS</sub> Mean	S <sub>5RS</sub> S.D.	T <sub>5RS</sub> Mean	T <sub>5RS</sub> S.D.
.4	2.67	1.39	.68	.35	2.42	1.11	.57	.50	1.02	.02	.96	.07
.8	1.63		.9073		1.45	.51	.87	.24	1.38	.44	.94	.02
1.2	1.54	.24	.89	.15	1.43	.37	.80	.24	1.20	.18	.92	.14
1.6	1.58	.48	.75	.25	1.24	.28	.87	.21	1.17	.22	.99	0
2.0	1.141		.9278		2.33	1.46	.77	.42	1.29	.28	.84	.23

TABLE IV

MEAN AND STANDARD DEVIATION OVER TESTS

F MAX Mean	F MAX S.D.	T FMAX Mean	T FMAX S.D.	S 1RS Mean	S 1RS S.D.	T 1RS Mean	T 1RS S.D.	S 2RS Mean	S 2RS S.D.	T 2RS Mean	T 2RS S.D.
89.23	32.0	.96	.02	2.16	.50	.52	.10	2.59	.50	.54	.08

S 3RS Mean	S 3RS S.D.	T 3RS Mean	T 3RS S.D.	S 4RS Mean	S 4RS S.D.	T 4RS Mean	T 4RS S.D.	S 5RS Mean	S 5RS S.D.	T 5RS Mean	T 5RS S.D.
1.72	.78	.81	.17	1.71	.56	.78	.12	1.22	.27	.93	.06



separation time between each sensor was approximately 1/10 of a second or more. There was no significant difference in stress magnitudes between the low and high deployment velocities.

Absolute filling times of the canopy decreased with increasing deployment velocity. The relationship between projected canopy area growth ratio,  $SP/SPFO$ , as a function of nondimensional time is shown in Appendix C for each of the test conditions. The figures illustrate a gradual and fairly smooth canopy area growth. When examining the curves for each of the test conditions, there are no differences. The five deployment velocities exhibit the exact trend in the area growth pattern.

On the ringslot model parachute, the maximum stress at the vent area occurs definitely before the maximum force occurs, while further toward the skirt the time ratio approaches unity, " $T$ " = 1.0. The total parachute force reaches its maximum value at the time of canopy full open. As is intuitively obvious, the total force of the parachute increases with increasing velocities. A presentation of the total parachute force versus time relationships for each test condition is included in Appendix D.

## SECTION VI

### CONCLUSIONS AND RECOMMENDATIONS

The stress distribution over the surface of a ringslot model parachute during the period of inflation and steady state was experimentally determined for the infinite mass operating condition during low speed wing tunnel tests. The area growth of the ringslot parachute during inflation was also determined.

The results are presented in detail and provide for the first time actual measurement of circumferential stresses on the surface of a model ringslot parachute. These results, however, can only present the general trend shown in the parachute's stress distribution and not actual stress values due to the manner of sensor calibration as mentioned earlier.

The general trend presented in this report was that the high stress concentrations during canopy inflation began early in the vent area and occur later at the skirt almost at the time of full-open. The canopy experienced low levels of circumferential stress at the middle and skirt sections of the canopy during inflation and at steady state.

Under steady state conditions, the model parachute experiences the same stress distribution trend as during inflation. That is, the stress concentration is highest in the vent area and lower in the middle and skirt regions.

This test program was entirely exploratory and unfortunately, the scope of the study was limited by time. Therefore, recommen-

dations are presented for further investigations in this area of study.

Along with the modifications of the Omega sensor, already mentioned, each of the sensor's electrical leads weaving through the suspension lines should be replaced with a higher strength insulation wire. This would eliminate inner breakage of the wire as was the case in this test program, producing unreasonable data.

Due to the findings of the fill strip tests, no satisfactory technique could be found to calibrate the Omega sensors mounted to the parachute's canopy. It is essential that a method be determined and used in future studies. In future programs, it is suggested that the Omega sensors be bonded to the inside of the canopy in the same manner as previously discussed. This would help to reduce the possibility of damage to the sensors during the deployment process.

APPENDIX A  
FILL STRIP TESTS

## APPENDIX A

### FILL STRIP TESTS

An investigation to determine the significance of altering the area (width) of an applied load and also altering the location of this load to the stresses measured by the Omega sensor was deemed important due to the manner in which an Omega sensor measures stress while mounted on the canopy. Therefore, an experimental test program was designed to look at this problem. A static loading test program was conducted on a nylon cloth strip specimen with an Omega sensor mounted on it. In static loading a known stress is applied and the related electrical output recorded. The relationship between applied load and electrical output establishes the static calibration.

Tests were conducted with a fill strip specimen with an Omega sensor mounted on it (Figure A-1). The Omega sensor was attached in the fill direction of the cloth corresponding to the sensor attachment on the fill of the model parachute. A small (.3-inch) slit was cut in the cloth beneath the slot in the Omega sensor for reasons previously mentioned.

A schematic presentation of the test arrangement is given in Figure A-2. A test of a strip specimen consisted of first clamping both ends of the strip specimen with the grips and suspending the cloth strip from a bending link. Then various weights were suspended from the cloth specimen to provide stress values and the electrical output of the sensor was recorded on a Honeywell visicorder.

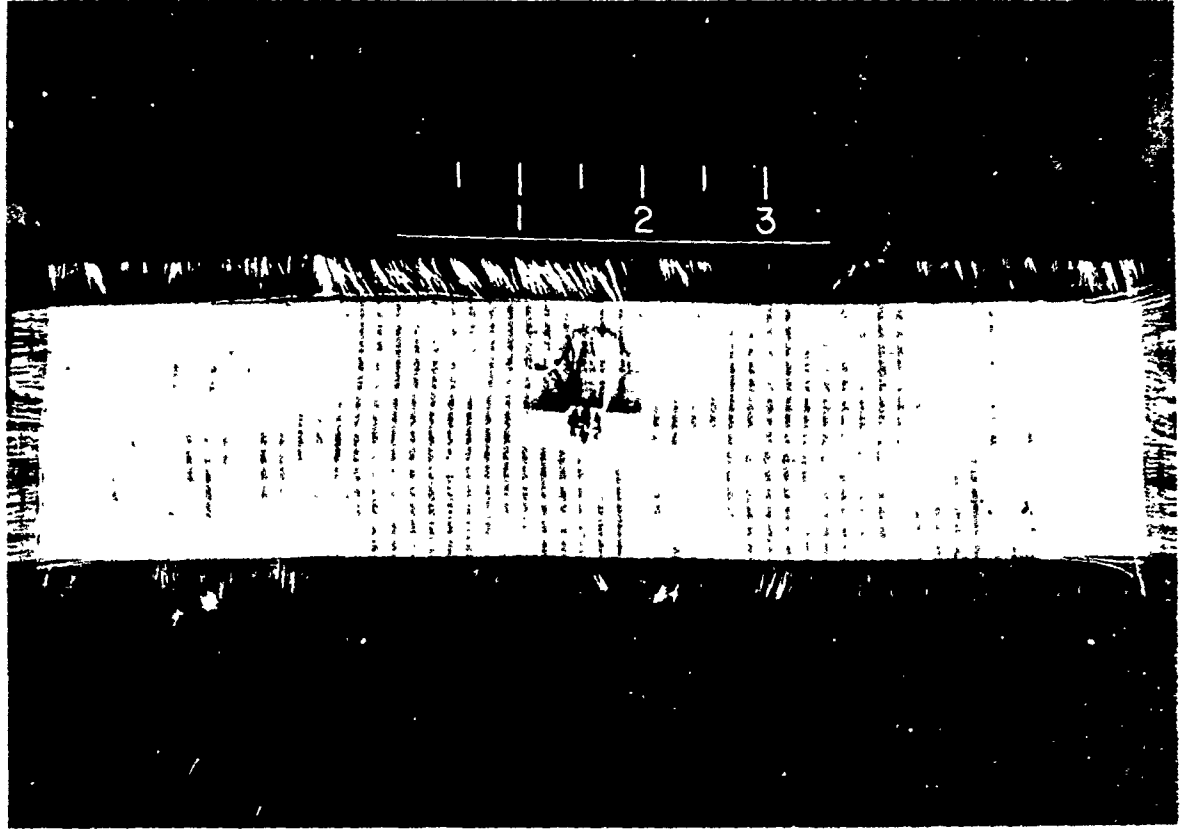


Figure A-1. Fill Strip Specimen.

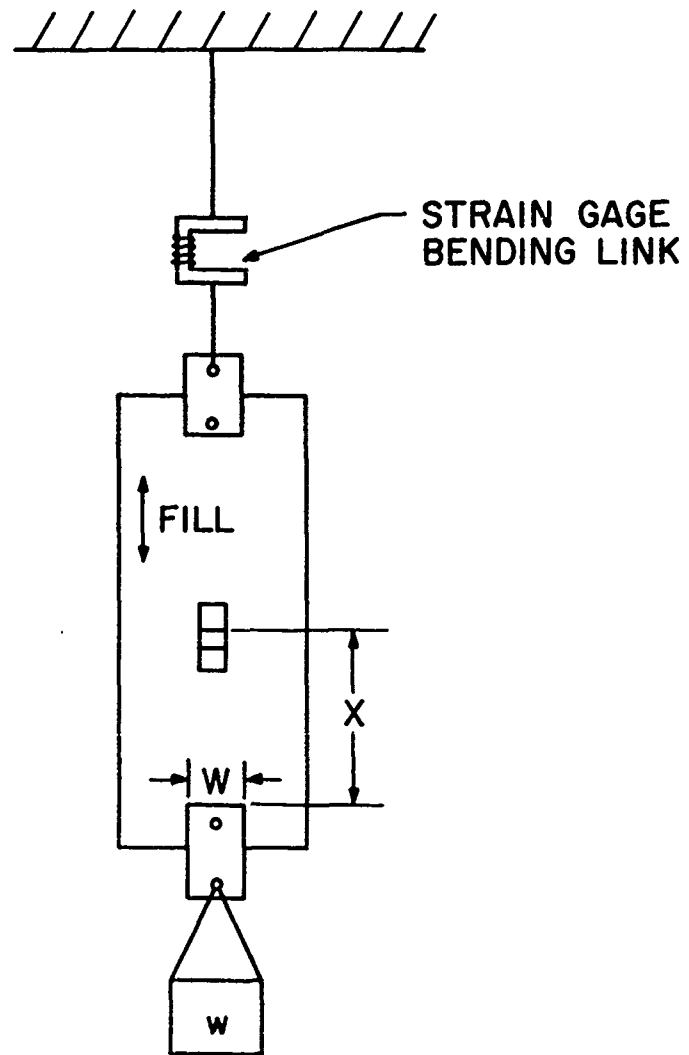


Figure A-2. Schematic of Fill Strip Test Arrangement

Two separate measurements were made for each load condition in order to determine the repeatability of the measurements and obtain valid average data.

A total of twenty-seven (27) tests were performed on the fill strip specimen.

Two supplementary tests were performed using two one-fourth ( $1/4$ -inch wide clothes pins as grips). One test was conducted with the clothes pins clamped approximately one-half ( $1/2$ )-inch from the Omega sensor and the next test the clothes pins were attached directly to the sensor's tabs (approximately  $3/8$ -inch).

These supplementary tests were conducted in order to validate the use of clothes pins as grips when calibrating the Omega sensors. Clothes pins were chosen for their convenience of gripping the cloth material firmly without damping it.

The oscillograms were transferred into applied stress versus galvanometer deflection diagrams as shown in Figures A-3 to A-9. These curves were linear and forced to pass through the origin.



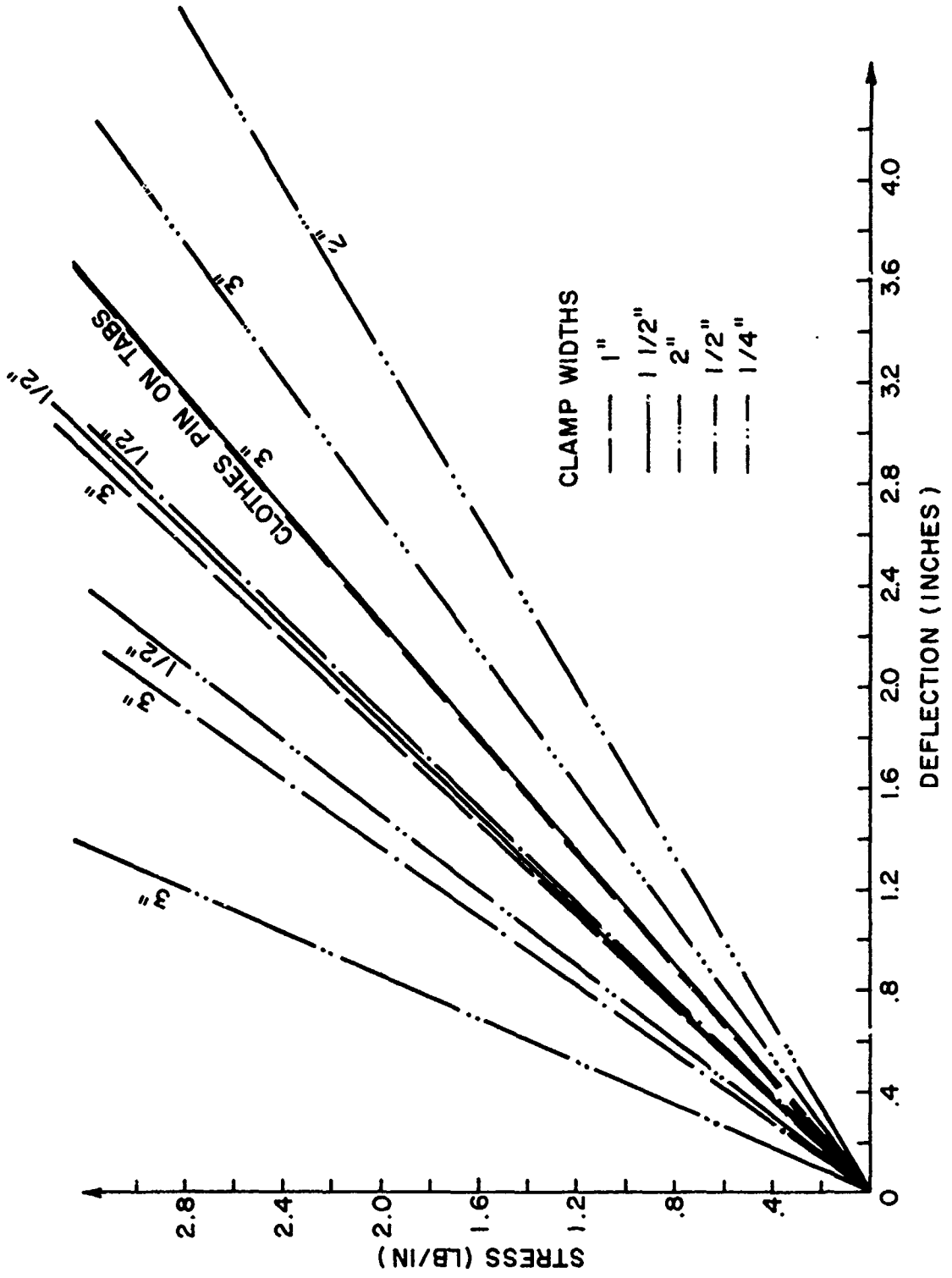


Figure A-3. Range of Outputs for Various Width Clamps and Distances from Sensor (1/4" to 3").

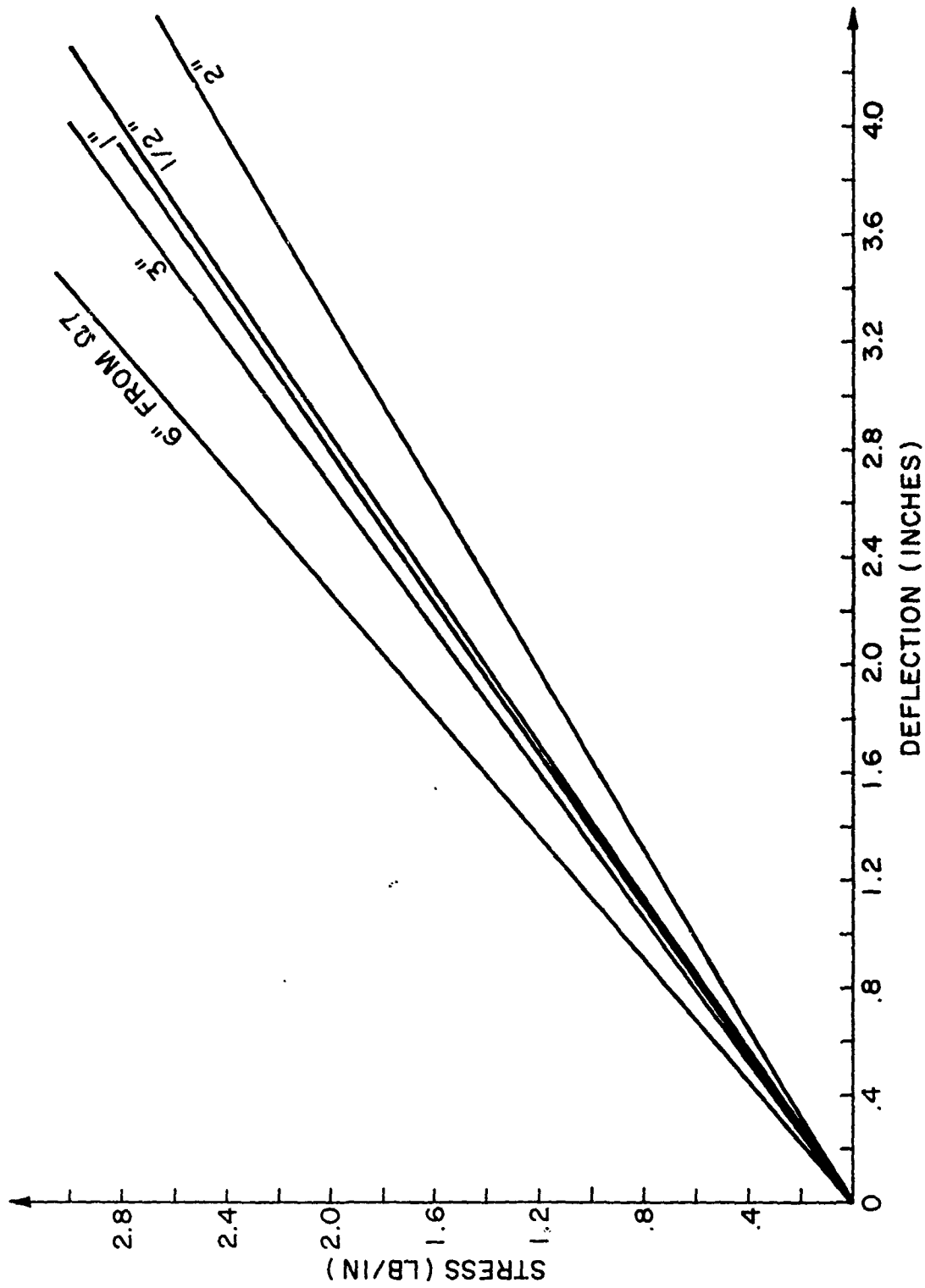


Figure A-4. Two (2) Inch Plates at Varying Distances.

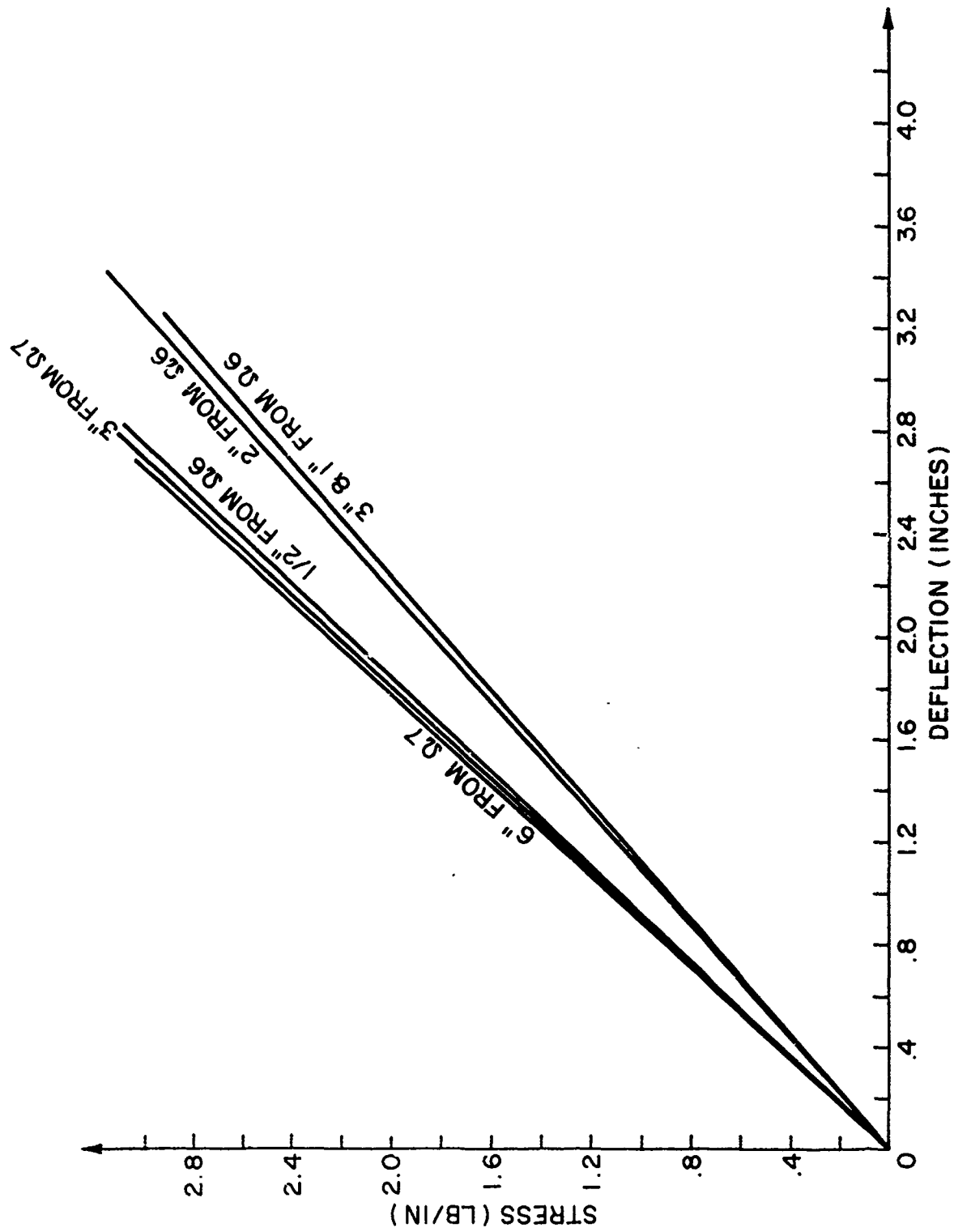


Figure A-5. One and One-Half (1 1/2) Plates at Varying Locations.

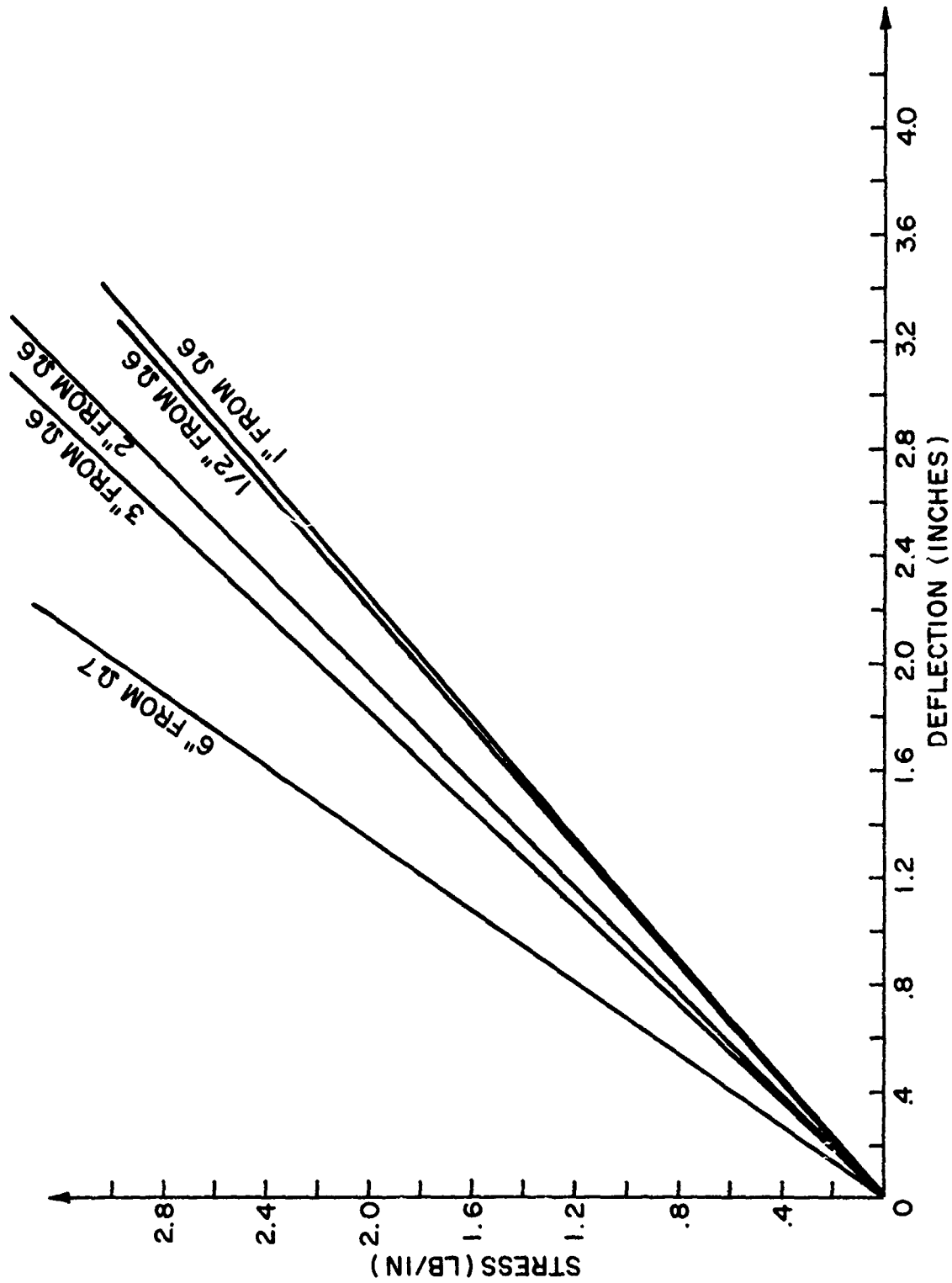


Figure A-6. One (1) Inch Plates at Varying Locations.

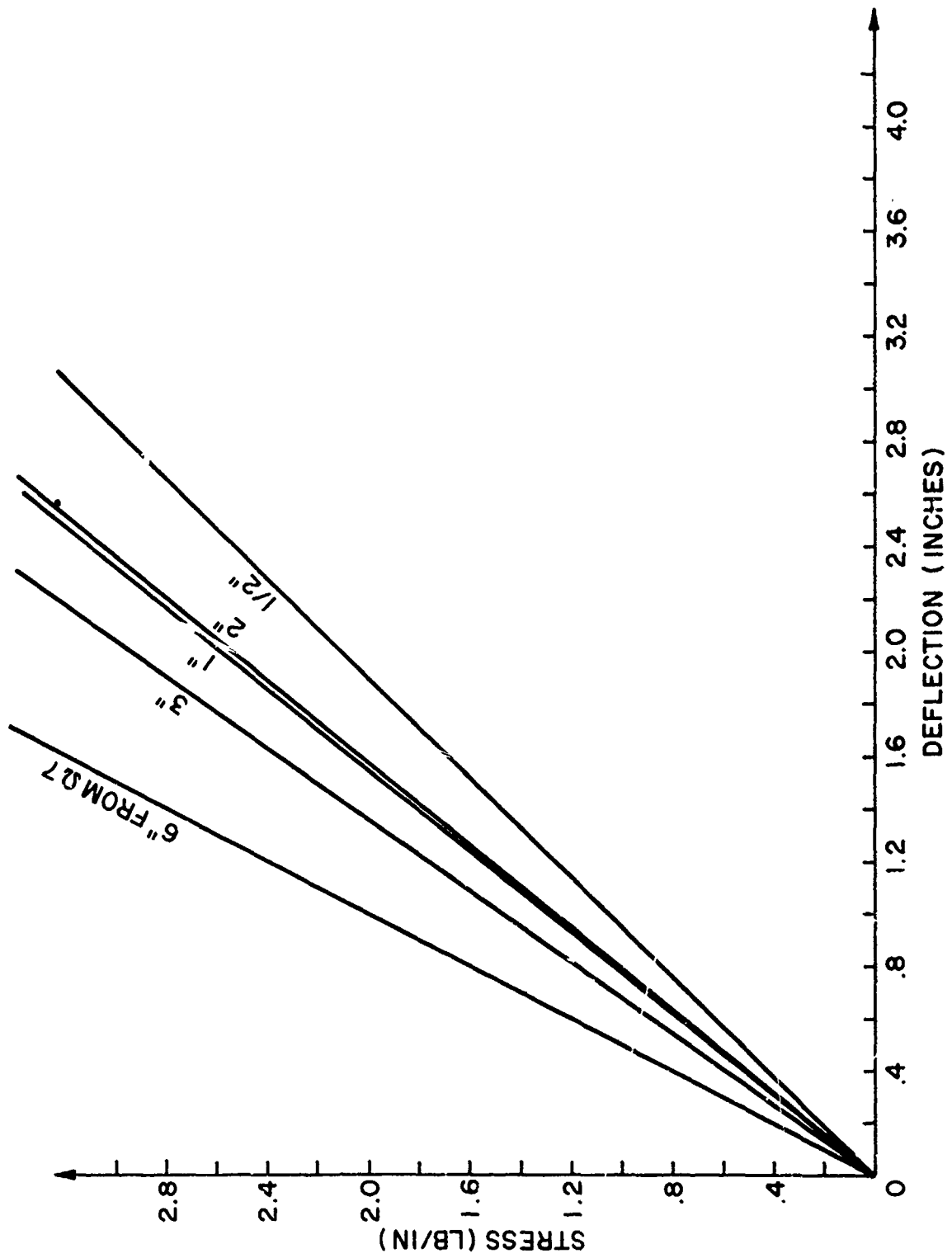


Figure A-7. One-Half (1/2) Inch Plates at Varying Locations.

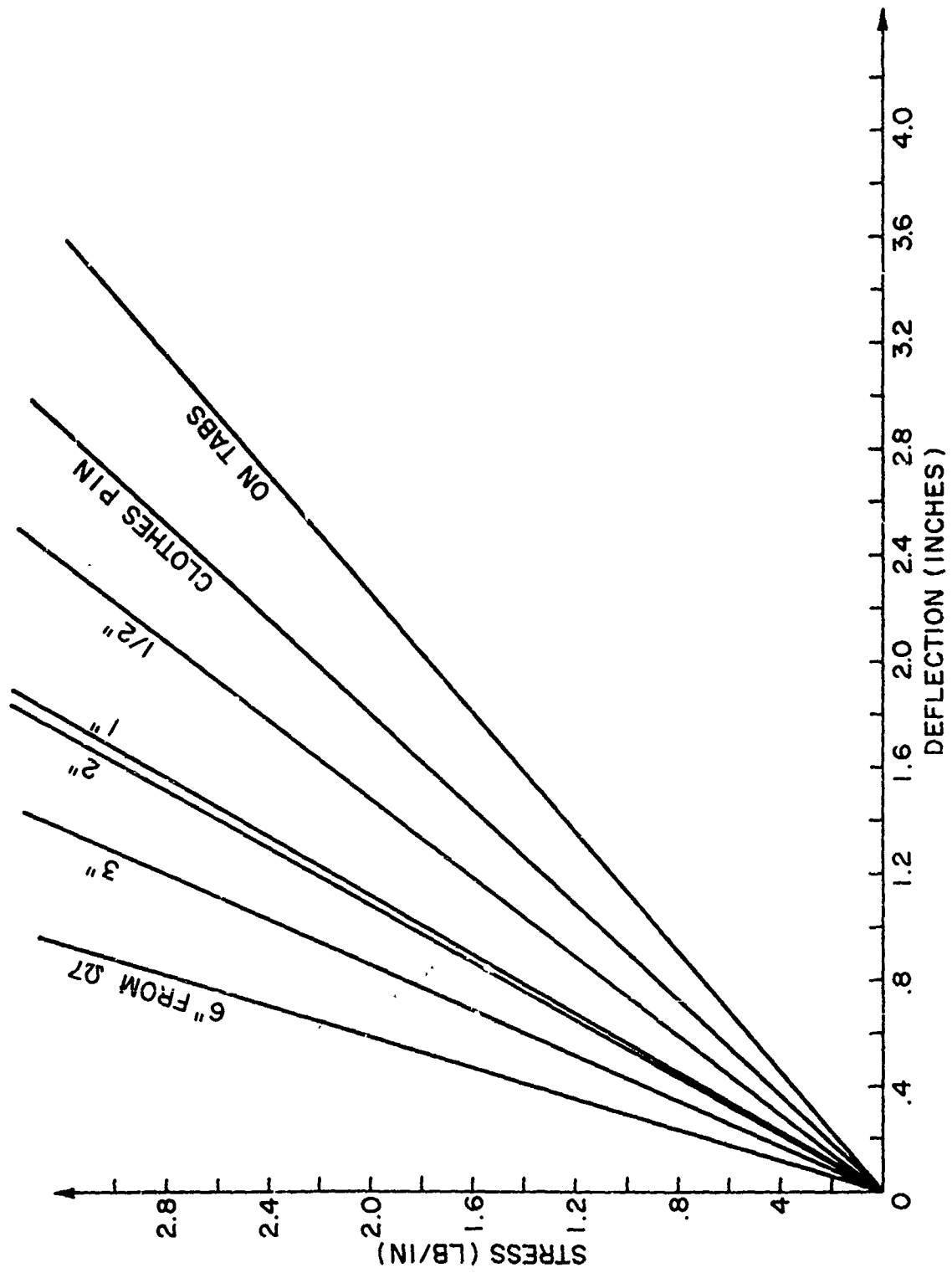


Figure A-8. One Fourth (1/4) Inch Plates at Varying Locations.

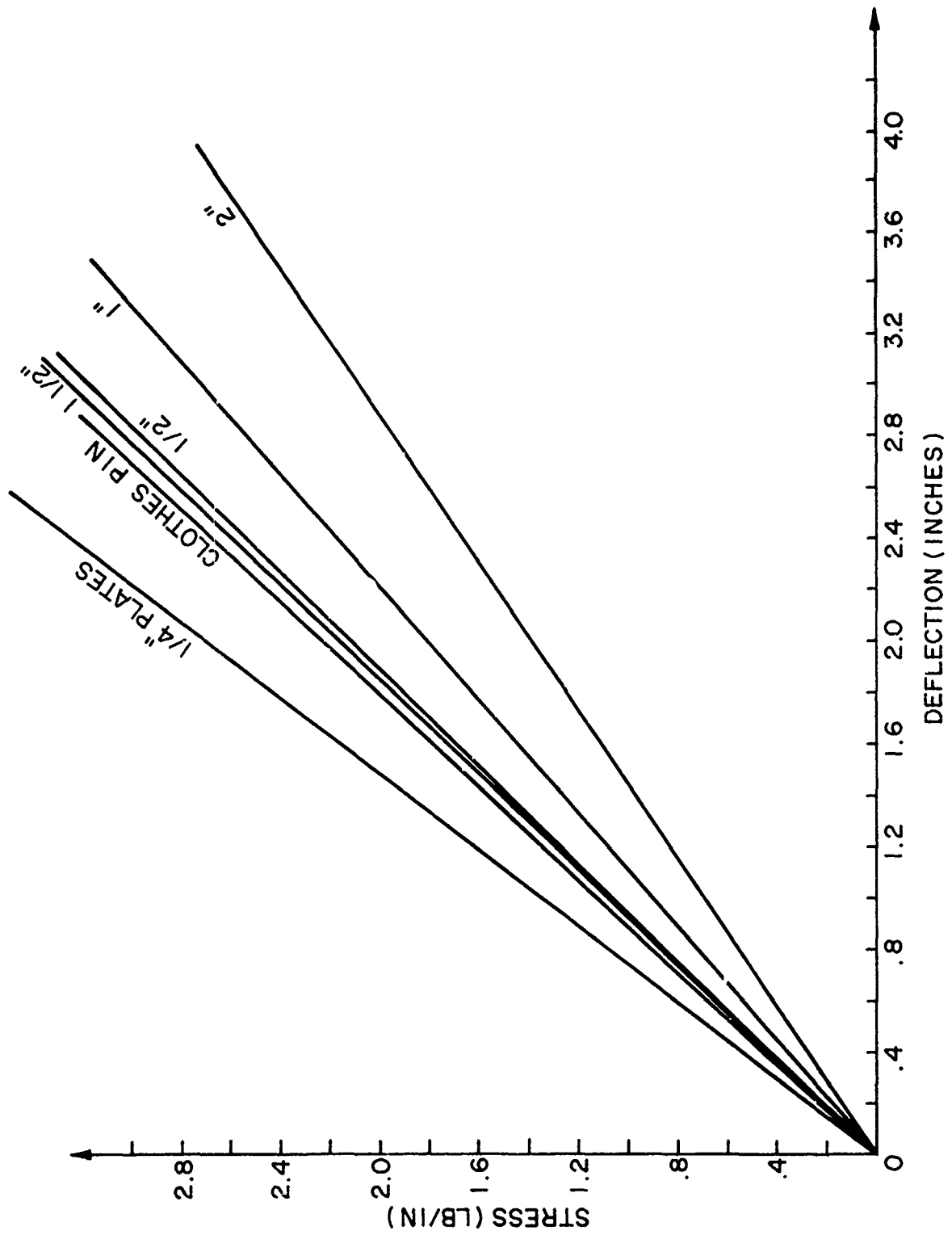


Figure A-9. Varying Plate Widths Placed One-Half (1/2) Inches from Sensor.

## TEST ARTICLES

### A. OMEGA SENSOR

The design of the Omega sensors used in these tests were described in the Test Articles Section.

### B. NYLON CLOTH STRIP SPECIMEN

The investigation was performed on a 2.5-inch wide by 12-inch long raveled strip specimen of MIL-C-7020, Type I, 1.1 oz/yd<sup>2</sup> rip-stop nylon cloth, the same type of cloth used in the fabrication of the model ringslot parachute canopy.



## GRIPS

To ensure a uniform load distribution which is applied to the cloth specimen, the cloth grips were half coated with rubber. The cloth was sandwiched between the rubber section of two plates and clamped together by a screw which was inserted through the cloth and both plates. A small hole had to be burned through the cloth to allow the screw to pass through it. When tightened, this proved to give a very sturdy hold on the cloth.

A plate adaptor was inserted between the upper portion of the two plates holding the cloth and used to hand the various weights from.

Therefore, the stress applied to the cloth strip is actually the total load of the 2 plates, 2 screws, 2 nuts, 2 plate adaptors, and the particular applied weight divided by the width of the grips.

## INSTRUMENTATION

The cloth strip was suspended from a 40-lb capacity bending link which measured the force created by the applied load to the specimen.

The wiring diagram of the test arrangement recording instruments is shown in Figure 11.

## RESULTS

Analyzing these diagrams, three general statements may be made:

1. The reproducibility of the two measurements made at any one test condition was relatively good. This applies in particular to the test points measured after the initial load had been applied. The little deviations that did occur were attributed to the stretching of the nylon material; this was not significant and therefore neglected.

2. The comparison of the two tests conducted with different Omega sensors, but tested at the same test condition was relatively good. Therefore, since no significant deviation occurred, the results of only one measurement for each clamp width is included in this report.

3. As the diagrams illustrate, the larger the clamps and also the closer the clamps were to the sensor the more sensitive the Omega sensor.

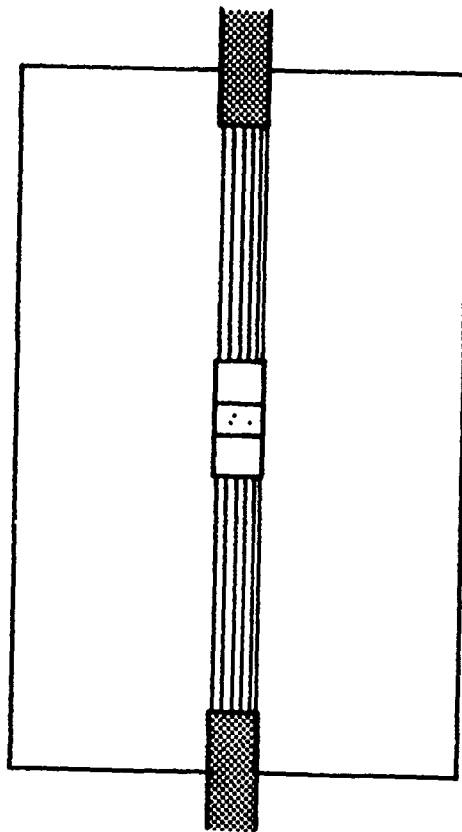
These results are demonstrated in particular in Figures 8 and 9. In Figure 8 (3-inches from Omega sensor) the varying clamps are located three-inches from the Omega sensor. It is shown that at a particular applied stress of 2.0 lb/in that the smaller clamp (1/4-inch in width) produces 0.86-inches of deflection where the largest clamps (2-inches in width) measures 2.69-inches of deflection, which is a considerable difference. Notice the order of increasing sensitivity of the sensor from the smallest clamps to the largest clamps.

Figure 9 (1/4-inch clamps) indicates the relationship of sensor

sensitivity to the location of the applied load. In this case, the 1/4-inch clamps were tested at various locations on the cloth specimen. Once again, when examining a particular applied stress, it is shown that the further away from the sensor, the lower the deflection measured. Therefore, the sensor is more sensitive the closer the load is applied to the sensor.

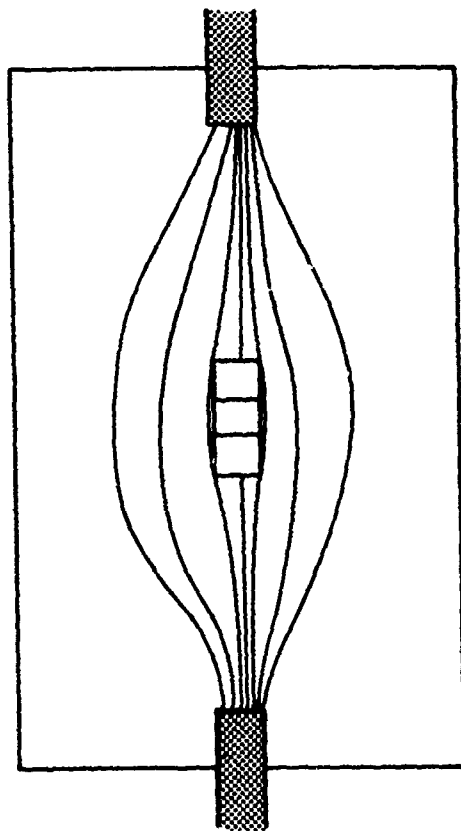
As the figures show, the results of the two (2)-inch clamps, located six (6)-inches from the Omega sensor, agreed identically with the off the cloth calibrations where the loads were applied directly to the tabs of the sensor. This was due to the boundary restrictions of the cloth strip, reducing the spreading of stress and creating a uniform stress distribution throughout the cloth strip. The Omega sensor was then capable of measuring all of the stress that was applied. The same ideal situation should occur with the smaller clamps (Figure A-10); however, that was not the case. Instead the stress was shown spreading to the outer boundaries of the cloth strip allowing the cloth material to carry some of the applied stress, causing the sensor to measure a smaller stress magnitude (Figure A-11).

It was also observed that the closer the two (2)-inch clamps were located relative to the sensor the greater the sensitivity. On occasion, more stress was indicated than had been applied. It was also noted that two (2)-inch clamps induce uniform load distribution in the cloth sample and the Omega sensor carries a higher percentage of the load when the cloth is uniformly loaded. However,



IDEAL STRESS  
DISTRIBUTION

Figure A-10.



ACTUAL STRESS  
DISTRIBUTION

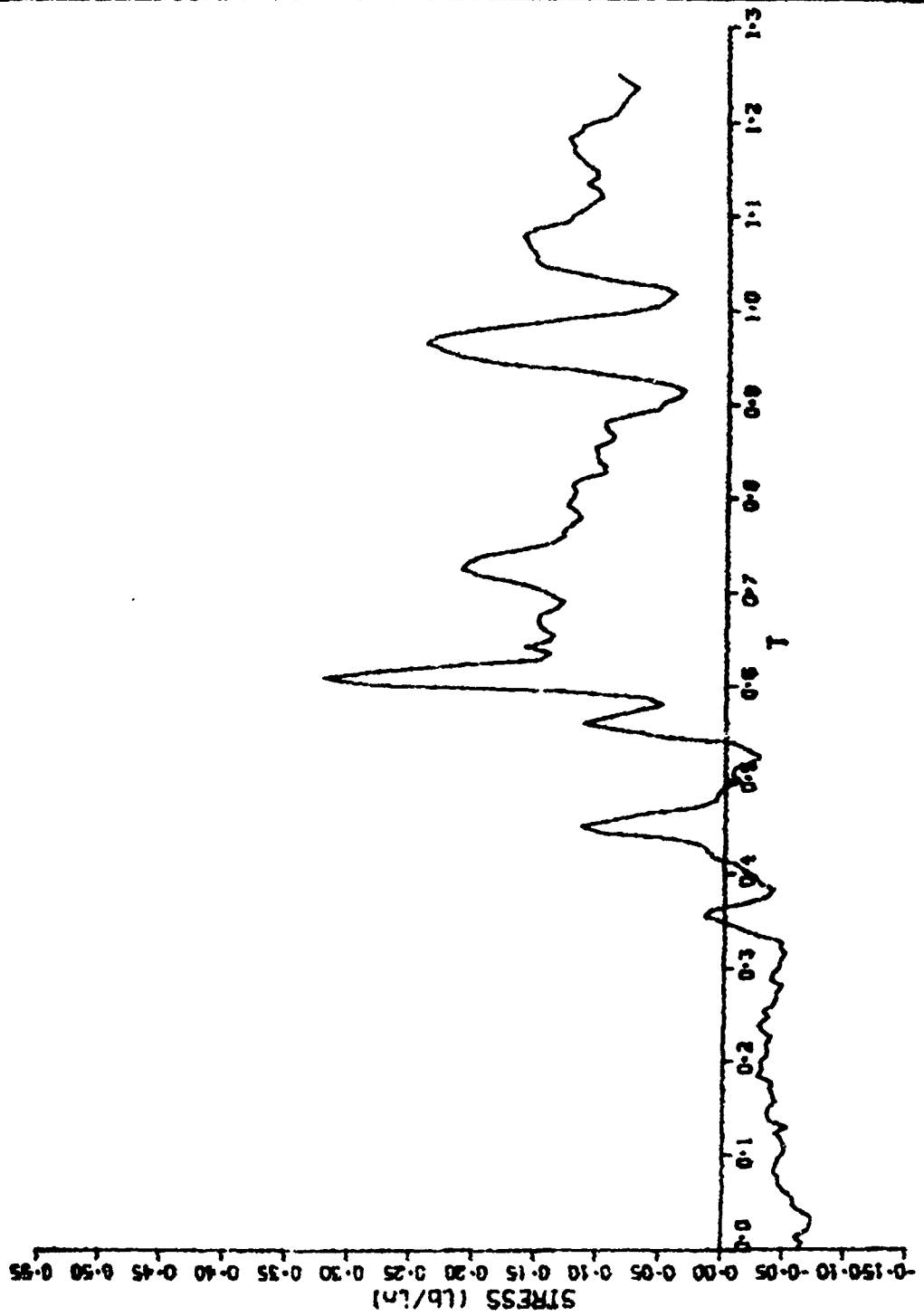
Figure A-11.

it is not understood at present why the sensor should indicate more stress than applied. Possibly, more tests and studies are required for adequate understanding and explanation.

APPENDIX B

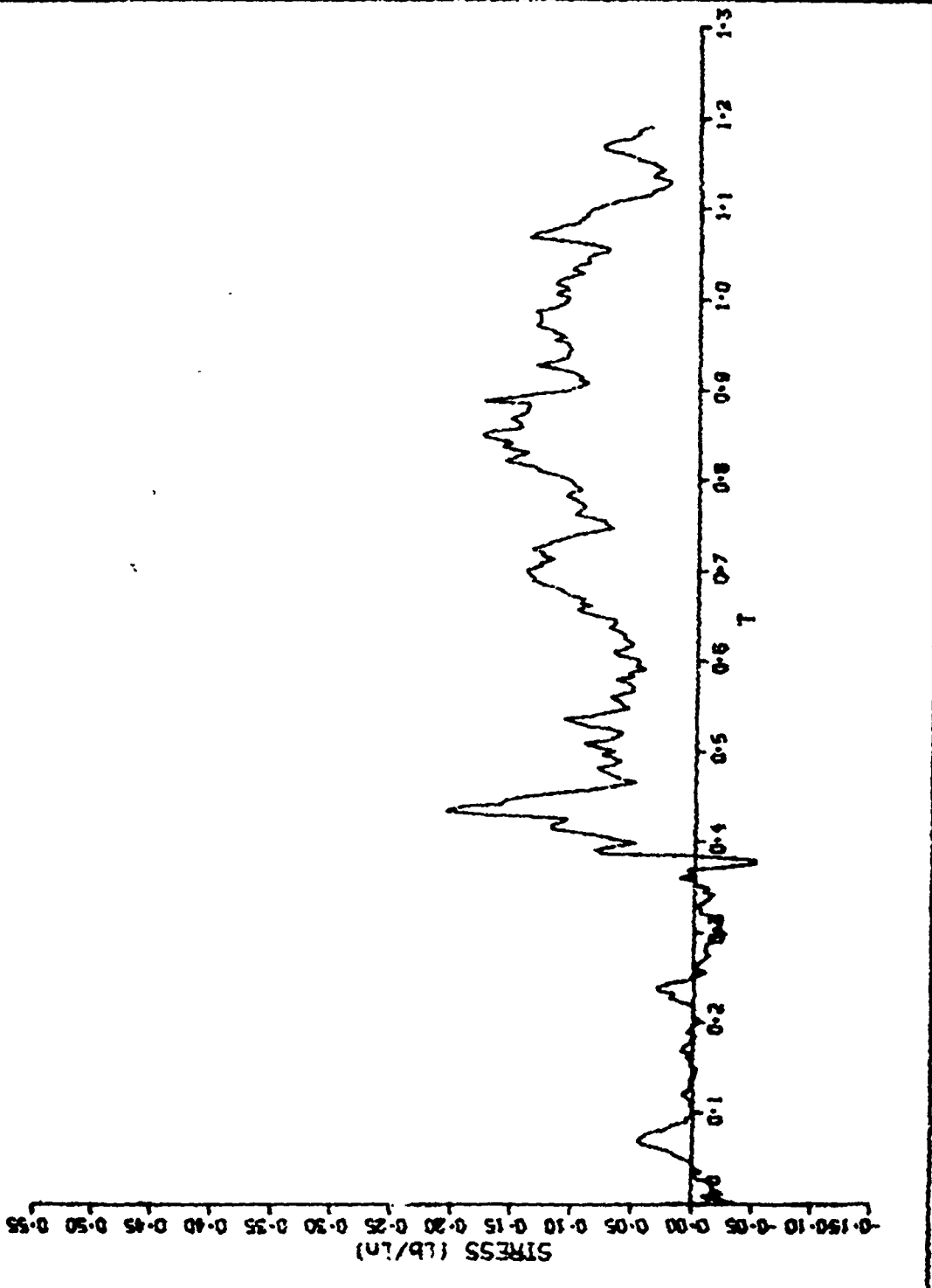
STRESS VS NON-DIMENSIONAL TIME

TEST NO. 4 SENSOR IRS - VENT 0- .4 (in H2O)

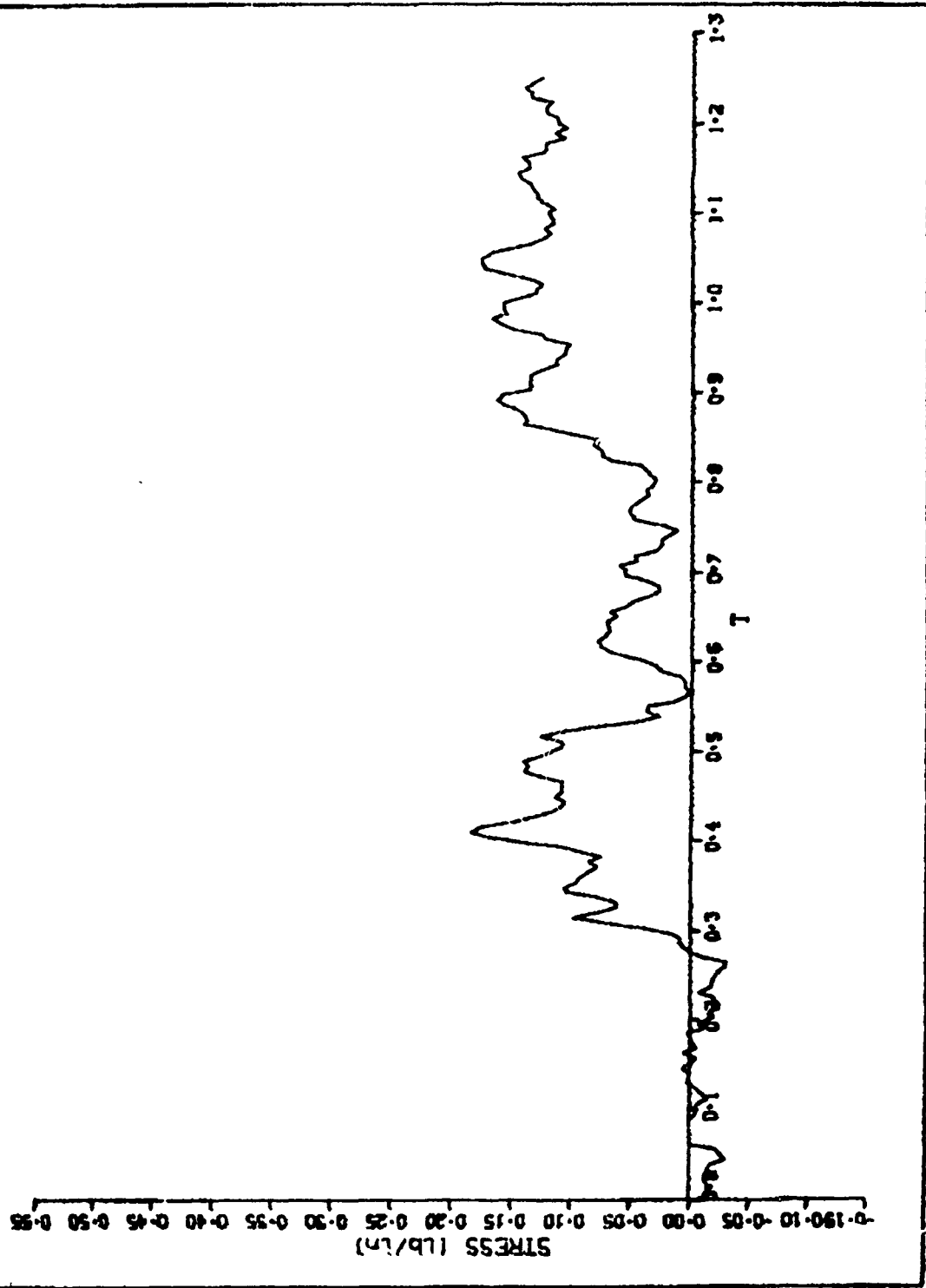




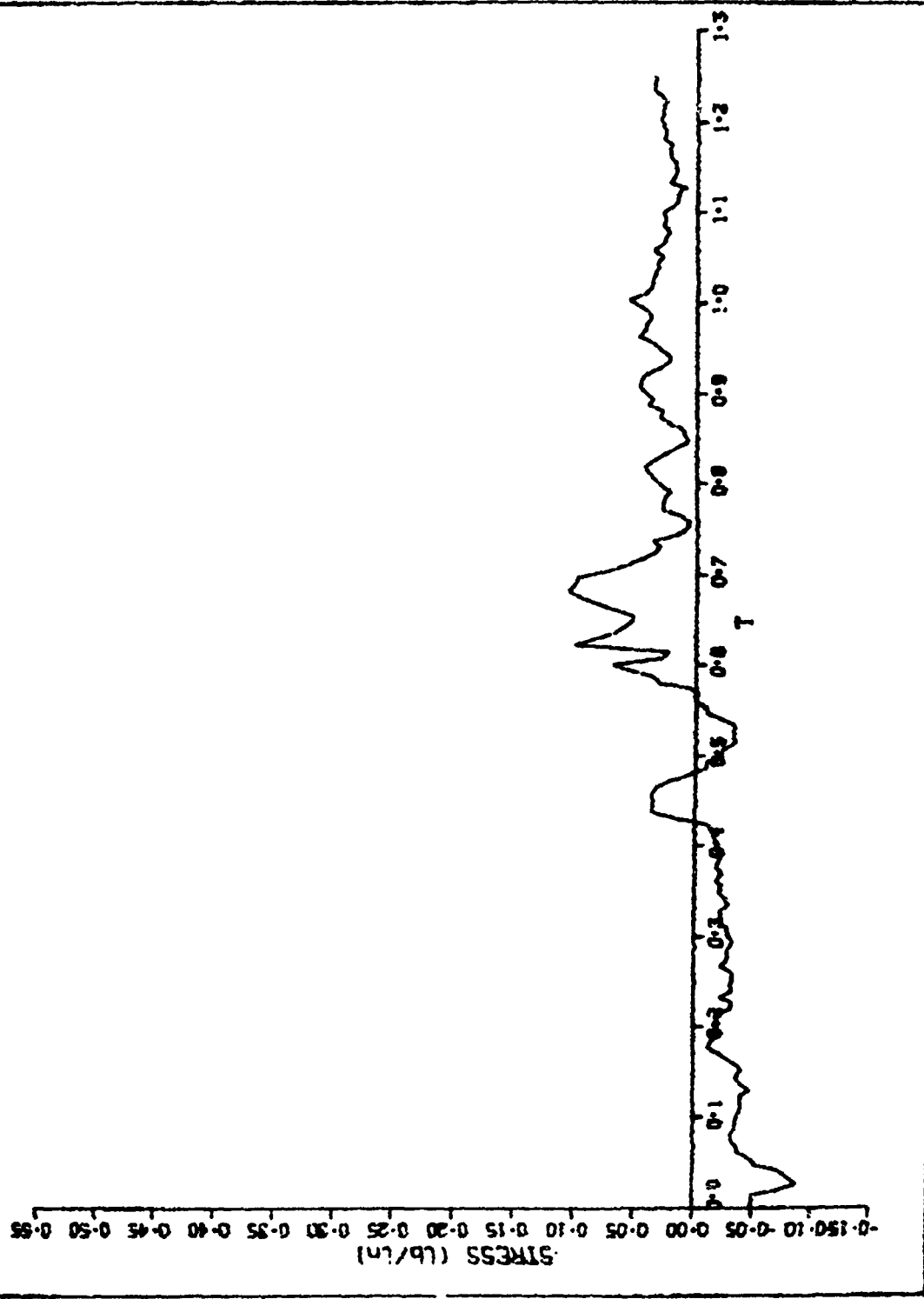
TEST NO. 5 SENSOR IRS - VENT 0- .4 (Ln H20)



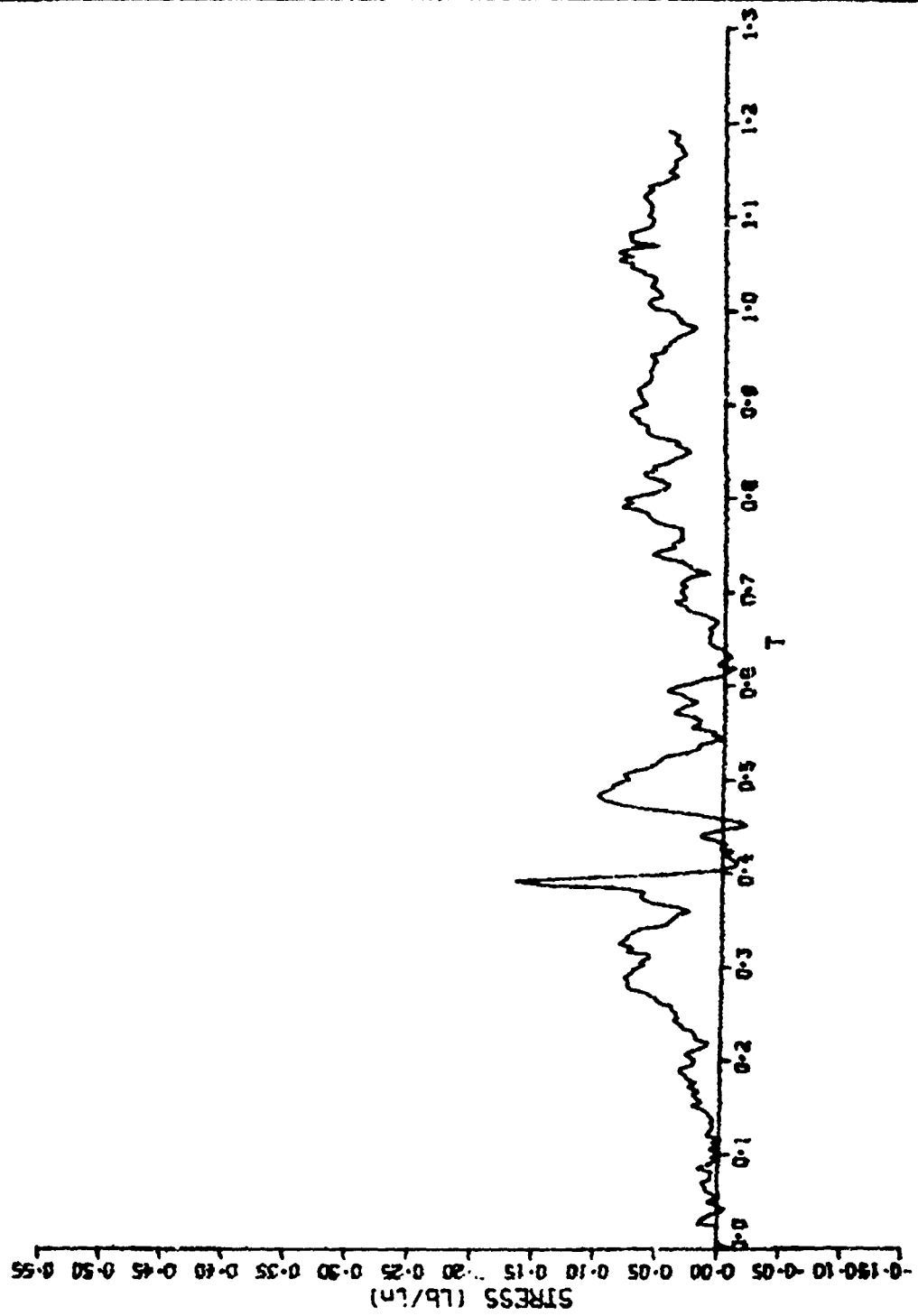
TEST NO. 6 SENSOR IRS - VENT 0- .4 (in H2O)



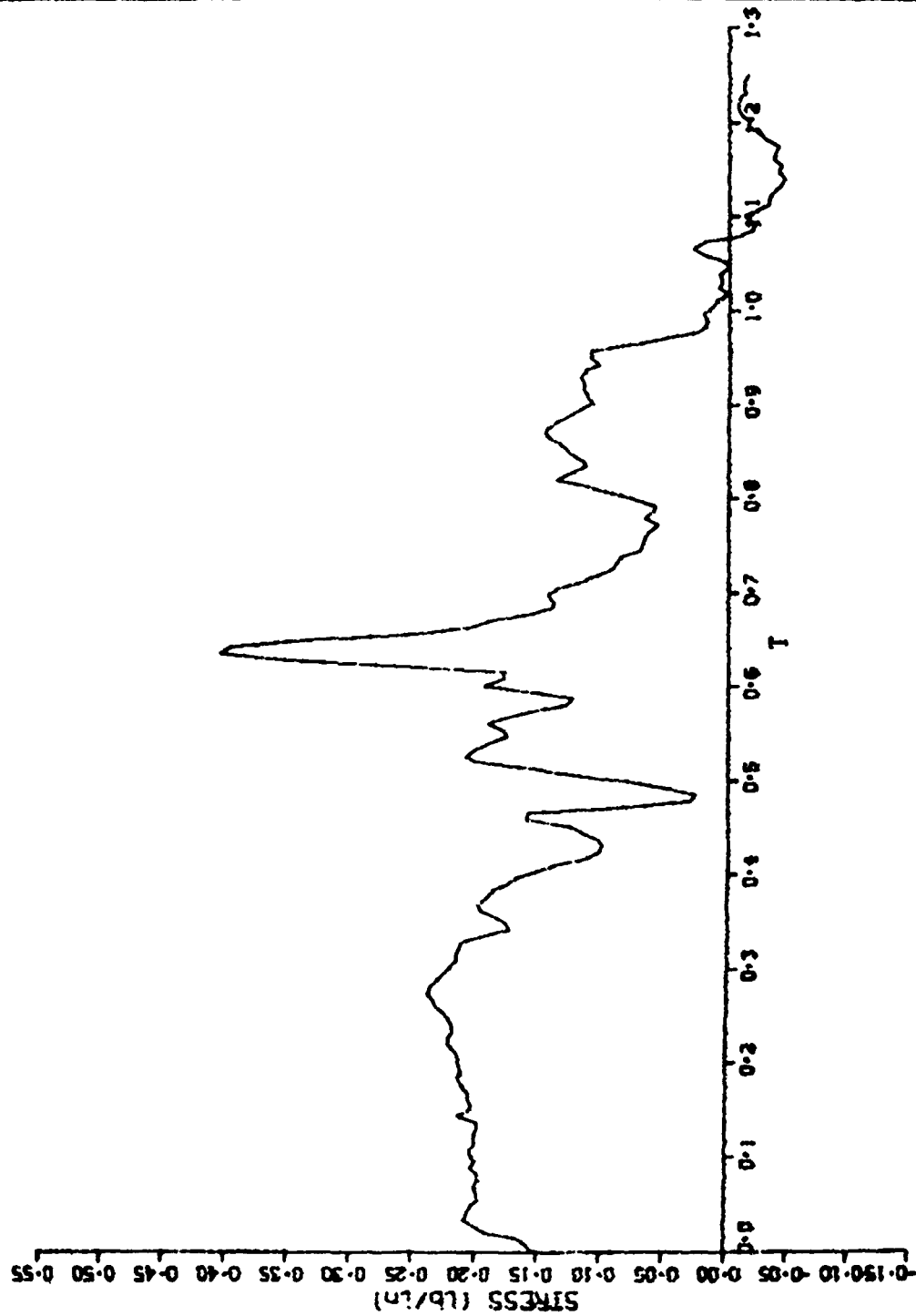
TEST NO. 4 SENSOR 2RS 0- .4 (in H2O)



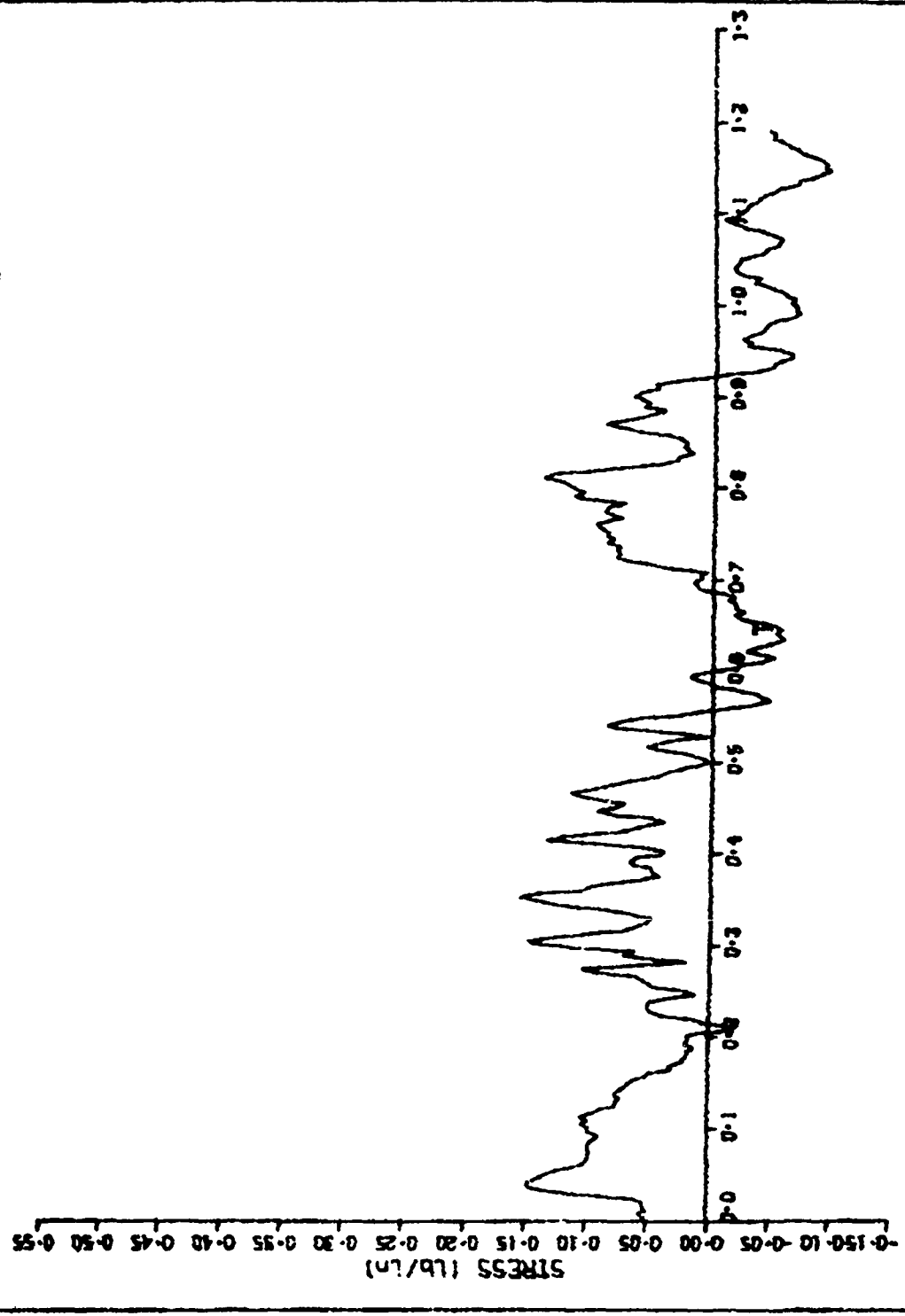
TEST NO. 5 SENSOR 2RS 0- .4(in H20)



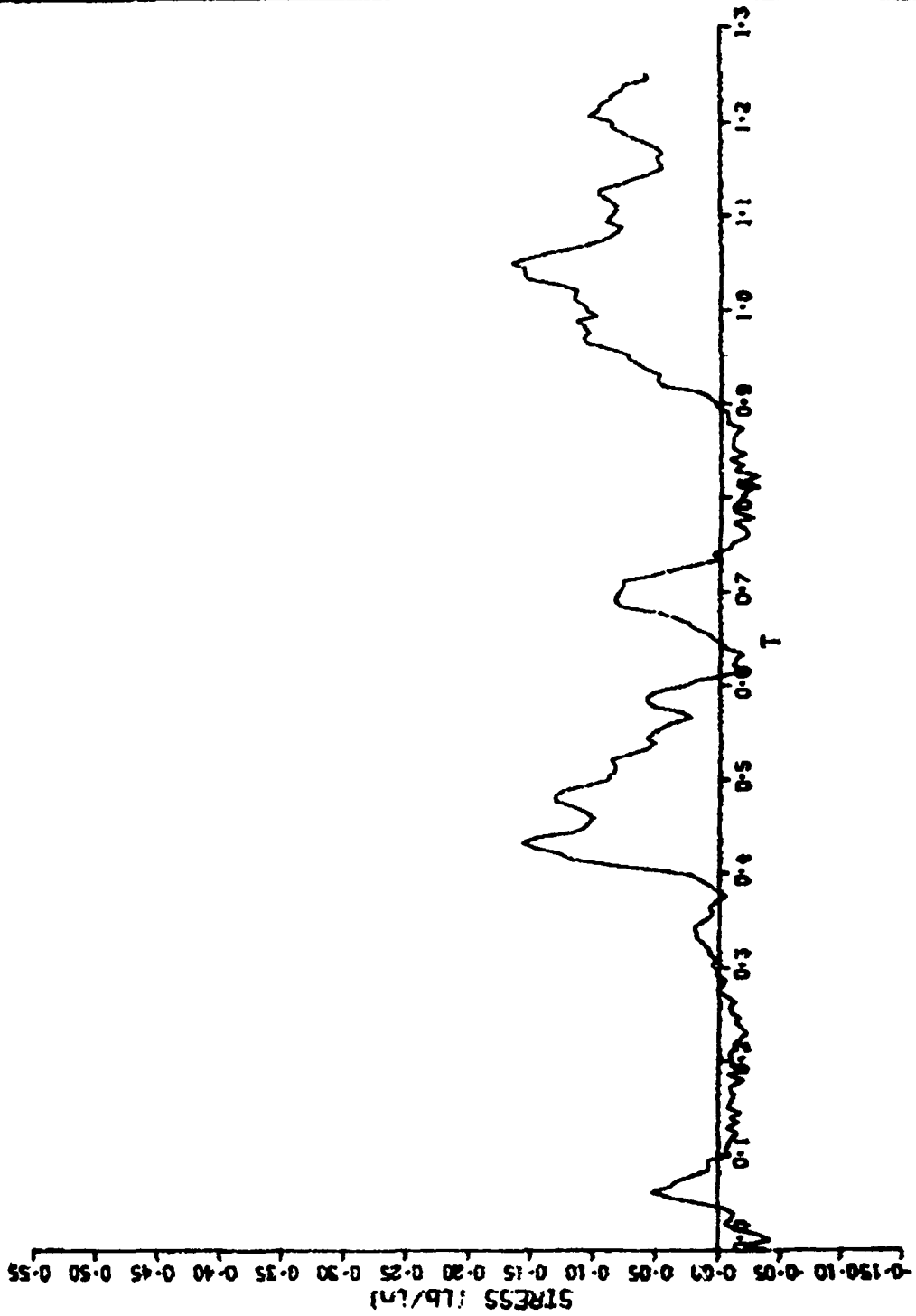
TEST NO. 4 SENSOR 3RS 0-.4(in H2O)



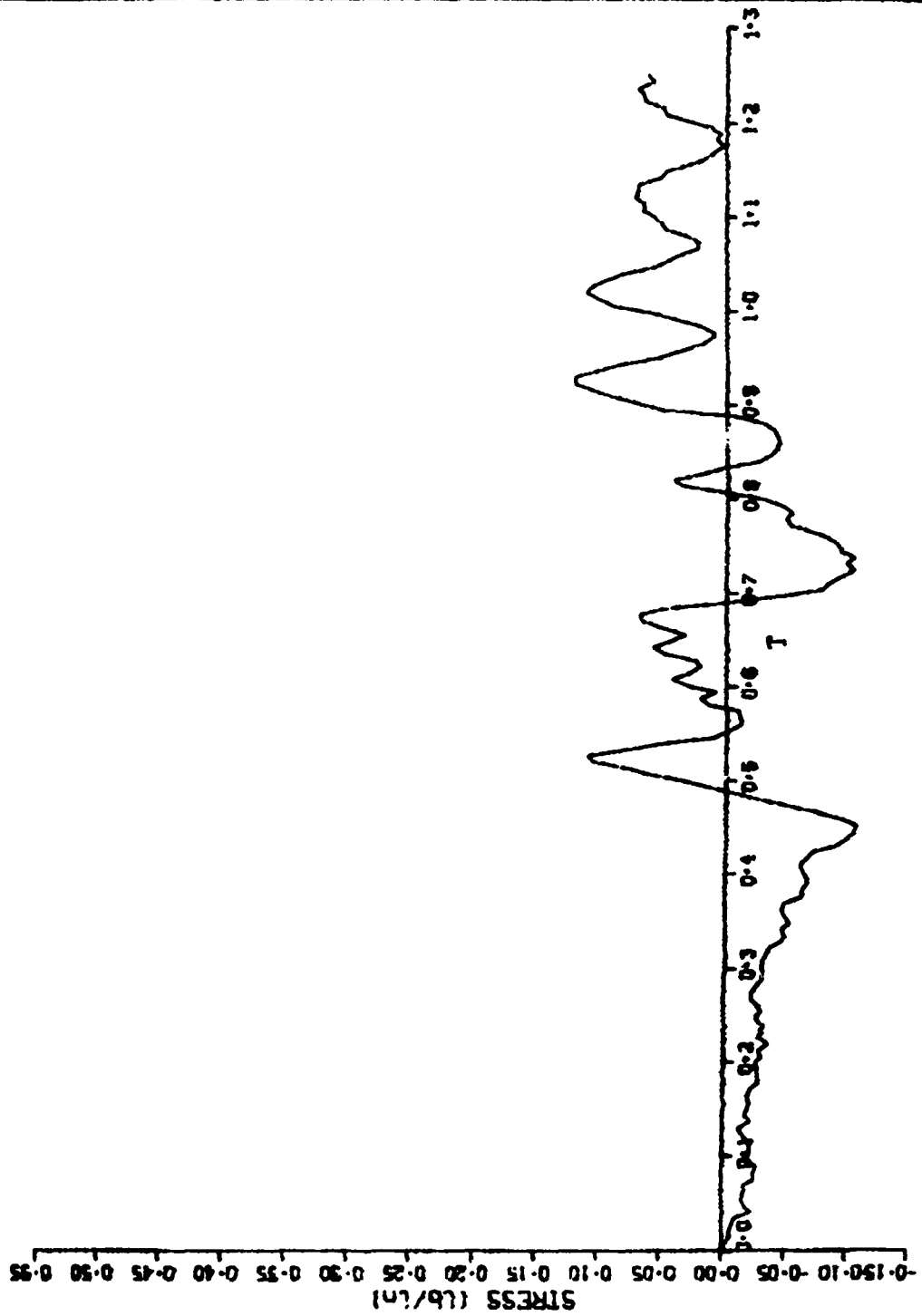
TEST NO. 5 SENSOR 3RS 0- .4 (ln H2O)



TEST NO. 6 SENSOR 3RS 0- .4 (in H2O)

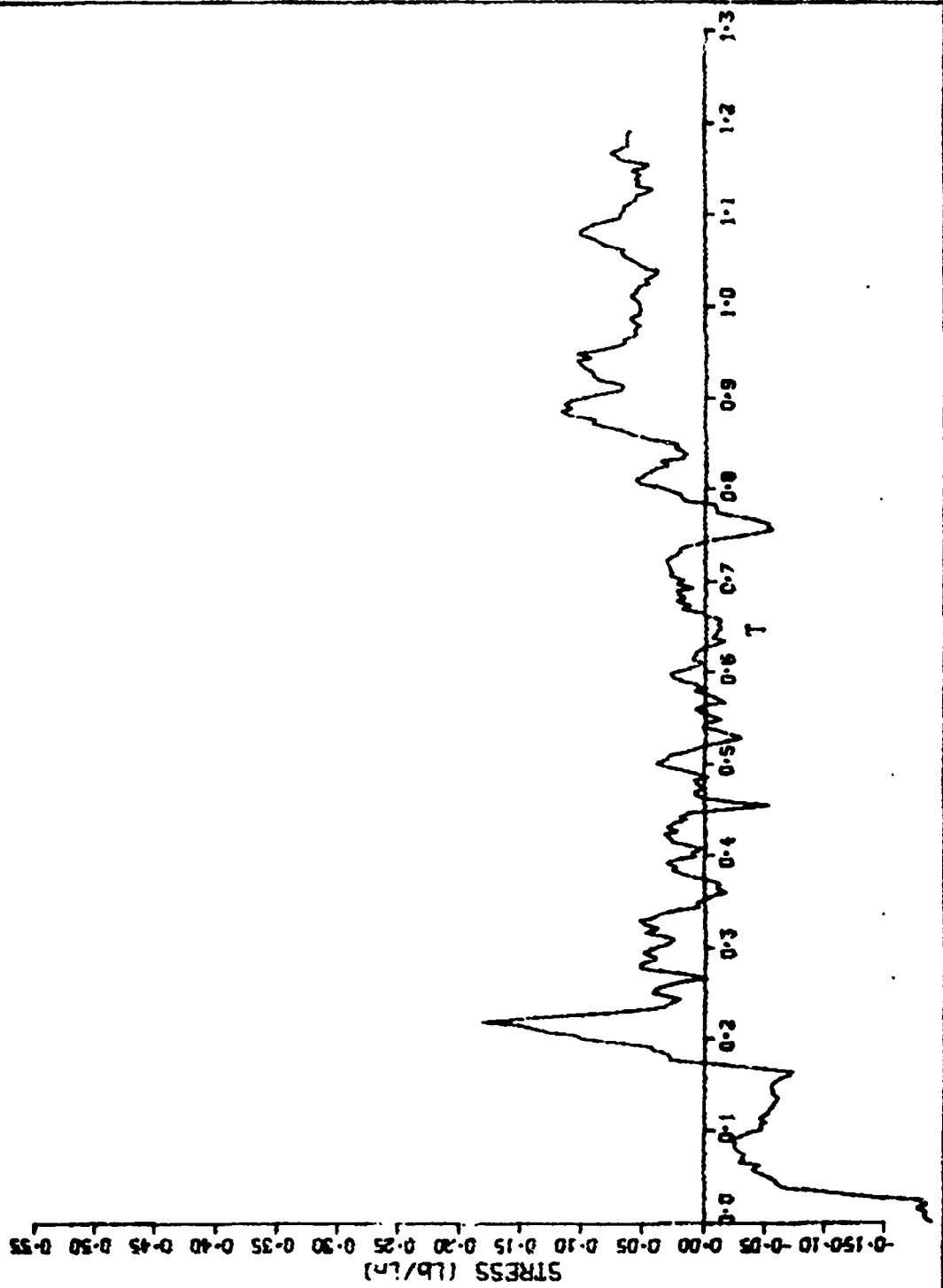


TEST NO. 4 SENSOR 4RS 0- .4 (in H2O)

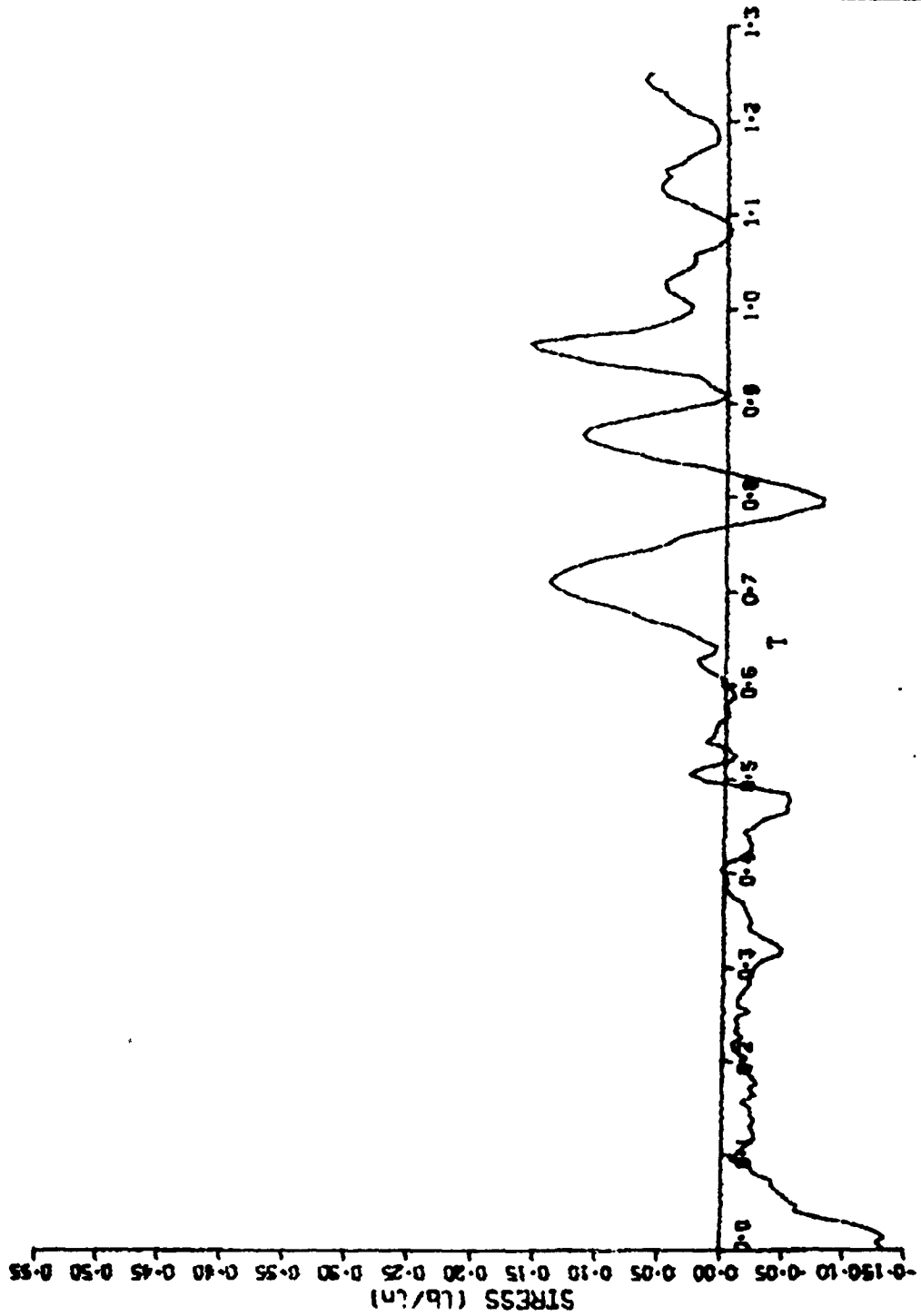




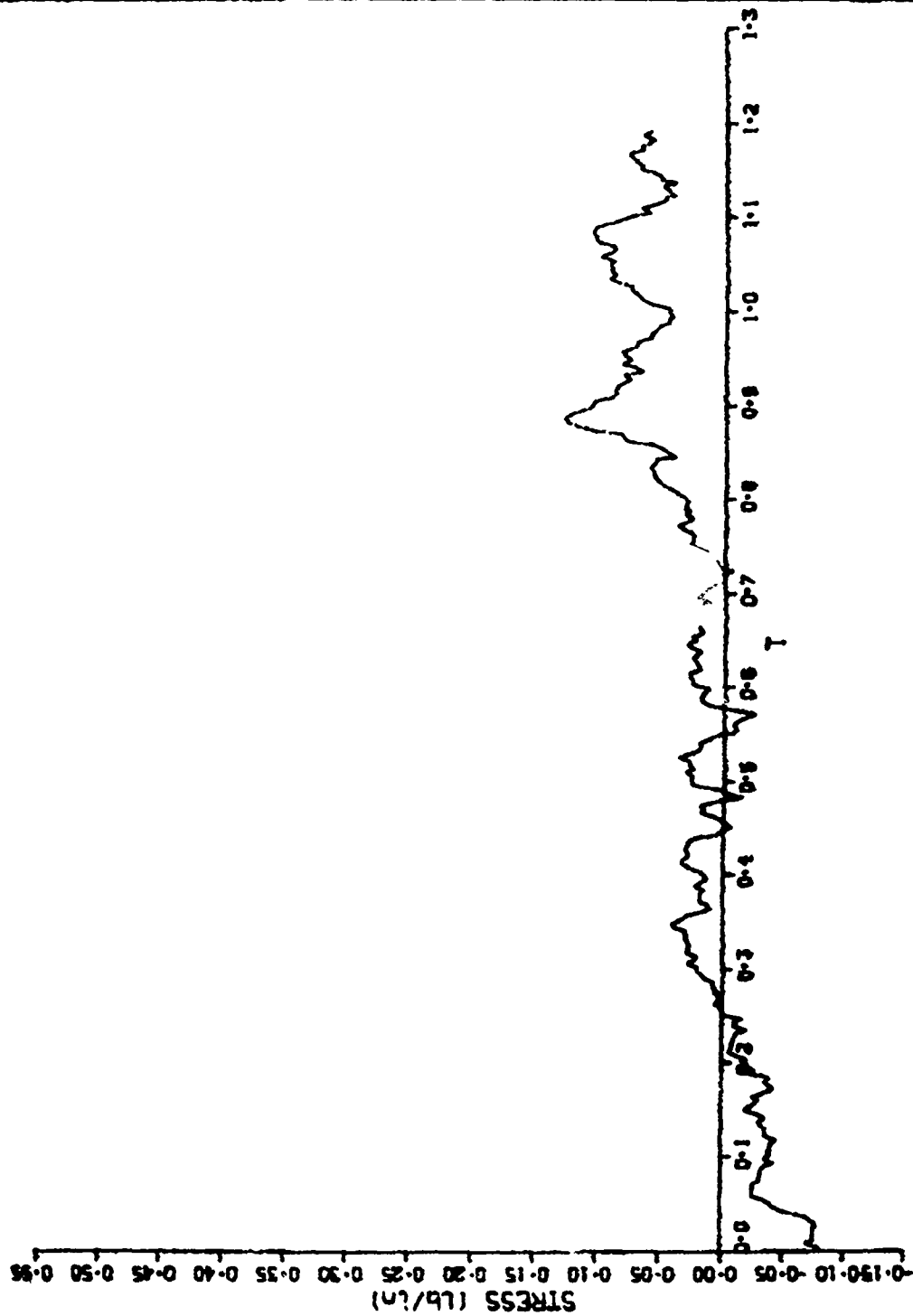
TEST NO. 5 SENSOR 4RS 0- .4 (in H2O)



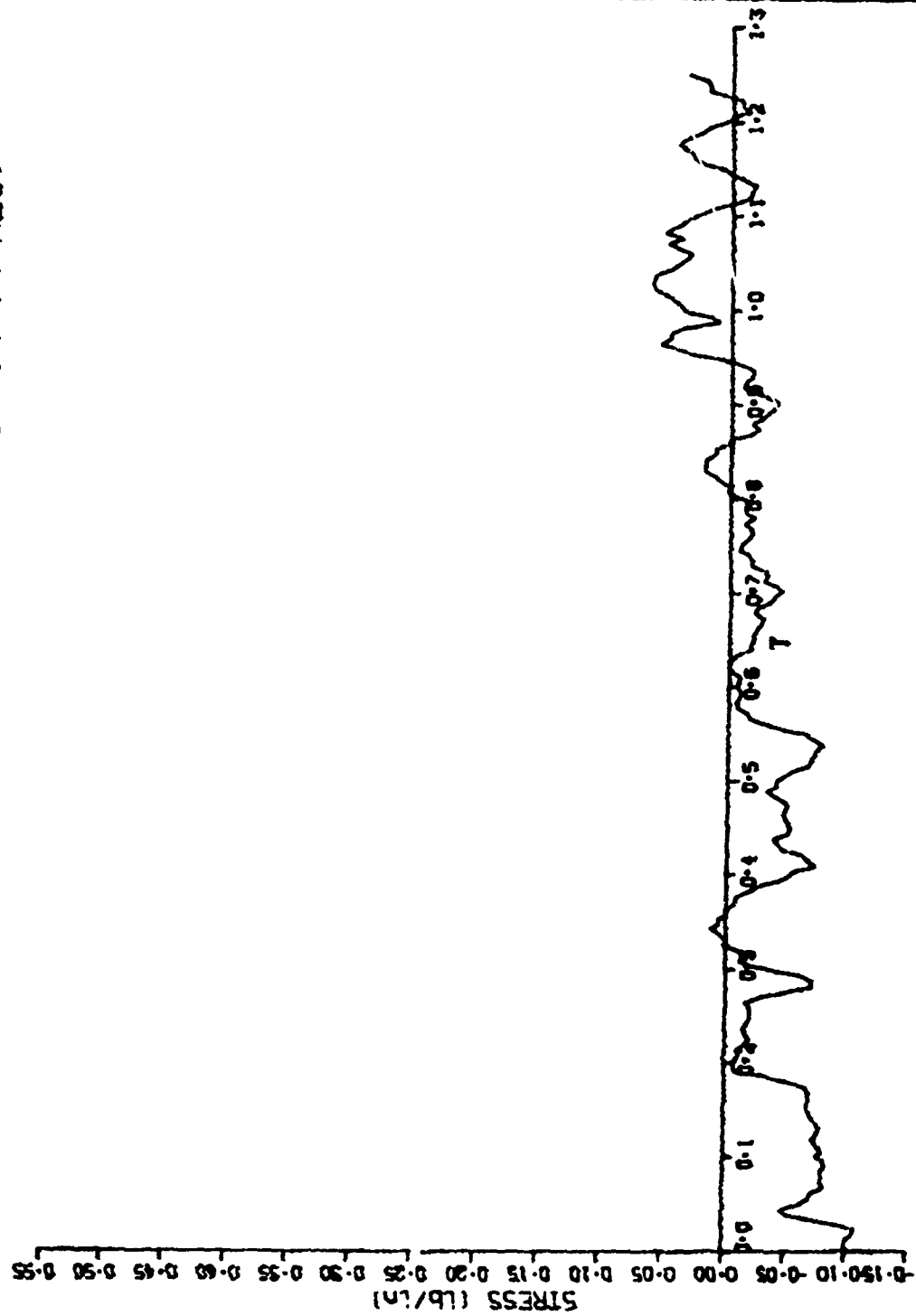
TEST NO. 4 SENSOR SRS - SKIRT 0- .4 (in H20)



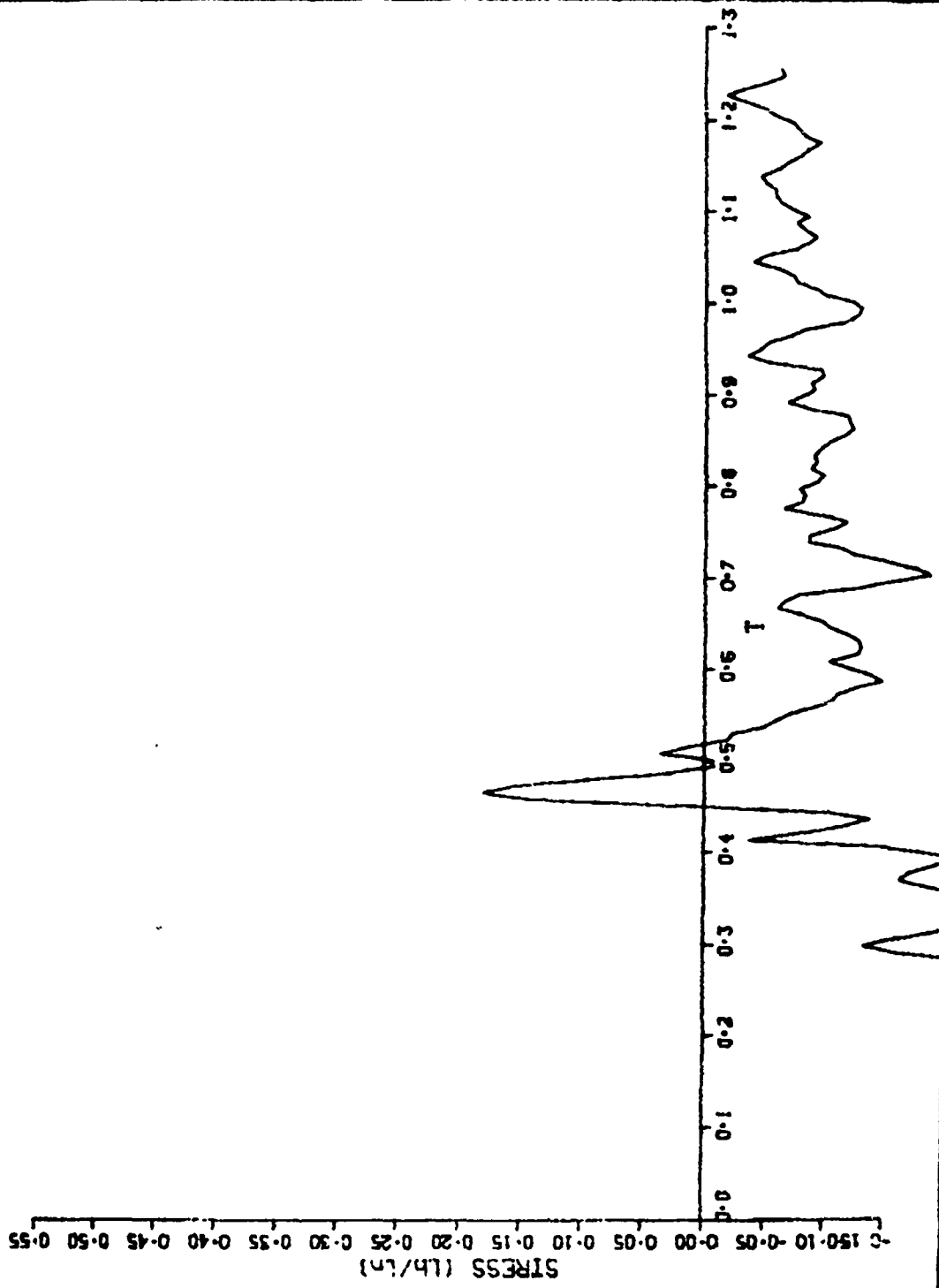
TEST NO. 5 SENSOR SRS - SKIRT 0- .4 (in H2O)



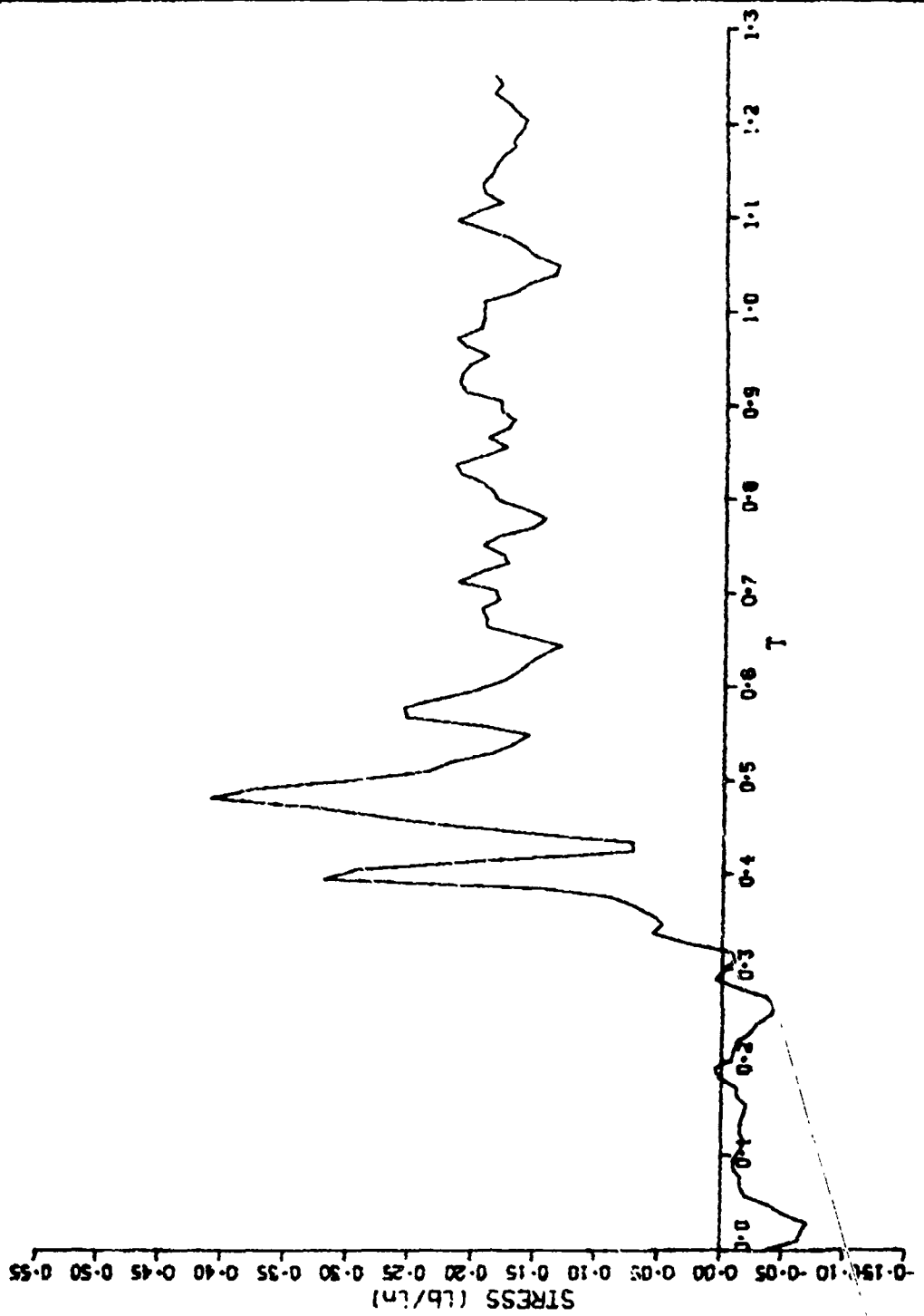
TEST NO. 6 SENSOR 5RS - SKIRT 0- .4 (in H20)



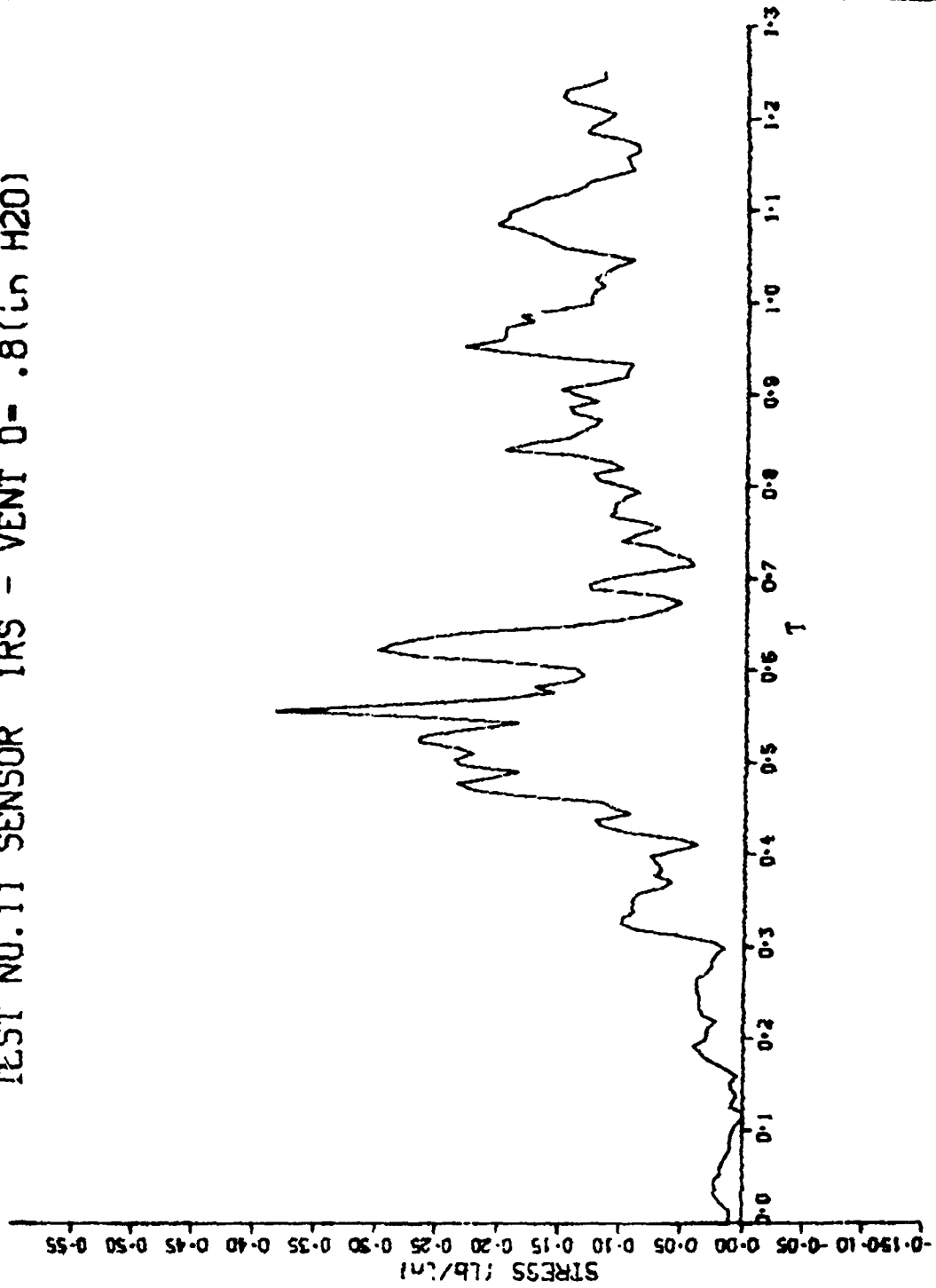
TEST NO. 7 SENSOR IRS - VENT 0- .8 (in H2O)



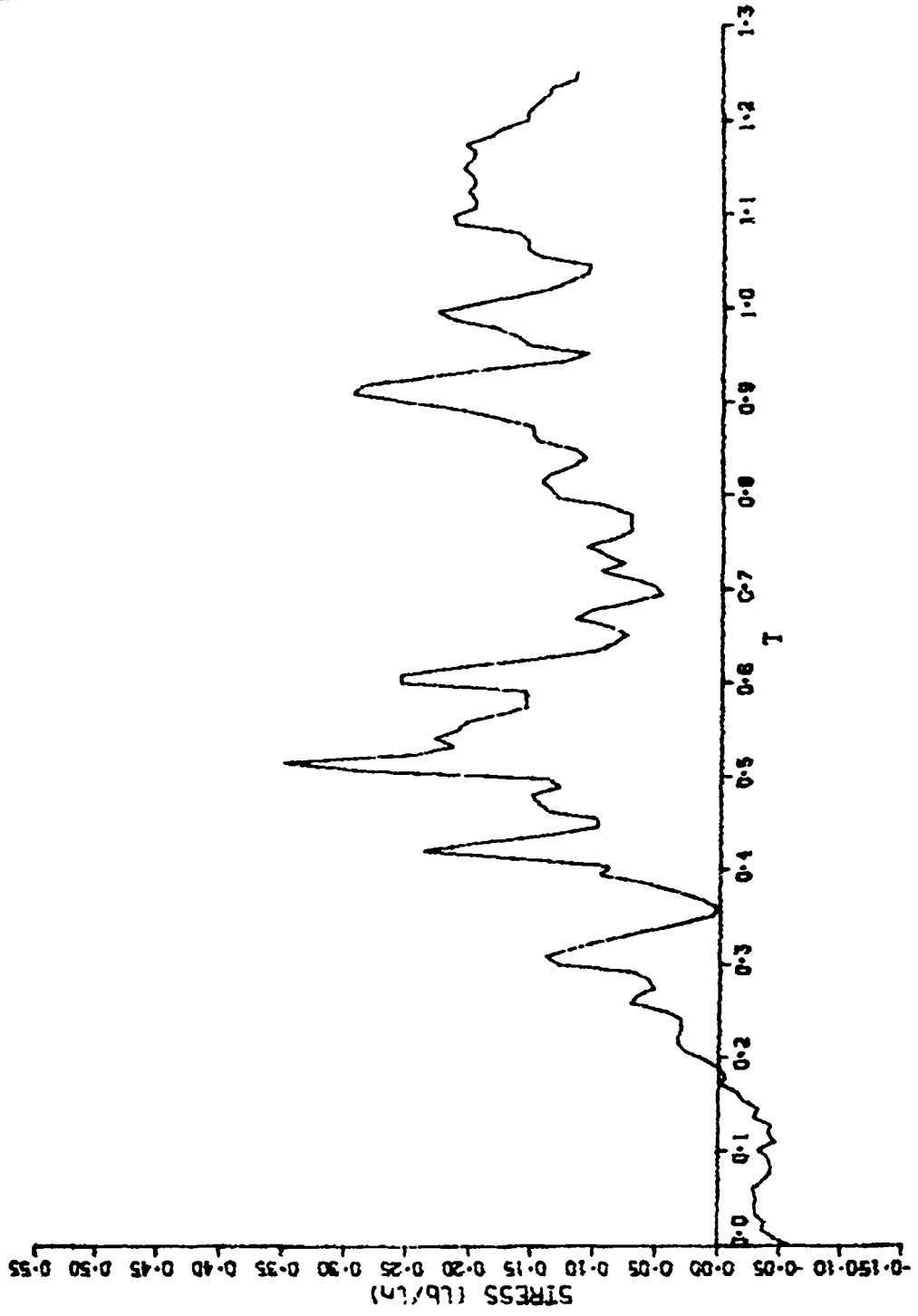
TEST NO. 9 SENSOR IRS - VENT 0- .8 (in H2O)



TEST NO.11 SENSOR IRS - VENT 0- .8 (in H2O)

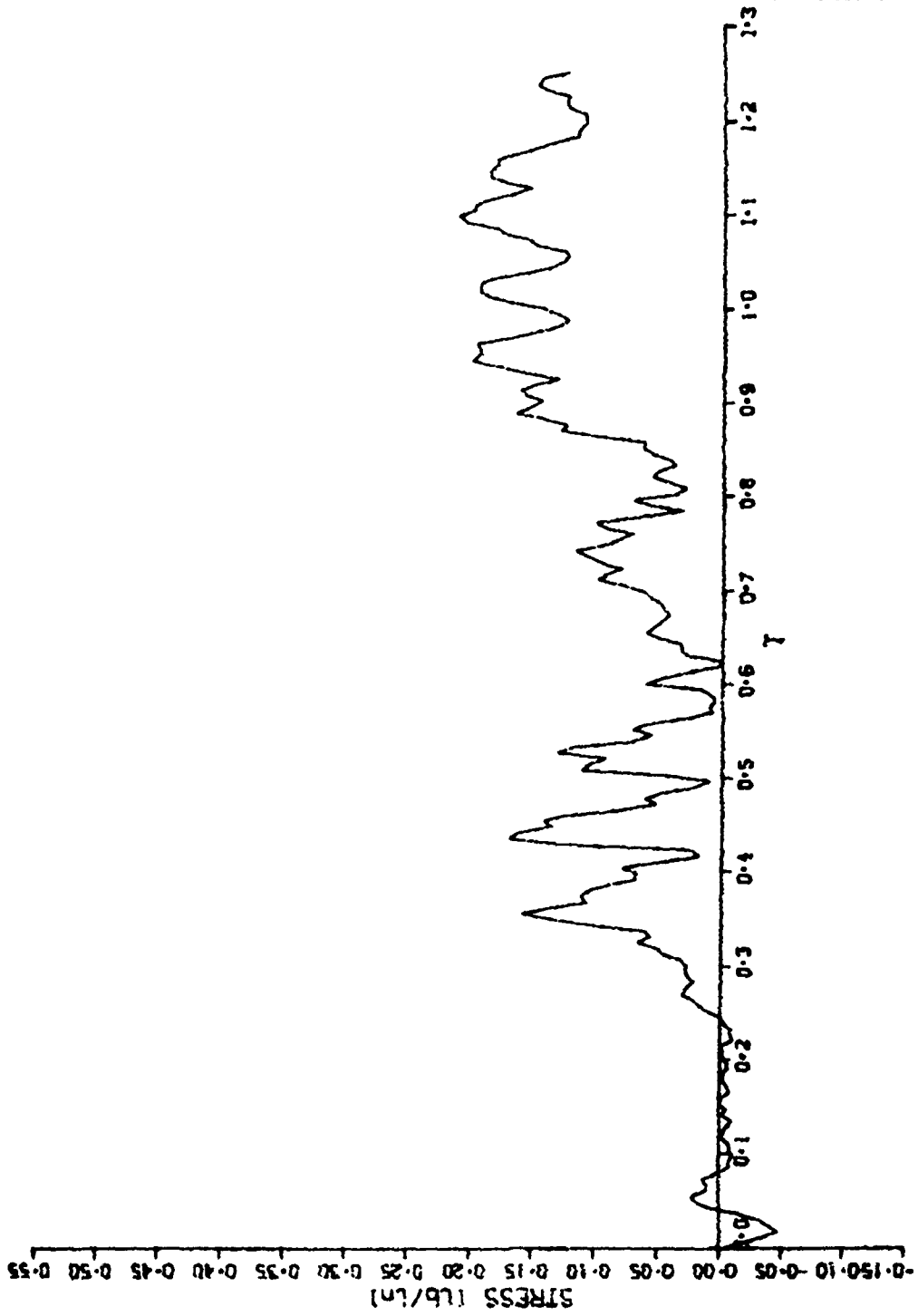


TEST NO.12 SENSOR IRS - VENT 0- .8 (in H2O)

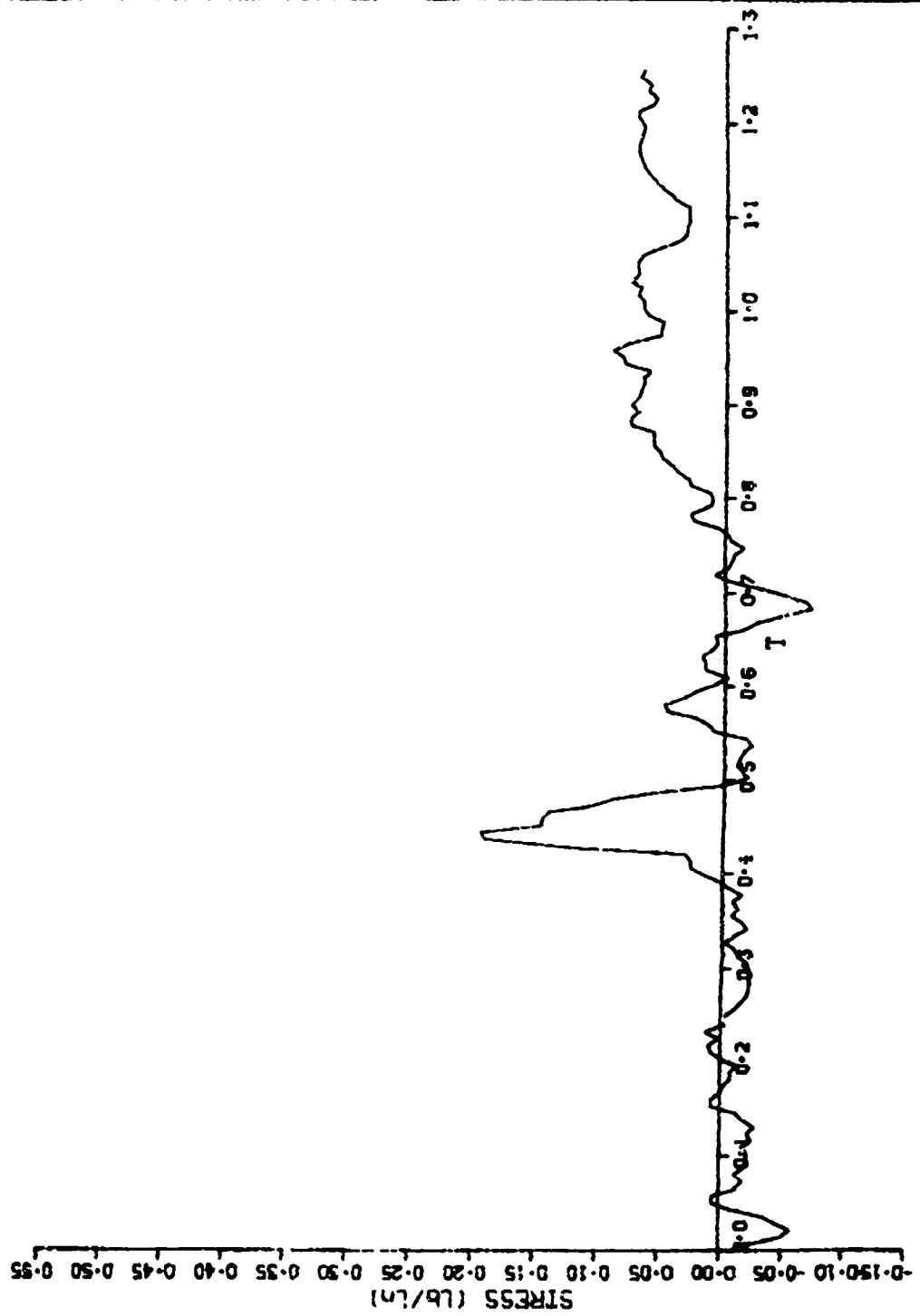




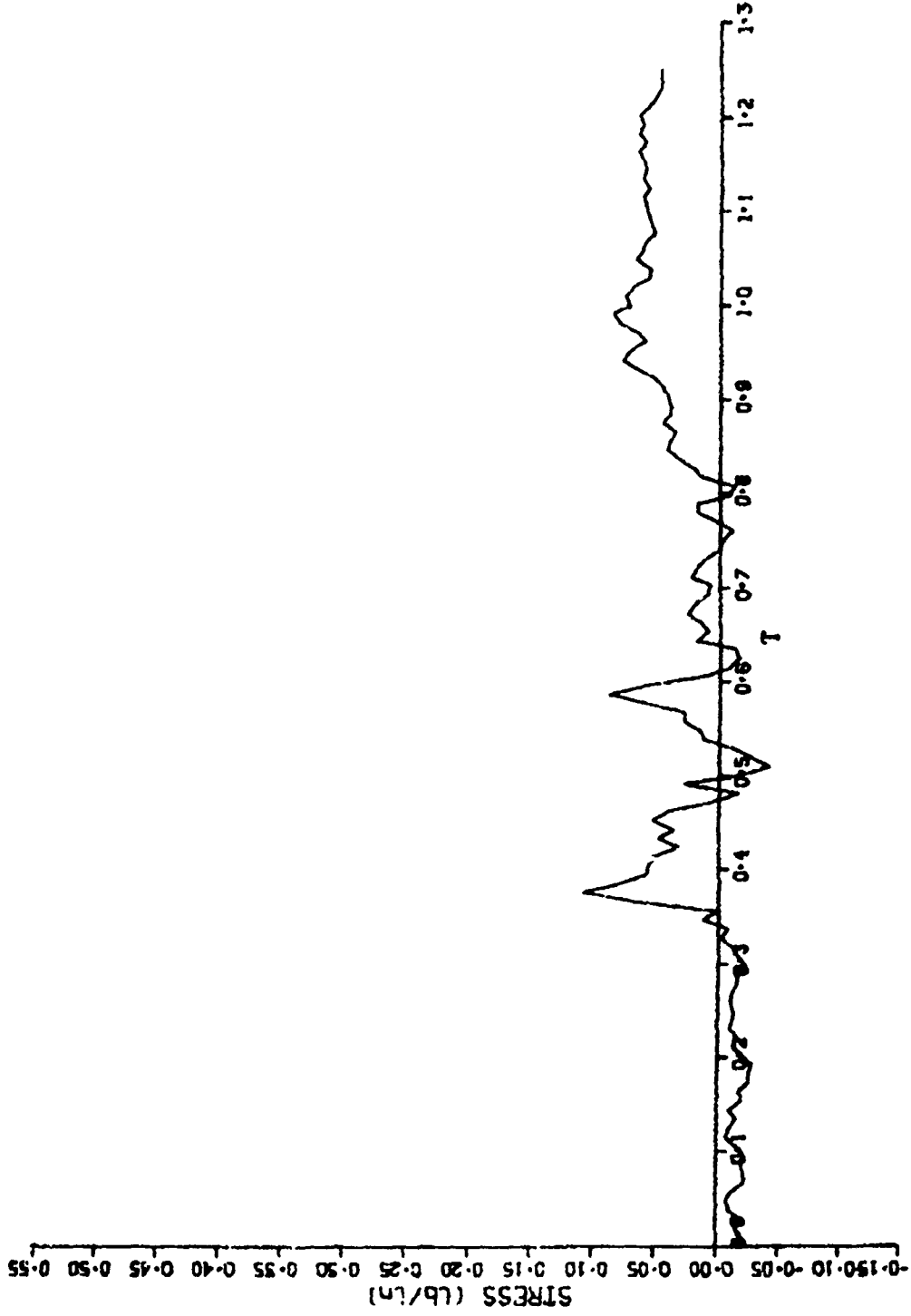
TEST NO. 13 SENSOR IRS - VENT 0- .8 (in H2O)



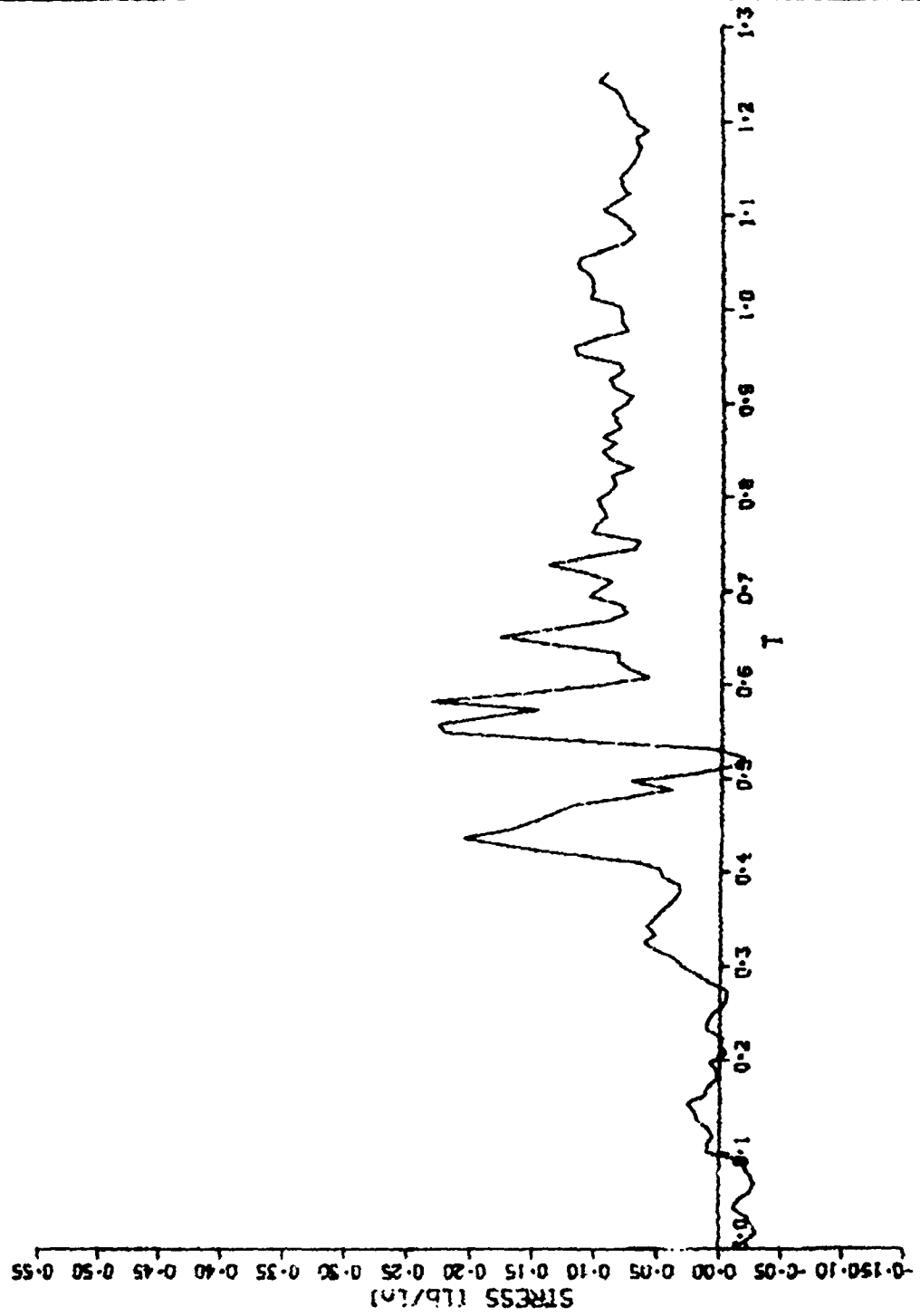
TEST NO. 7 SENSOR 2RS 0- .8 (in H2O)



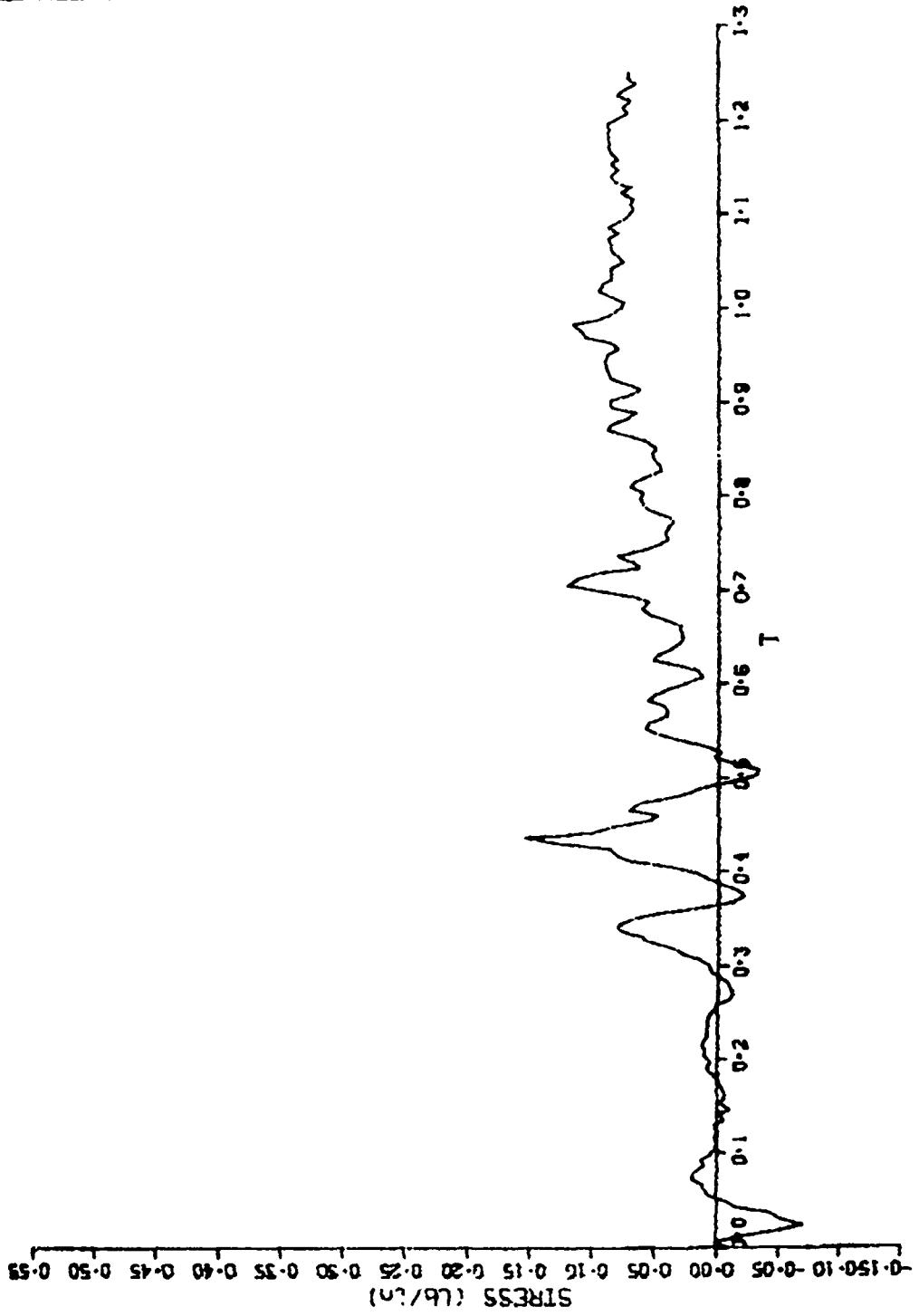
TEST NO. 9 SENSOR 2RS 0- .8(in H2O)



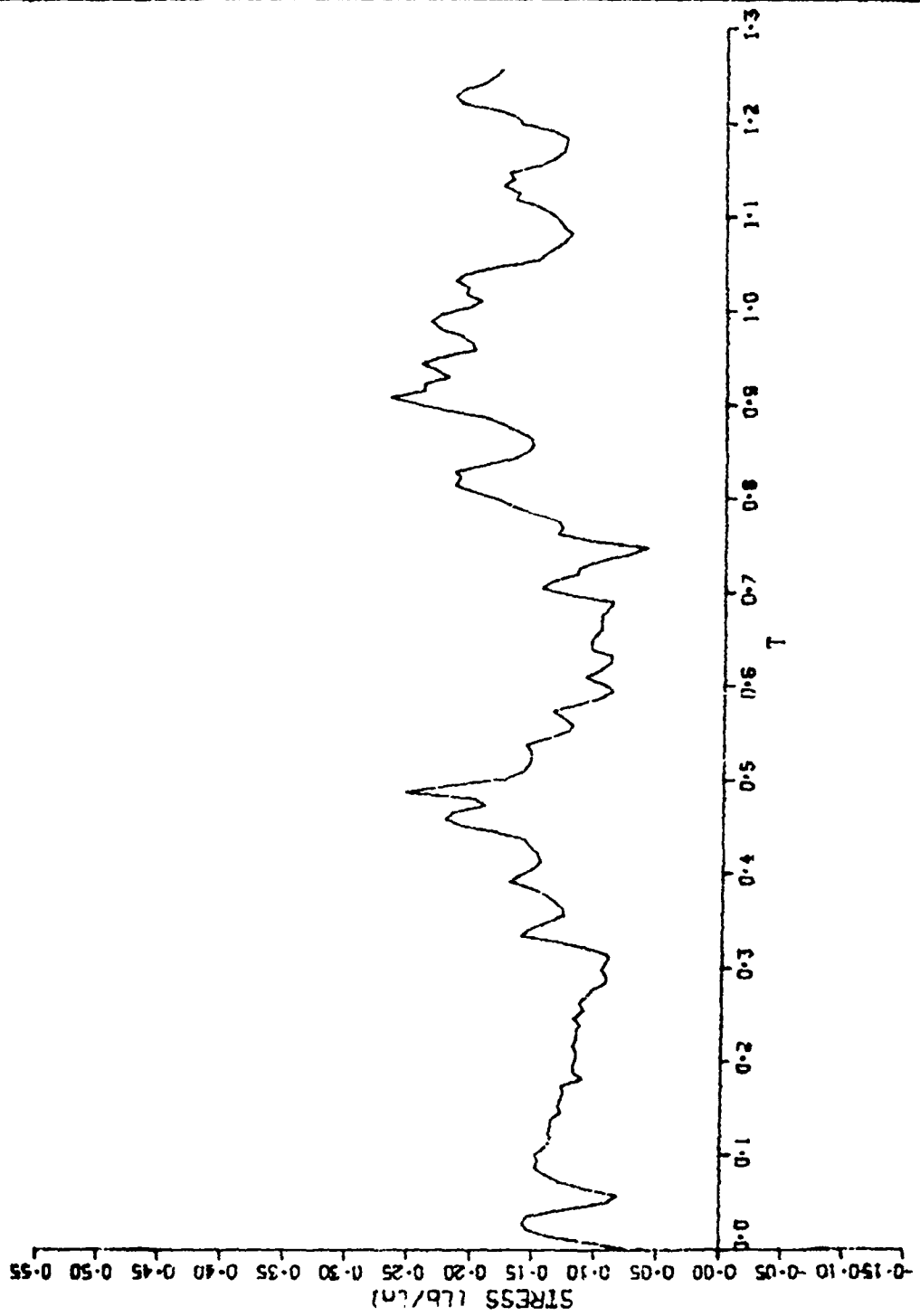
TEST NO. 12 SENSOR 2RS 0- .8 (in H2O)



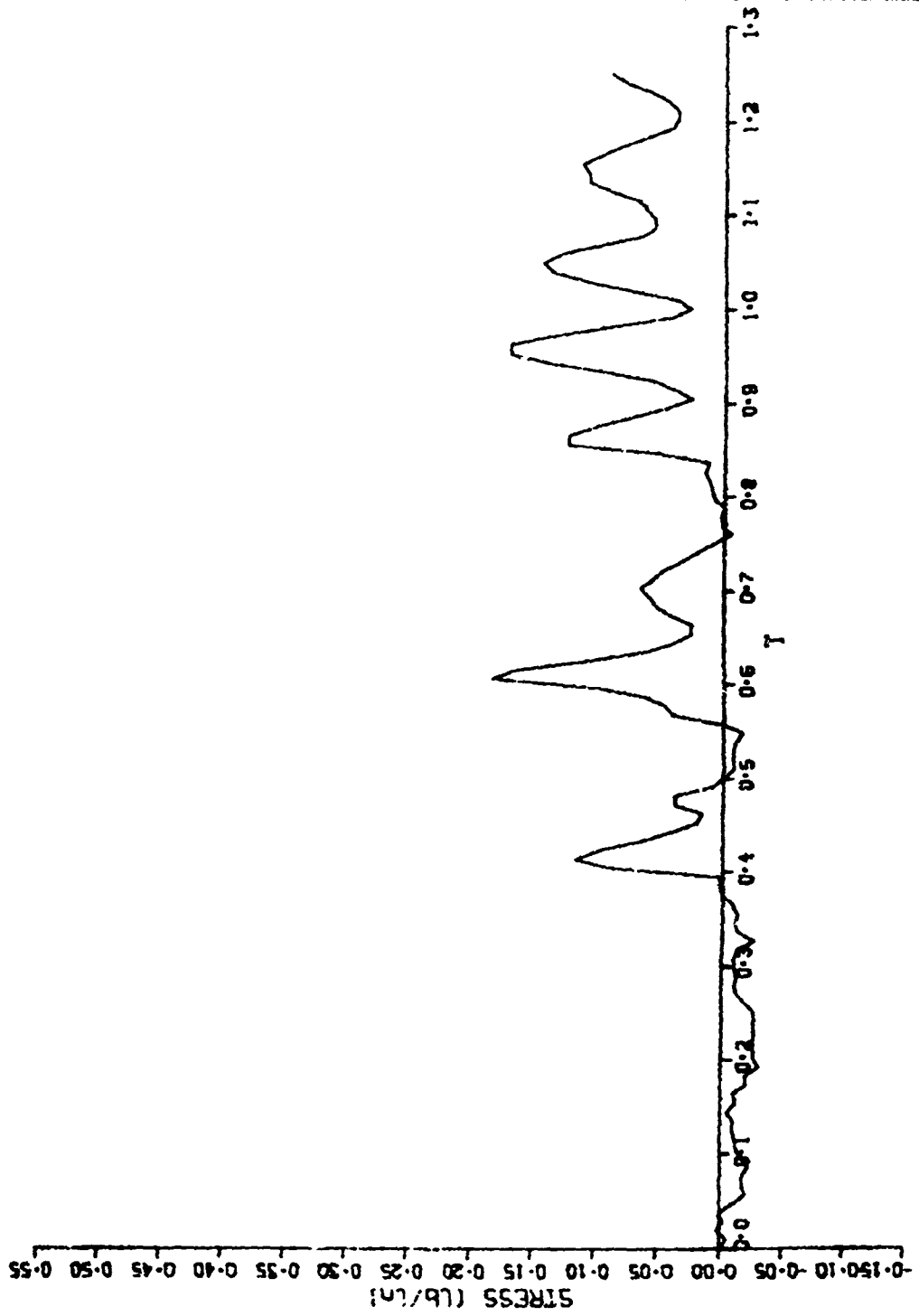
TEST NO.13 SENSOR 2RS 0- .8(in H2O)



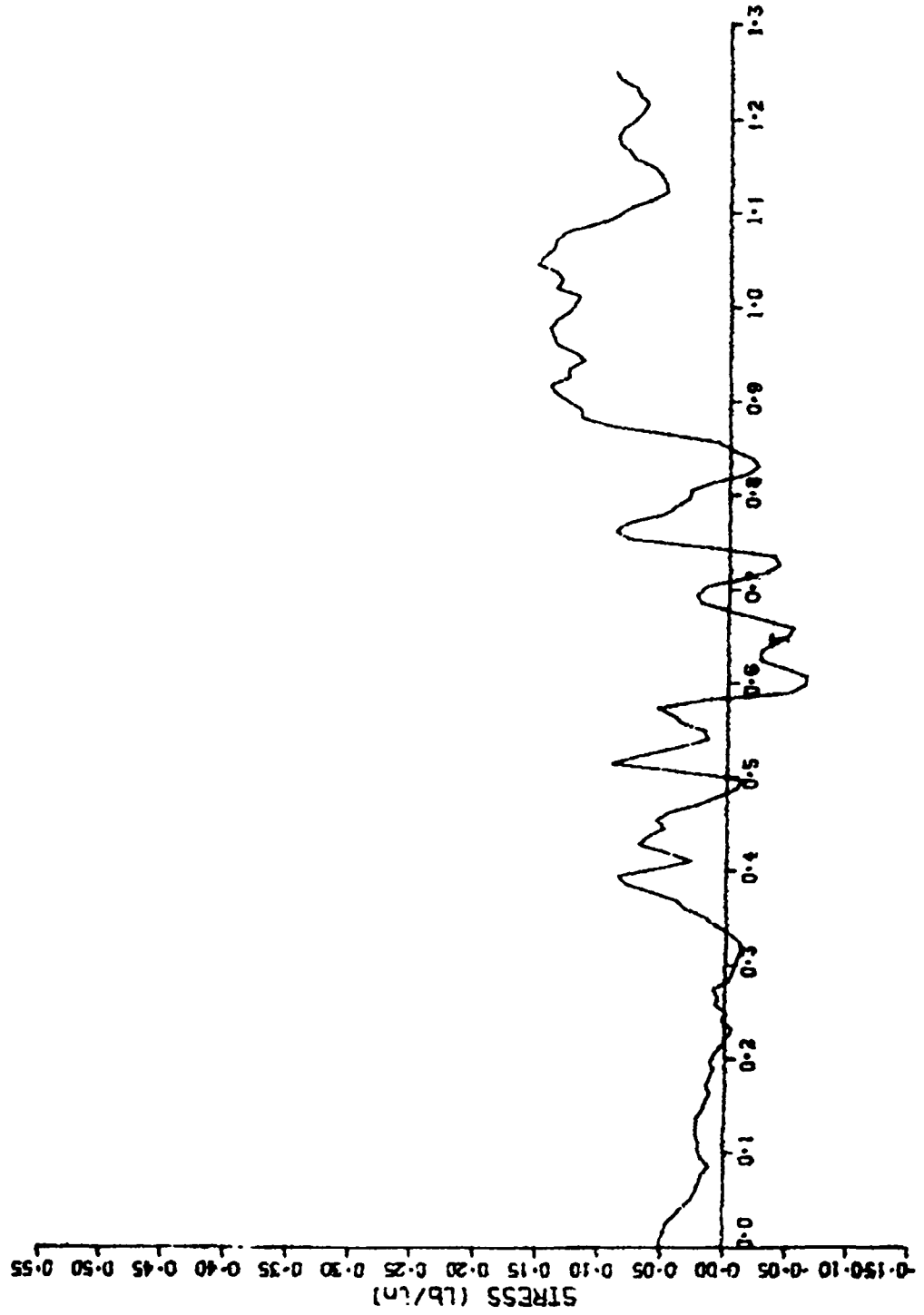
TEST NO. 7 SENSOR 3RS 0- .8 (in H2O)



TEST NO. 9 SENSOR 4RS 0- .8 (in H2O)

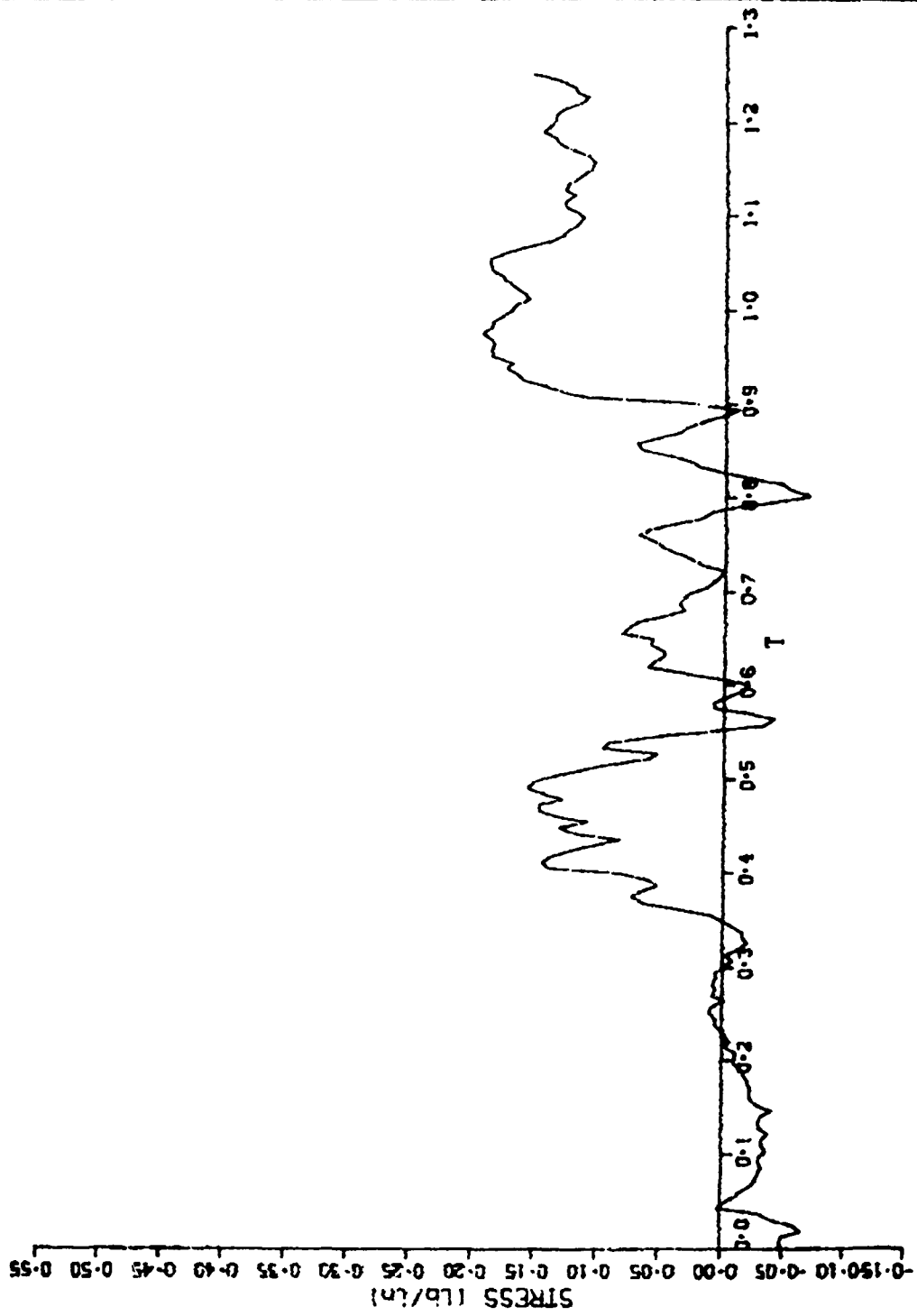


TEST NO. 12 SENSOR 4RS 0- .8 (in H2O)

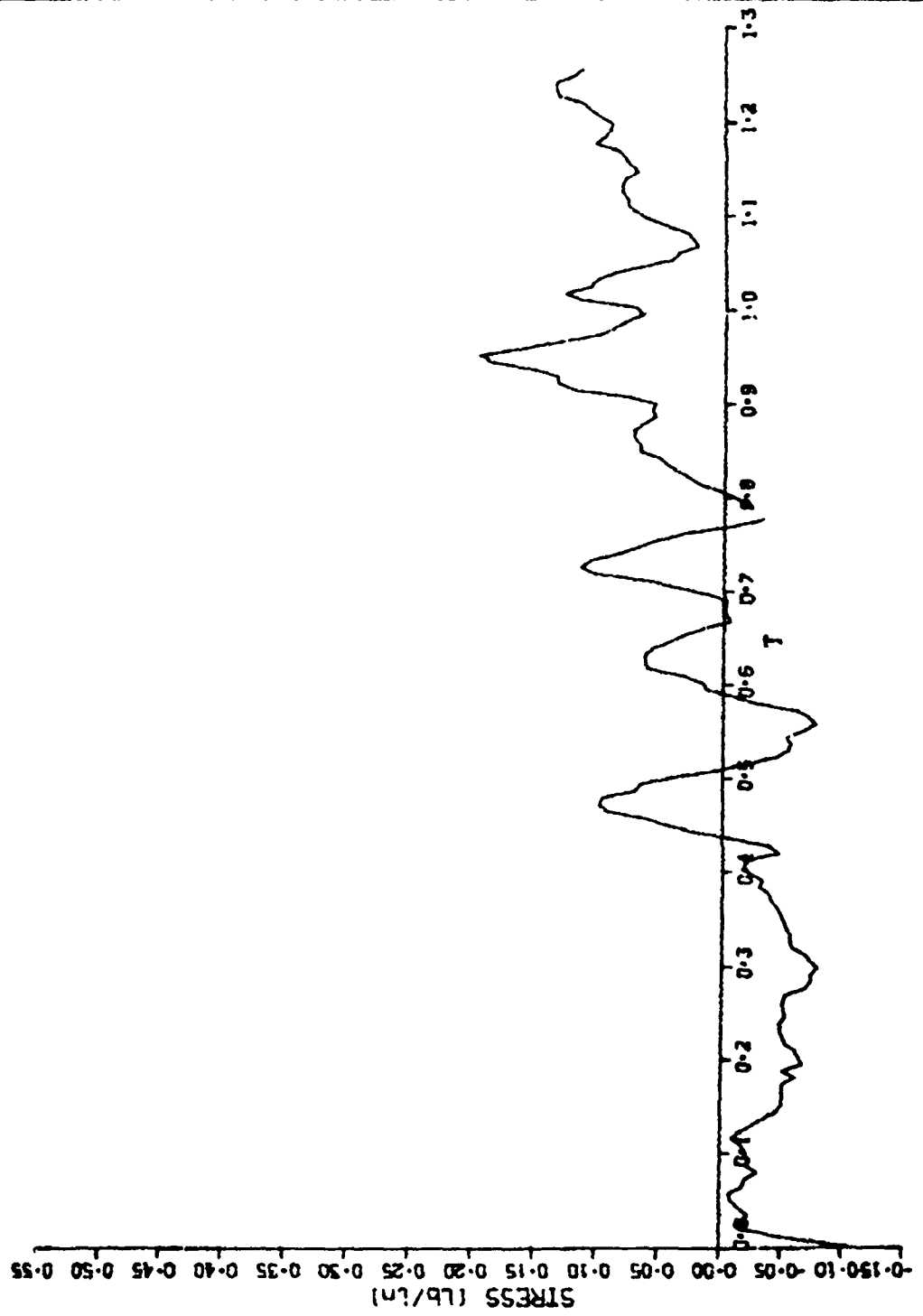




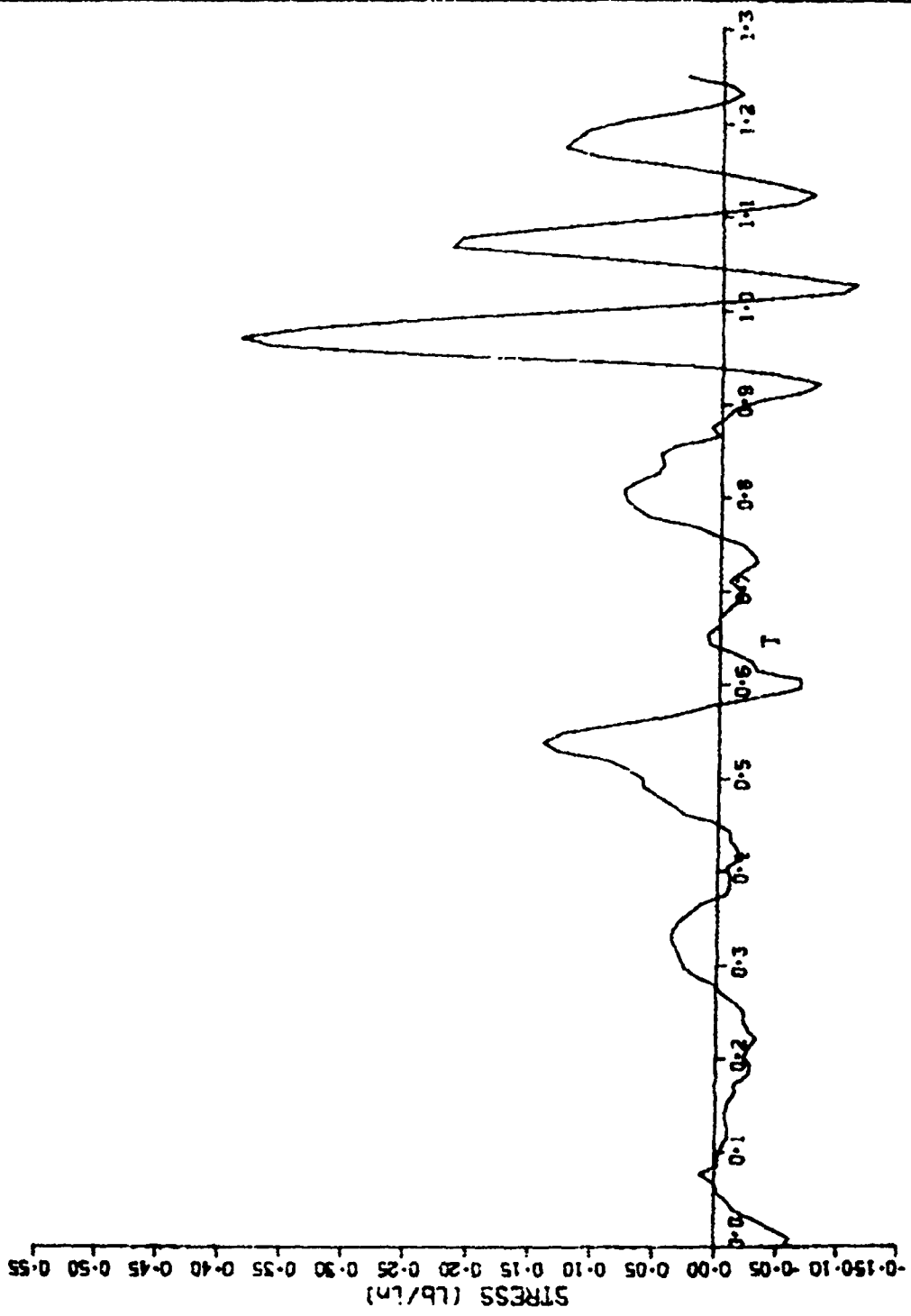
TEST NO. 13 SENSOR 4RS 0- .8 (in H2O)



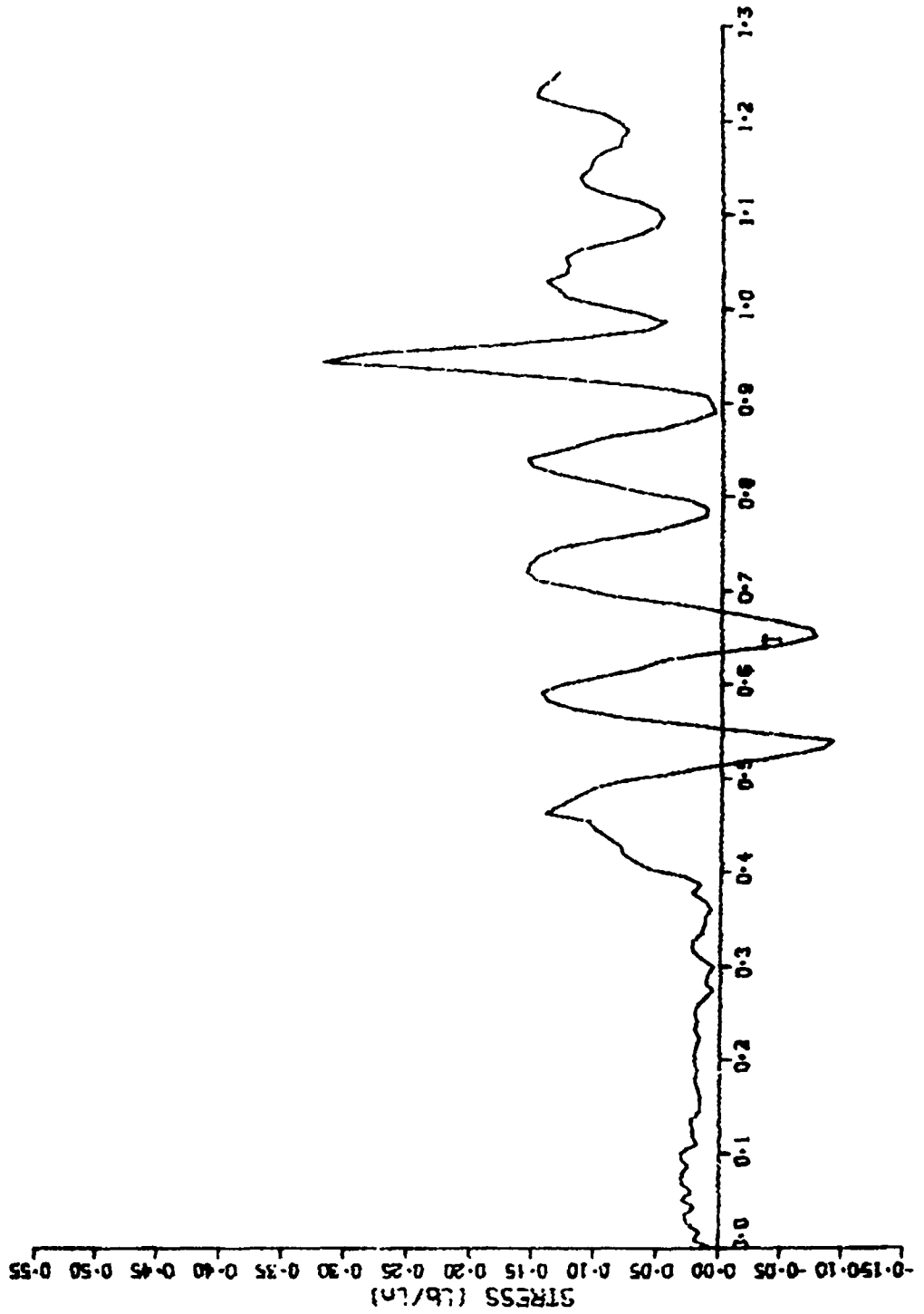
TEST NO. 7 SENSOR SRS - SKIRT 0- .8 (in H2O)



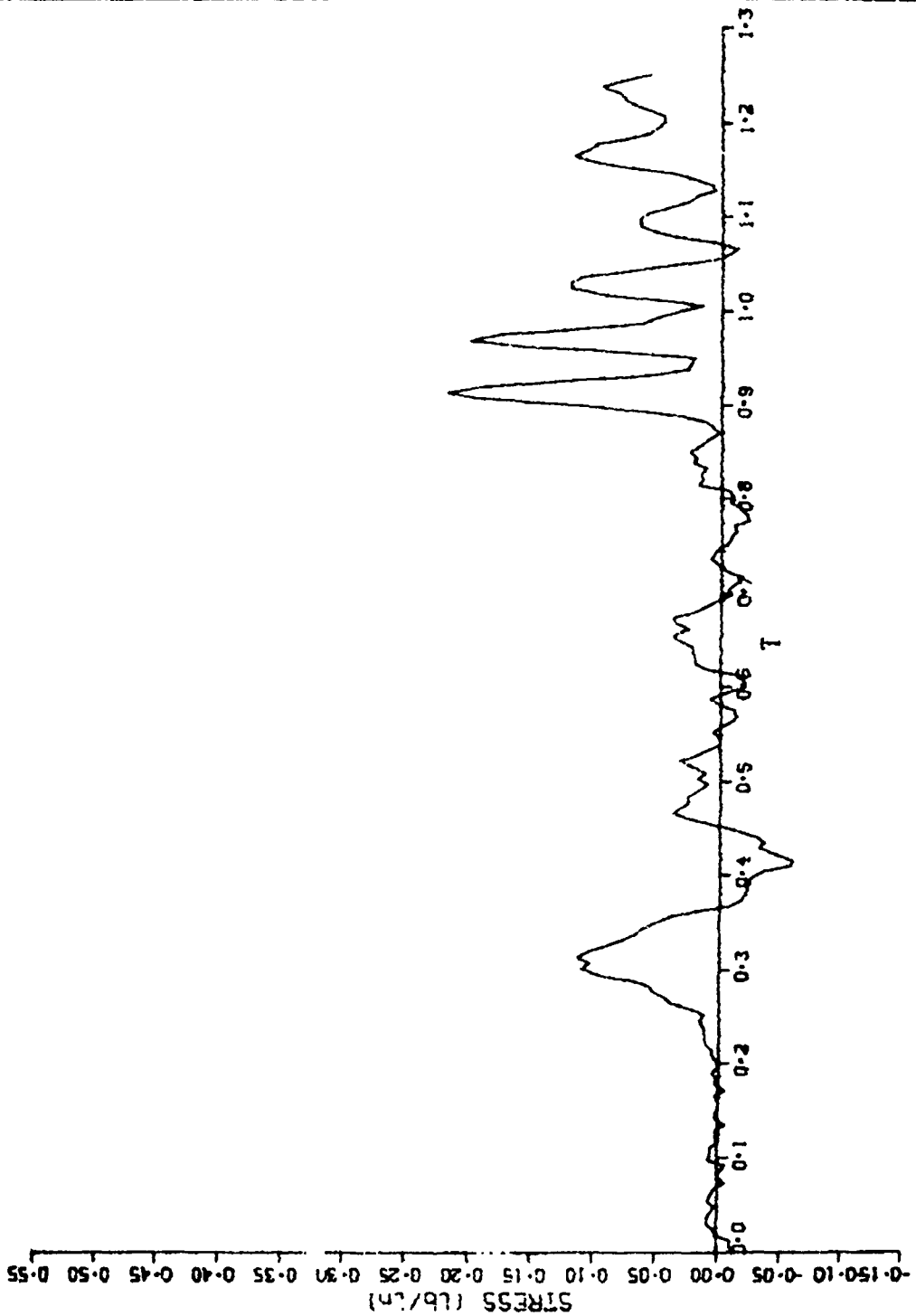
TEST NO. 9 SENSOR 5RS - SKIRT 0- .8 (in H20)



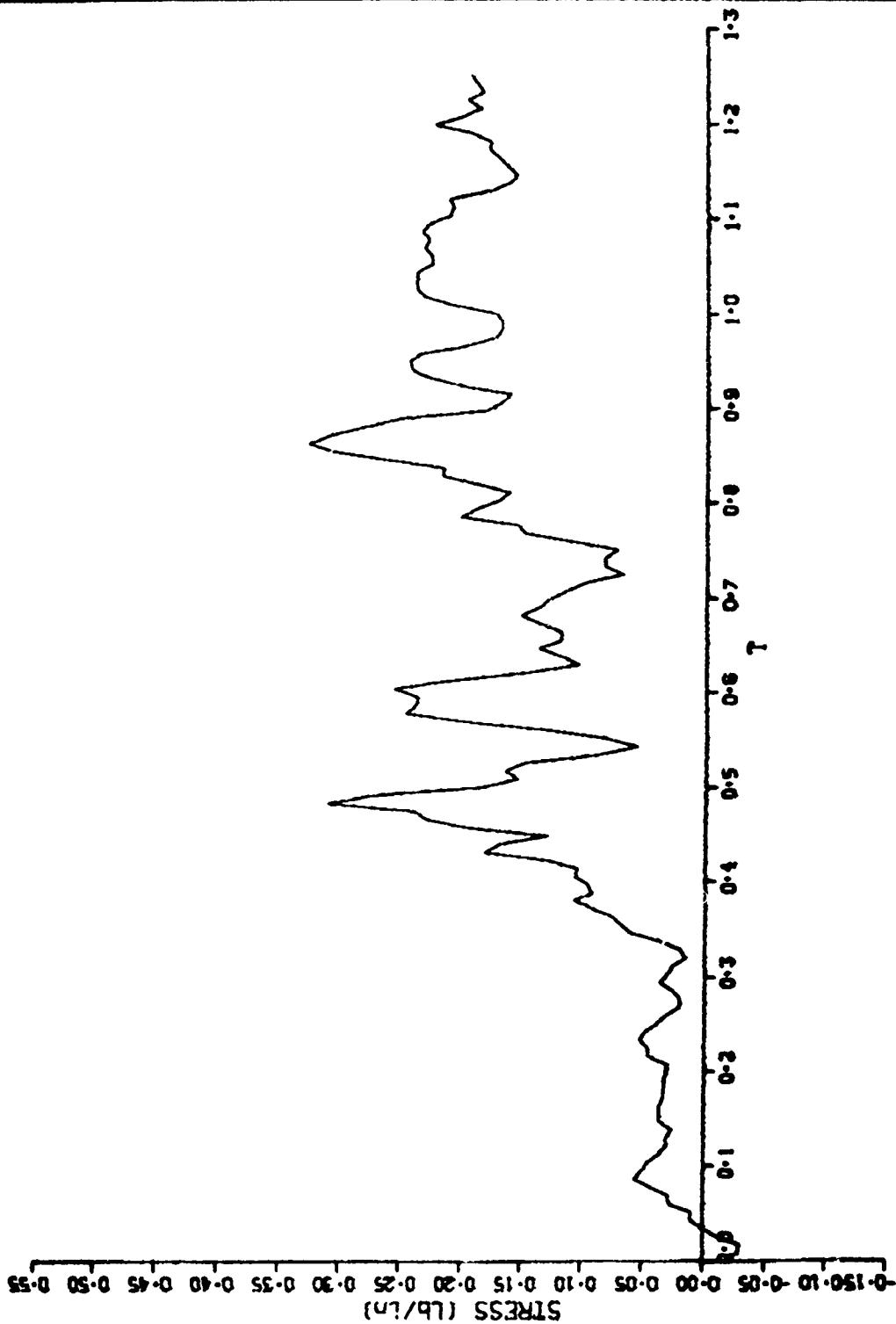
TEST NO. 12 SENSOR 5RS - SKIRT 0- .8 (in H2O)



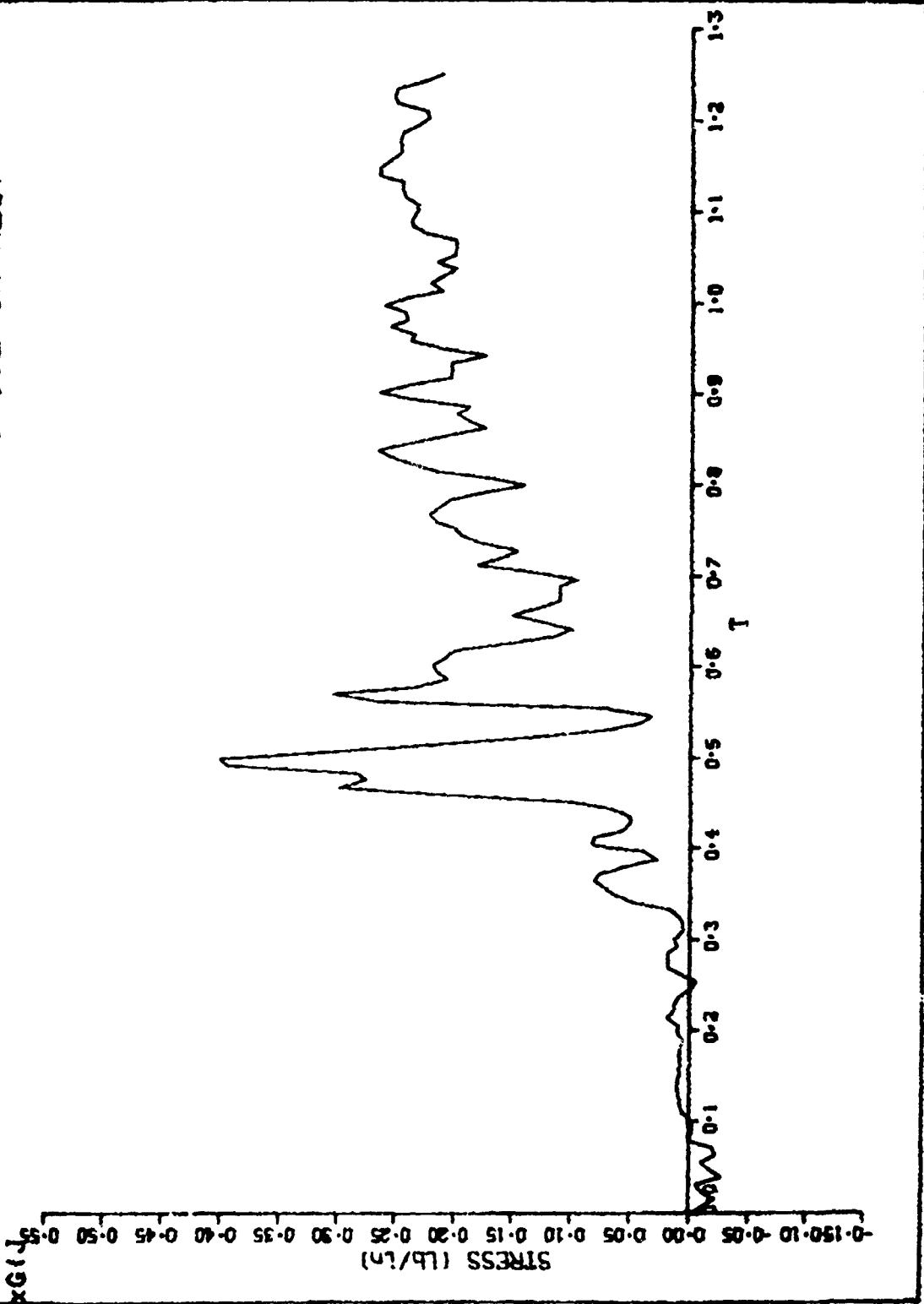
TEST NO. 13 SENSOR 5RS - SKIRT 0- .8 (Ln H20)



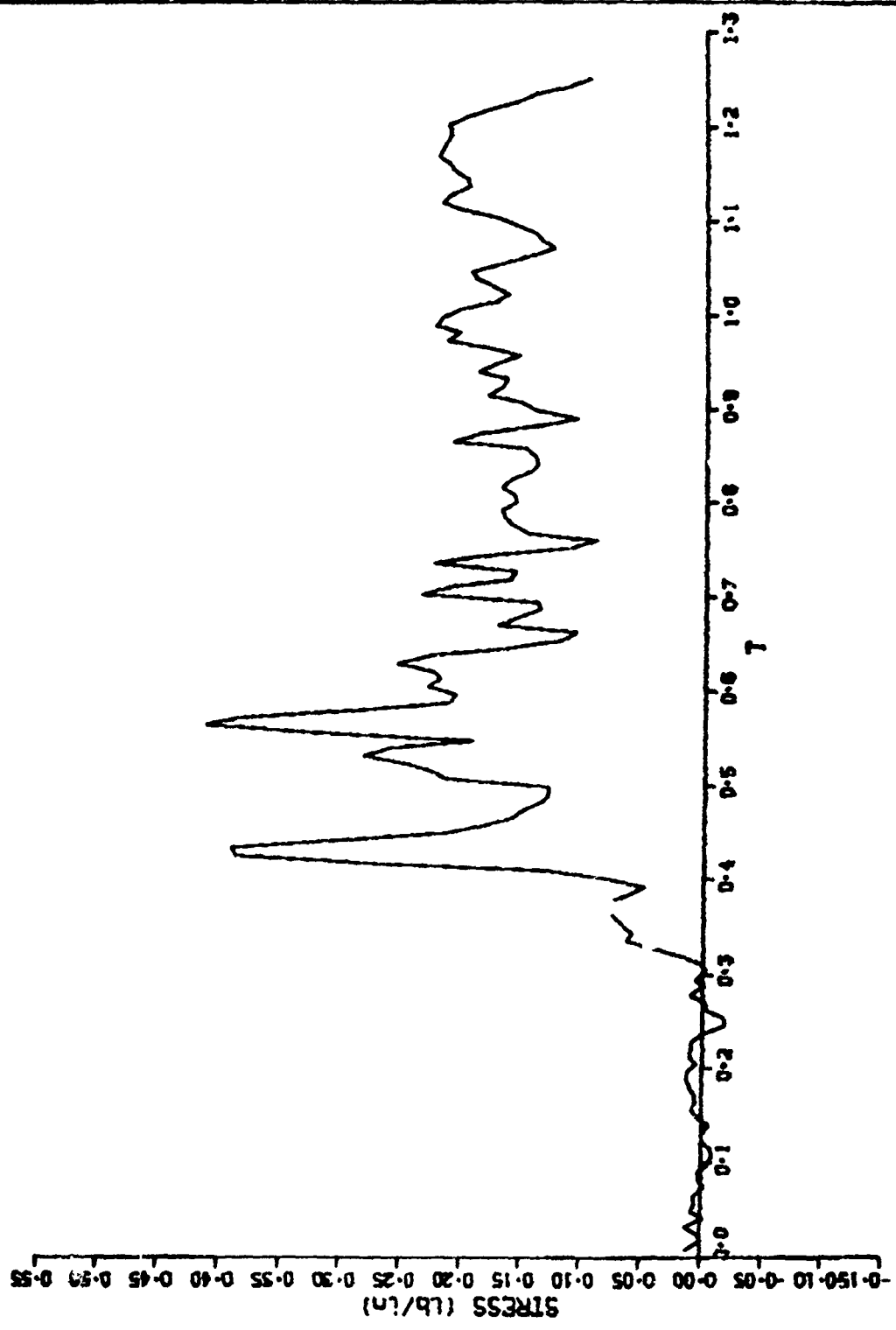
TEST NO. 14 SENSOR IRS - VENT 0-1.2 (in H2O)



TEST NO. 15 SENSOR IRS - VENT 0-1.2 in H2O)

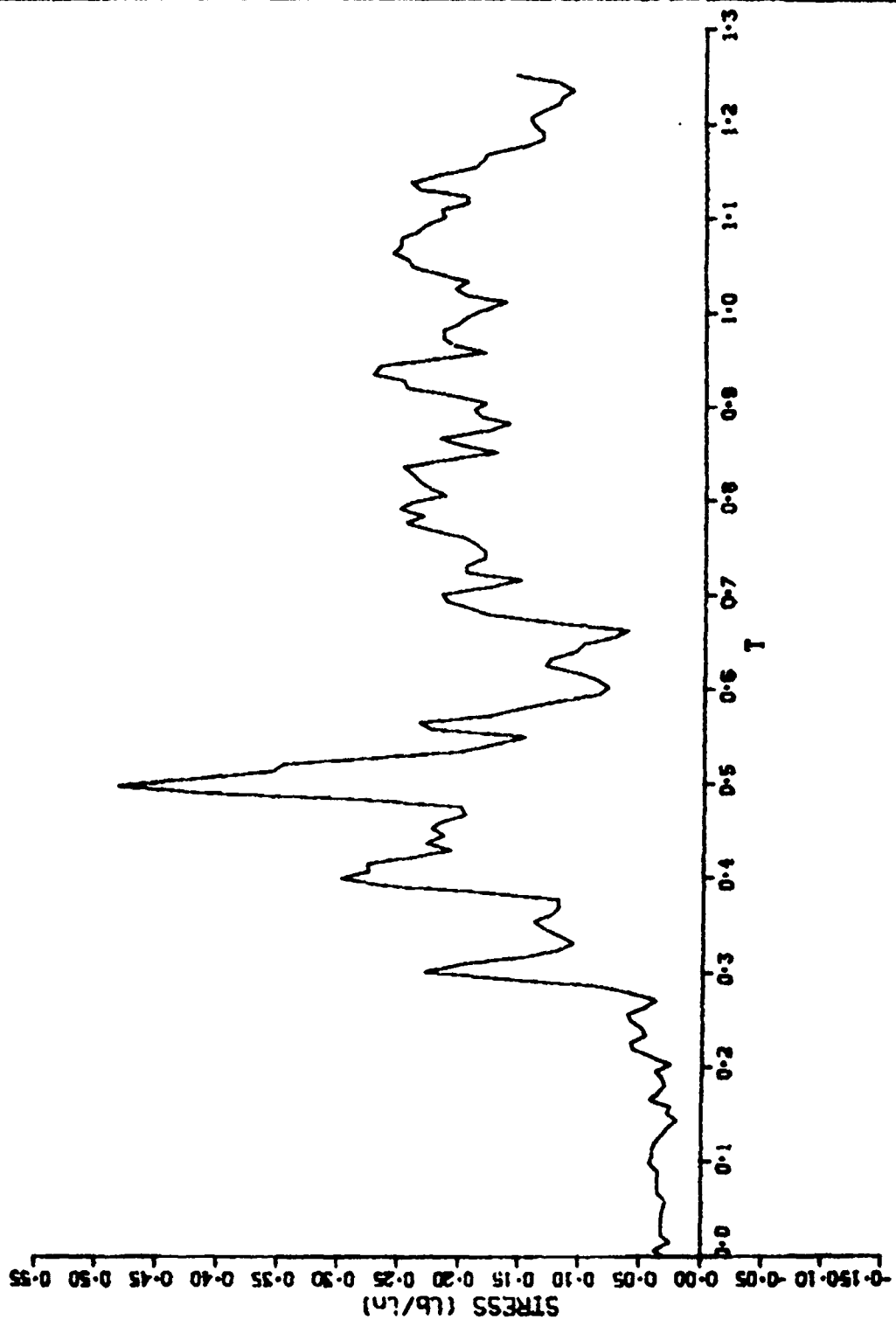


TEST NO. 16 SENSOR IRS - VENT 0-1.2 (in H2O)

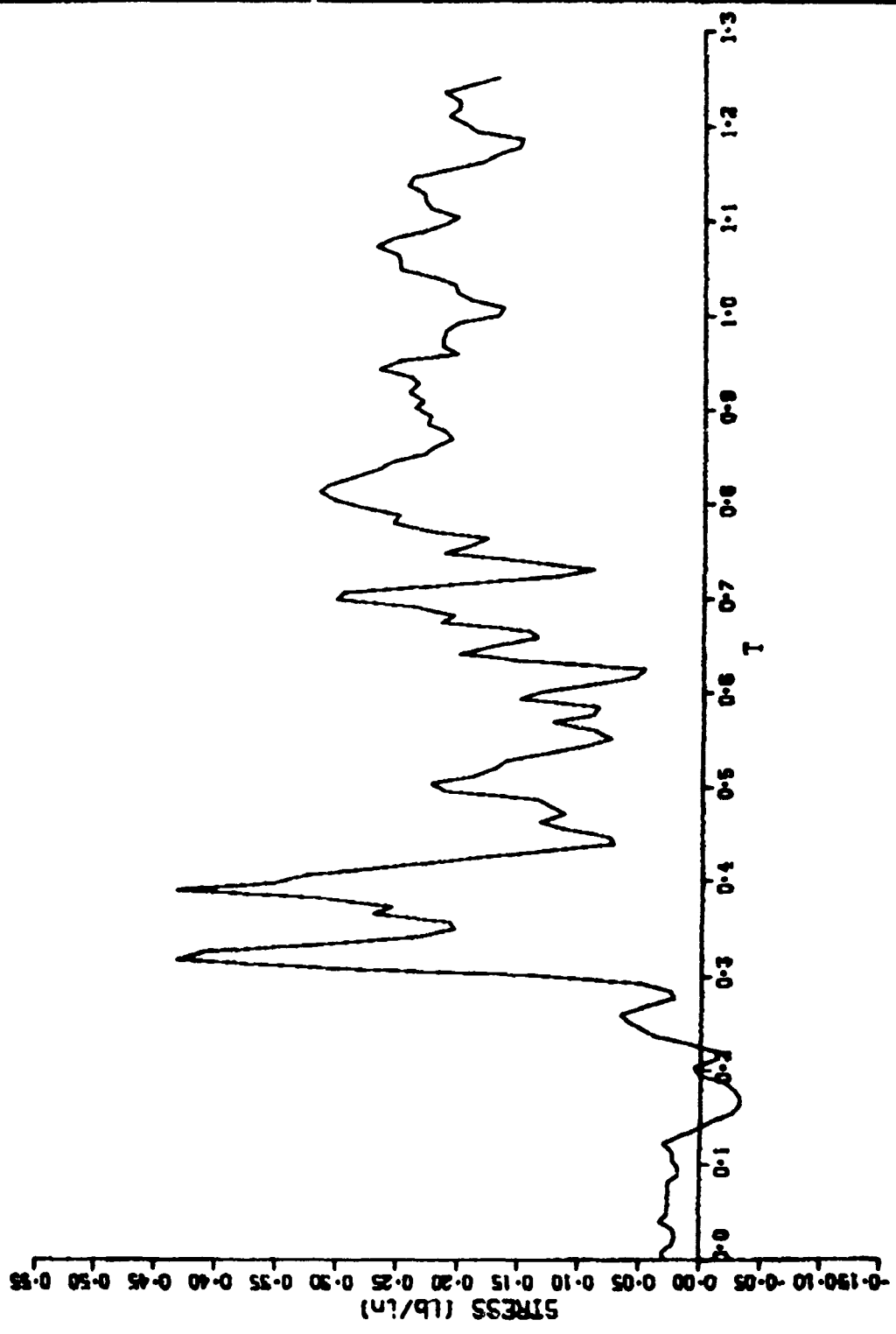




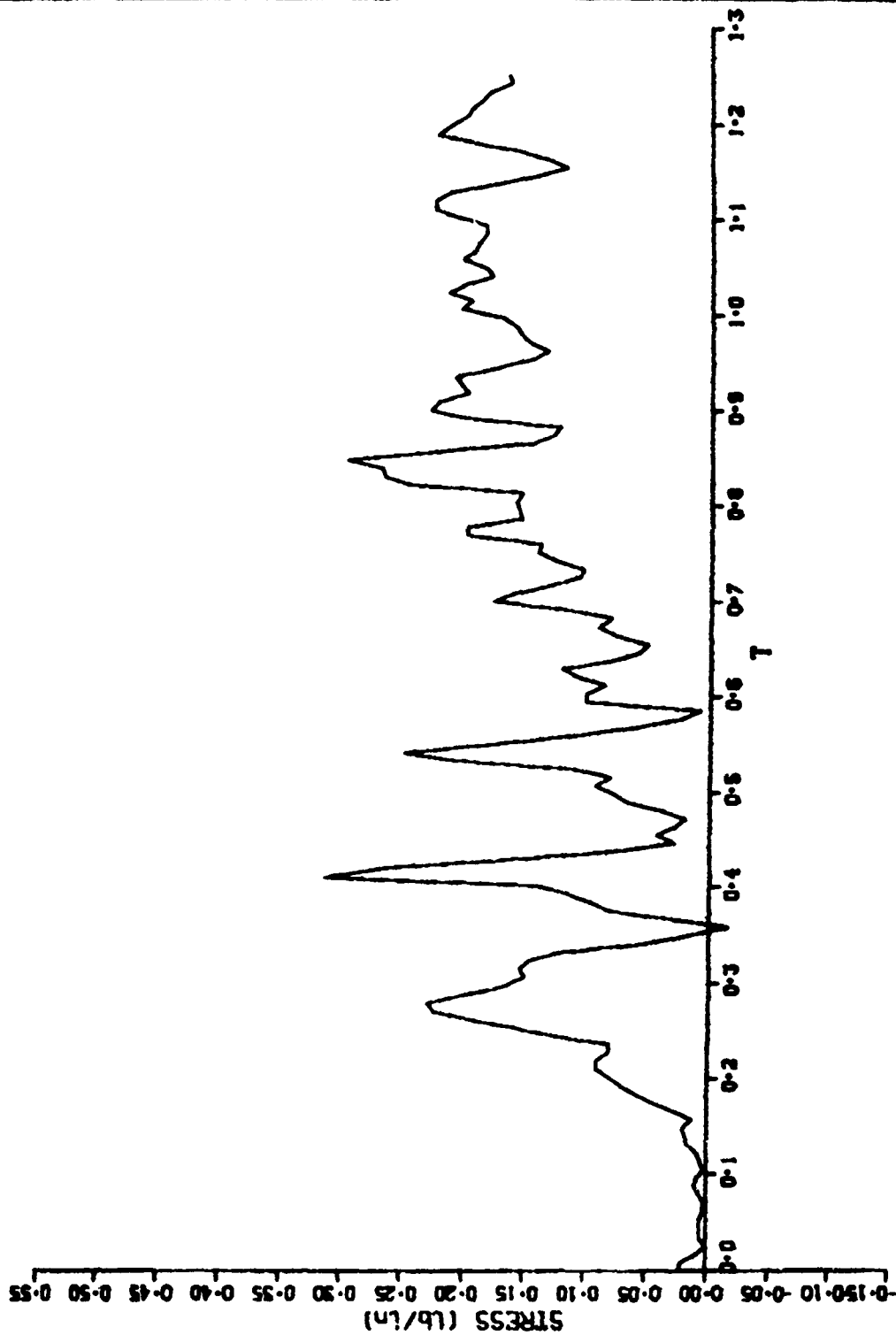
TEST NO. 17 SENSOR IRS - VENT 0-1.2 (in H2O)



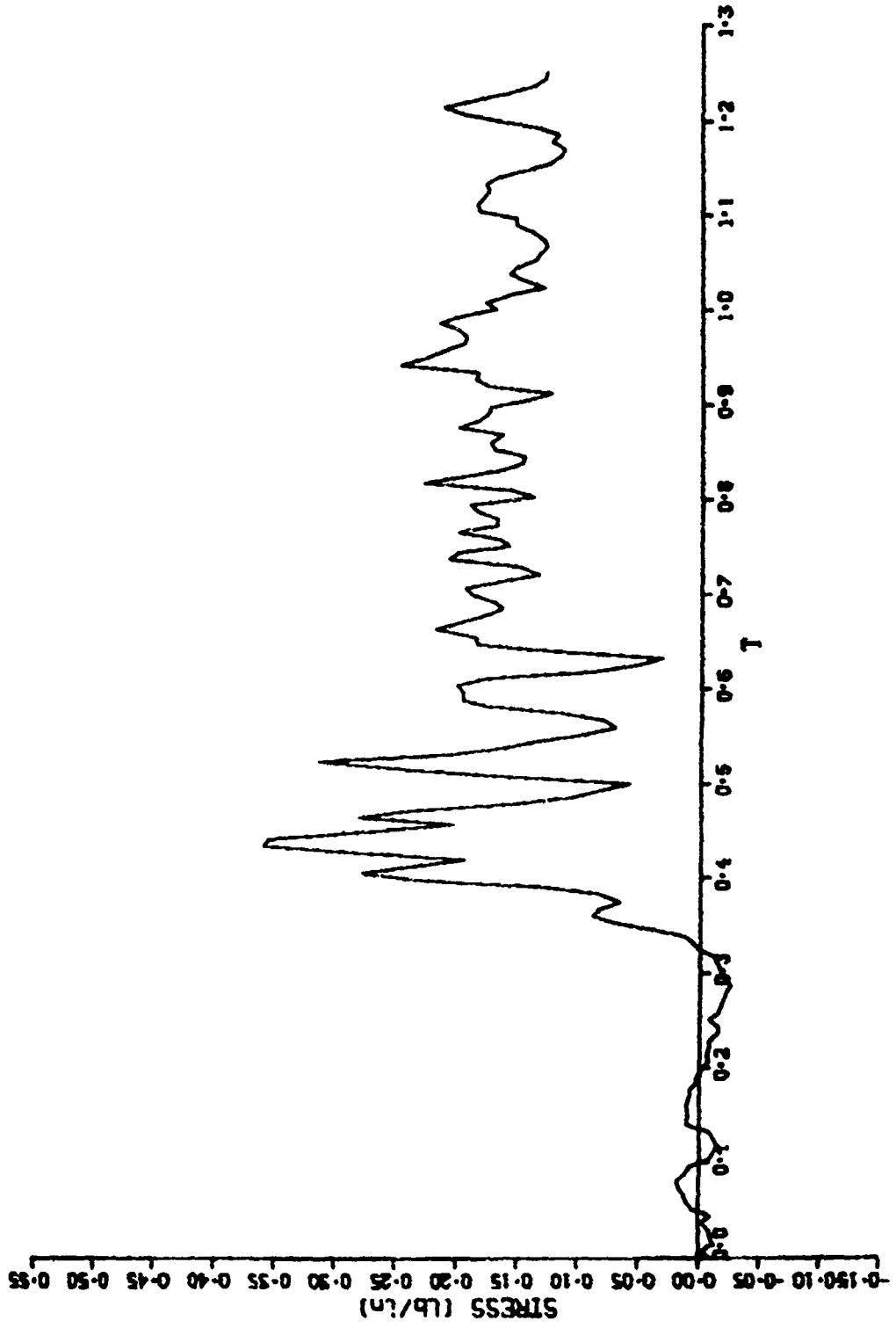
TEST NO. 18 SENSOR IRS - VENT 0-1.2 (in H2O)



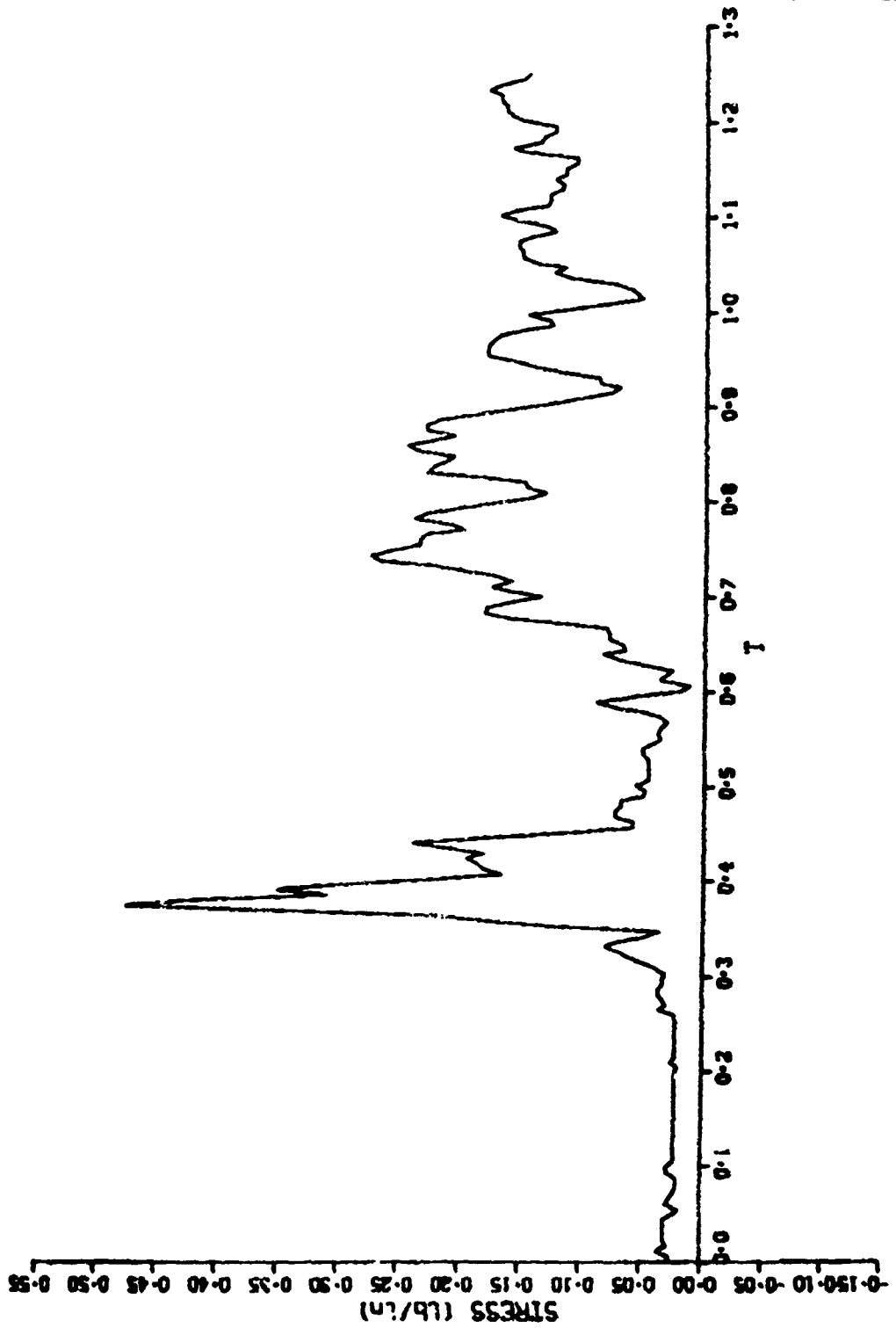
TEST NO.19 SENSOR IRS - VENT 0-1.2 (in H2O)



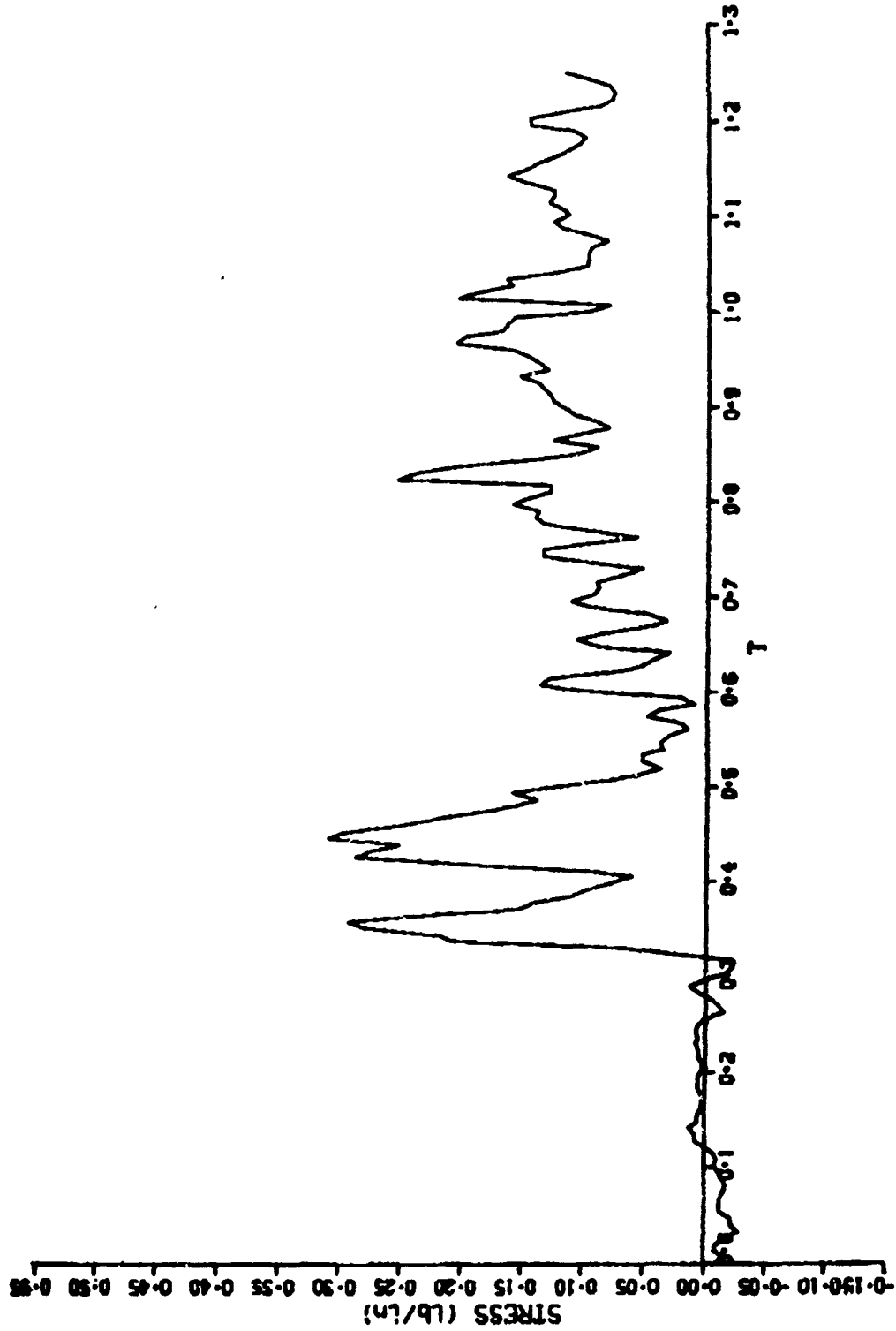
TEST NO.20 SENSOR IRS - VENT 0-1.2(in H2O)



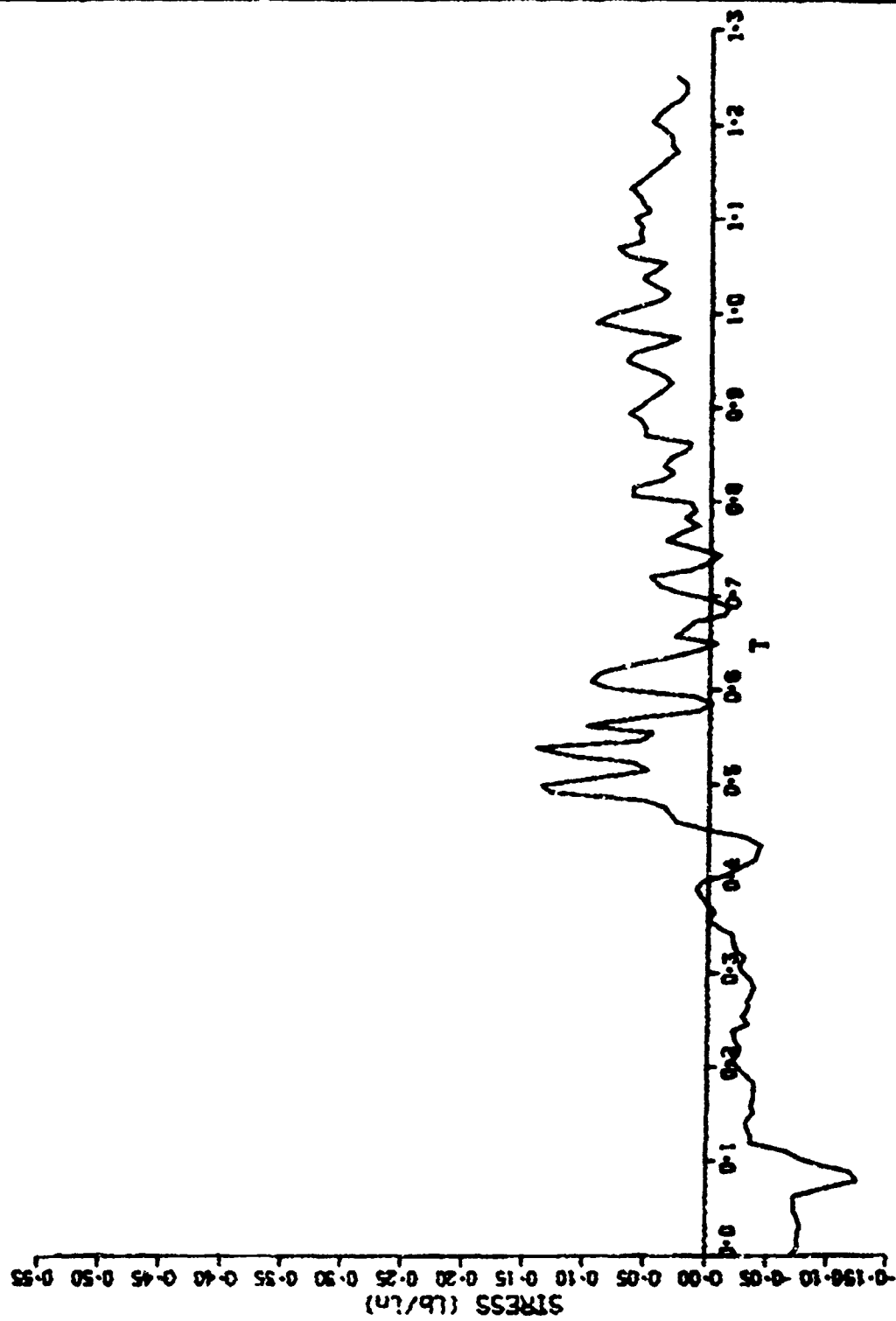
TEST NO.32 SENSOR IRS - VENT 0-1.2(in H2O)



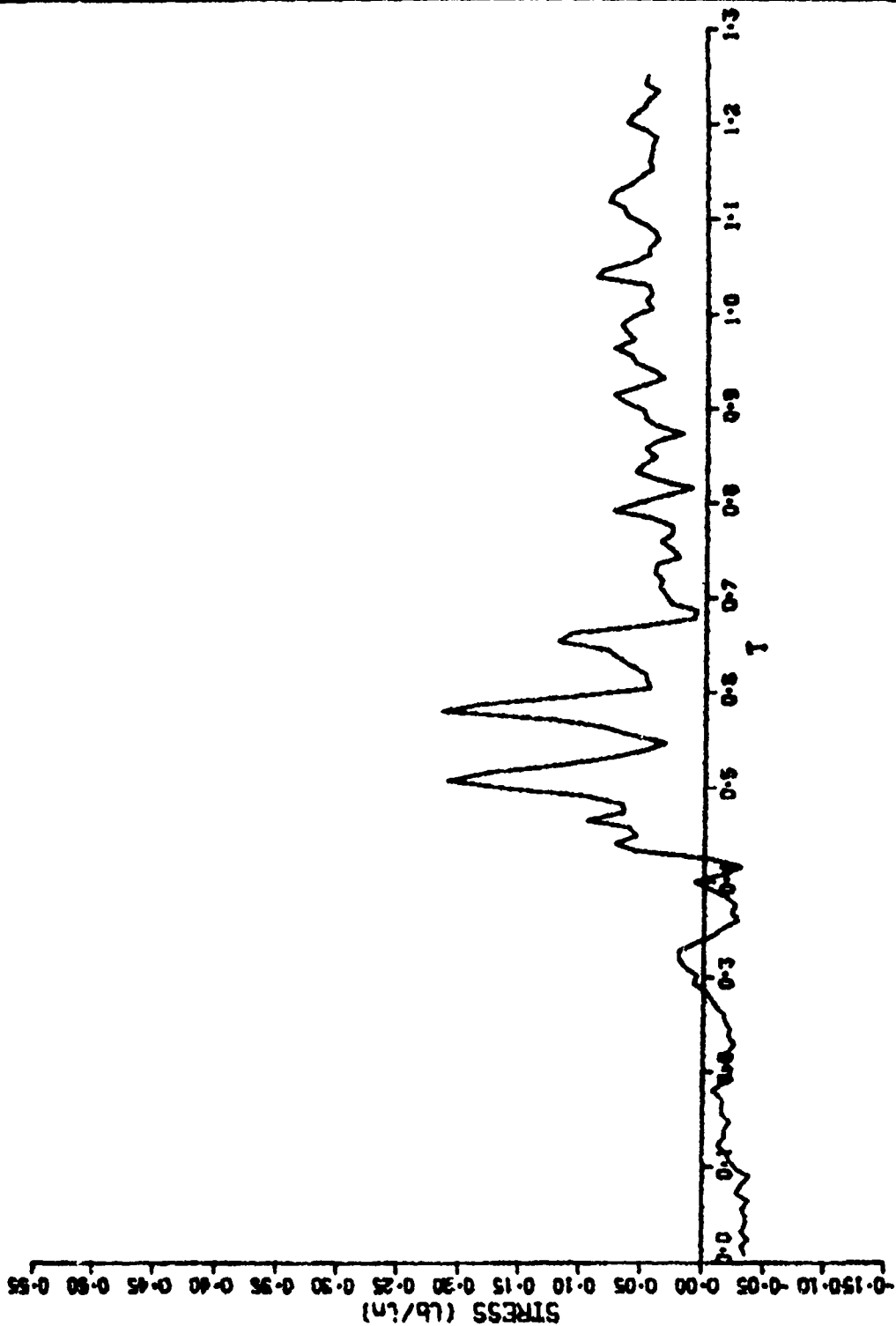
TEST NO.36 SENSOR IRS - VENT 0-1.2 (in H2O)



TEST NO. 15 SENSOR 2RS 0-1.2 (in H2O)

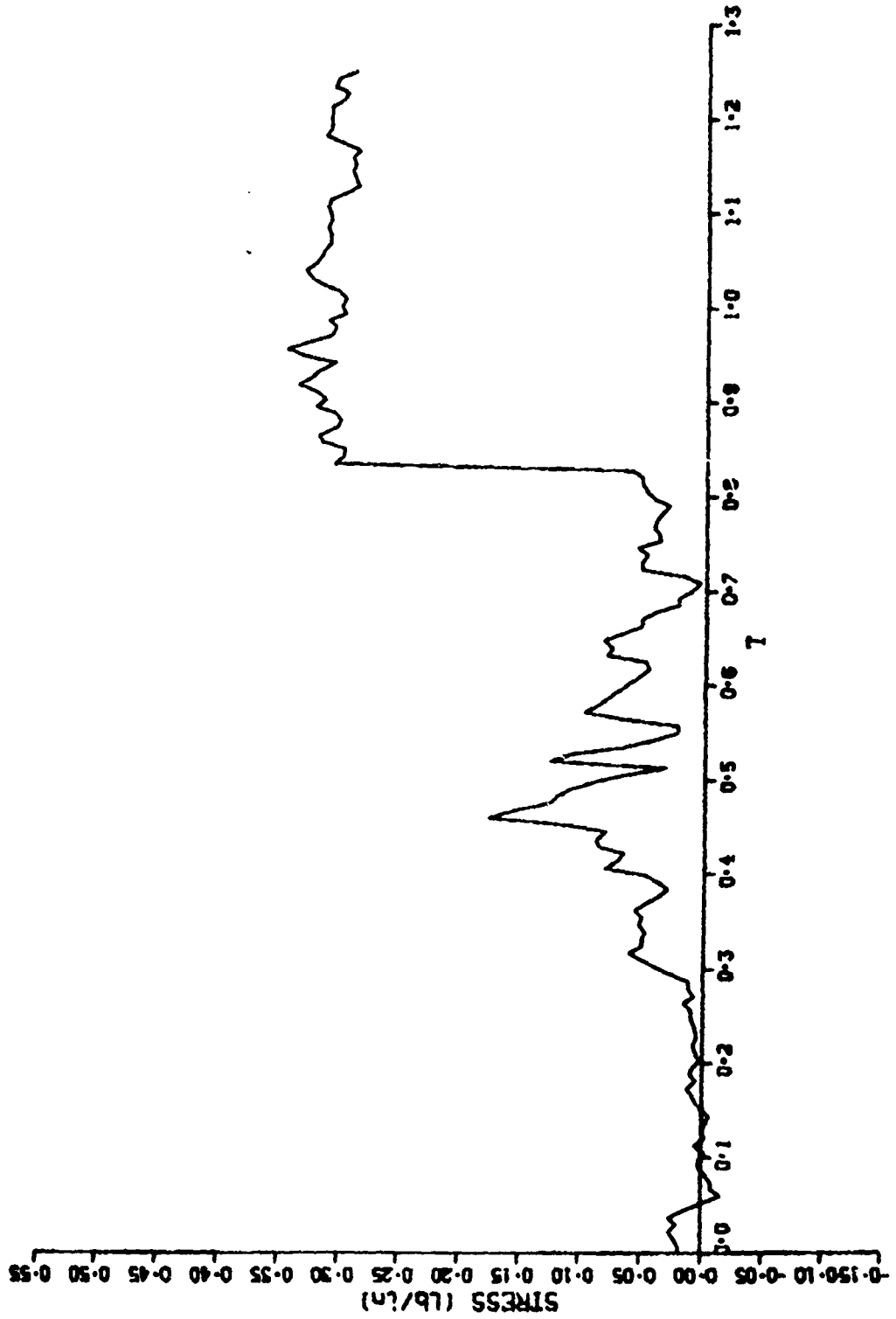


TEST NO.16 SENSOR 2RS 0-1.2(in H2O)

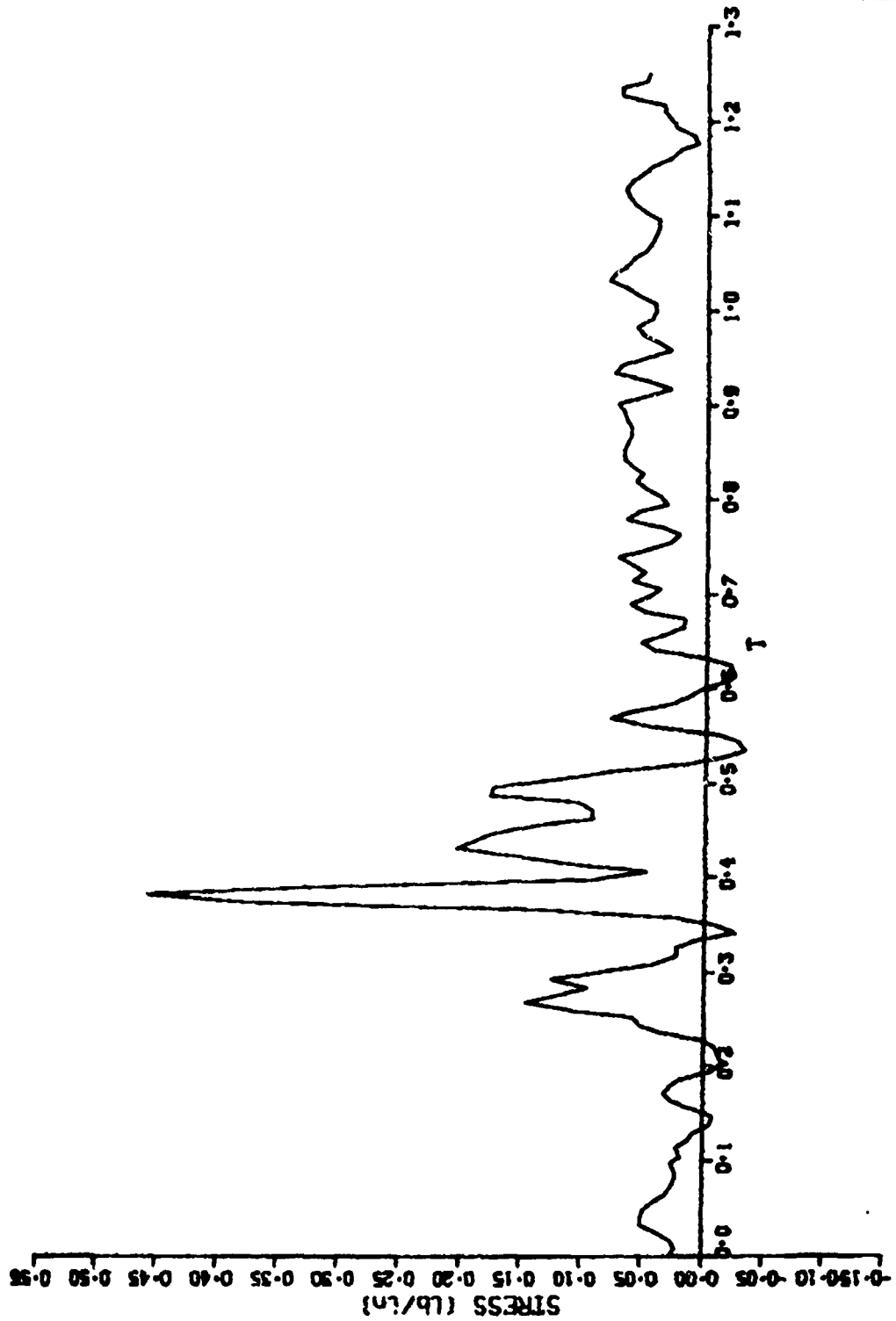




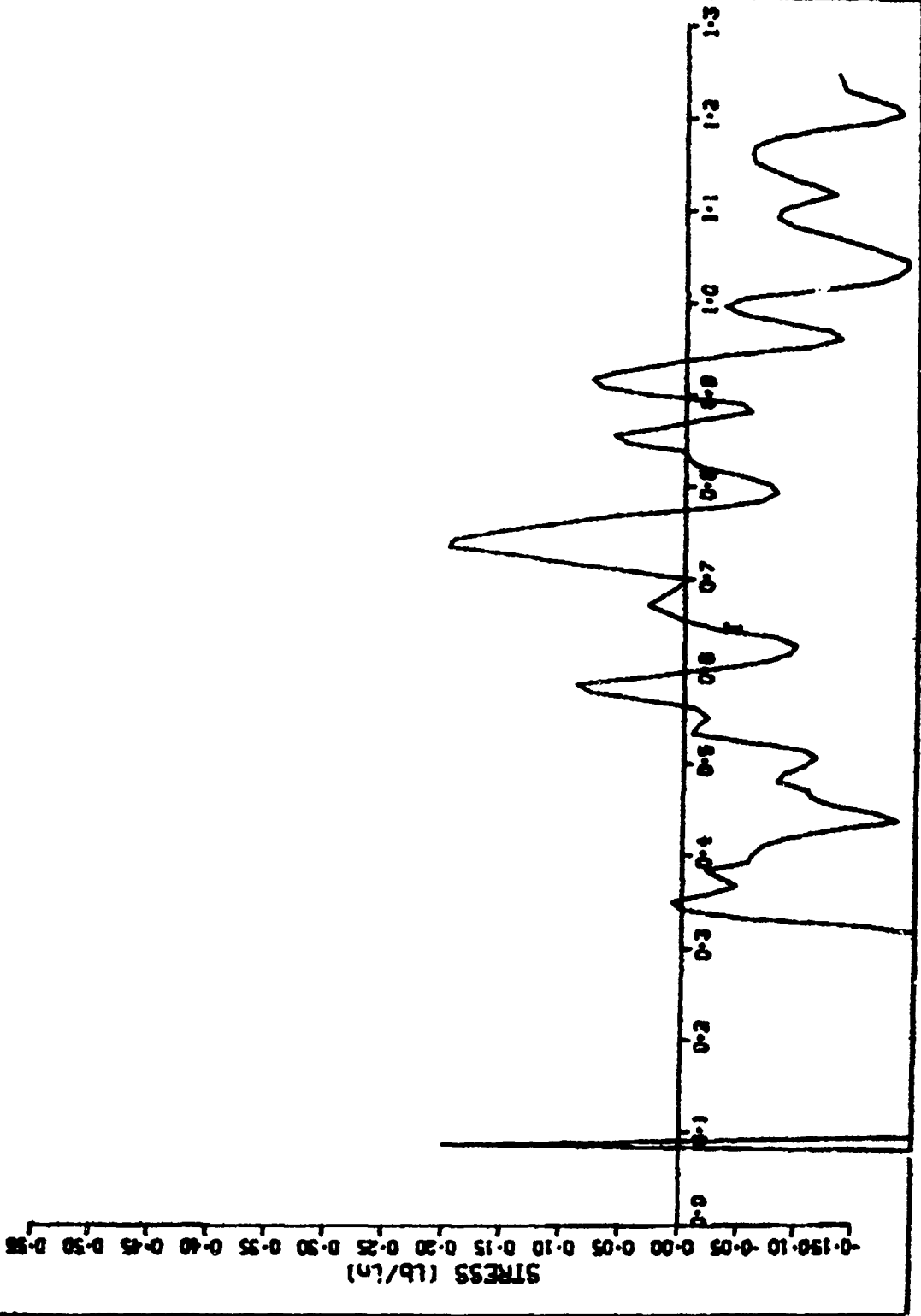
TEST NO. 17 SENSOR 2RC 0-1.2 (In H2O)



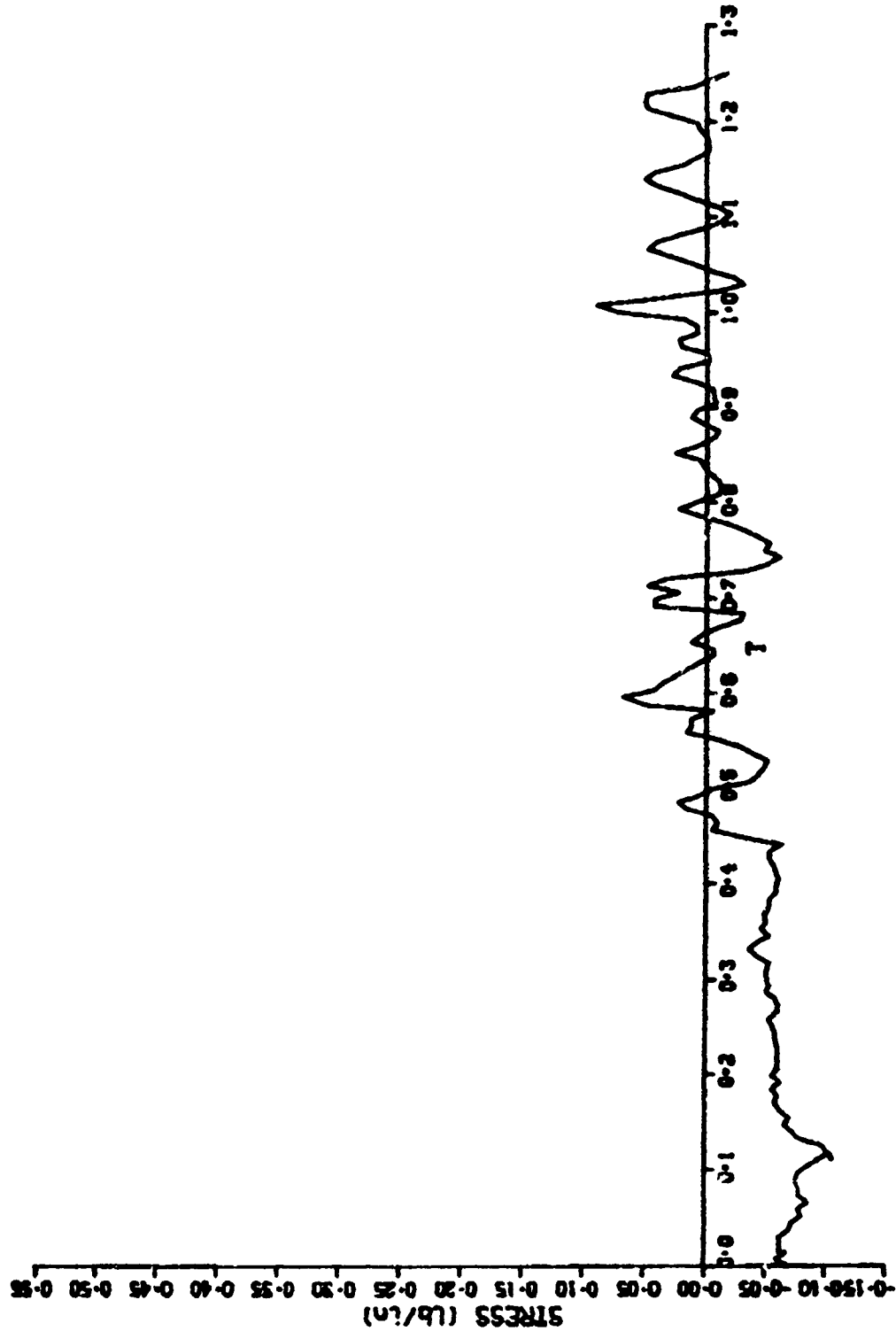
TEST NO. 18 SENSOR 2RS 0-1.2 (in H2O)



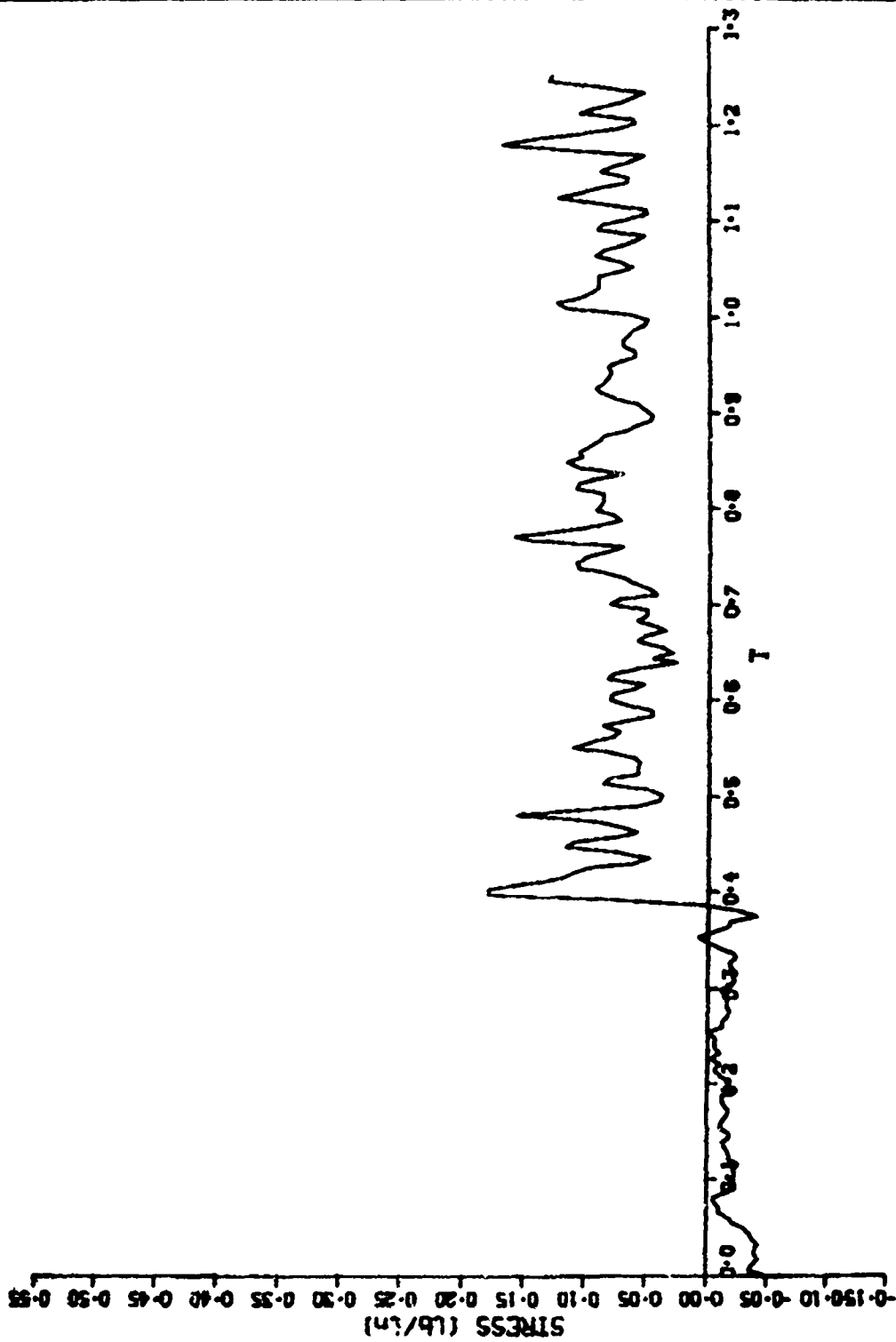
TEST NO. 19 SENSOR 2RS 0-1.2 (in H2O)



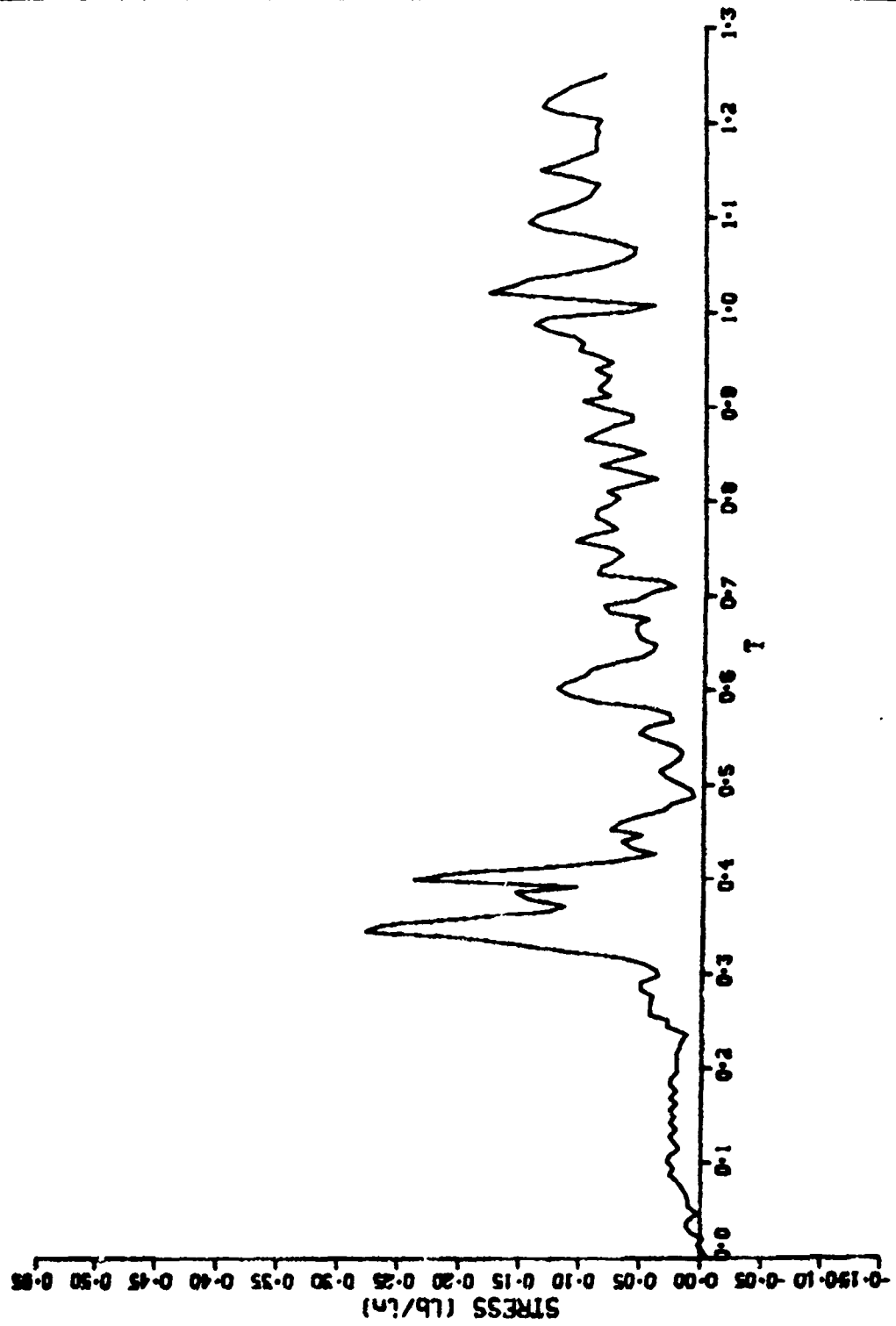
TEST NO.20 SENSOR 2RS 0-1.2(in H2O)



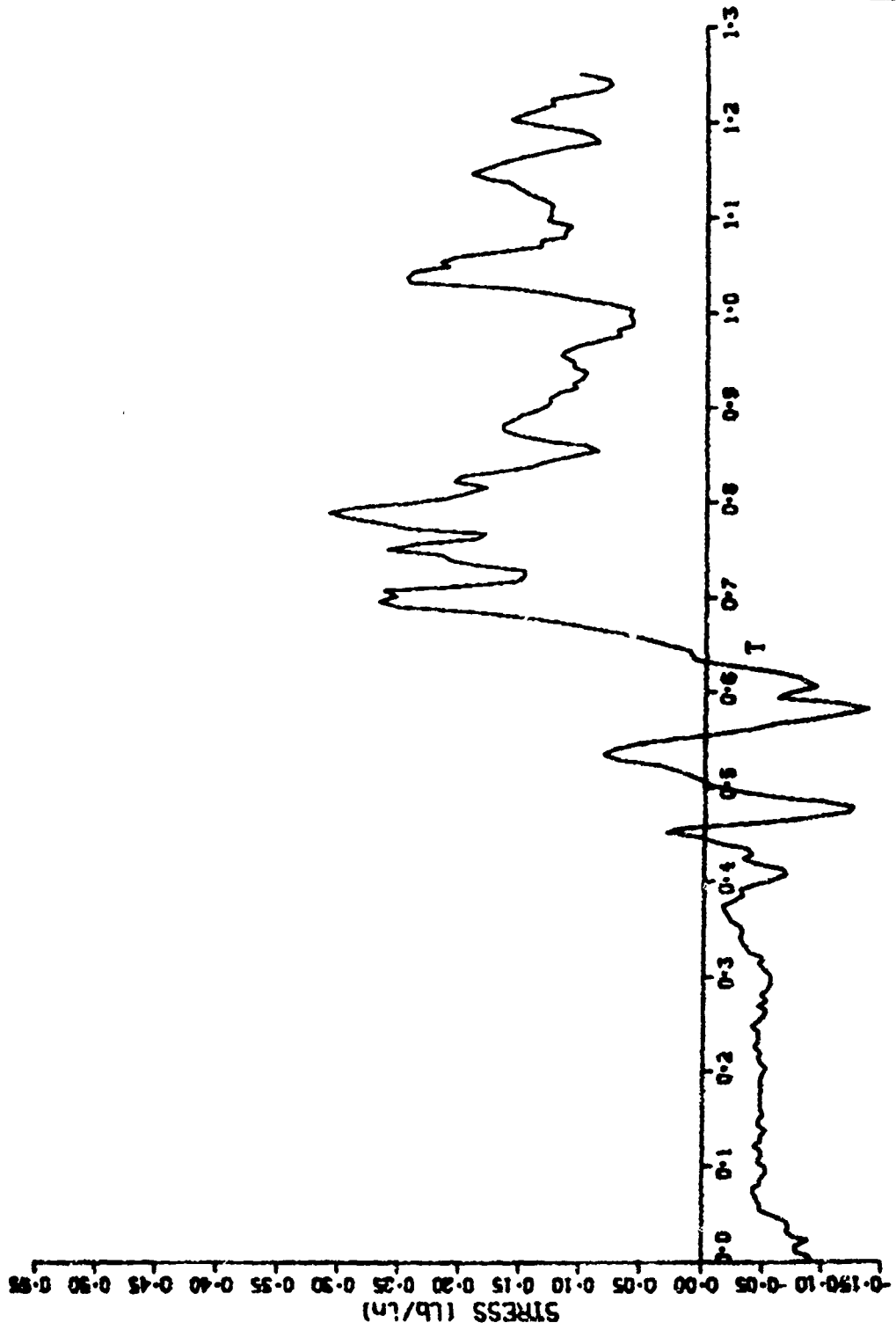
TEST NO. 32 SENSOR 2RS 0-1.2 (in H2O)



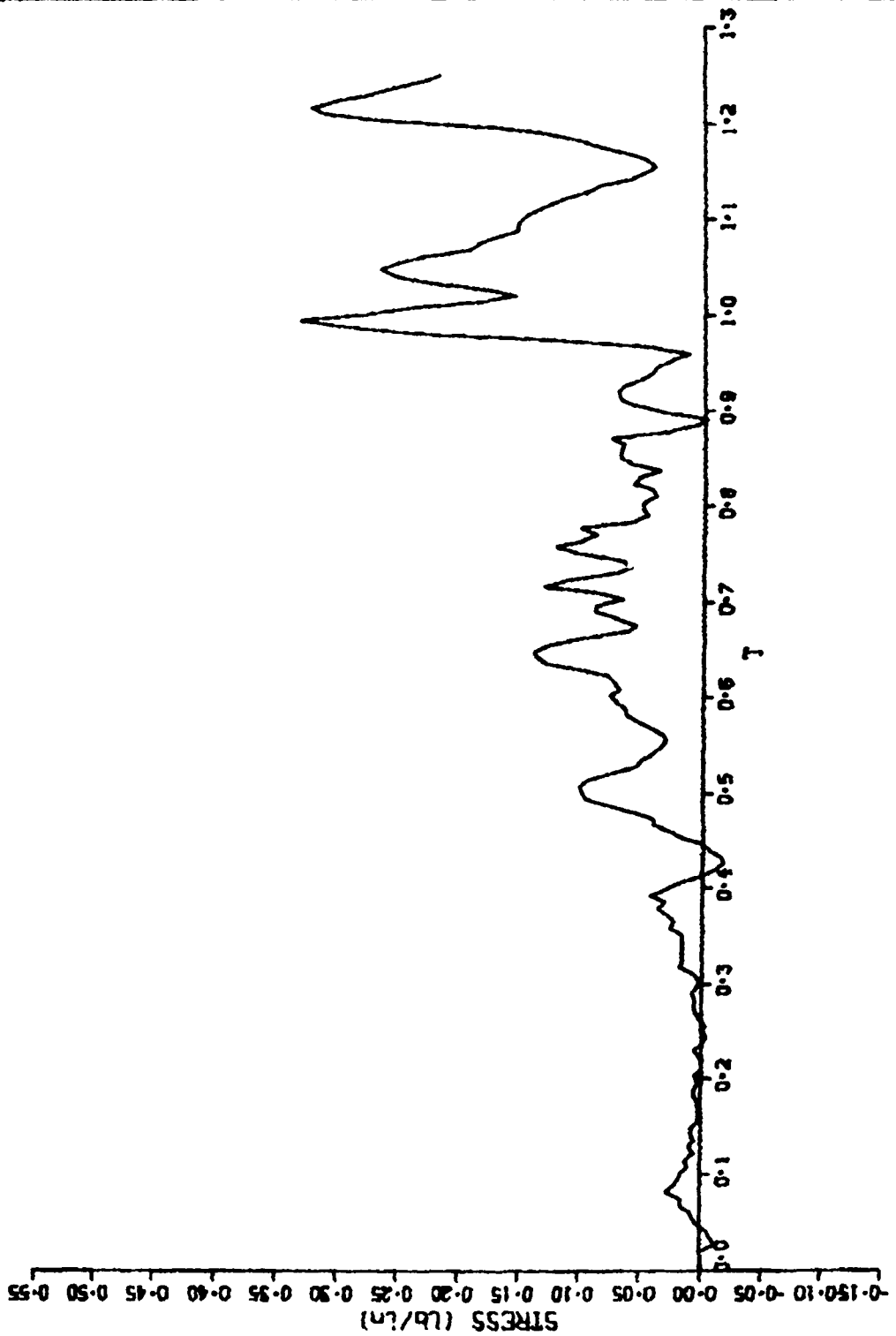
TEST NO.36 SENSOR 2RS 0-1.2(in H2O)



TEST NO.32 SENSOR 3RS 0-1.2 (in H20)

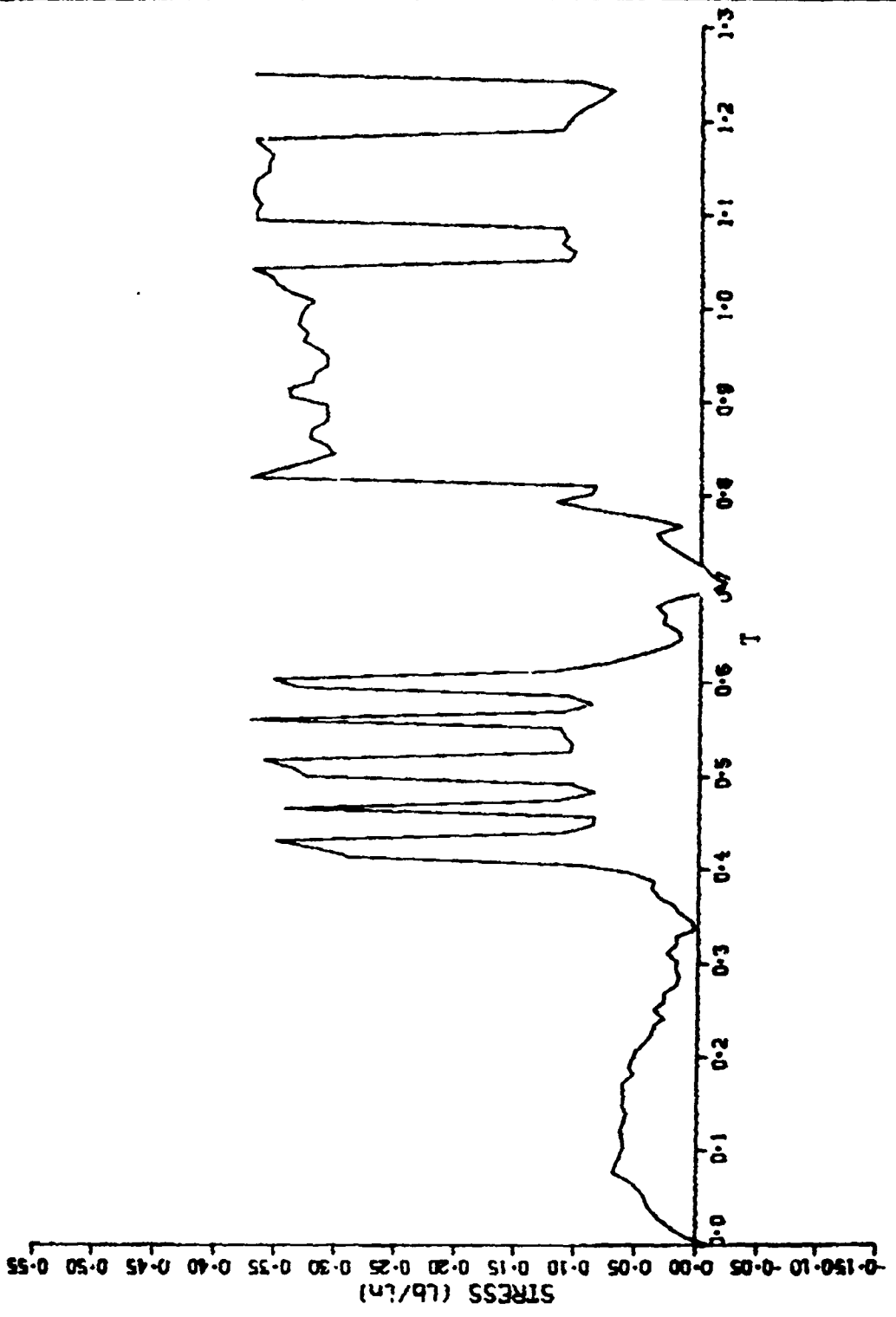


TEST NO.36 SENSOR 3RS 0-1.2(IN H2O)

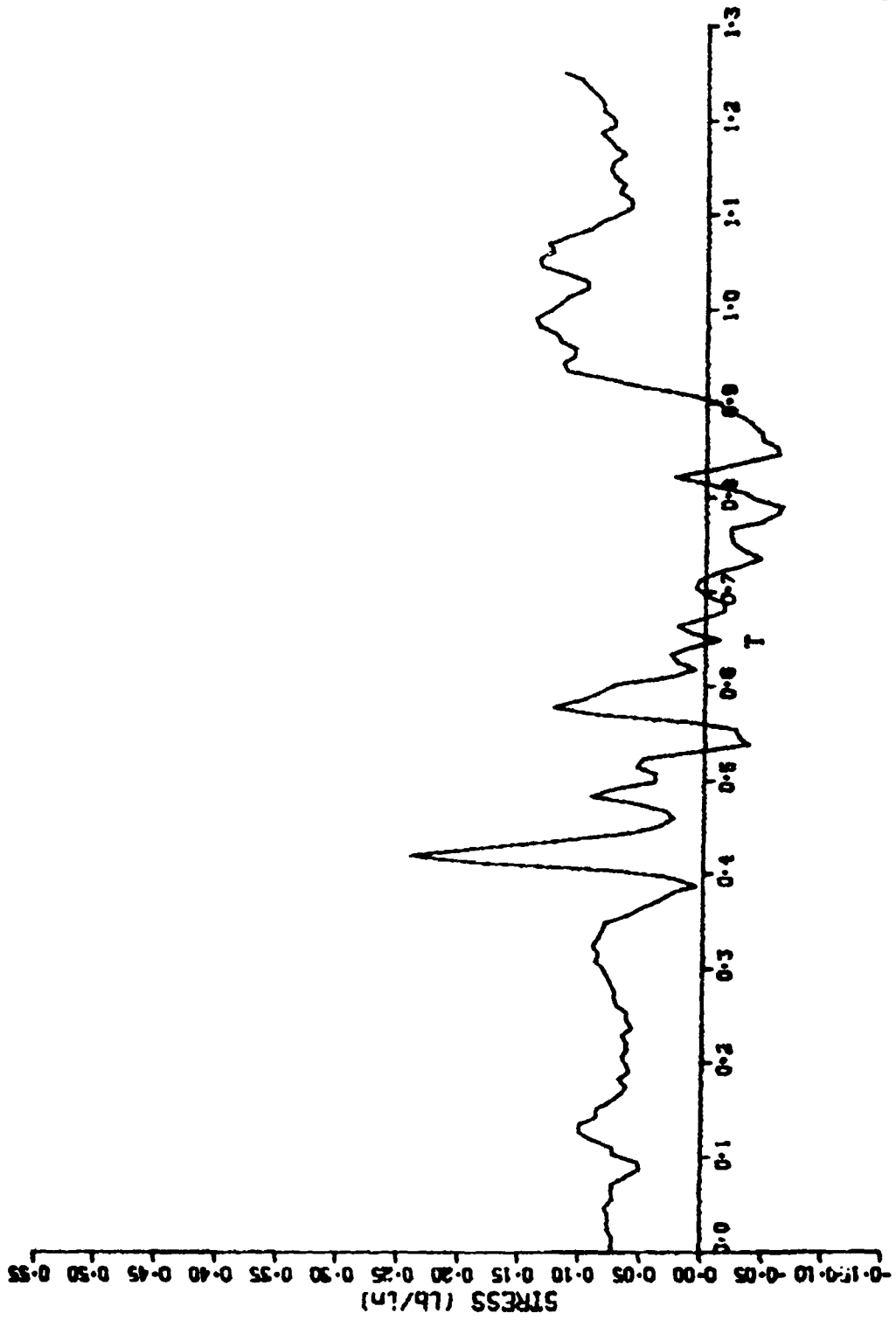




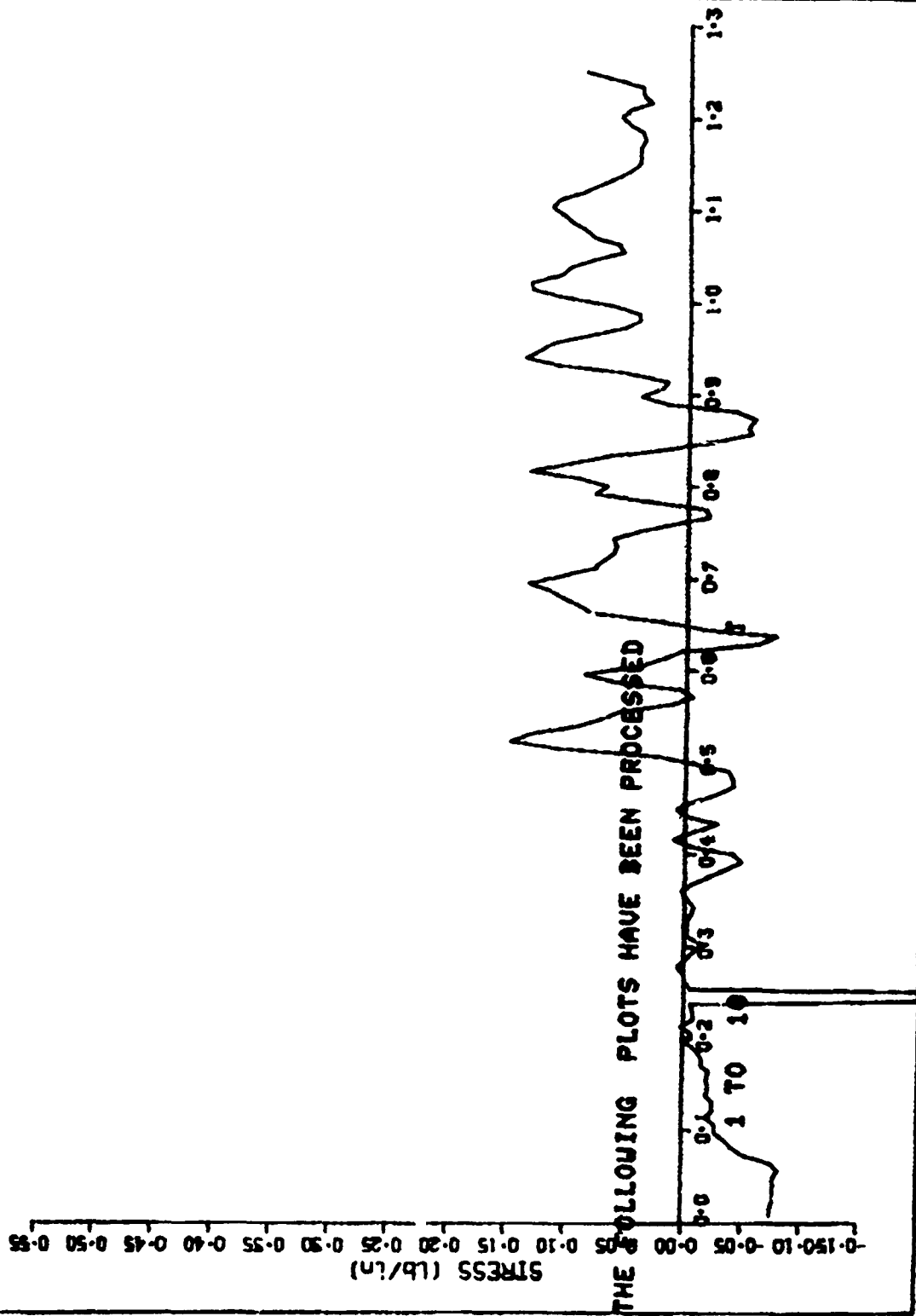
TEST NO. 14 SENSOR 4RS 0-1.2 (in H2O)



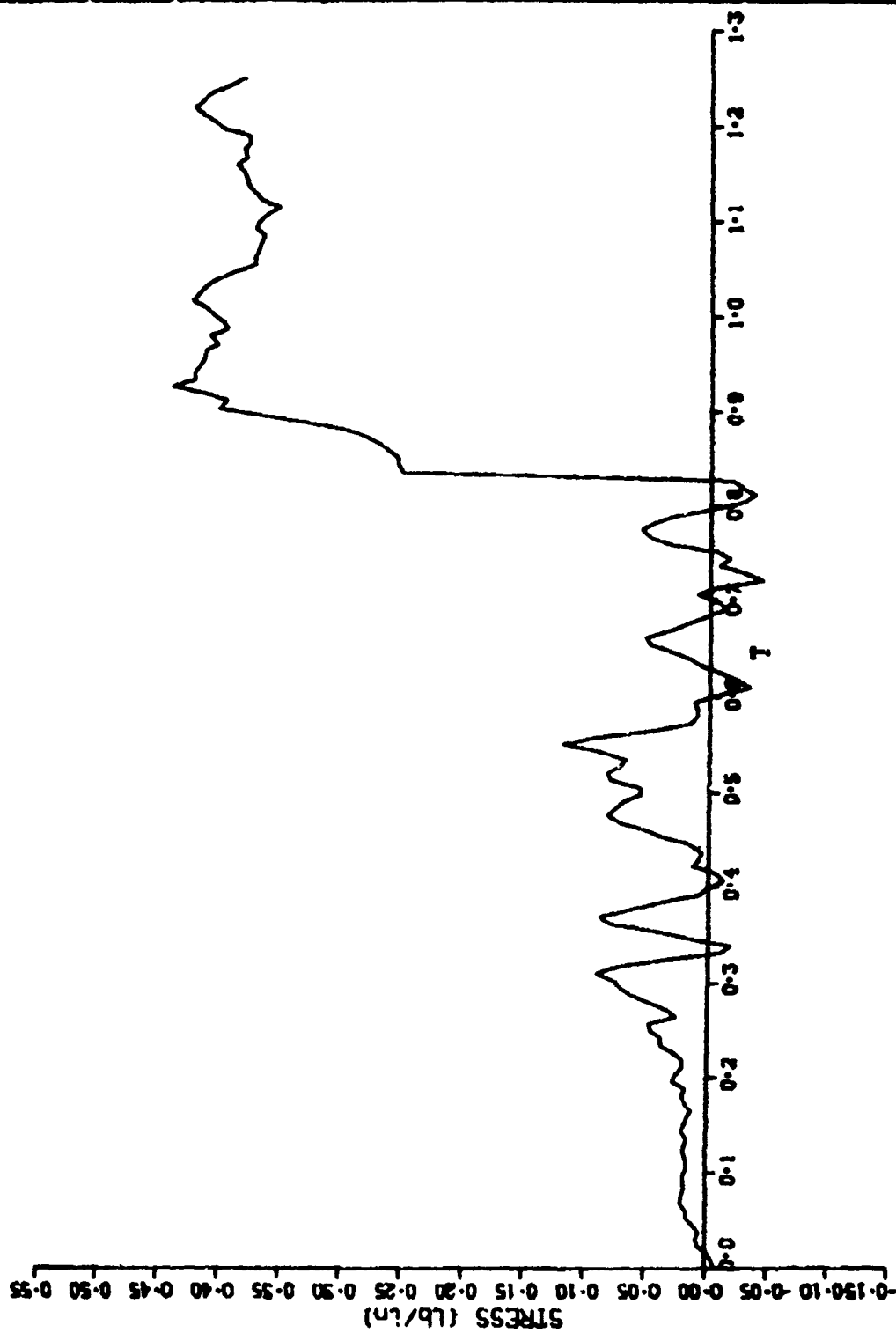
TEST NO. 15 SENSOR 4RS 0-1.2 (in H2O)



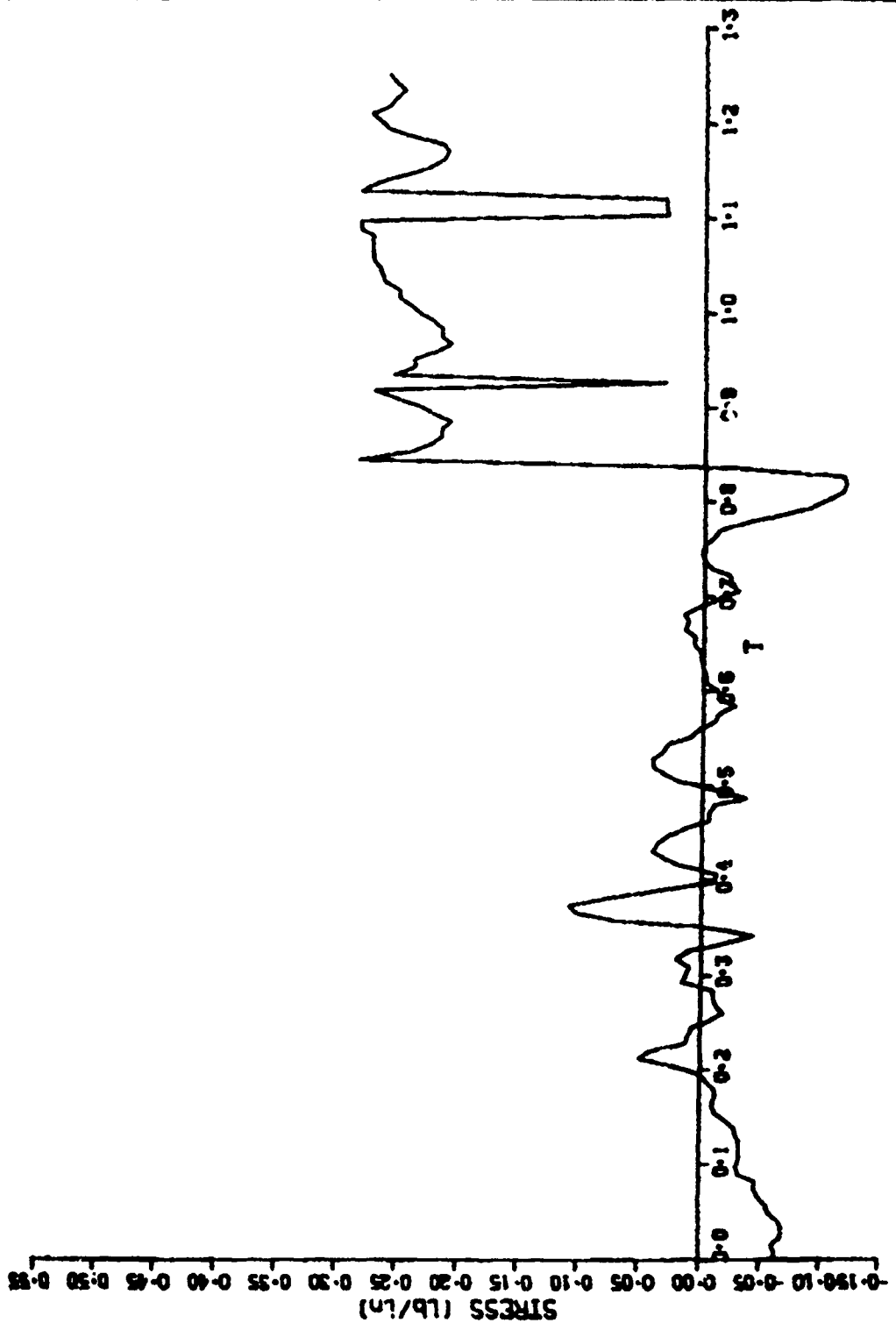
TEST NO. 16 SENSOR 4RS 0-1.2 (in H2O)



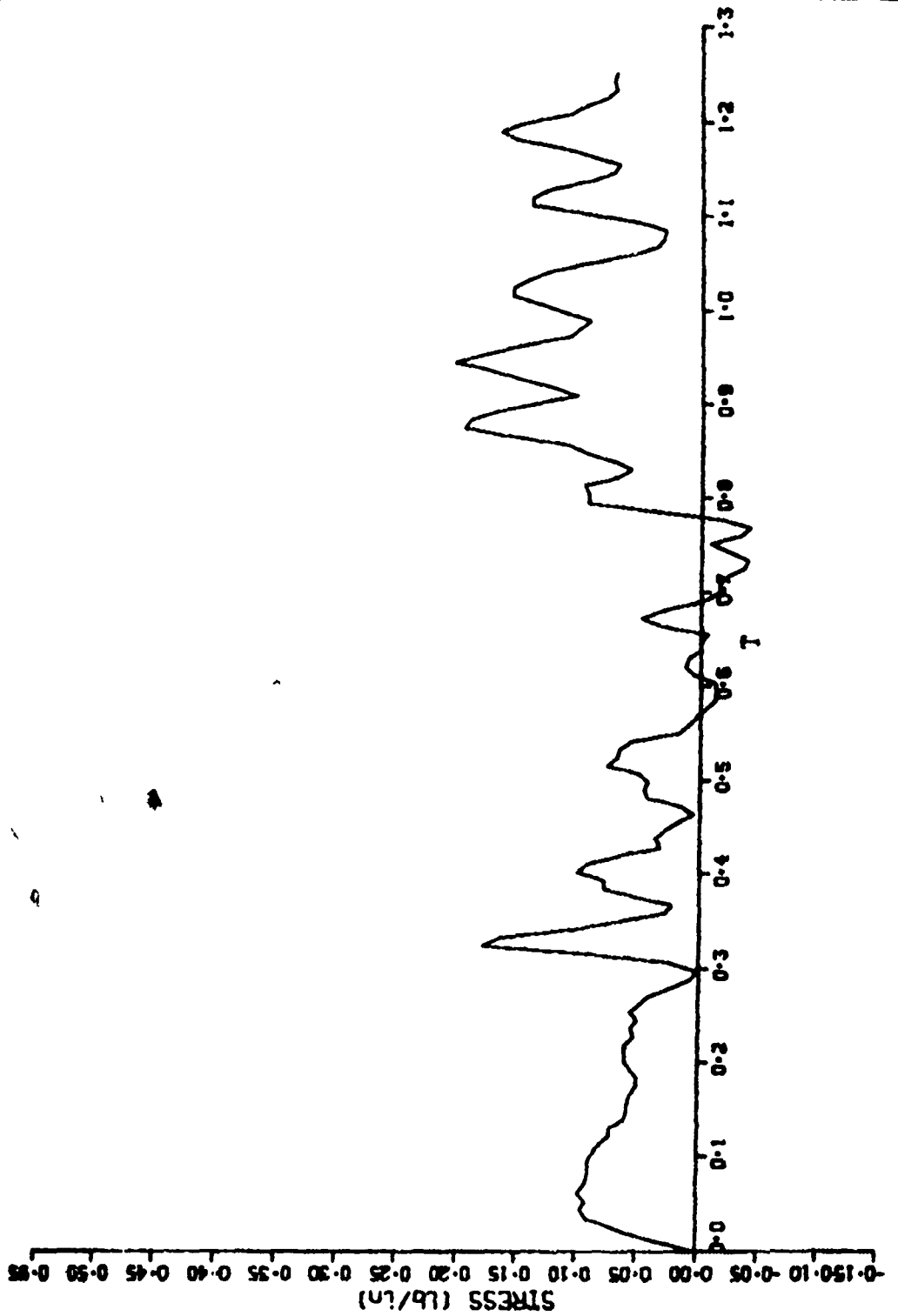
TEST NO. 17 SENSOR 4RS 0-1.2 (in H2O)



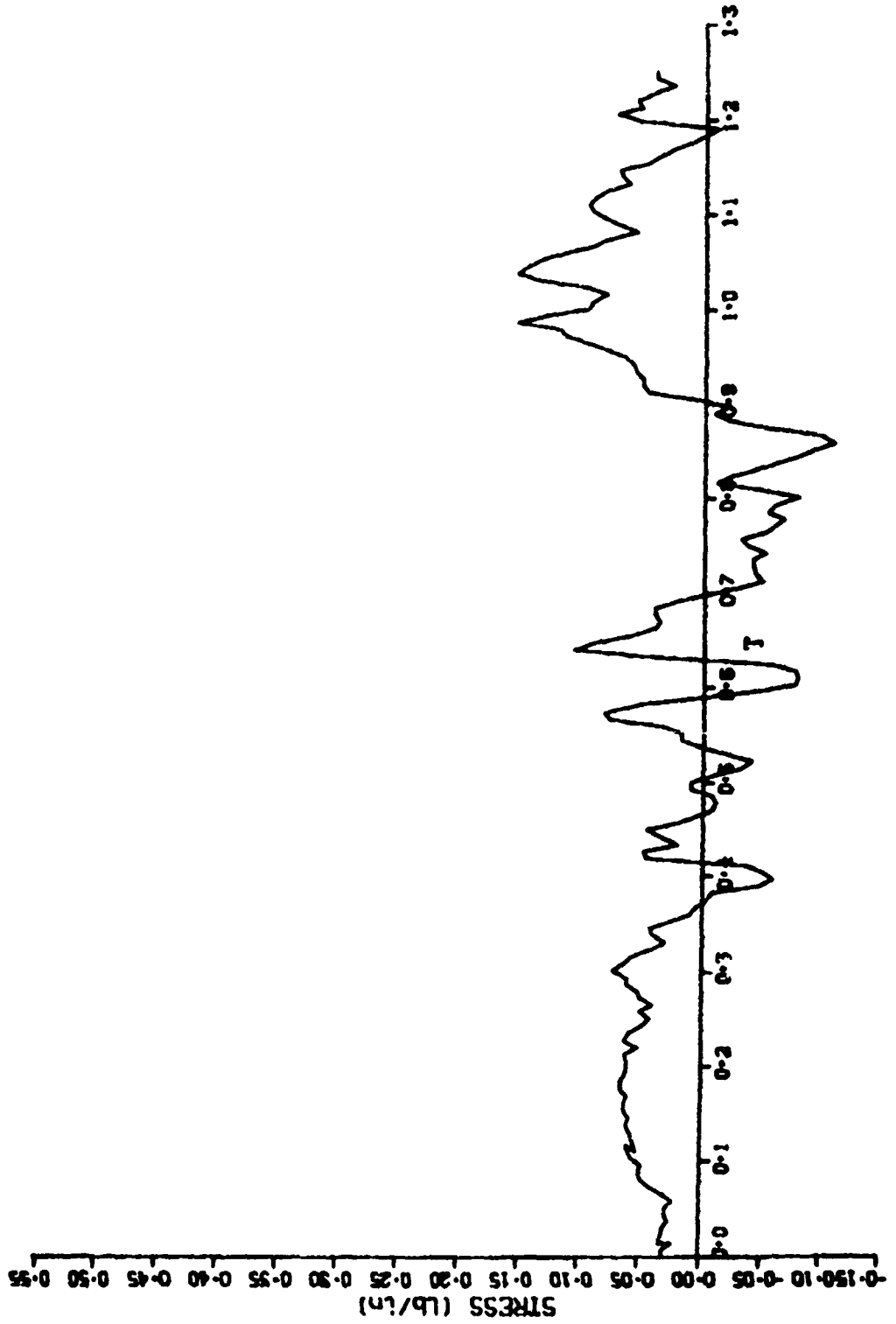
TEST NO. 18 SENSOR 4RS 0-1.2 (in H2O)



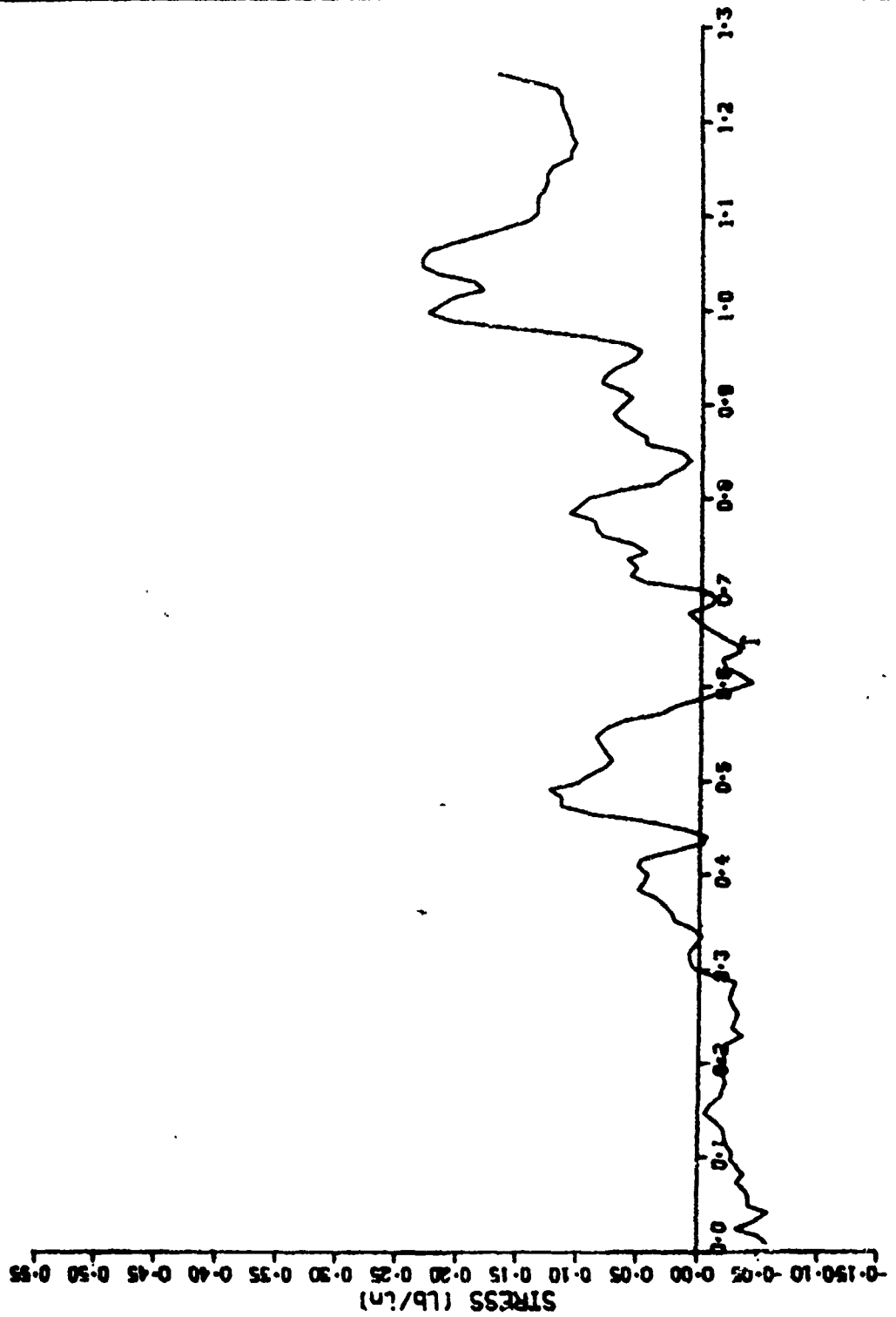
TEST NO. 19 SENSOR 4RS 0-1.2 (in H2O)



TEST NO. 20 SENSOR 4RS 0-1.2 (in H2O)

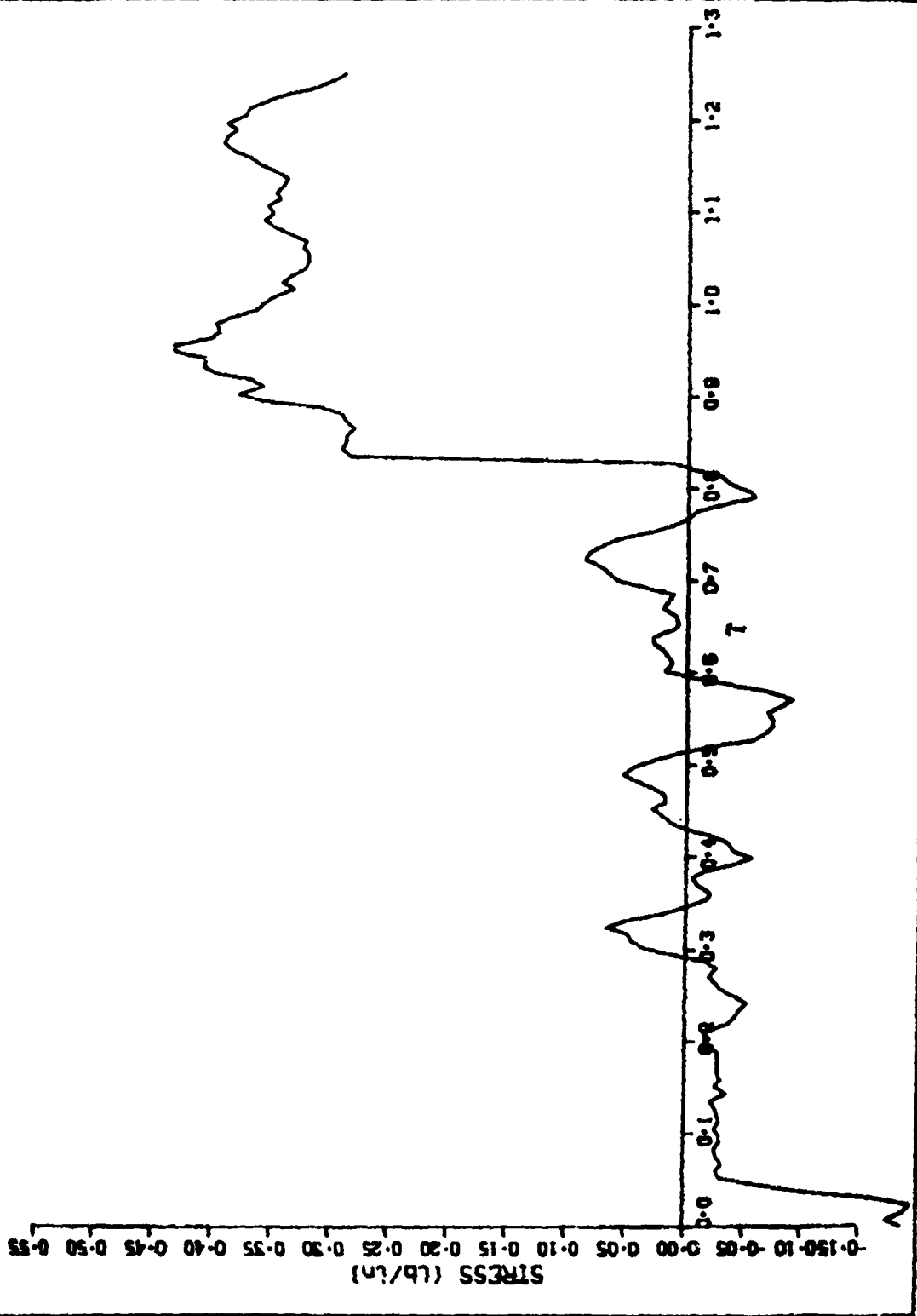


TEST NO.16 SENSOR SRS - SKIRT 0-1.2(in H2O)

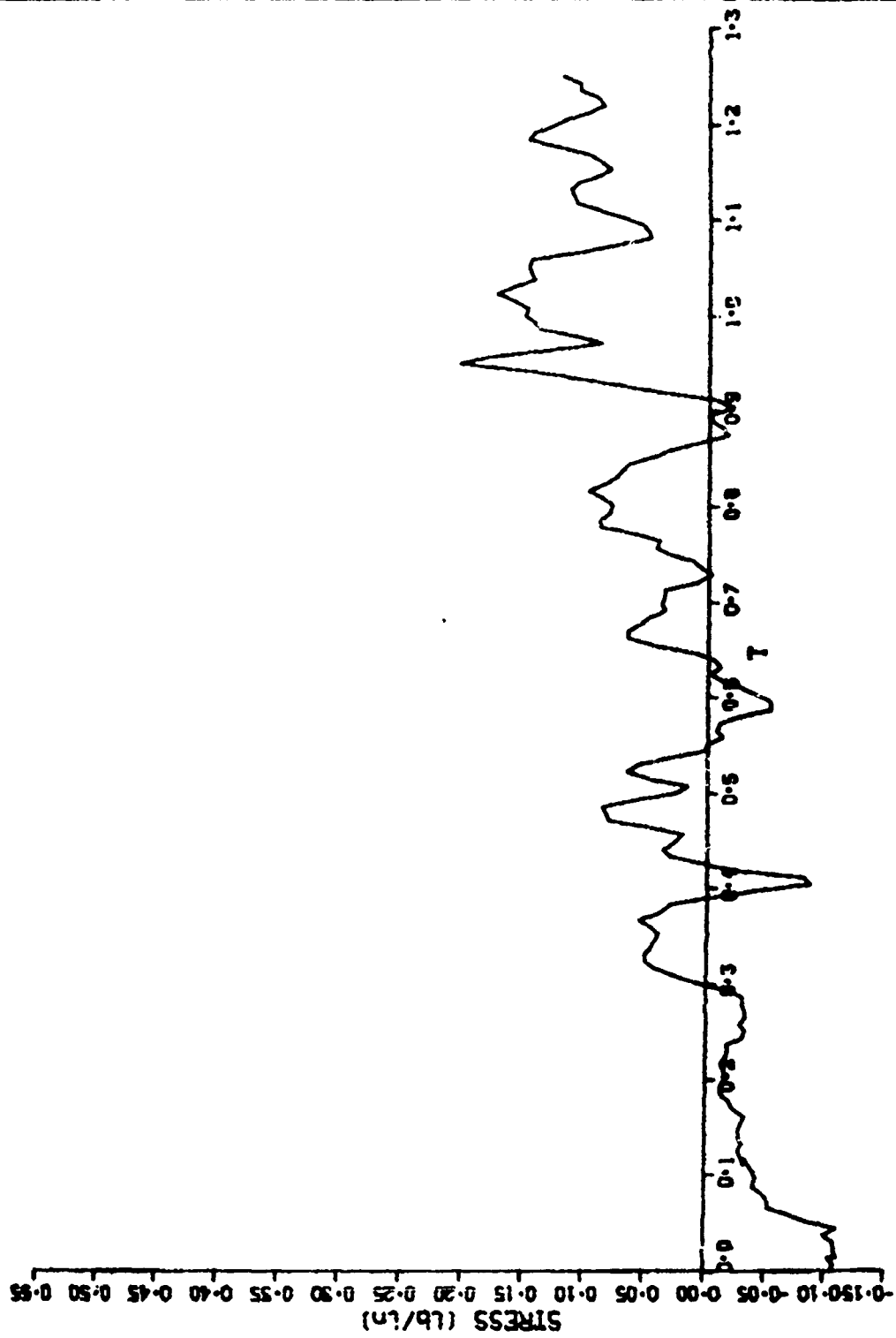




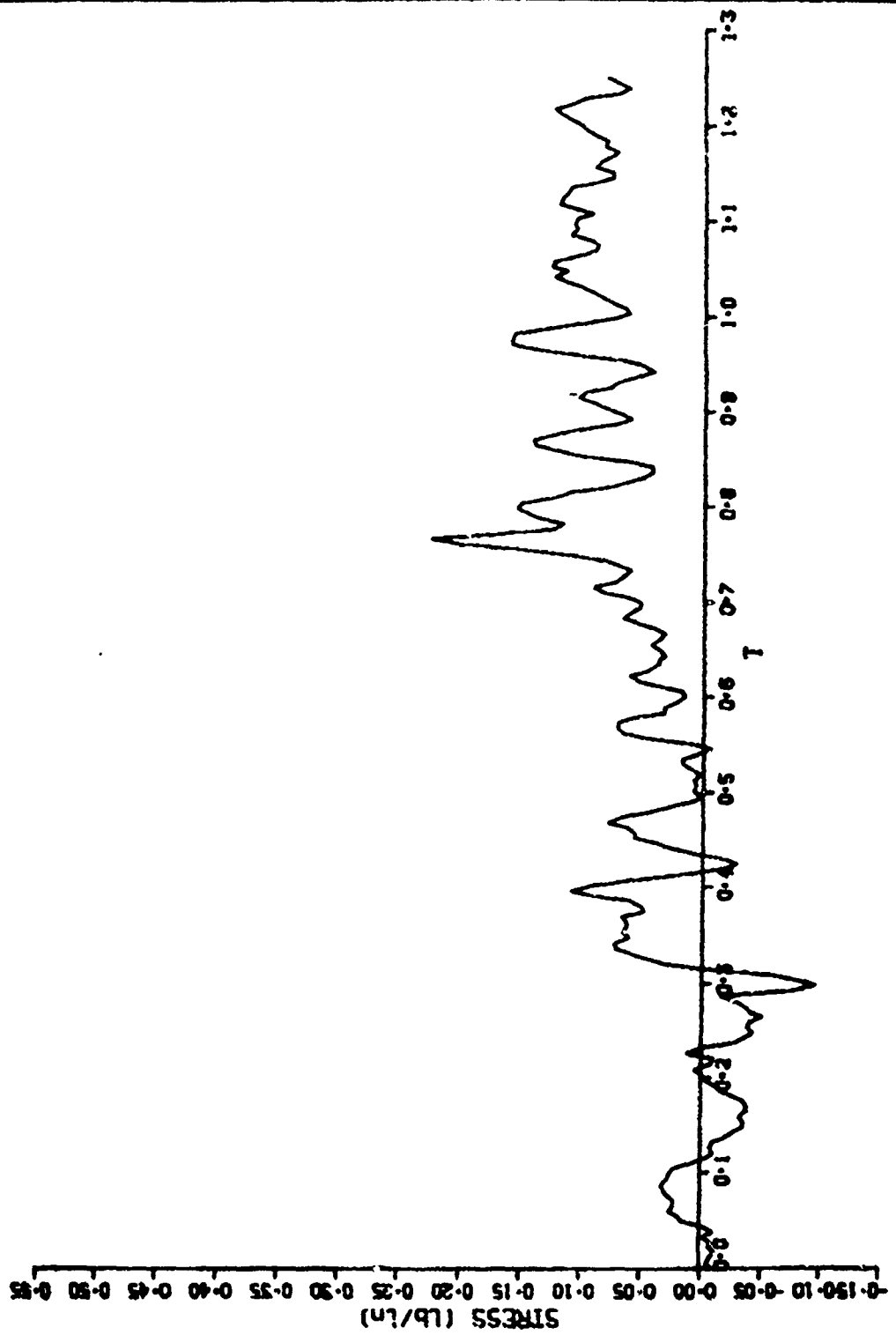
TEST NO. 17 SENSOR SRS - SKIRT 0-1.2 (in H2O)



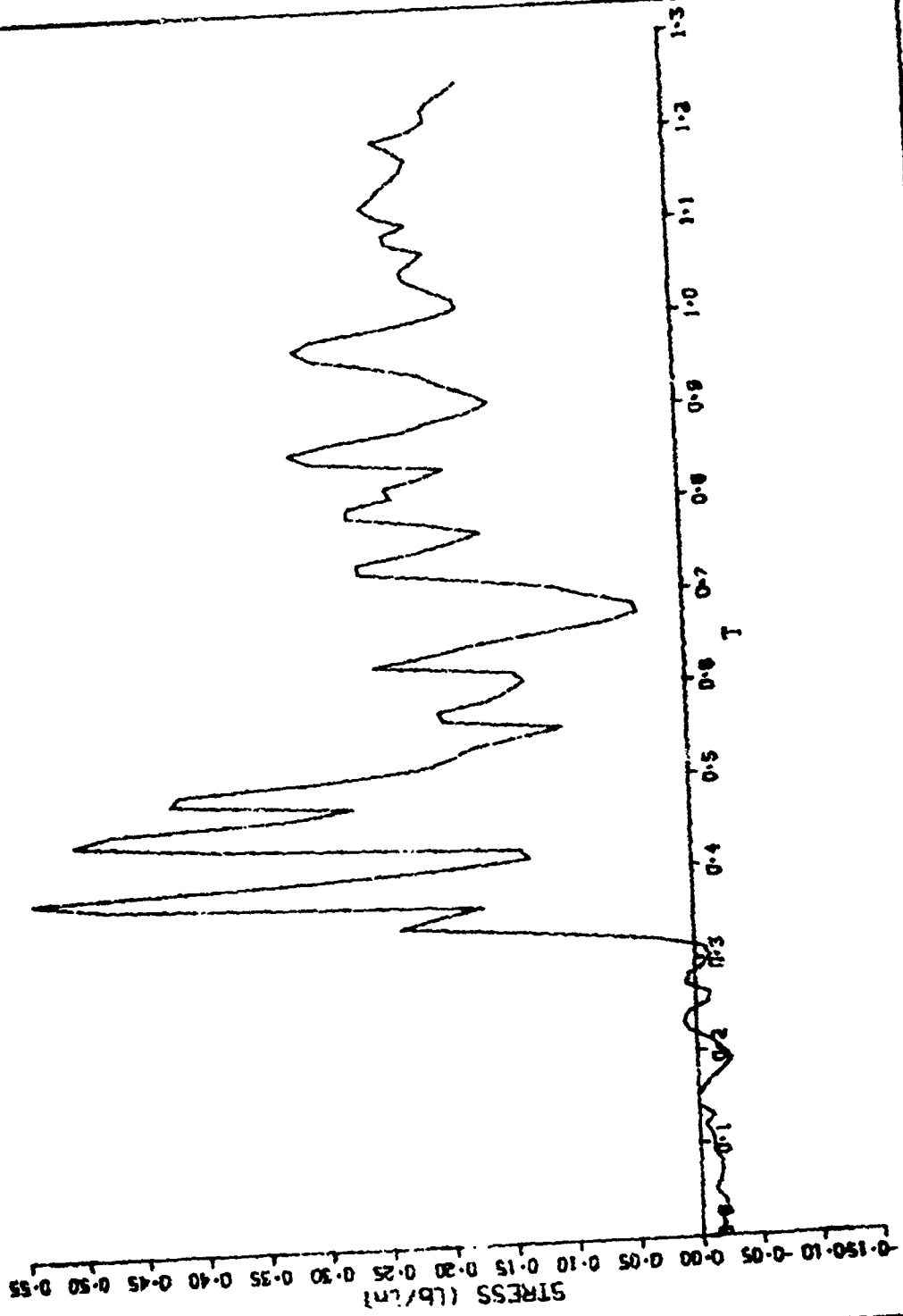
TEST NO. 20 SENSOR 5RS - SKIRT 0-1.2 (in H20)



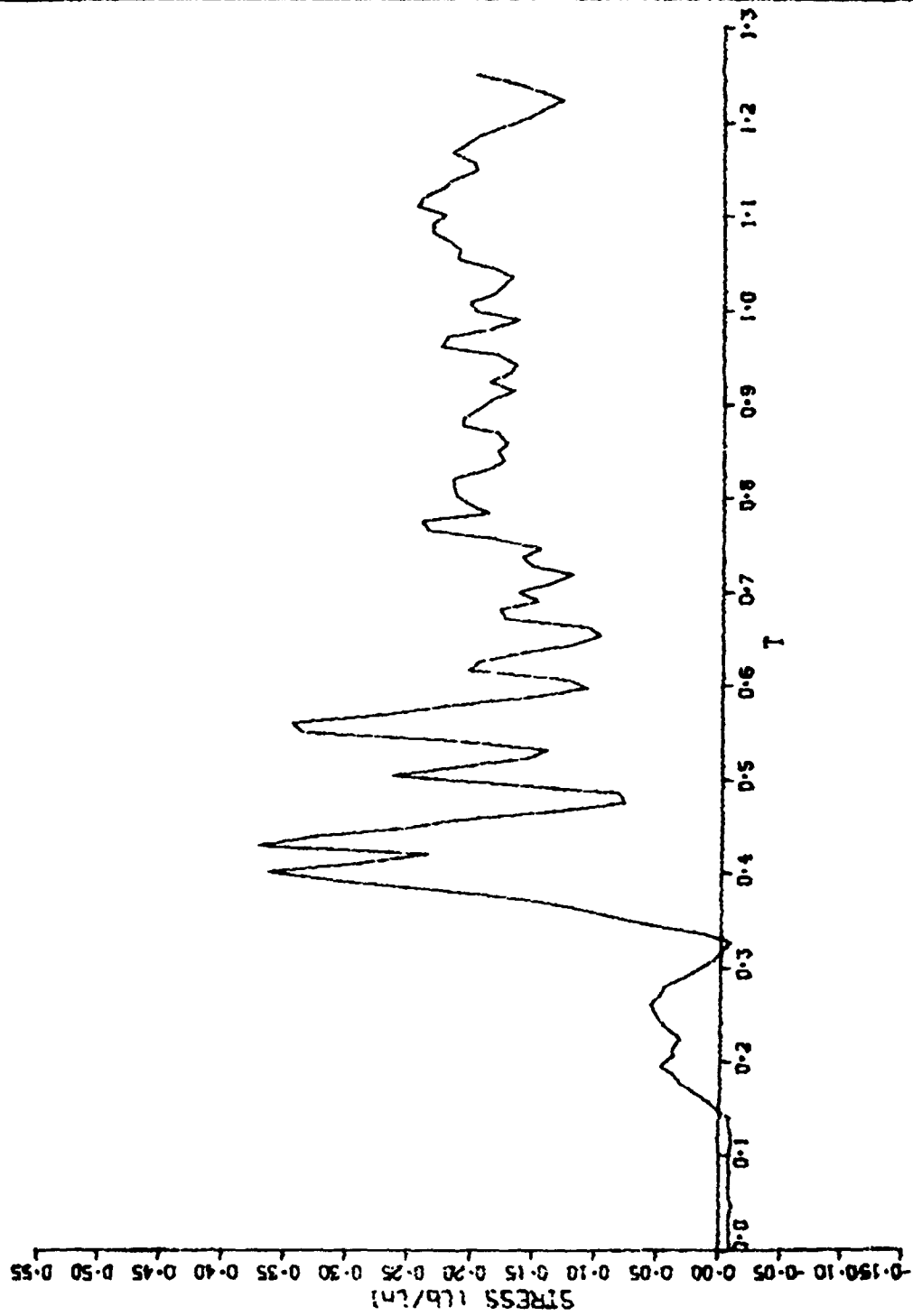
TEST NO.32 SENSOR SRS - SKIRT 0-1.2 (in H2O)



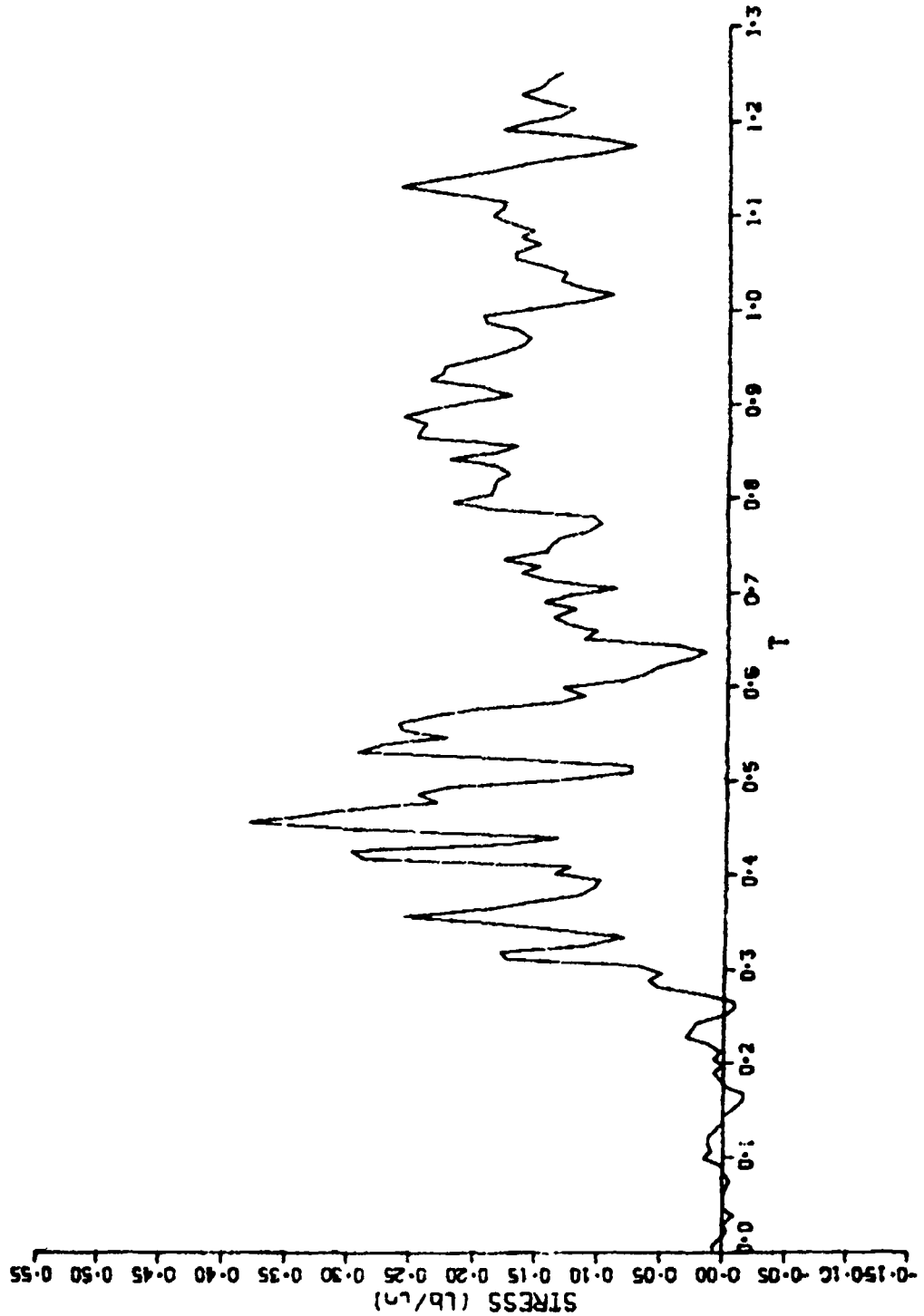
TEST NO.21 SENSOR IRS - VENT 0-1.6 (in H2O)



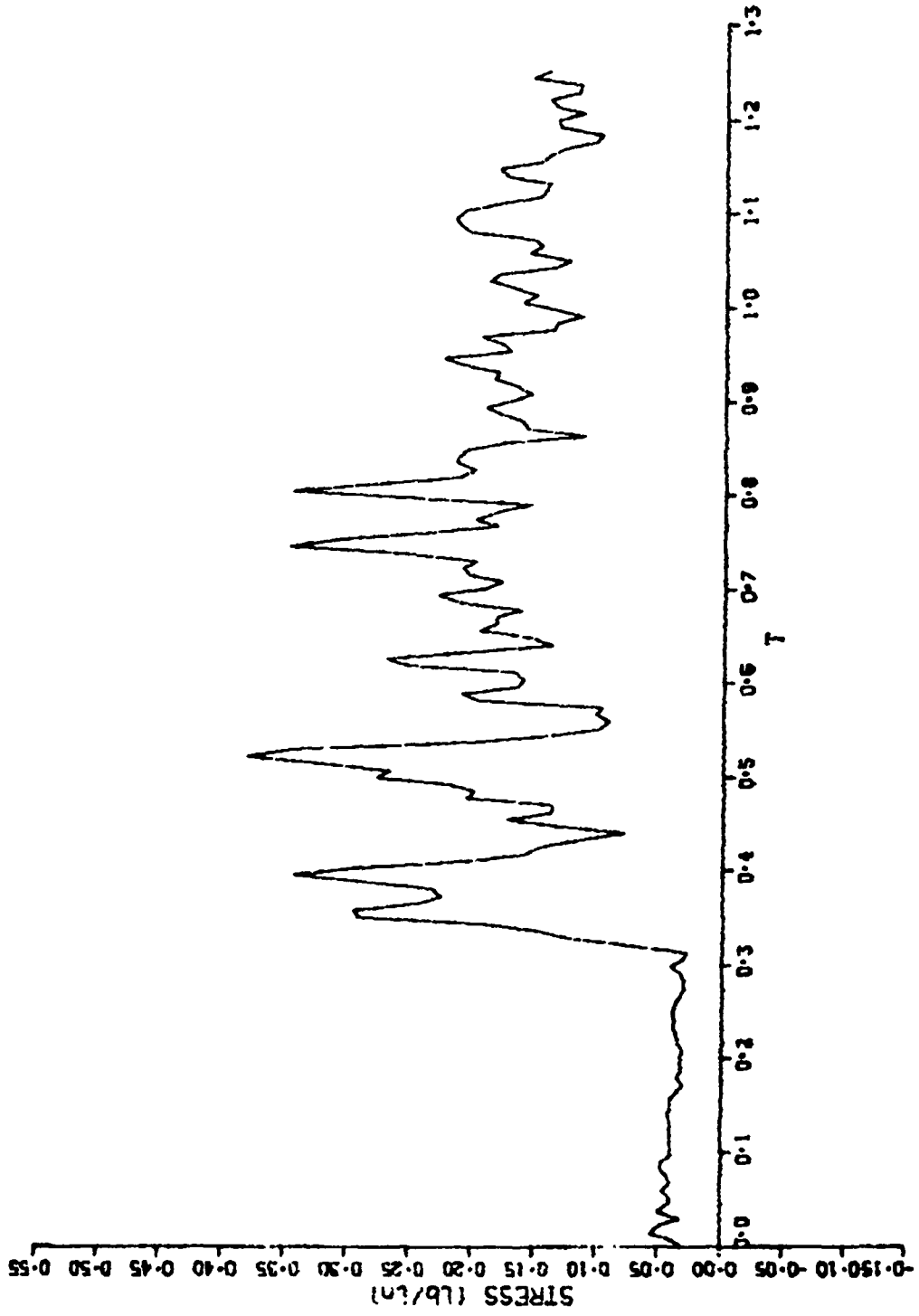
TEST NO.22 SENSOR IRS - VENT Q-1.6 (in H2O)



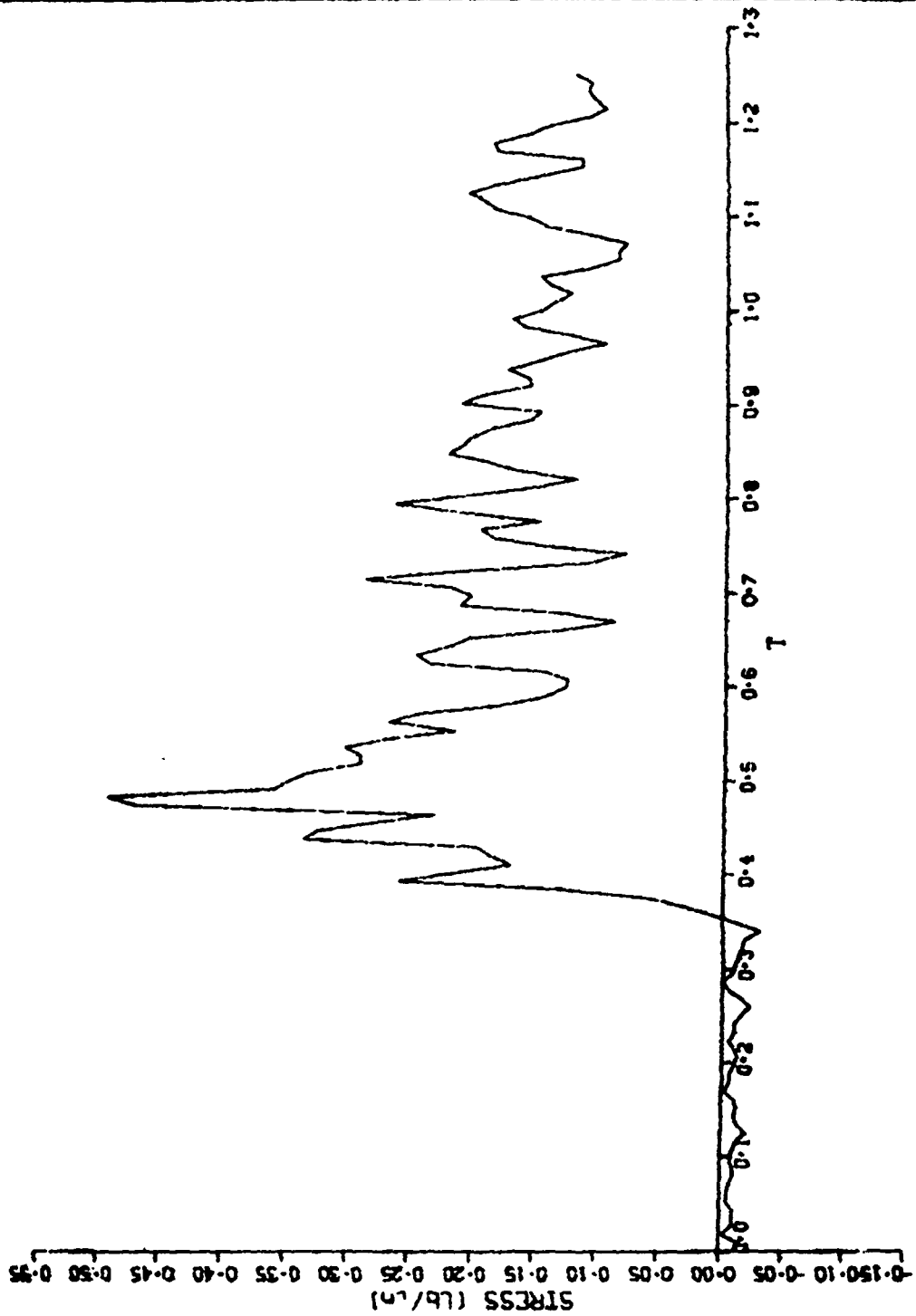
TEST NO.26 SENSOR IRS - VENT 0-1.6 (in H2O)



TEST NO.33 SENSOR IRS - VENT 0-1.6 (in H2O)

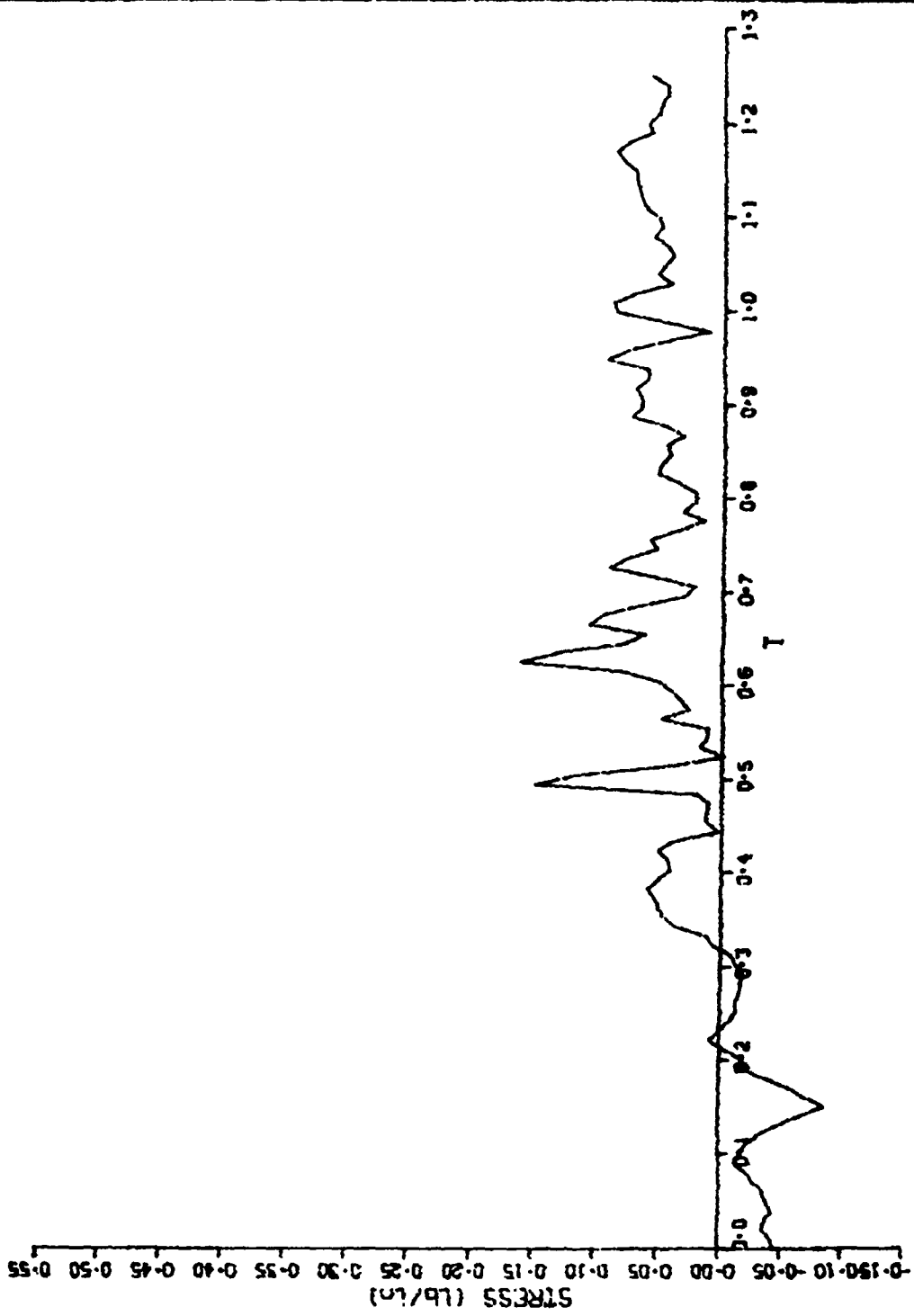


TEST NO. 37 SENSOR IRS - VENT 0-1.6 (in H2O)

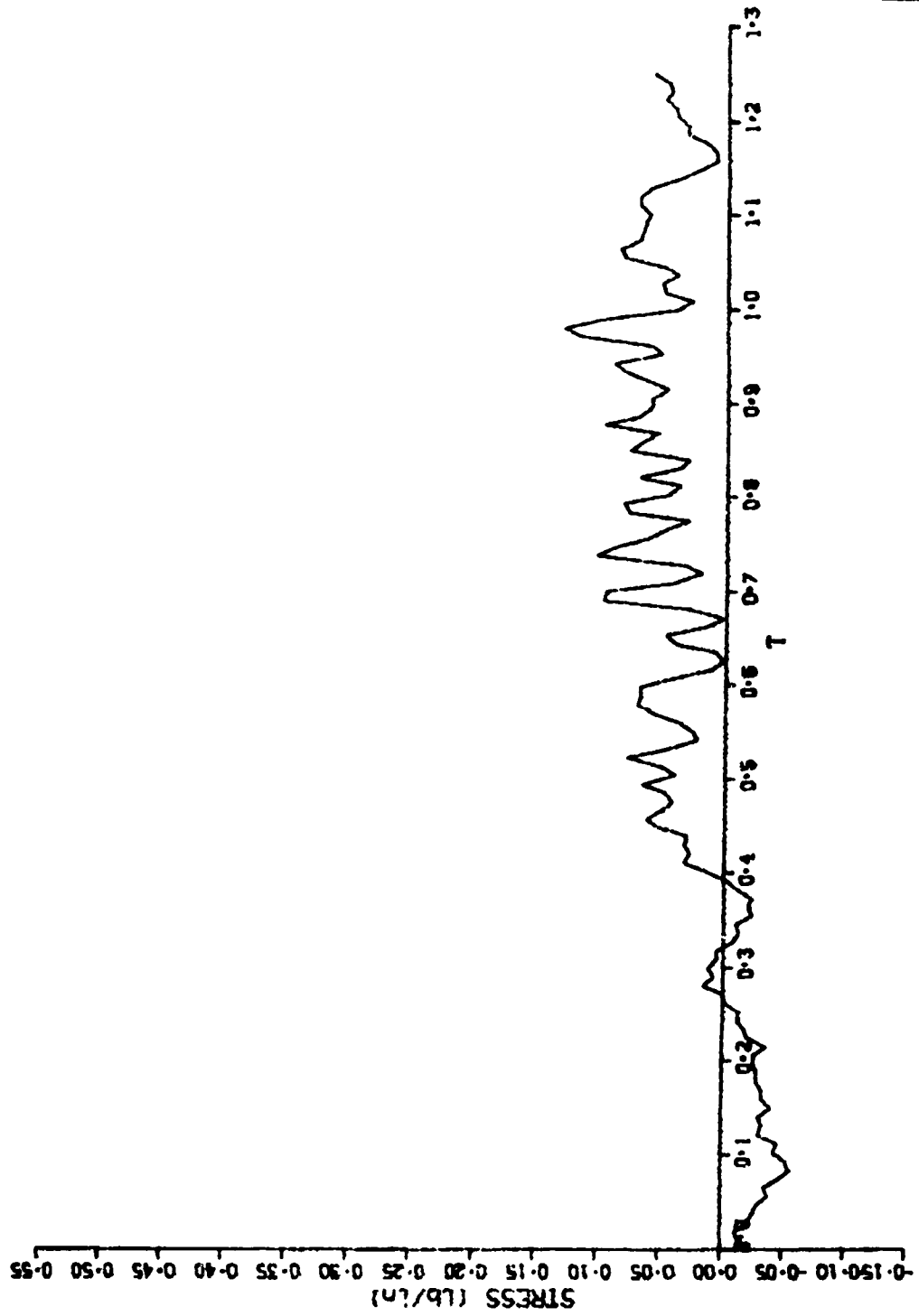




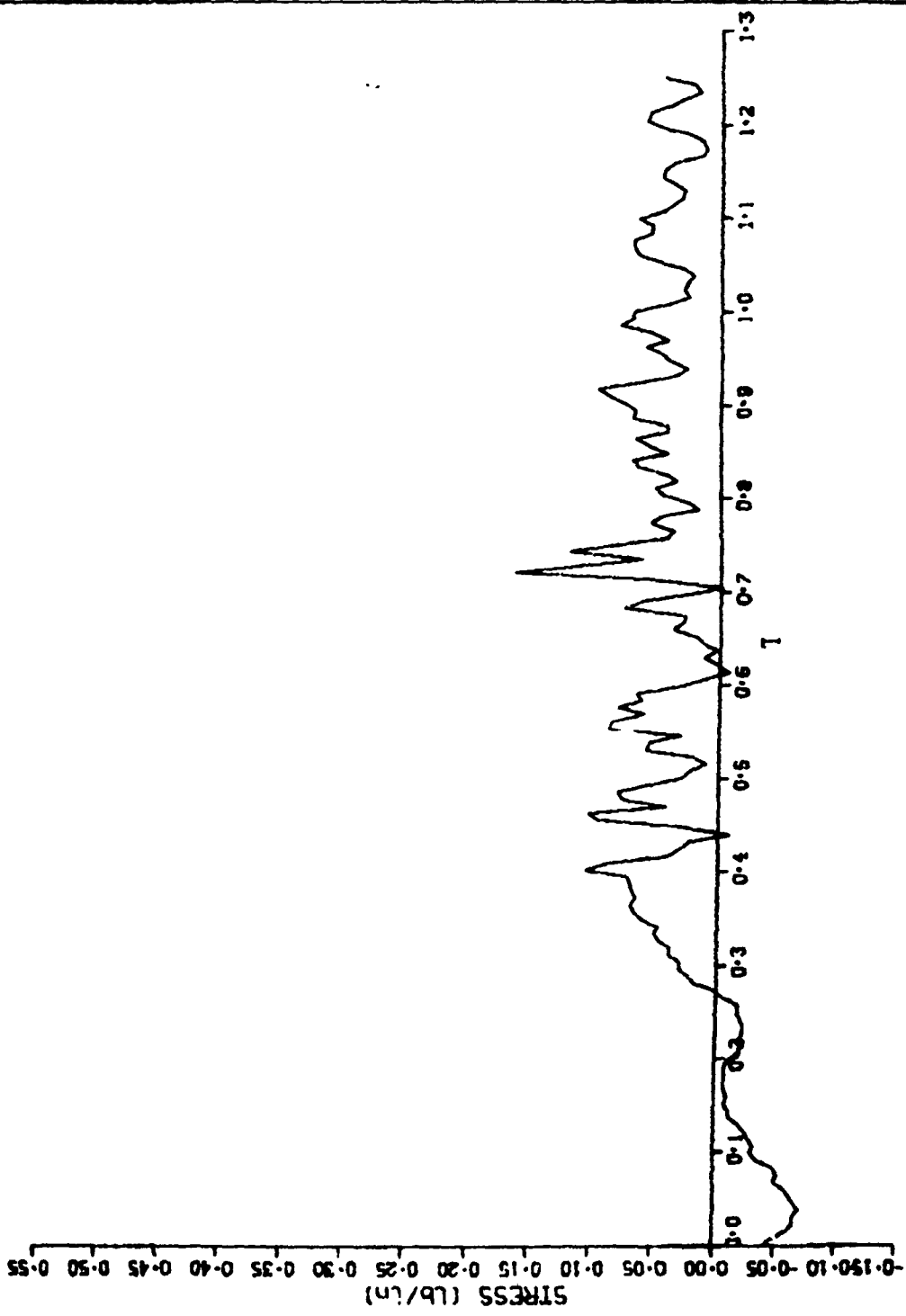
TEST NO.21 SENSOR 2RS 0-1.6 (in H2O)



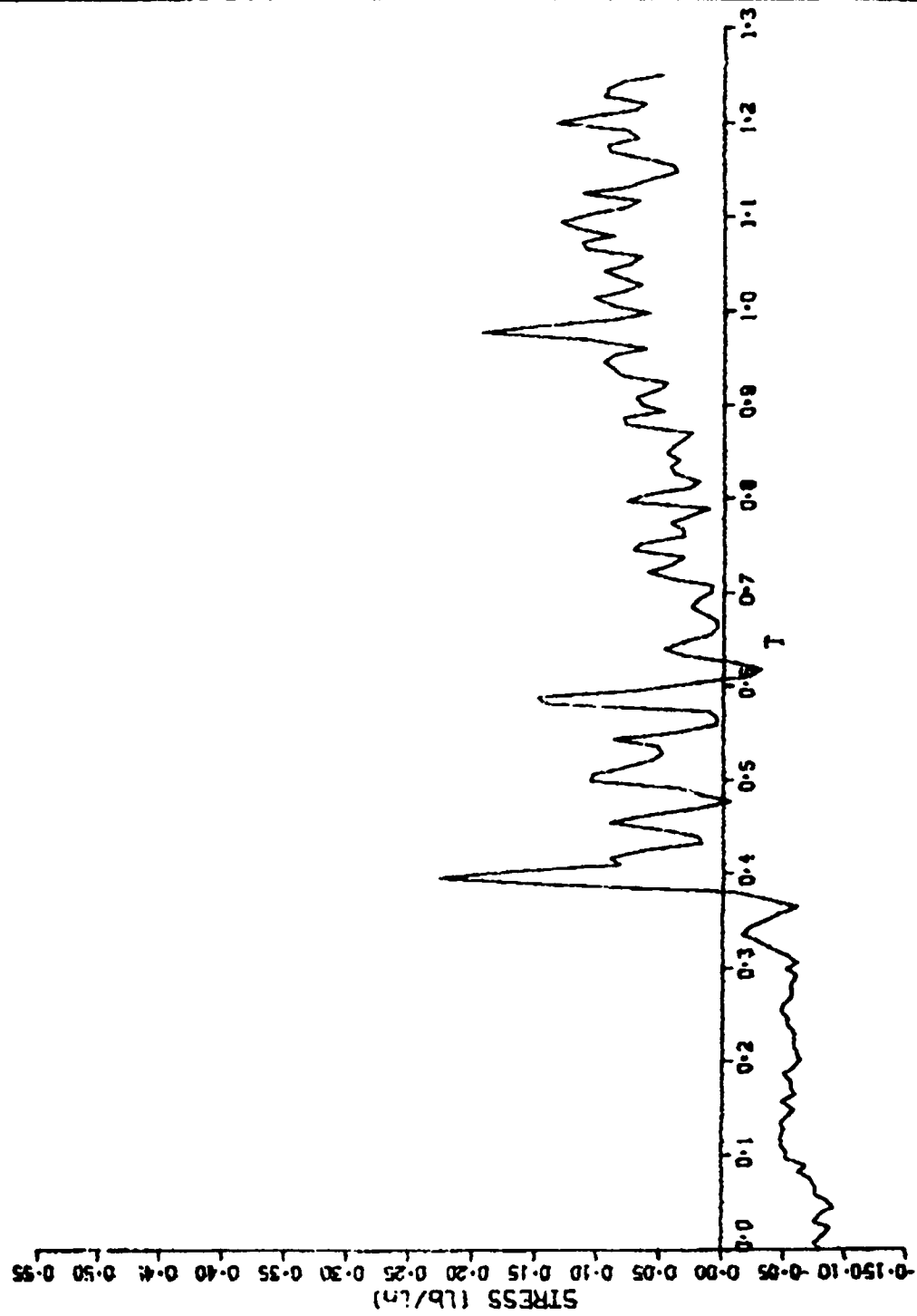
TEST NO.22 SENSOR 2RS 0-1.6(in H2O)



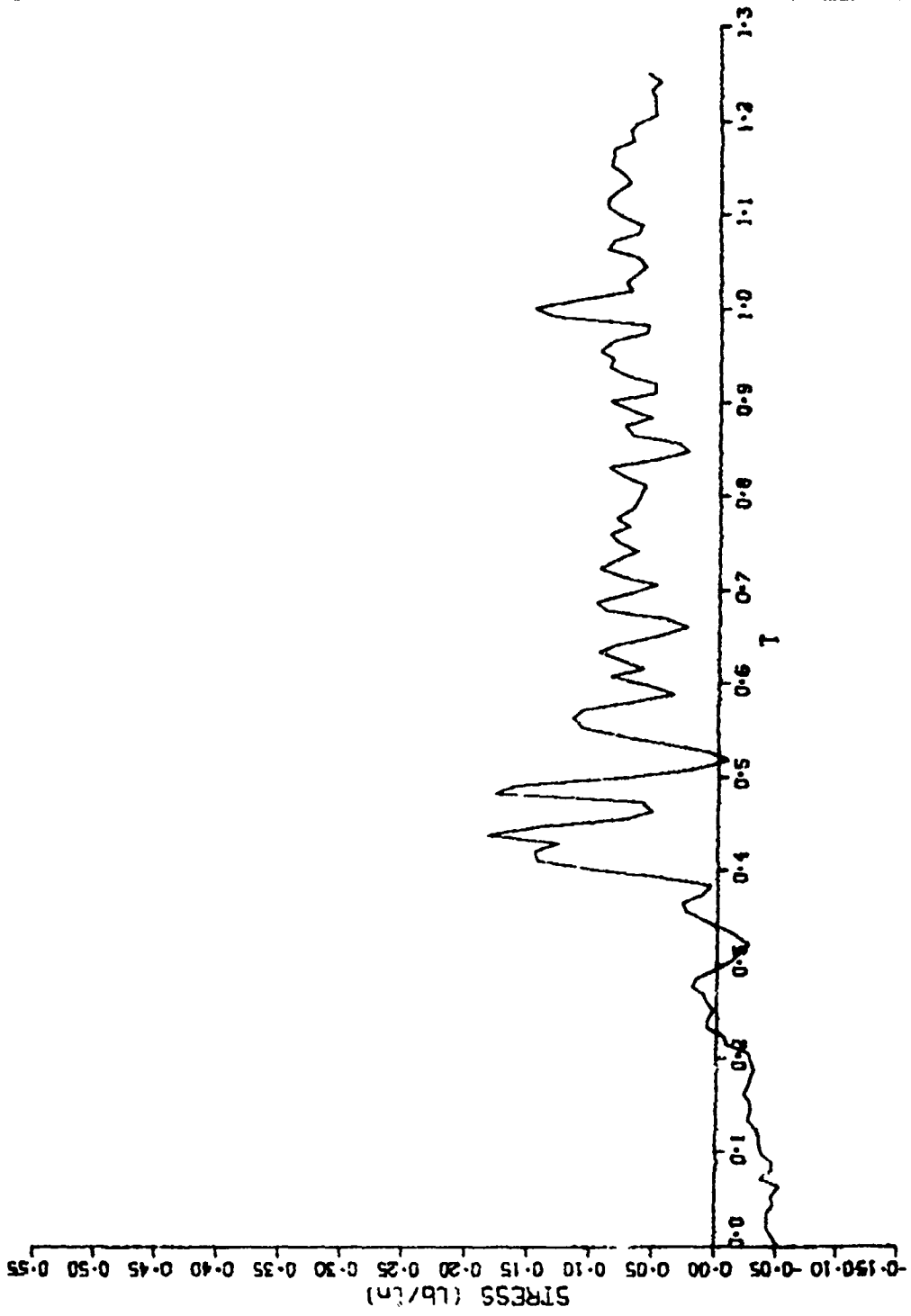
TEST NO.26 SENSOR 2RS 0-1.6(in H20)



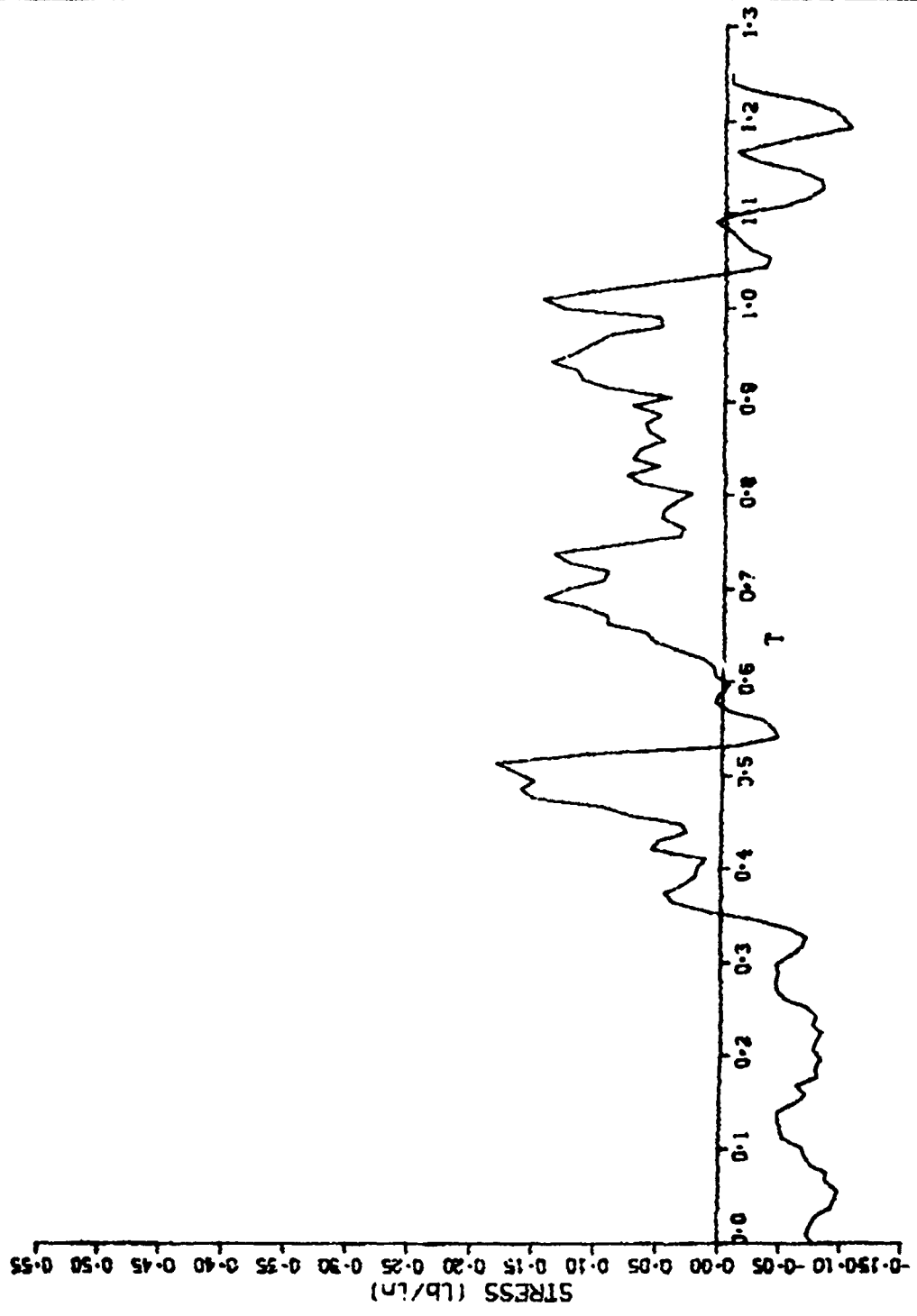
TEST NO. 33 SENSOR 2RS 0-1.6 (in H2O)



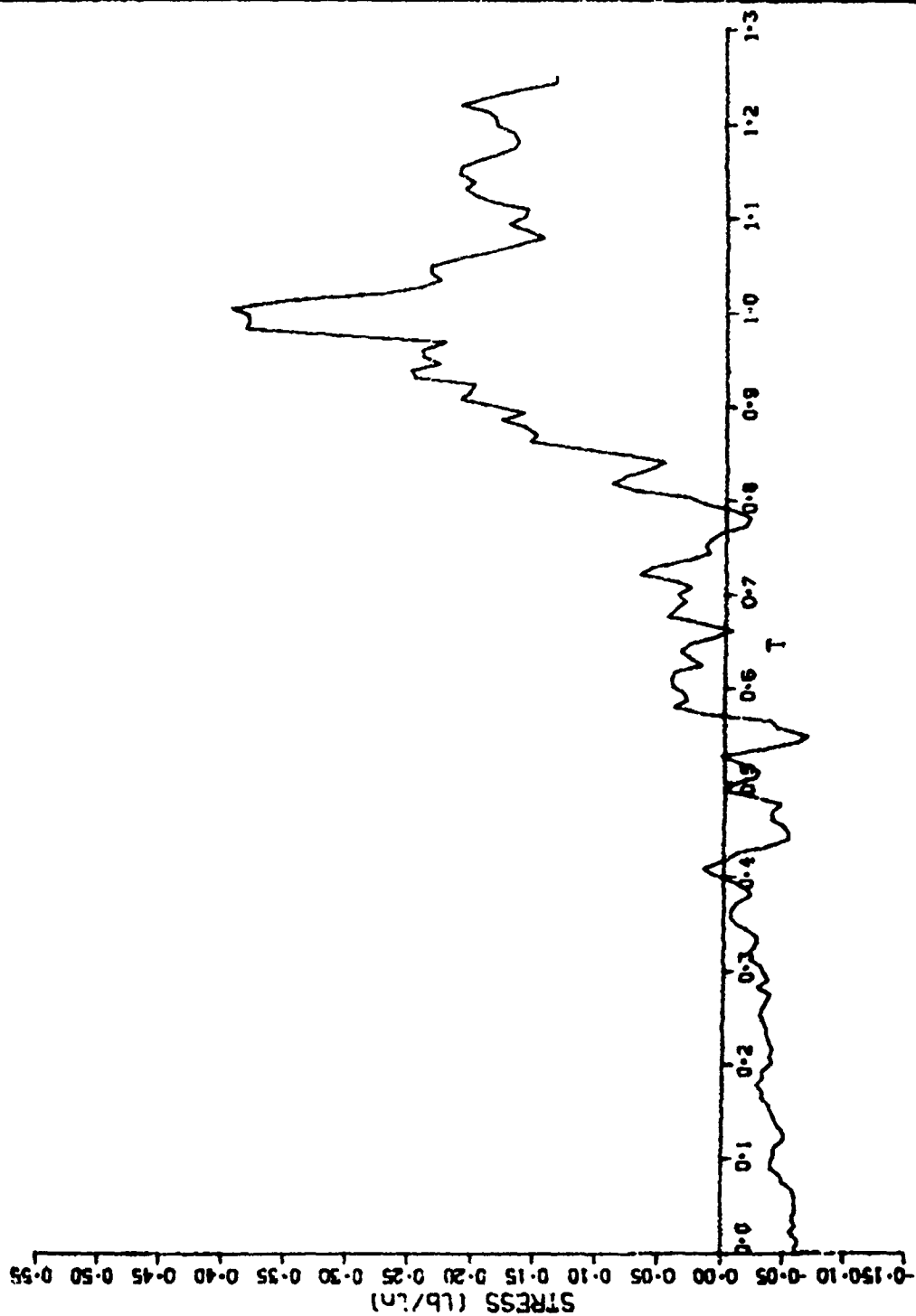
TEST NO. 37 SENSOR 2RS 0-1.6 (Ln H20)



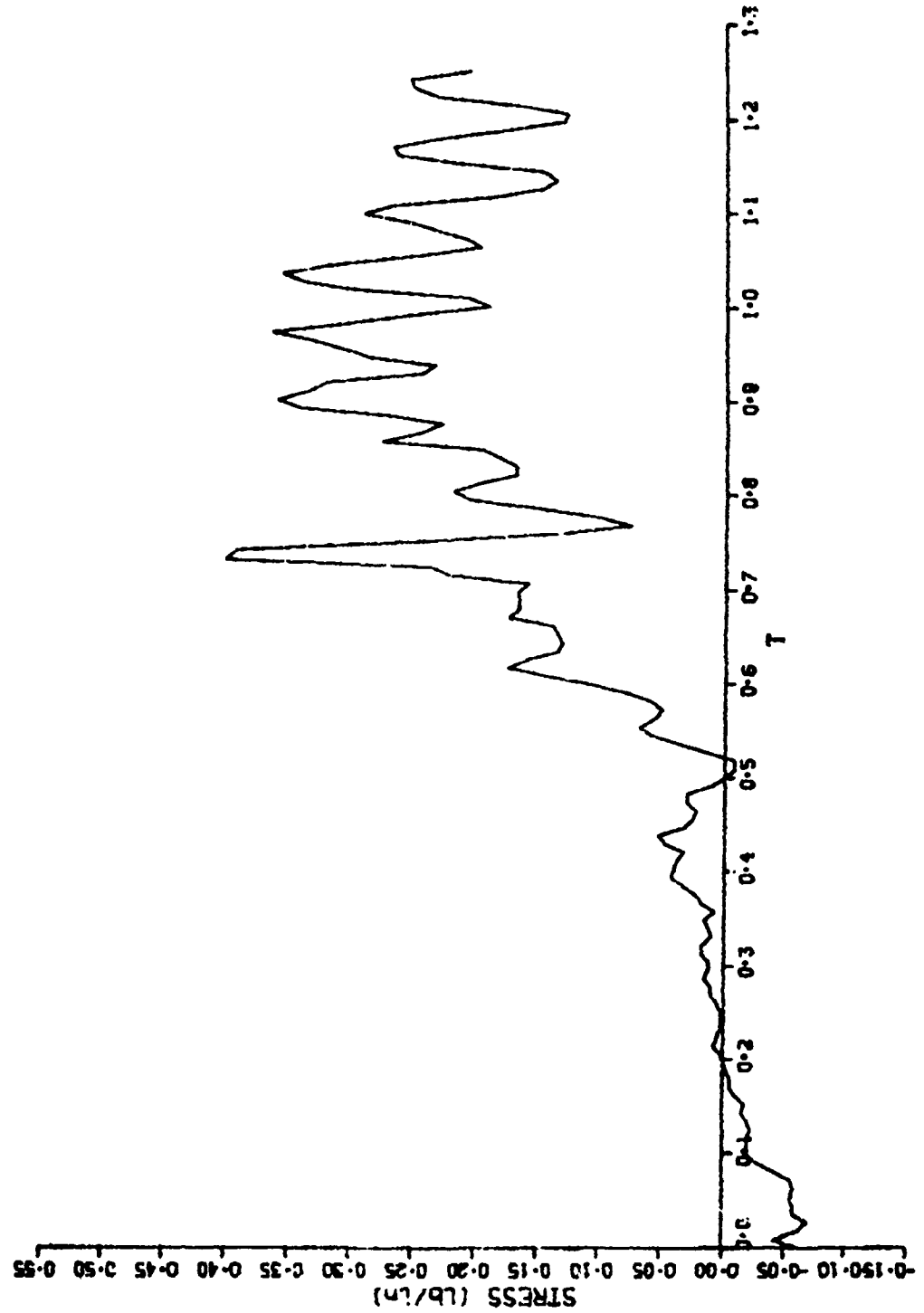
TEST NO.22 SENSOR 3RS 0-1.6(in H2O)



TEST NO. 33 SENSOR 3RS 0-1.6 (in H2O)

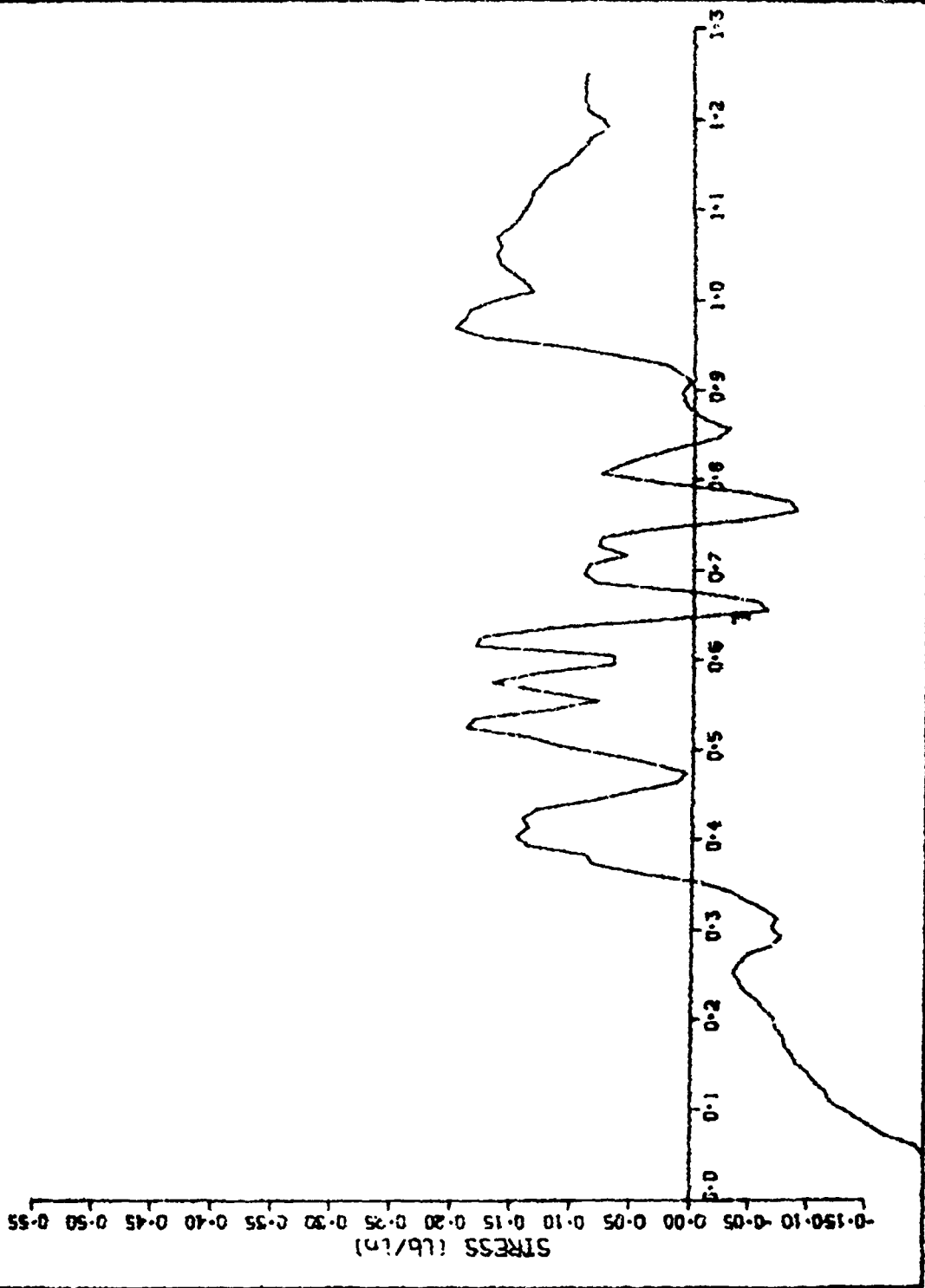


TEST NO. 37 SENSOR 3RS 0-1.6 (in H2O)

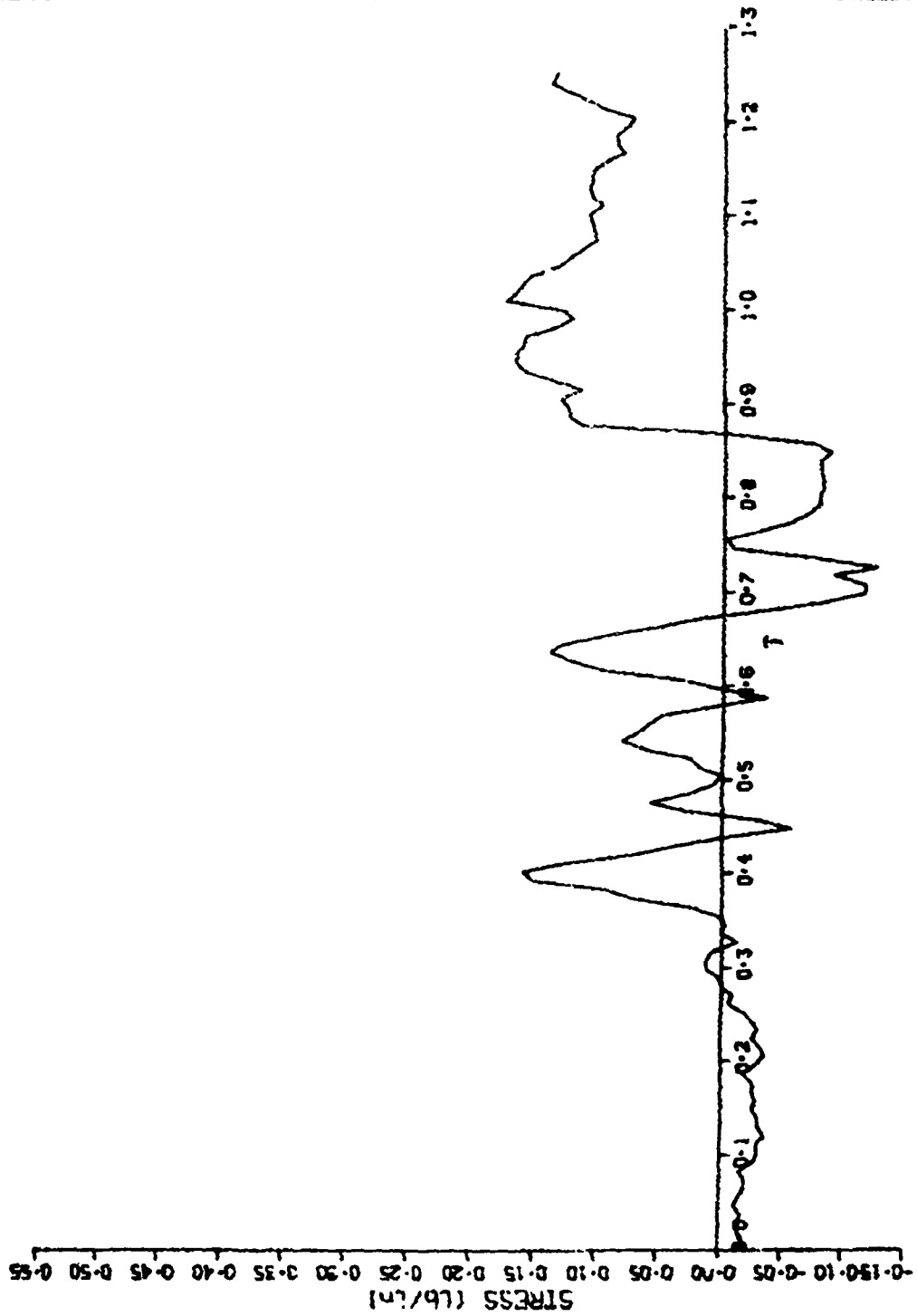




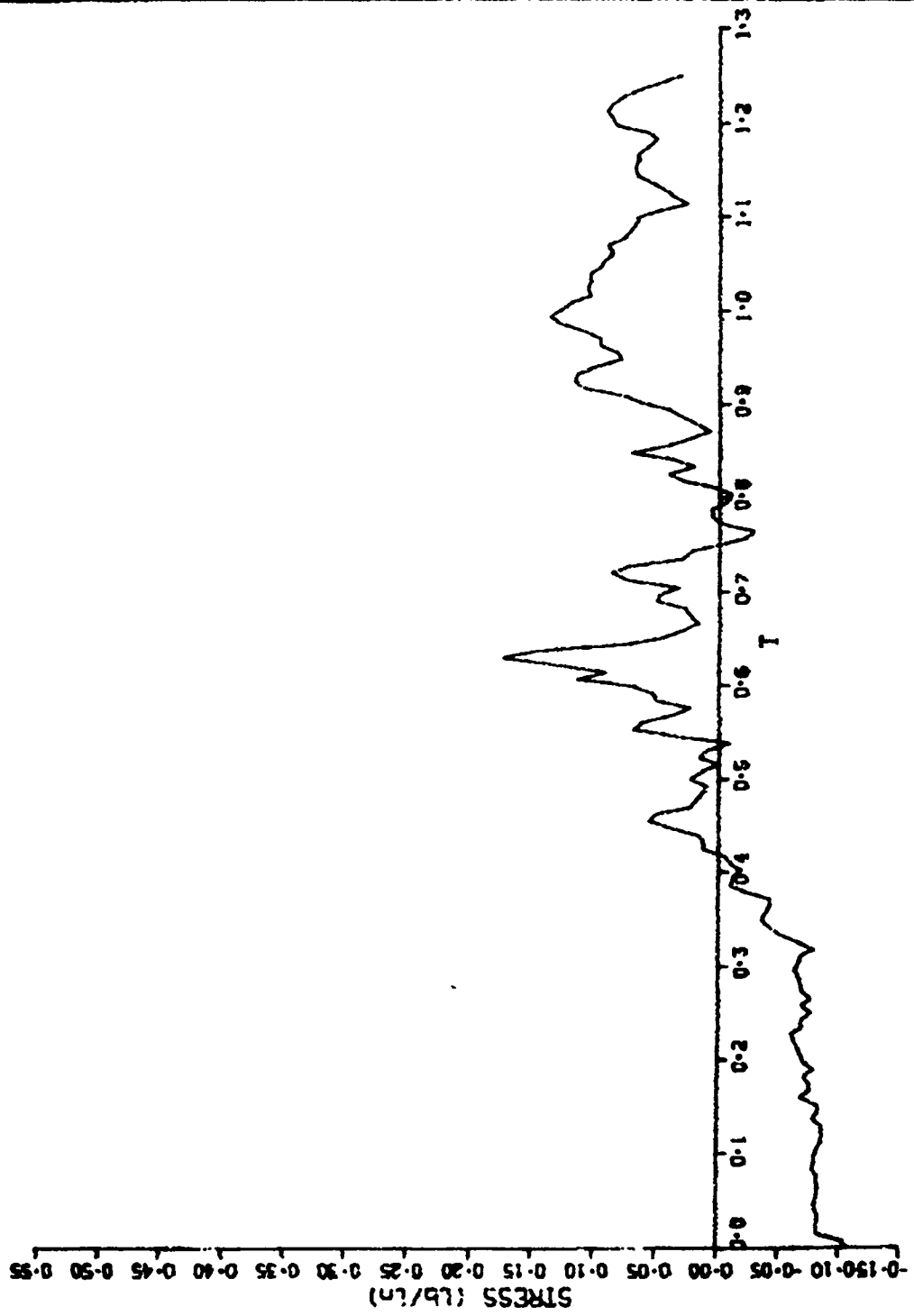
TEST NO.21 SENSOR 4RS 0-1.6 (in H20)



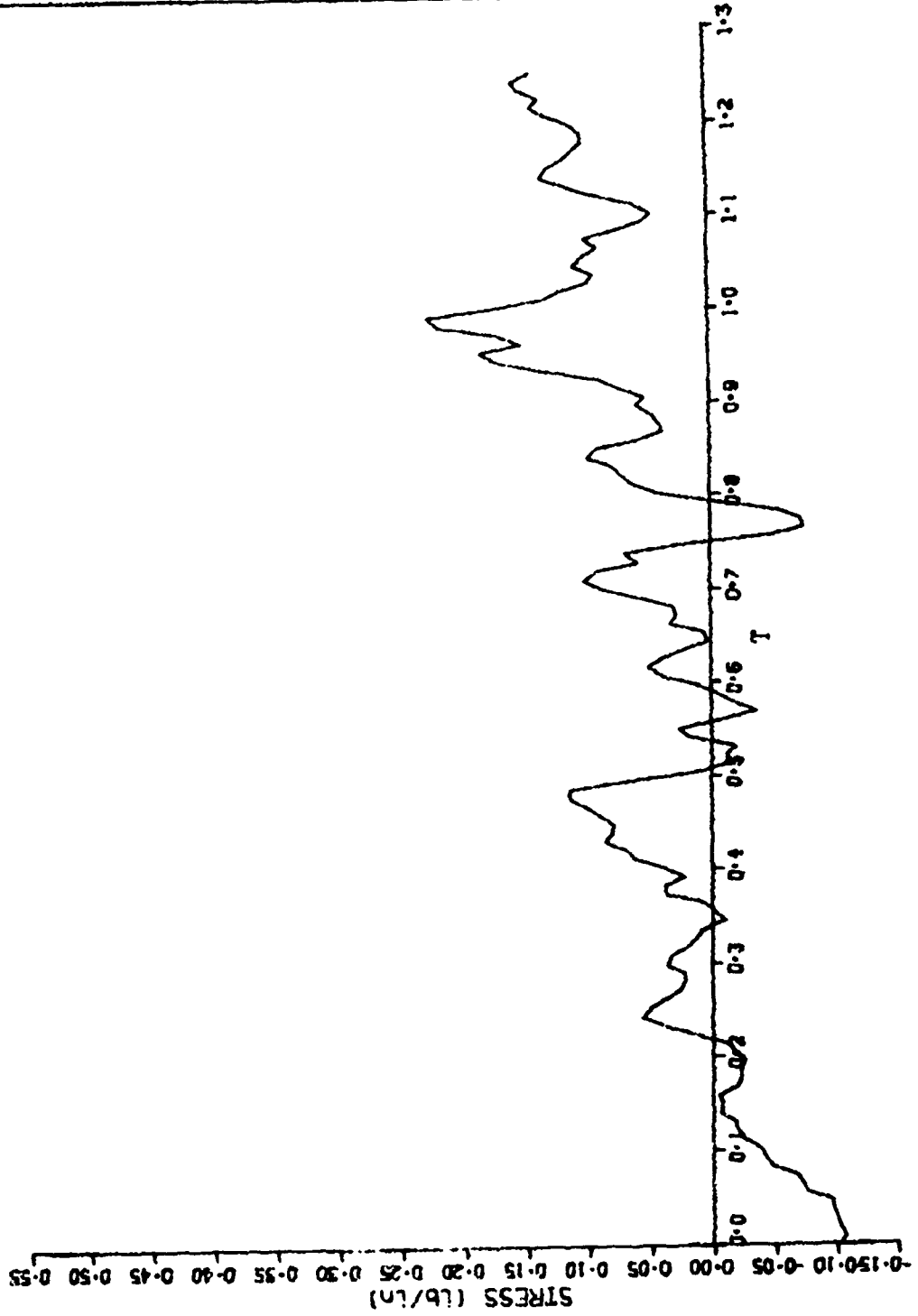
TEST NO. 22 SENSOR 4RS 0-1.6 (in H2O)



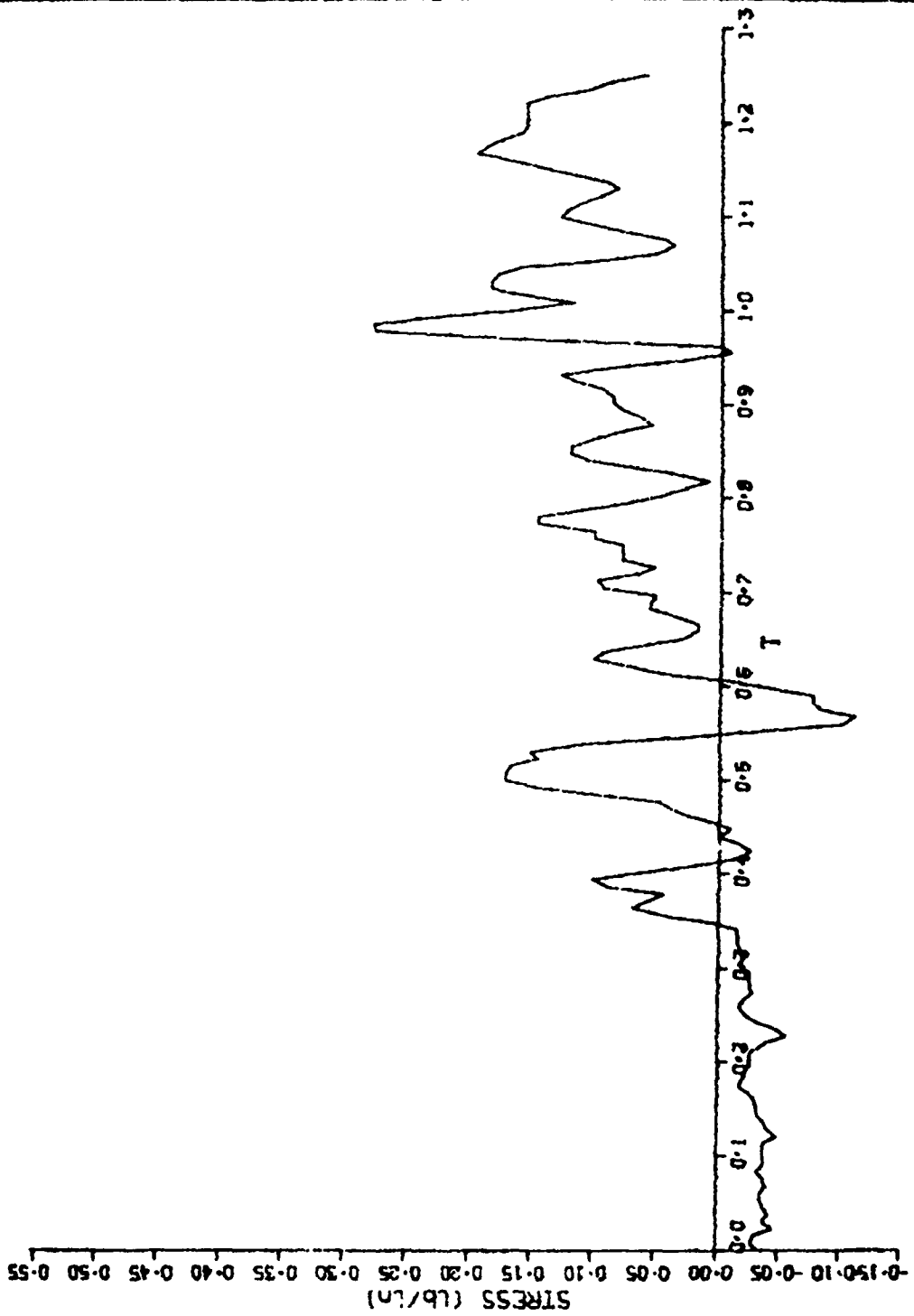
TEST NO.26 SENSOR 4RS 0-1.6 (in H2O)



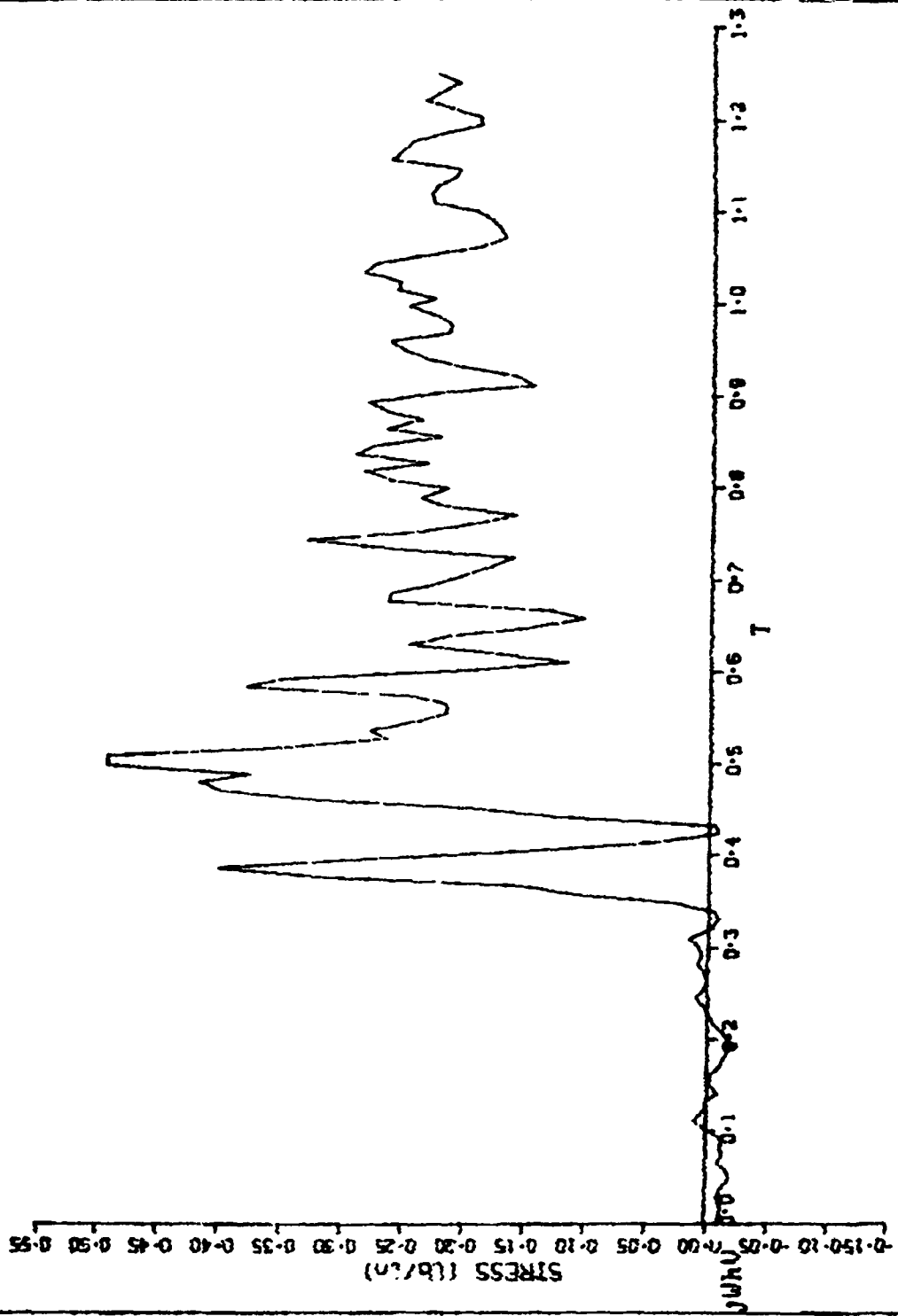
TEST NO. 22 SENSOR 5RS - SKIRT 0-1.6 (in H20)



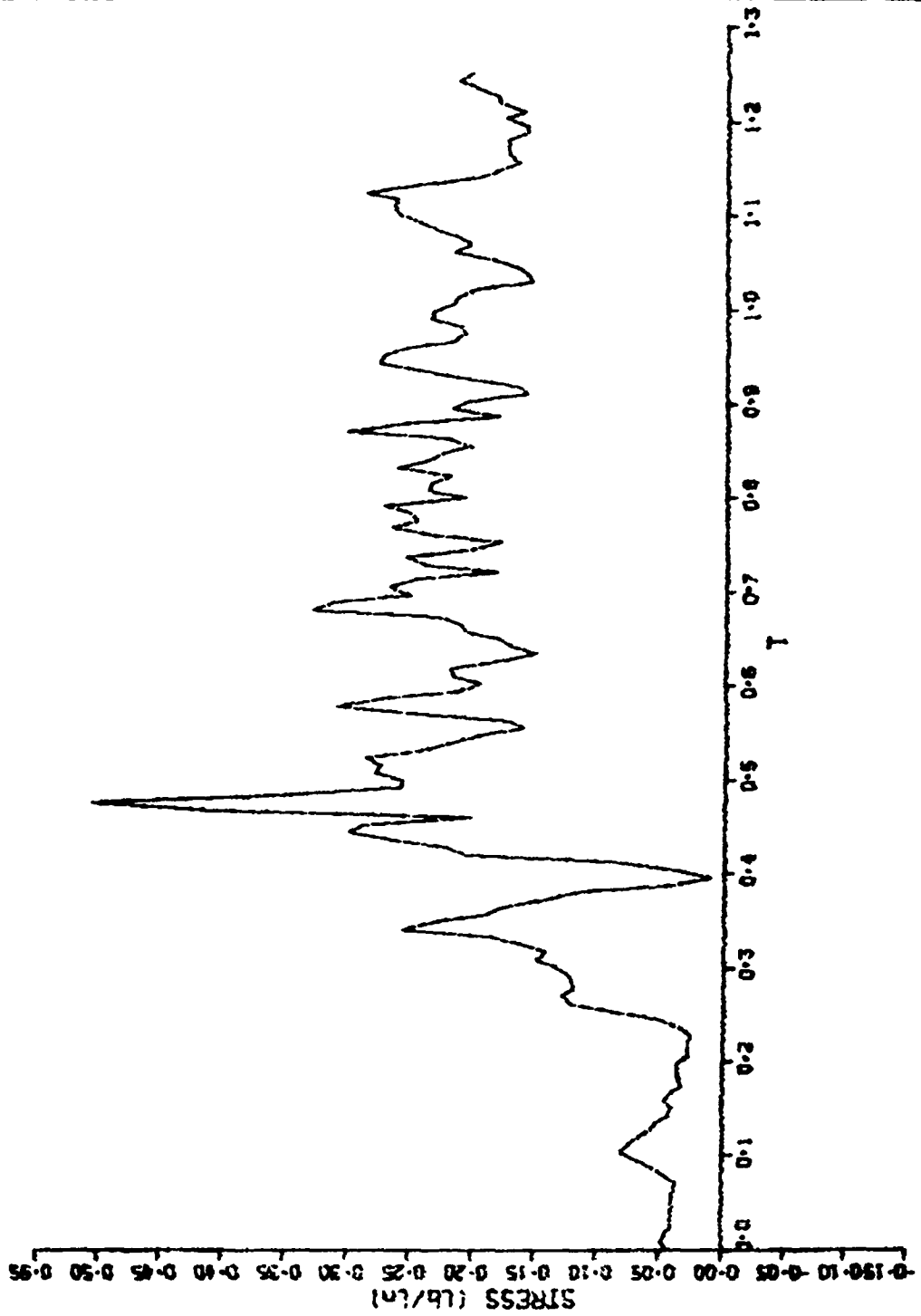
TEST NO.26 SENSOR 5RS - SKIRT 0-1.6 (ln H2O)



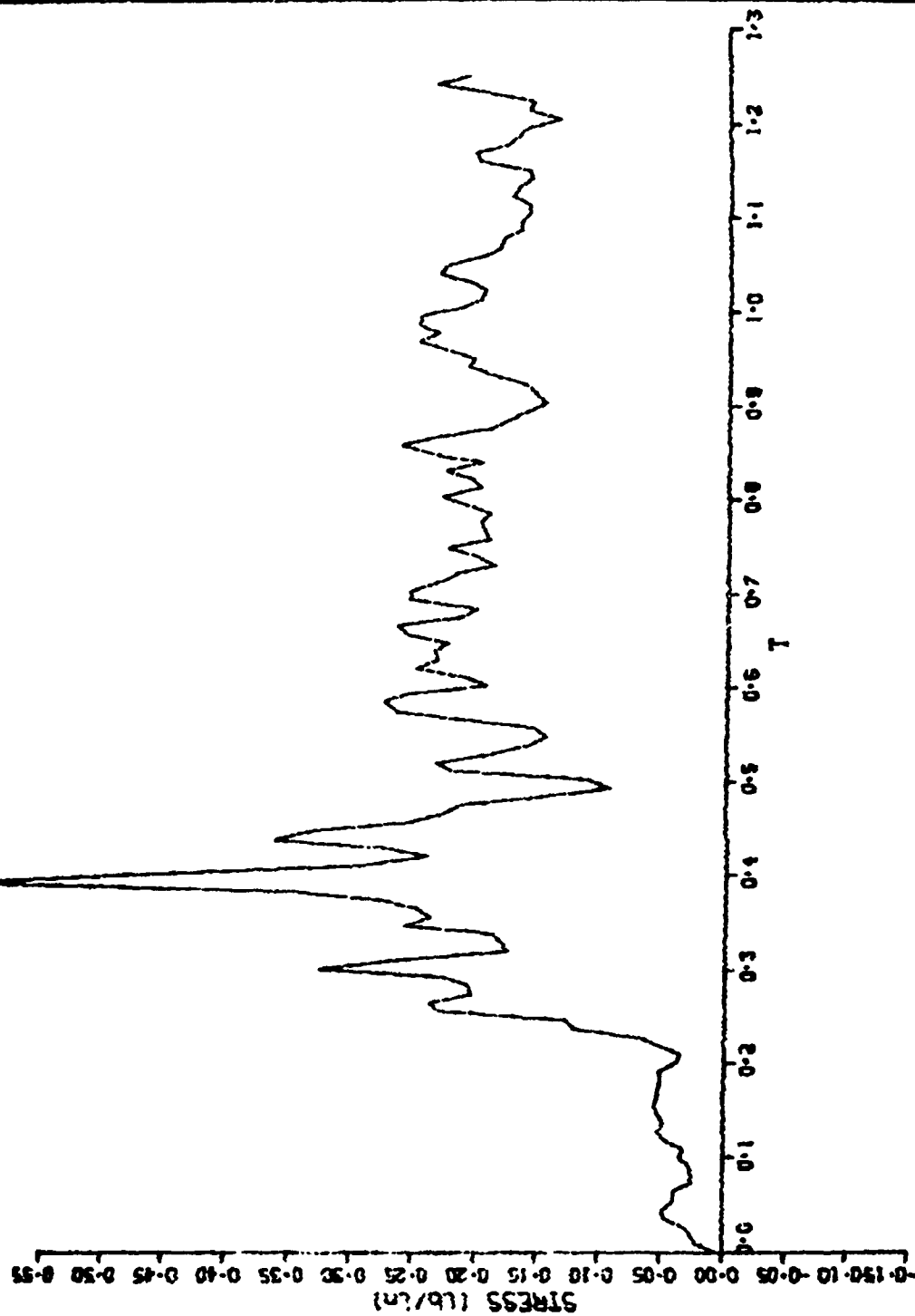
TEST NO.27 SENSOR IRS - VENT 0-2.0(in H2O)



TEST NO.28 SENSOR IRS - VENT 0-2.0 (in H2O)

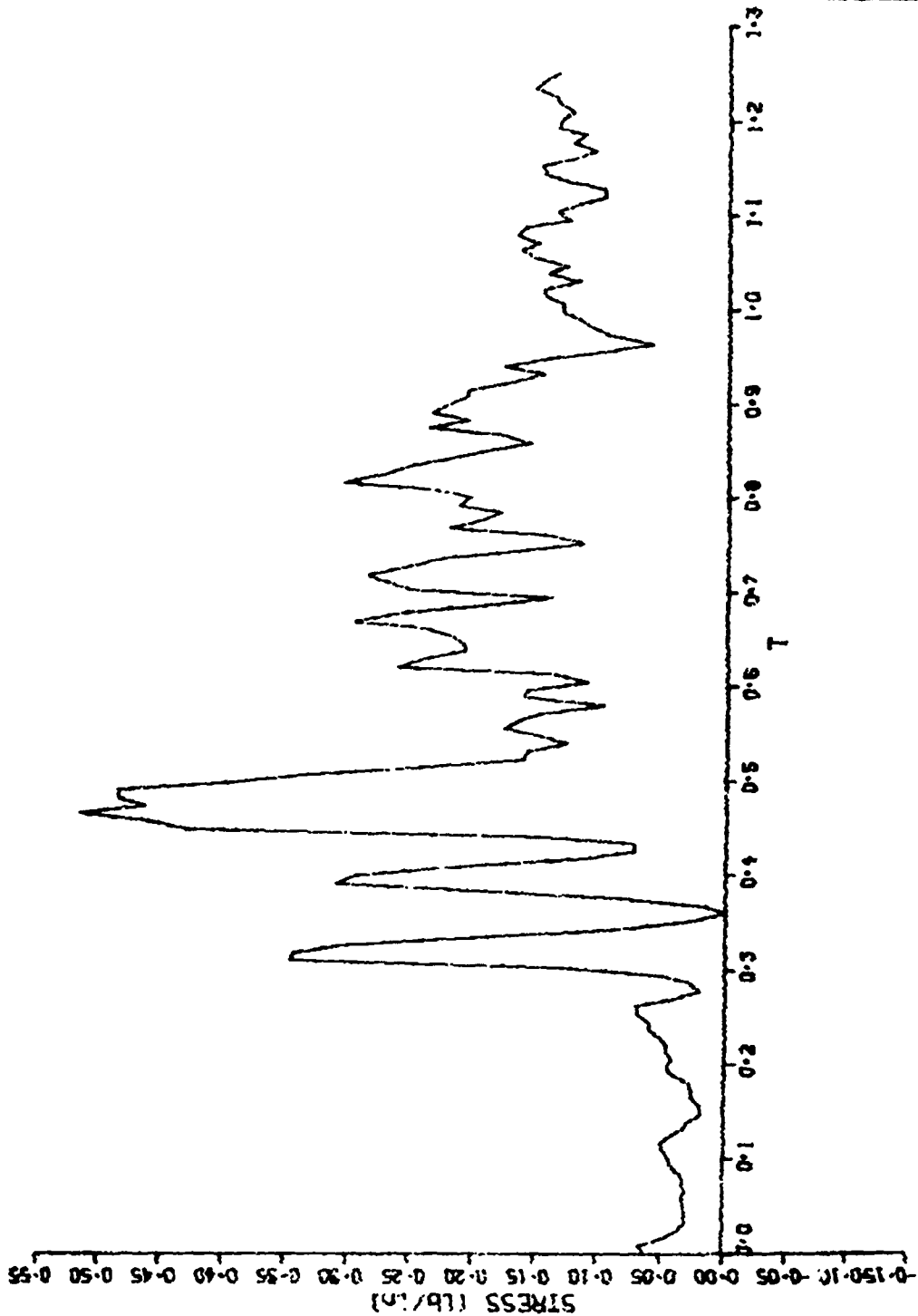


TEST NO.29 SENSOR IRS - VENT 0-2.0(in H2O)

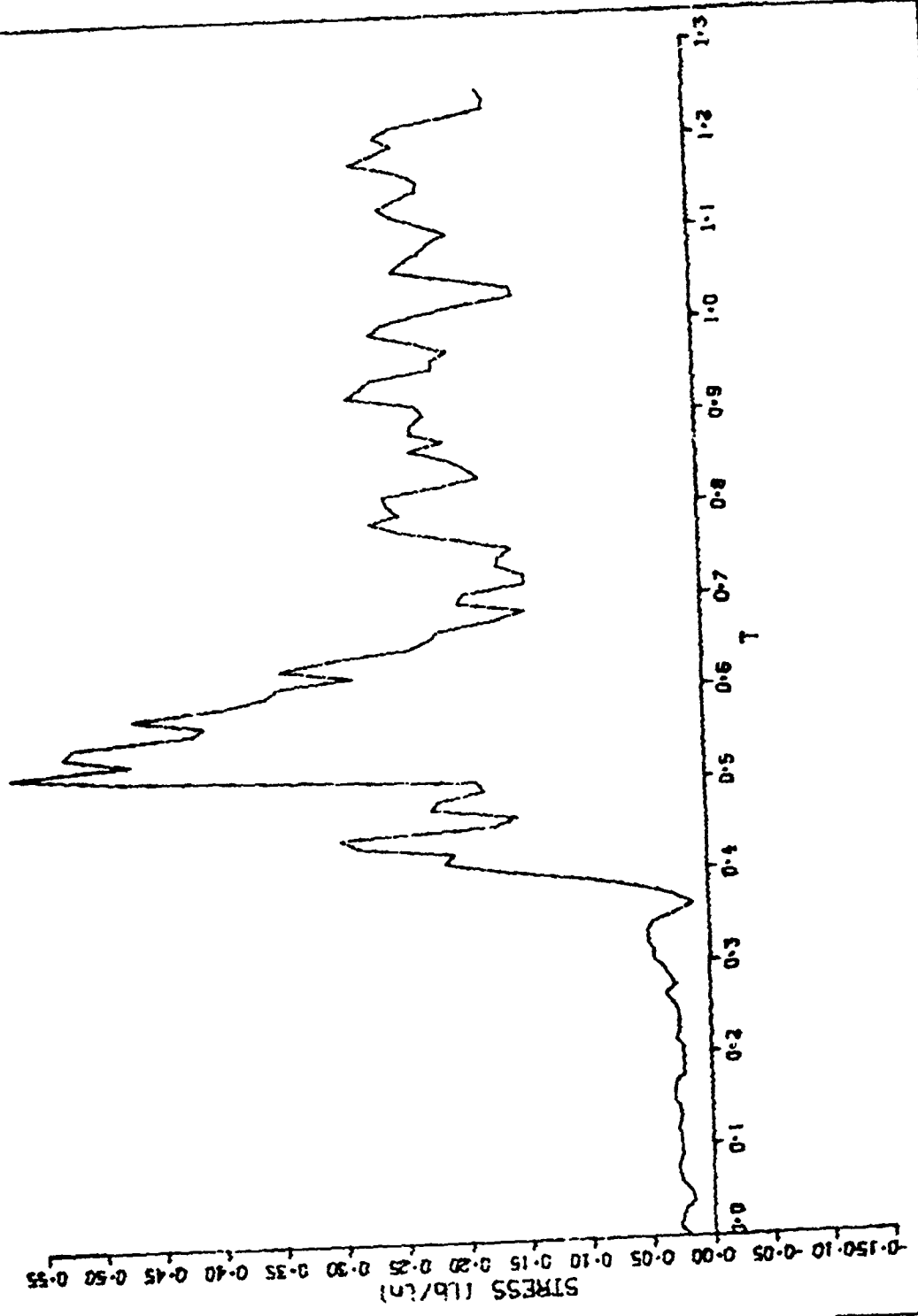




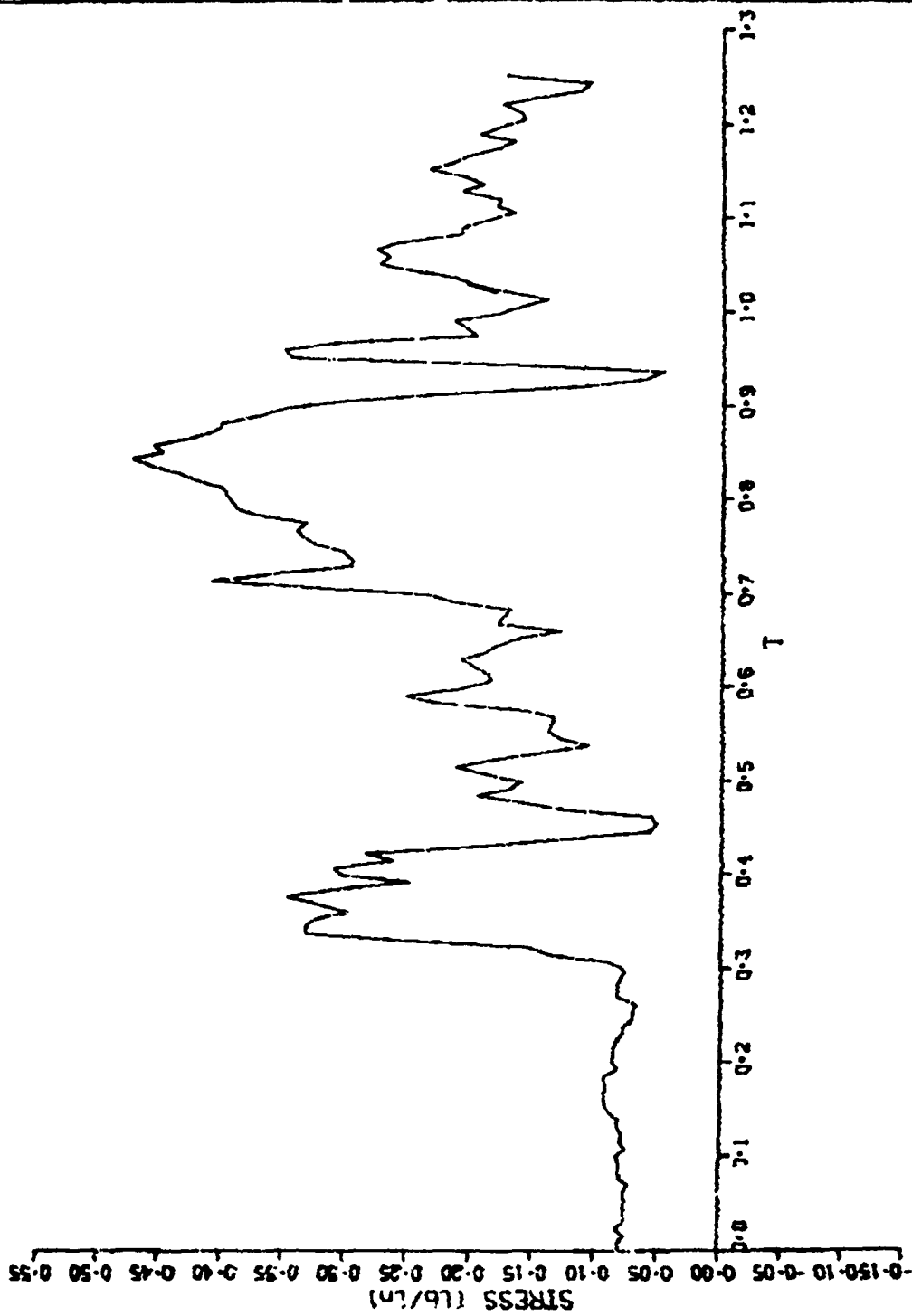
TEST NO.30 SENSOR IRS - VENT 0-2.0 (in H2O)



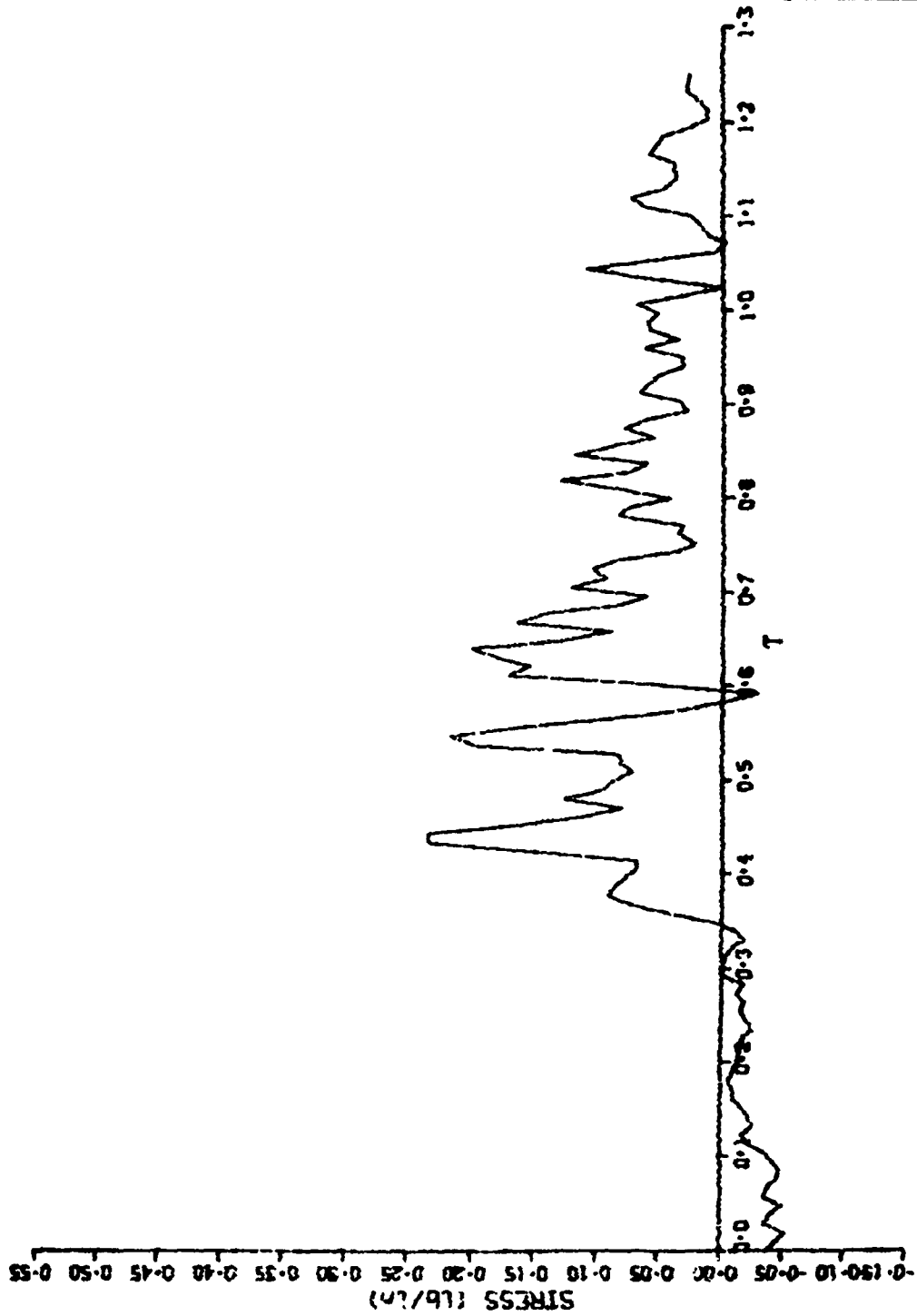
TEST NO.31 SENSOR IRS - VENT 0-2.0 (in H2O)



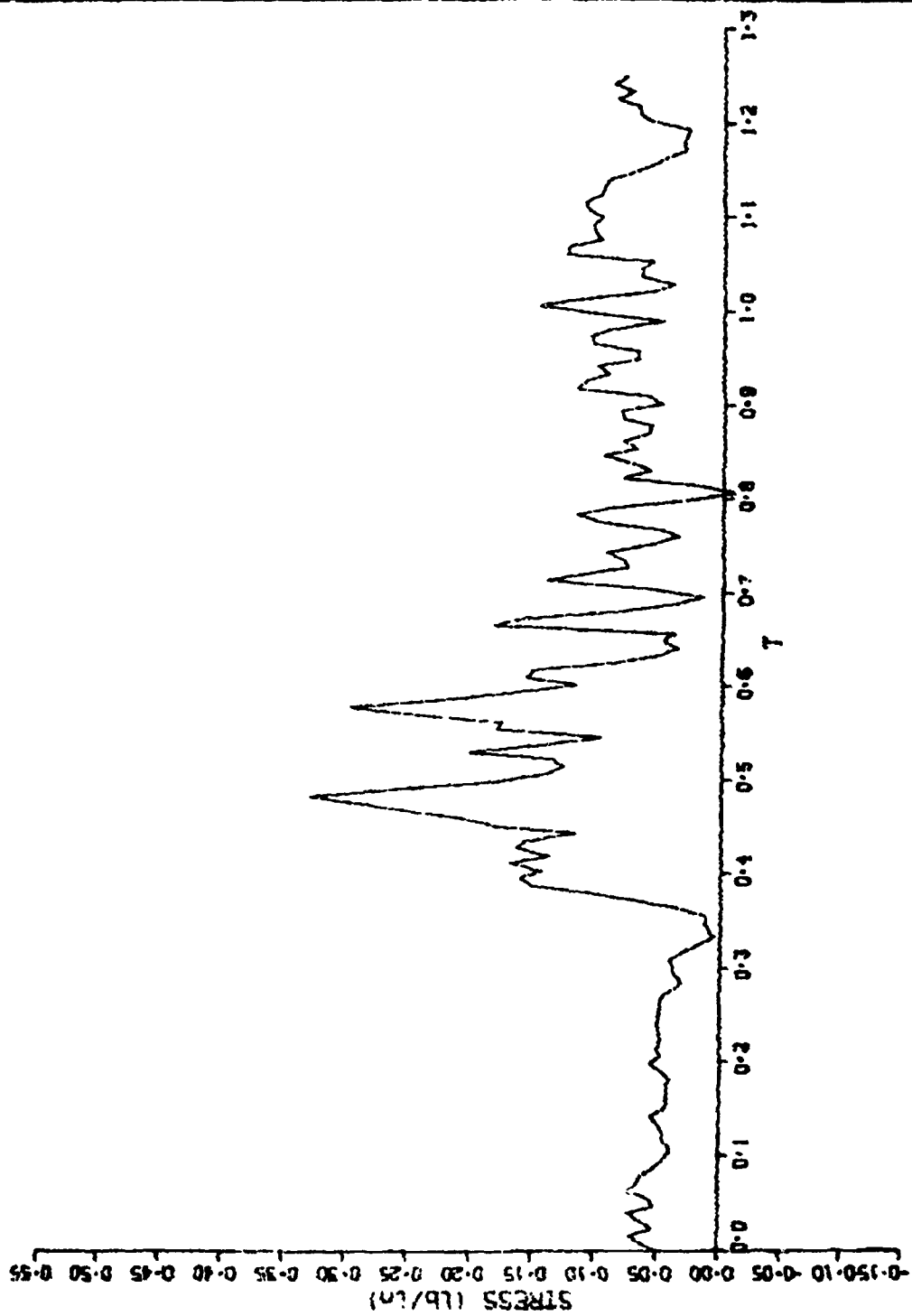
TEST NO.34 SENSOR IRS - VENT 0-2.0 (Ln H2O)



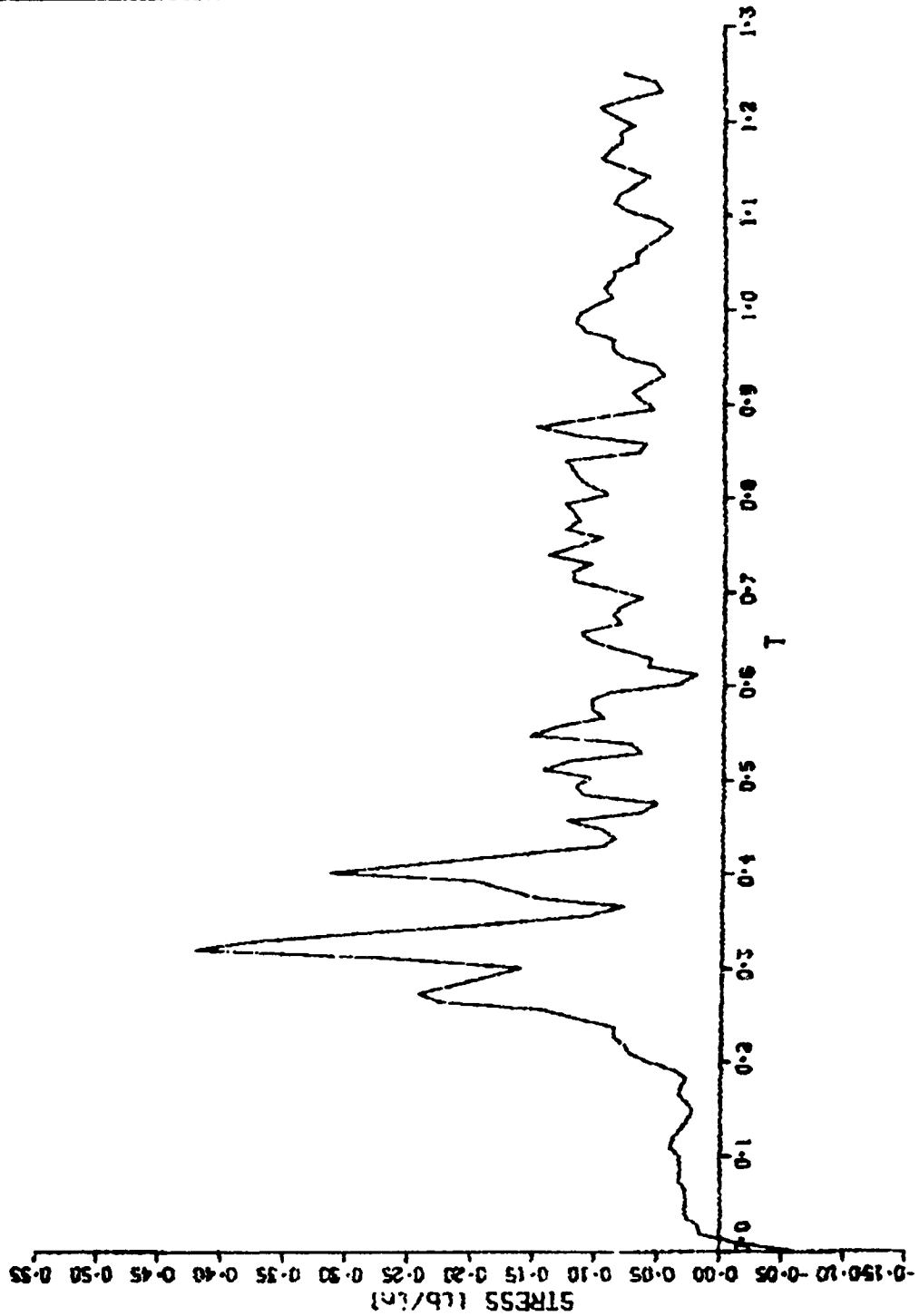
TEST NO.27 SENSOR 2RS 0-2.0(in H2O)



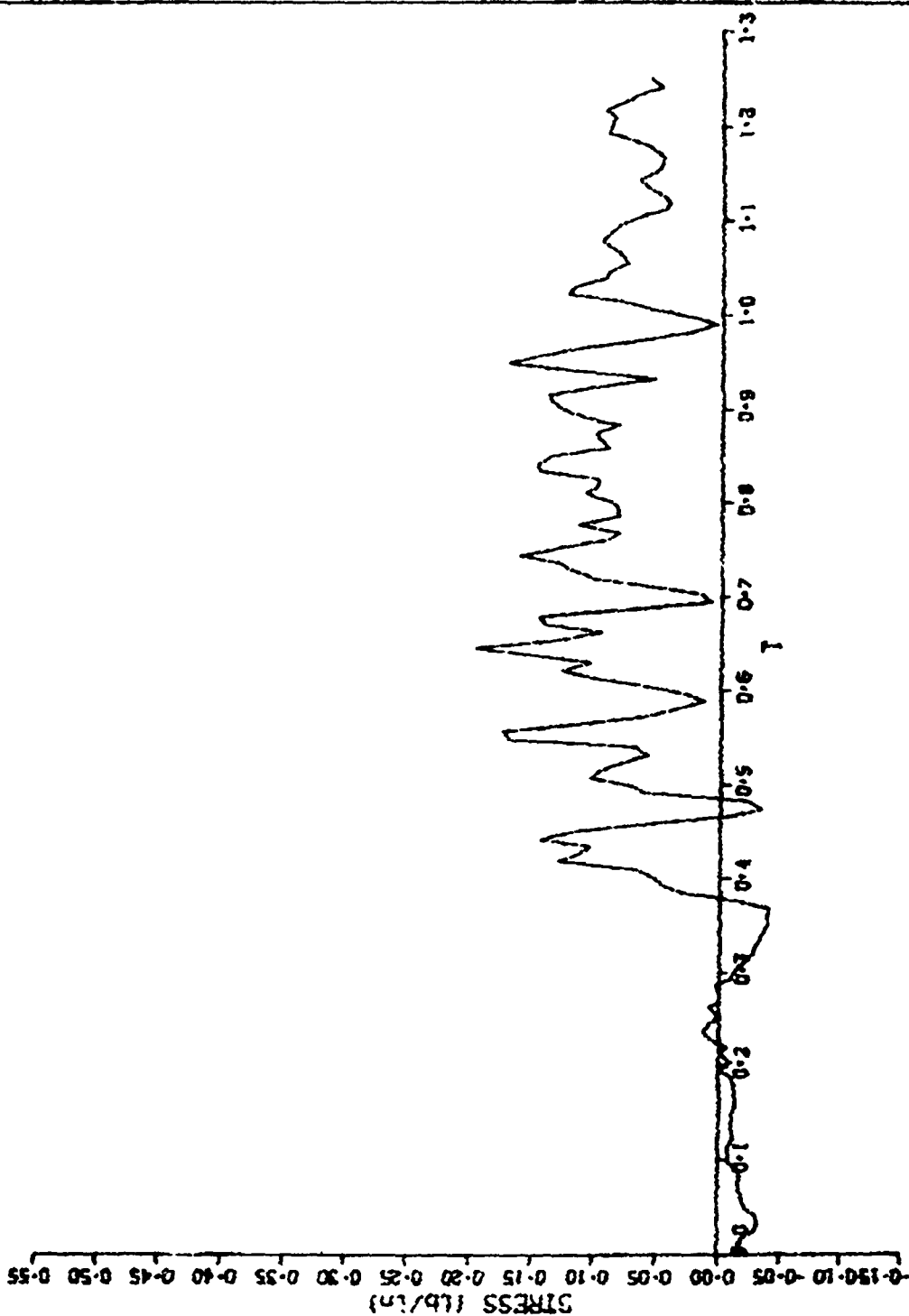
TEST NO. 26 SENSOR 2RS 0-2.0 (in H2O)



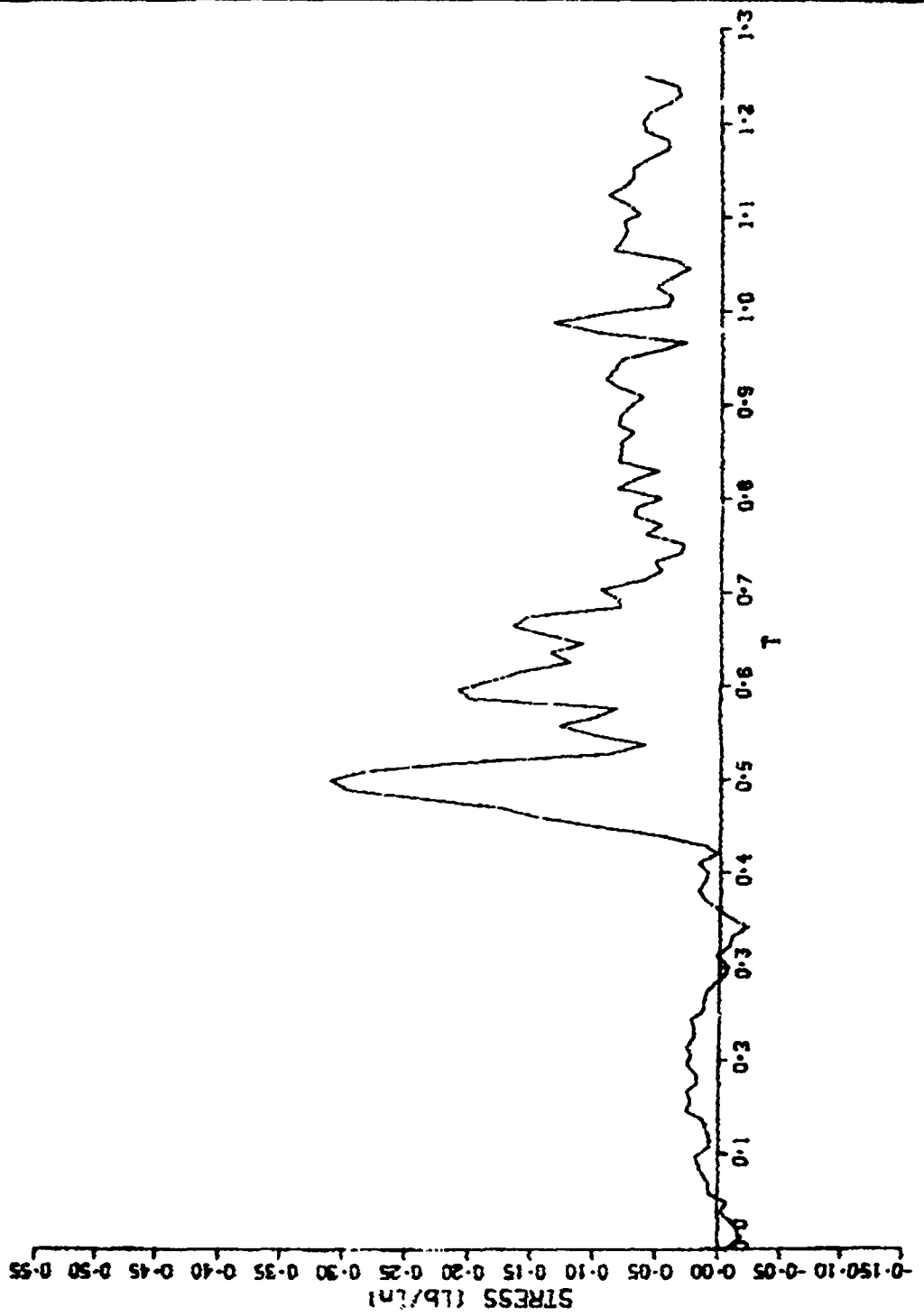
TEST NO. 29 SENSOR 2RS 0-2.0 (in H2O)



TEST NO. 30 SENSOR 2RS 0-2.0 (in H20)

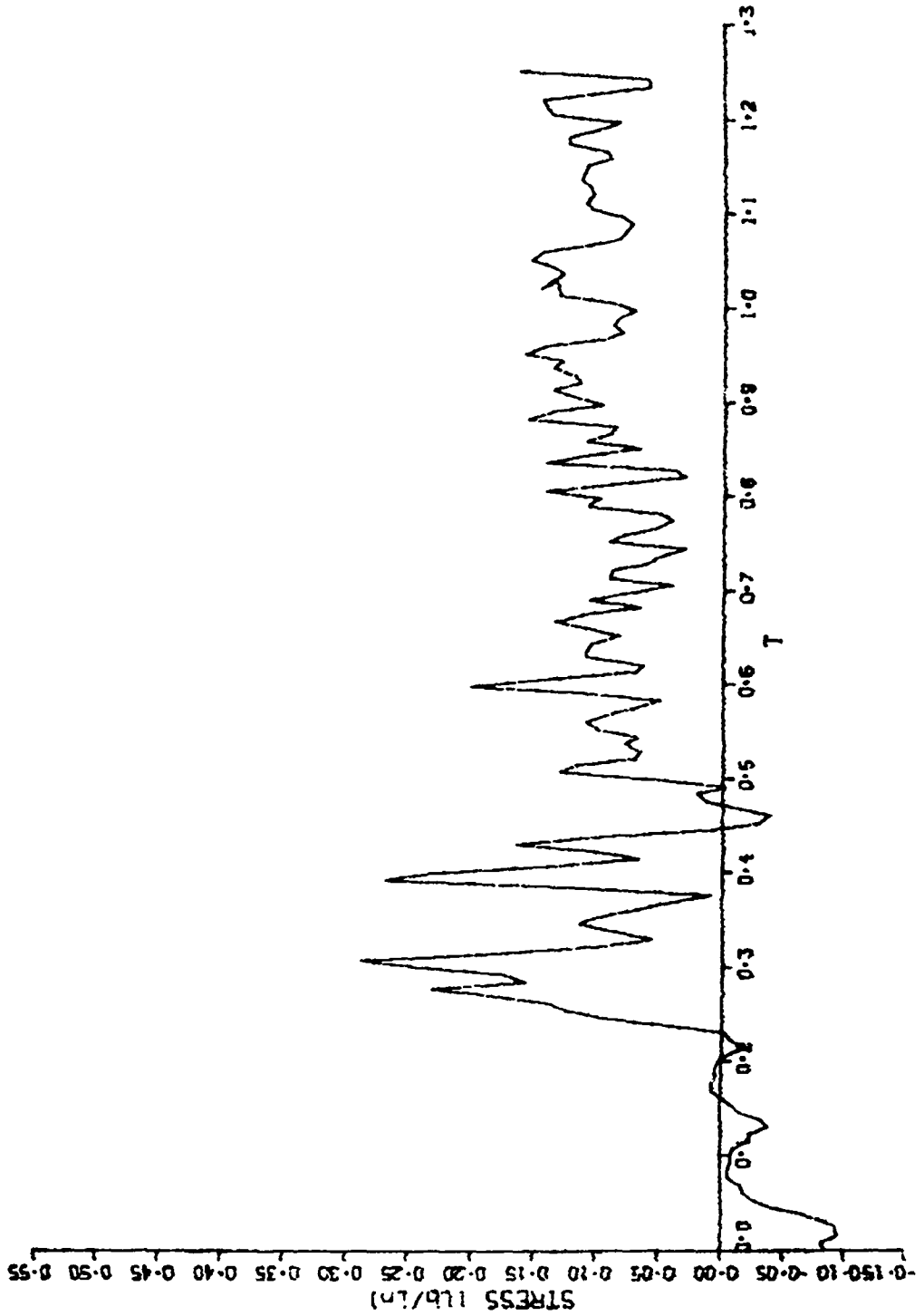


TEST NO.31 SENSOR 2RS 0-2.0 (in H20)

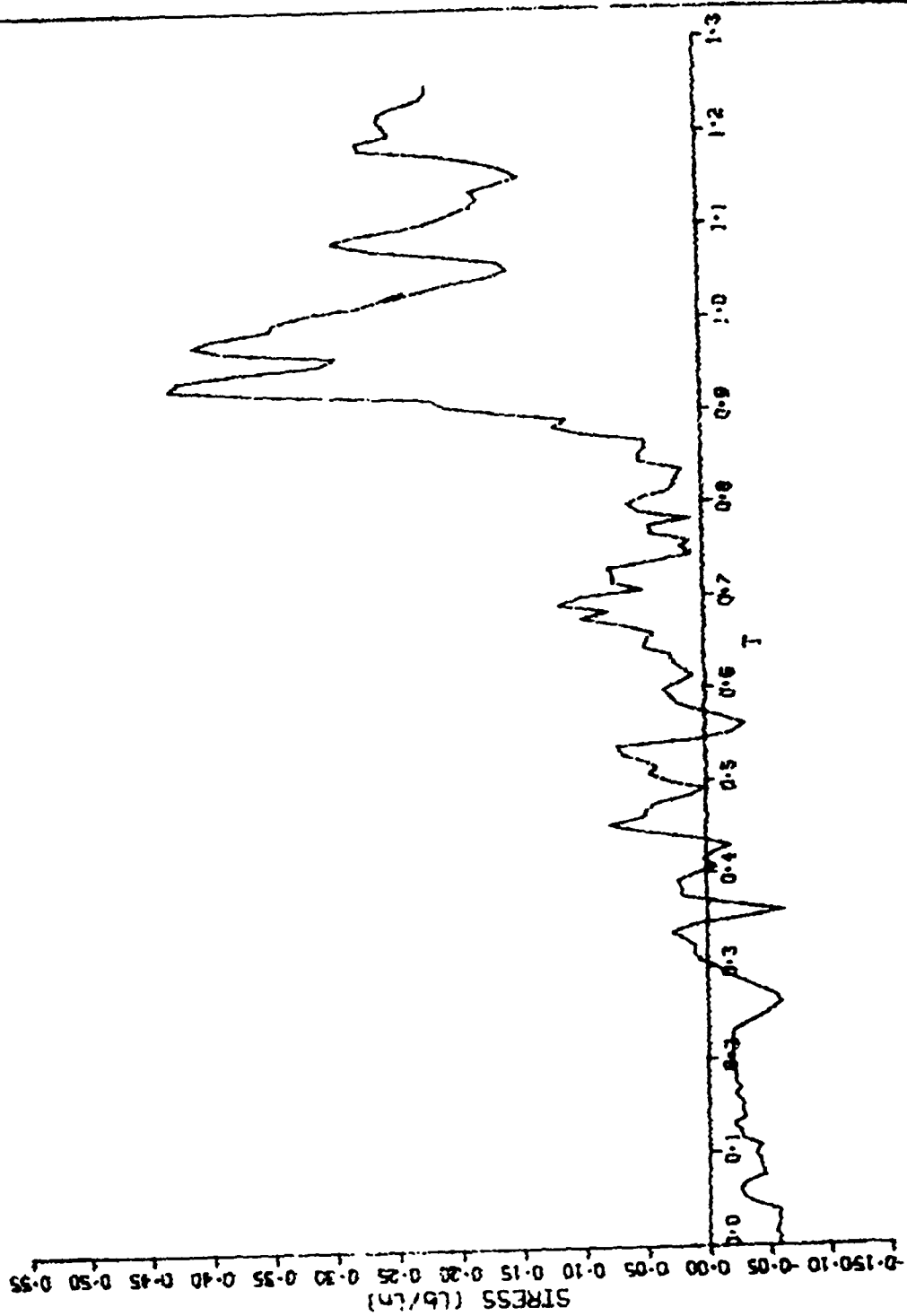




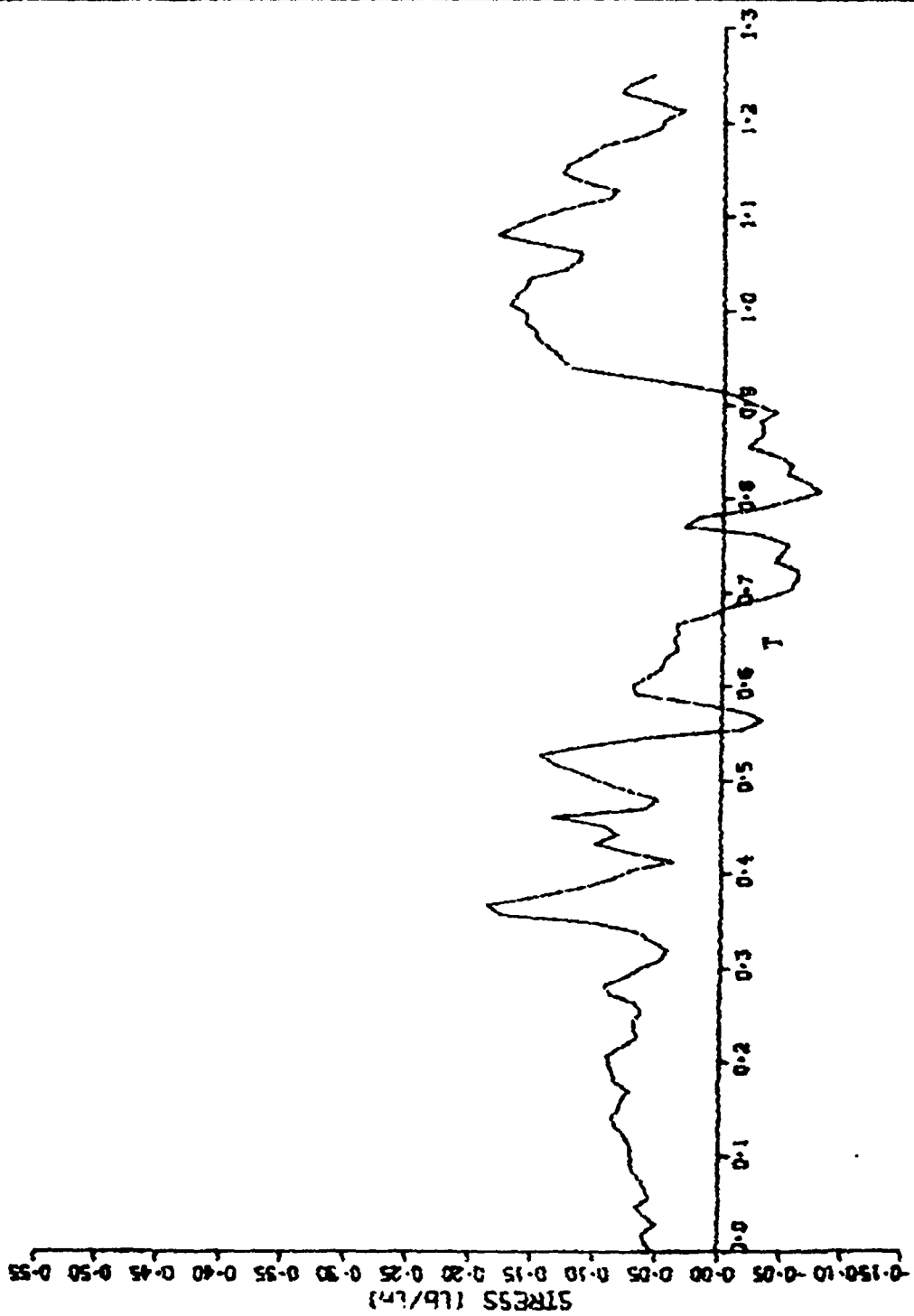
TEST NO. 34 SENSOR 2RS 0-2.0 (in H2O)



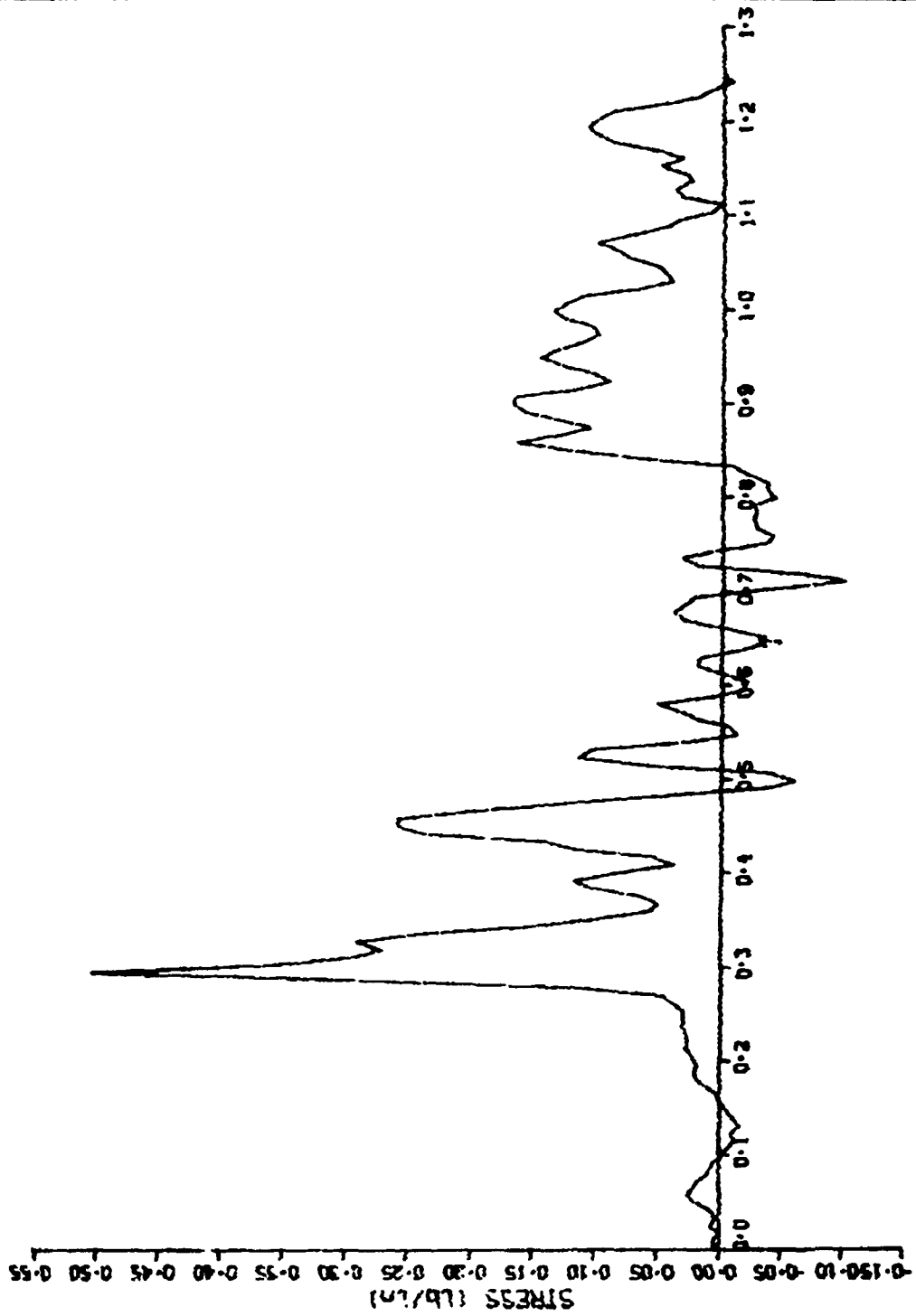
TEST NO. 34 SENSOR 3RS 0-2.0 (in H2O)



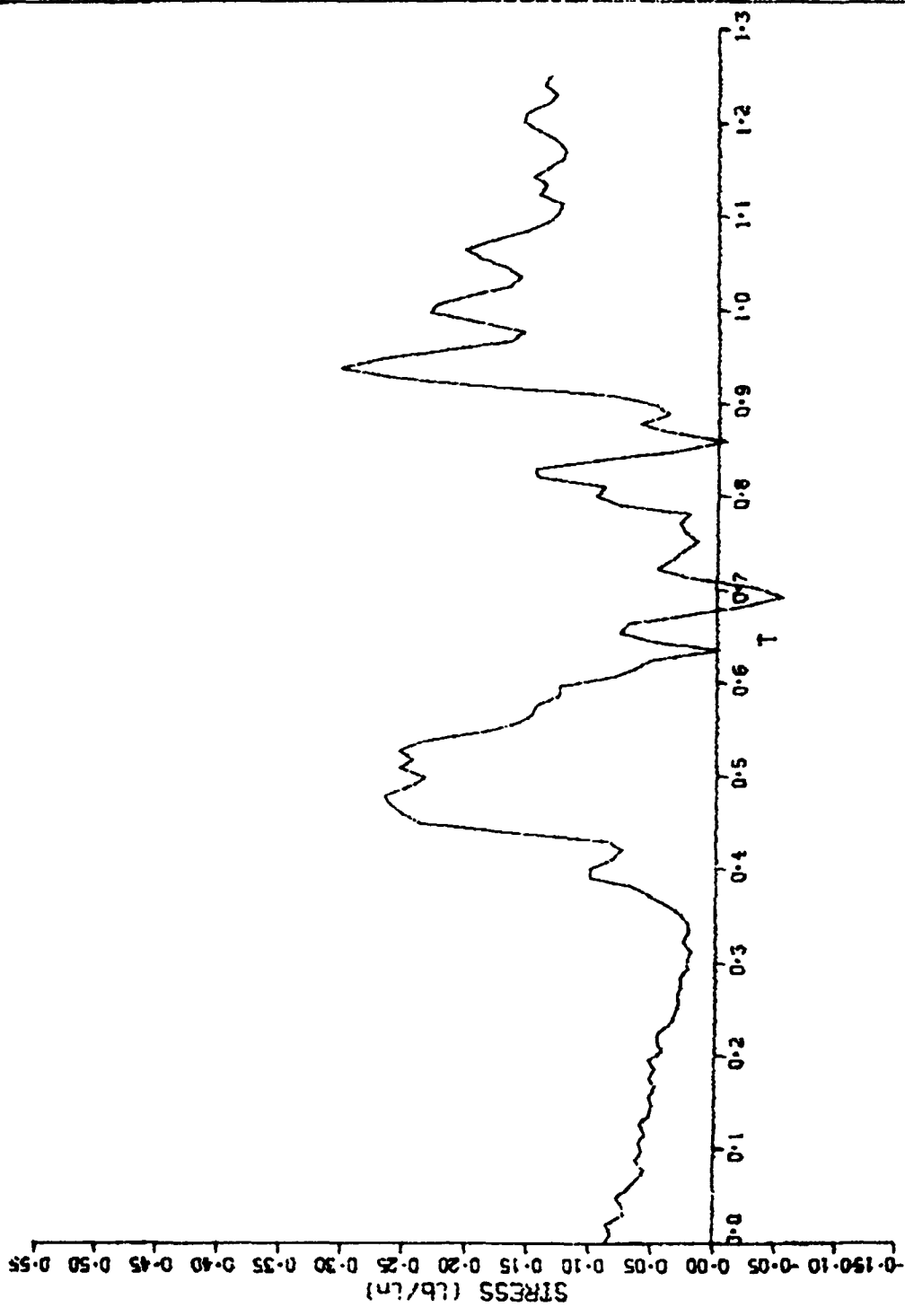
TEST NO. 27 SENSOR 4RS 0-2.0 (in H2O)



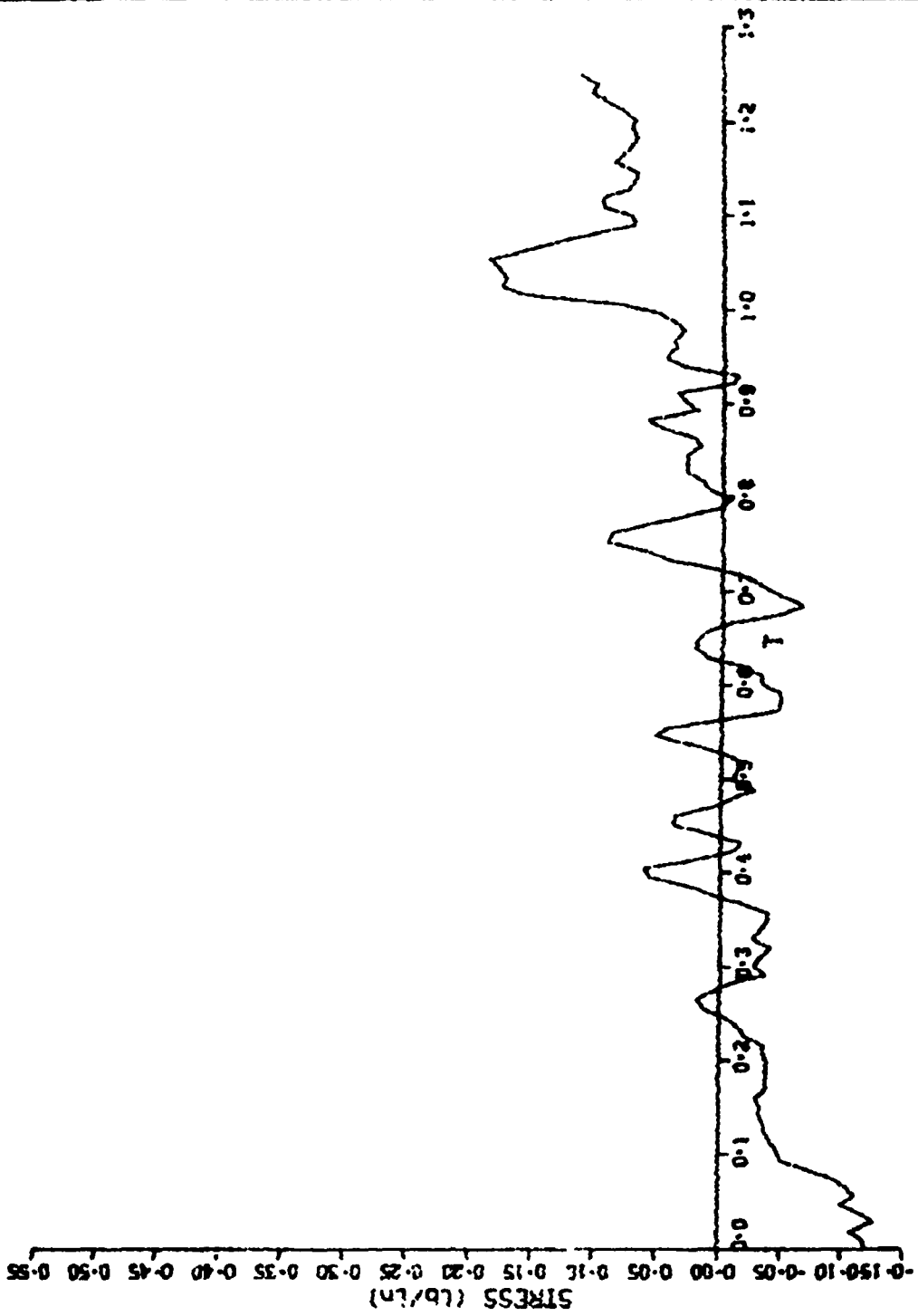
TEST NO. 30 SENSOR 4RS 0-2.0 (in H2O)



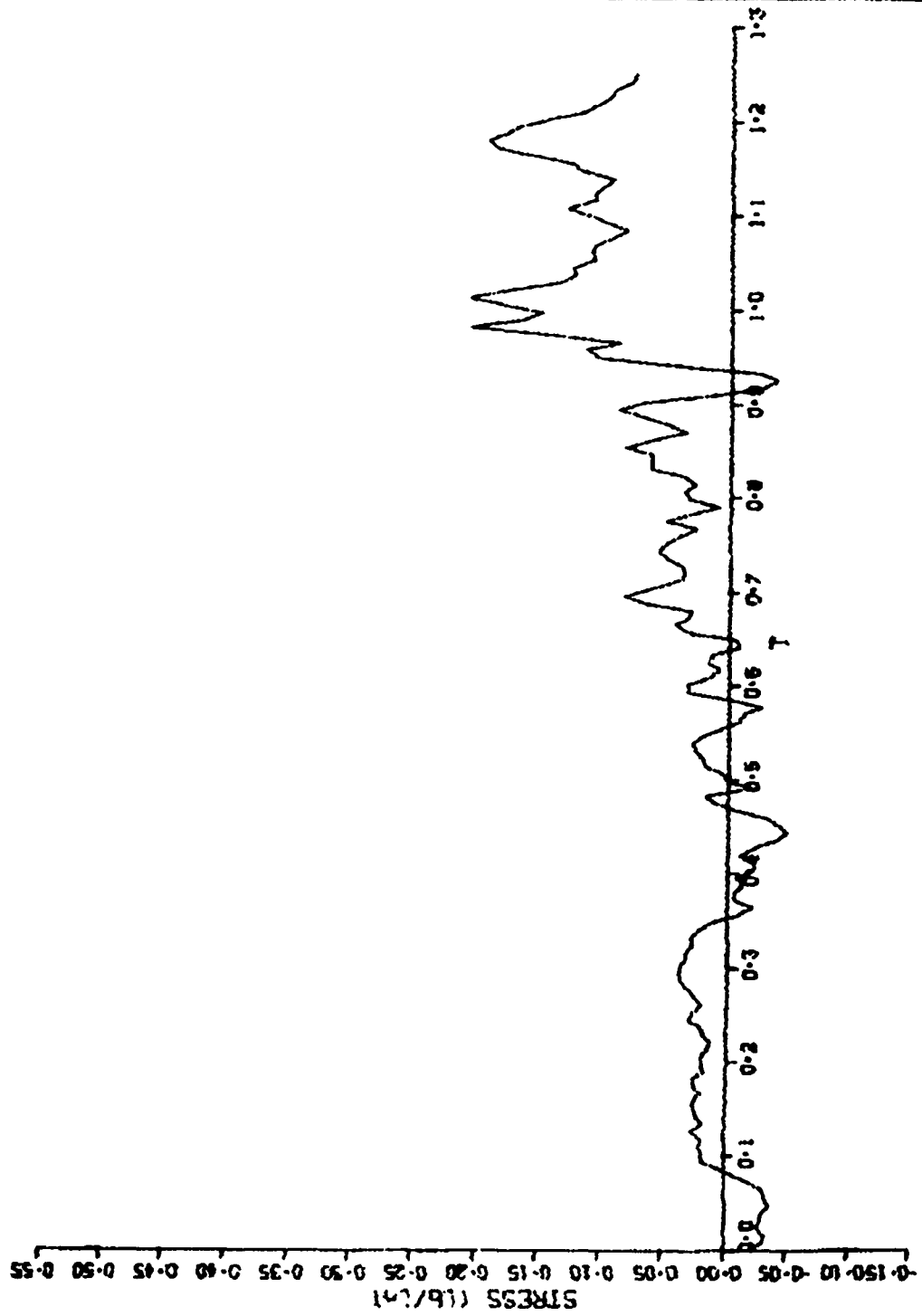
TEST NO. 31 SENSOR 4RS 0-2.0 (Ln H2O)



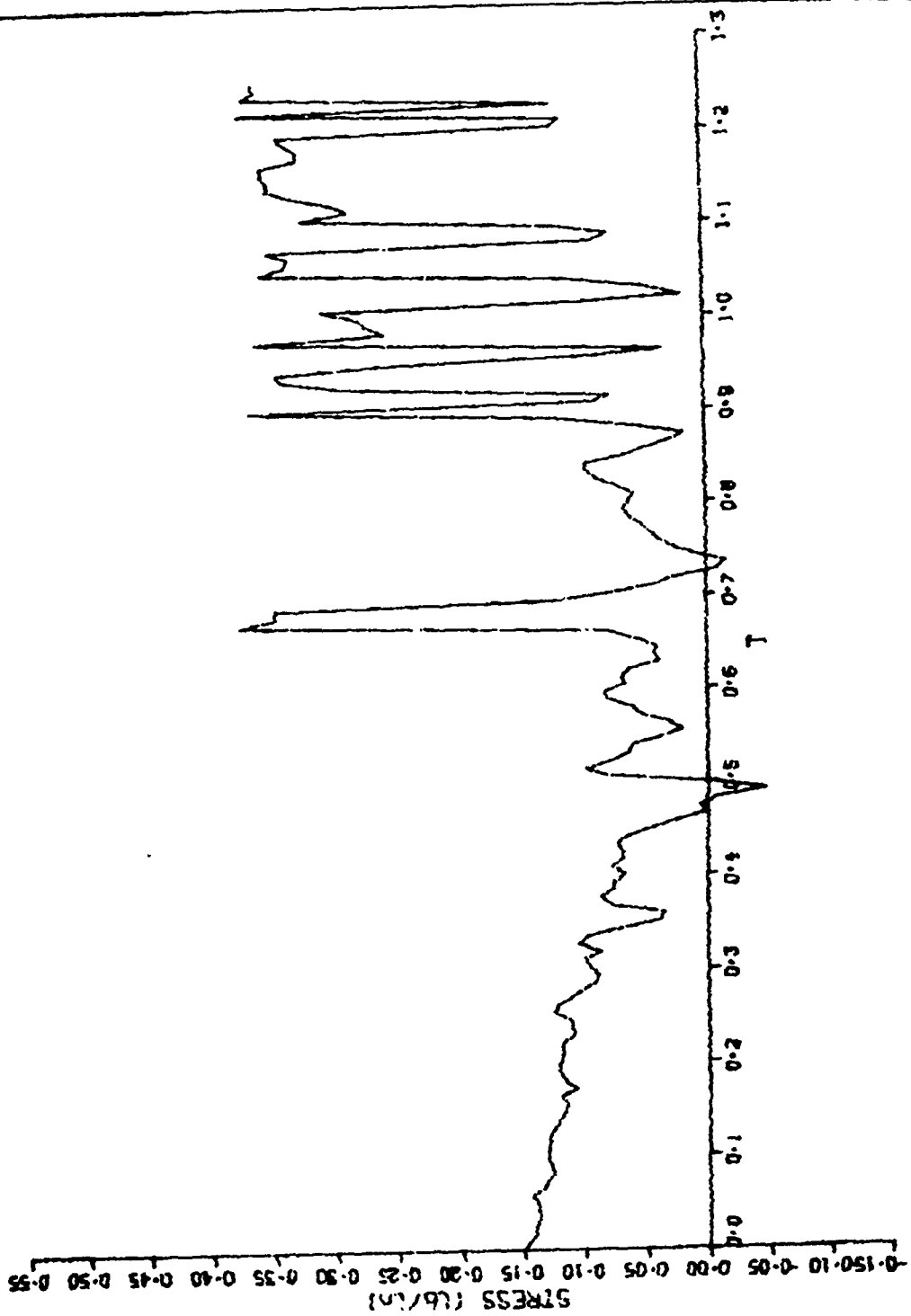
TEST NO. 27 SENSOR 5RS - SKIRT 0-2.0 (in H2O)



TEST NO. 28 SENSOR SRS - SKIRT 0-2.0 (in H2O)

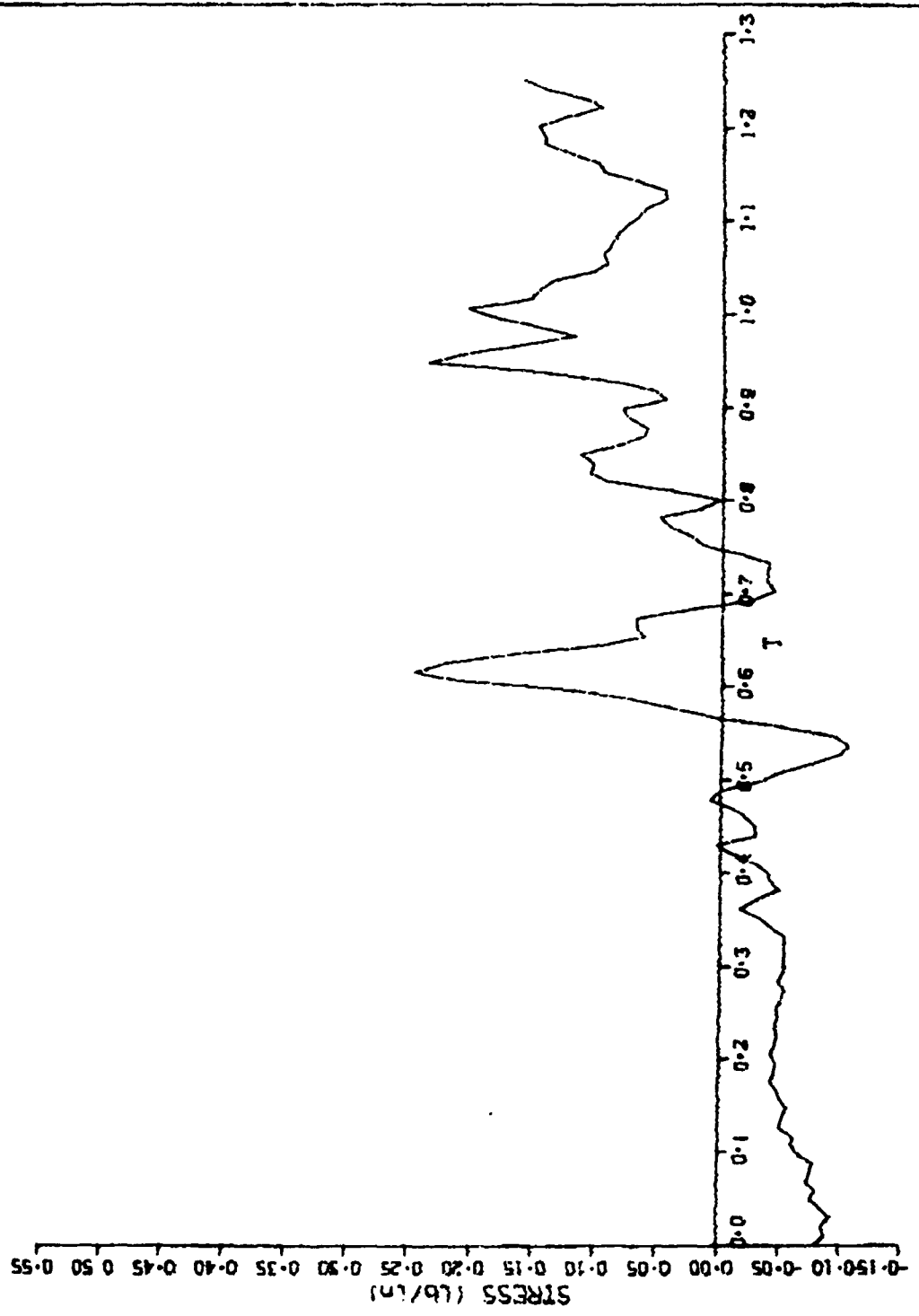


TEST NO. 30 SENSOR SRS - SKIRT 0-2.0 (in H2O)



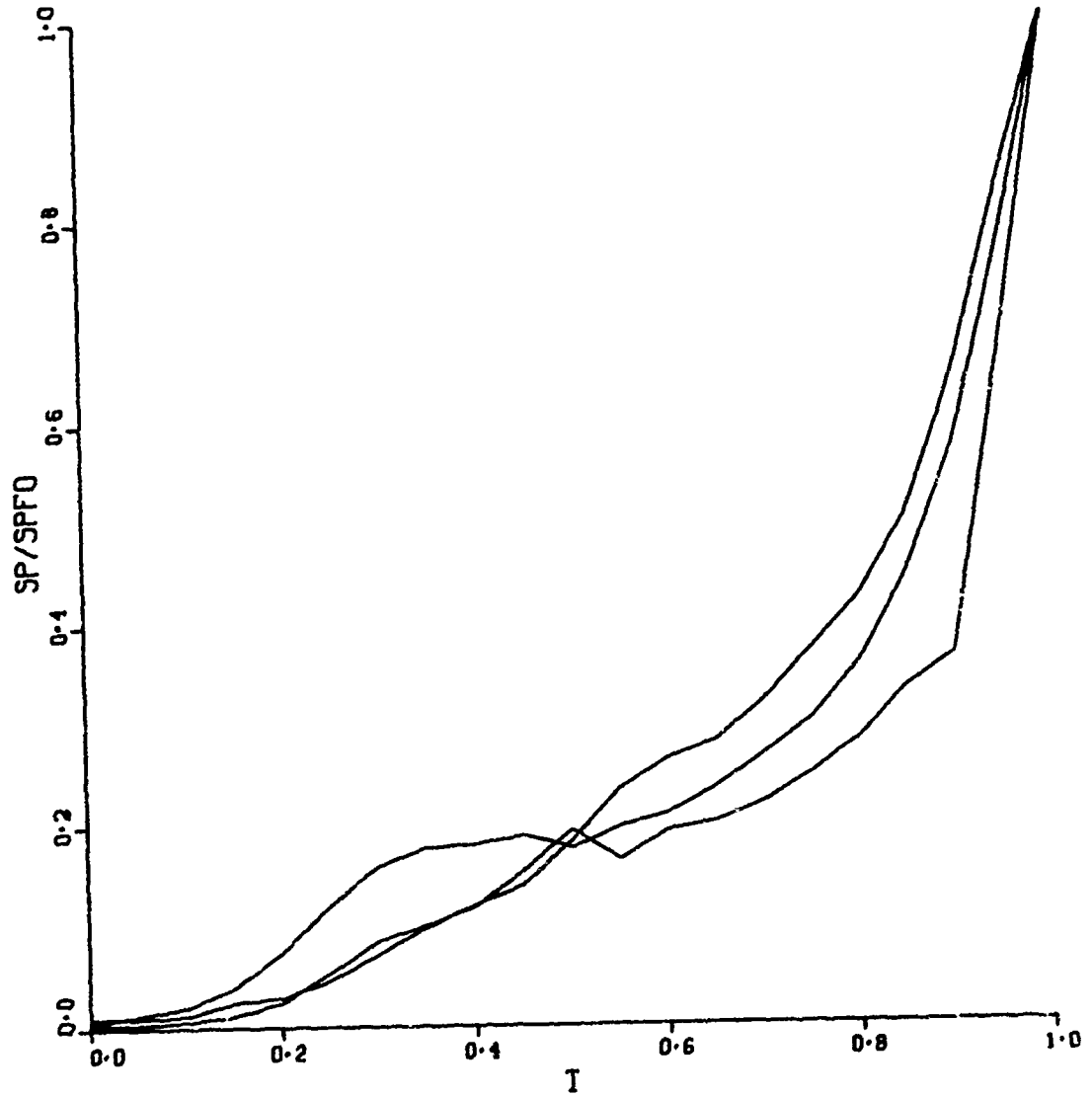


TEST NO.31 SENSOR 5RS - SKIRT 0-2.0 (in H20)

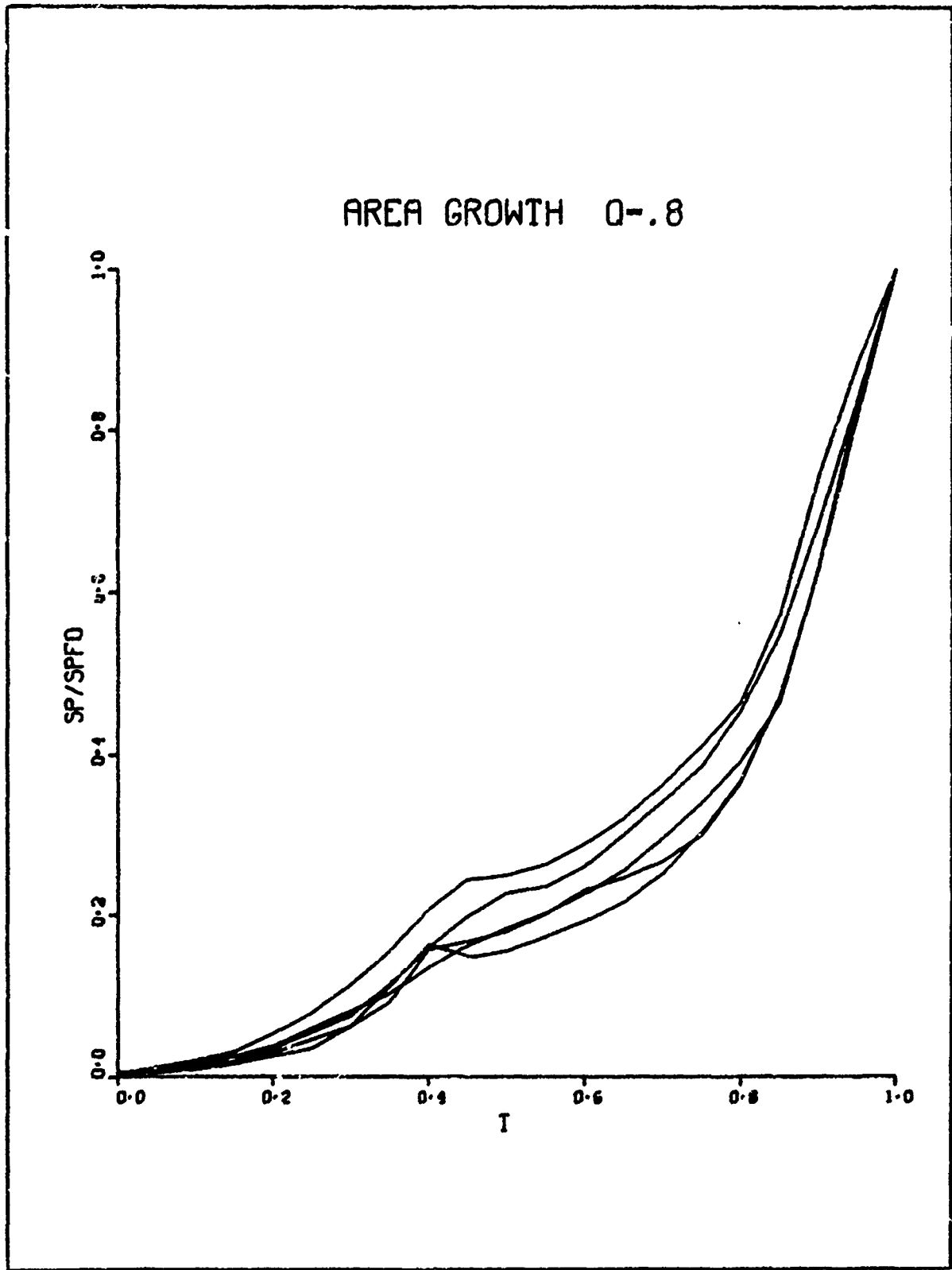


APPENDIX C  
AREA GROWTH PLOTS

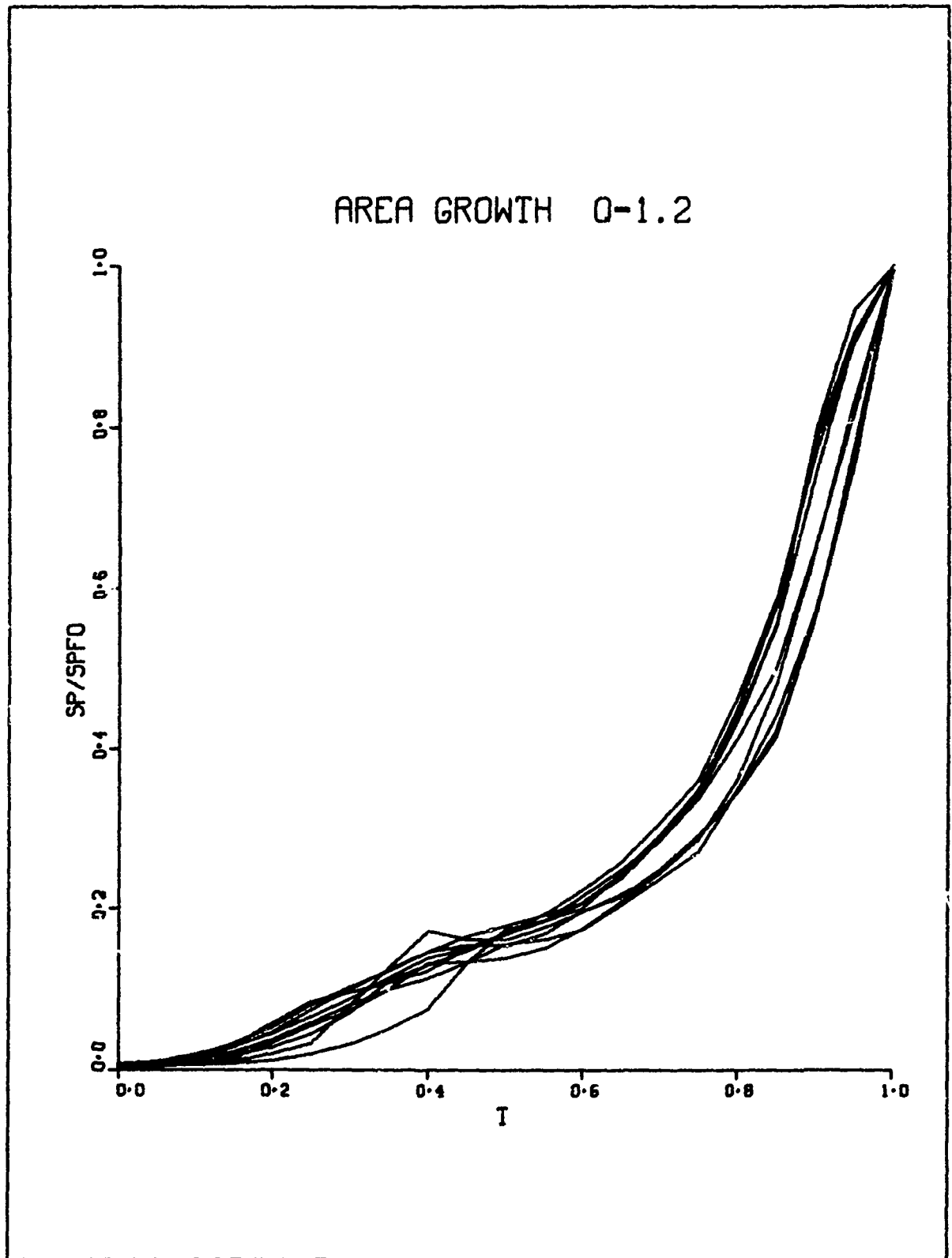
AREA GROWTH Q-.4



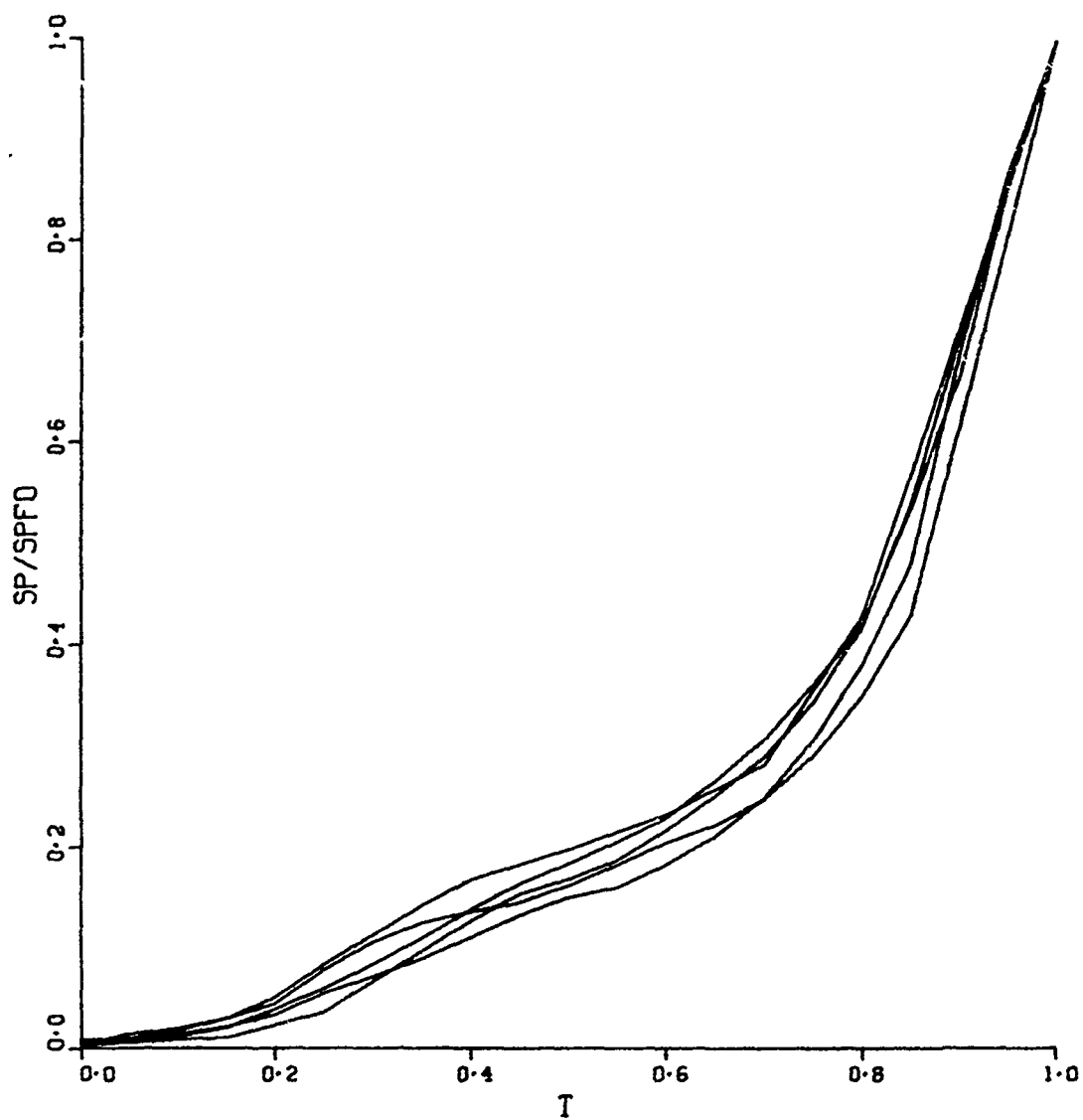
AREA GROWTH 0-.8



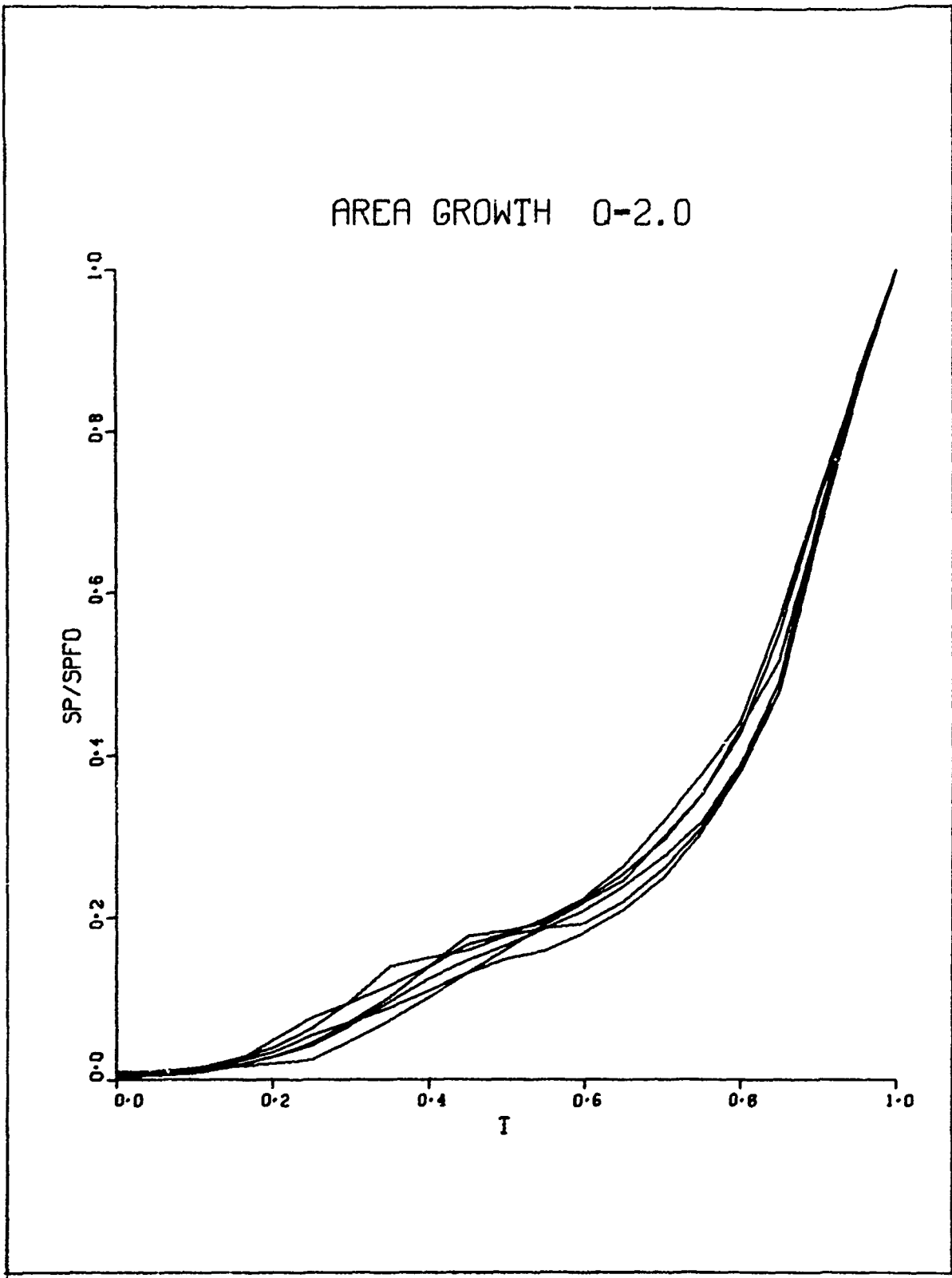
AREA GROWTH 0-1.2



AREA GROWTH 0-1.6



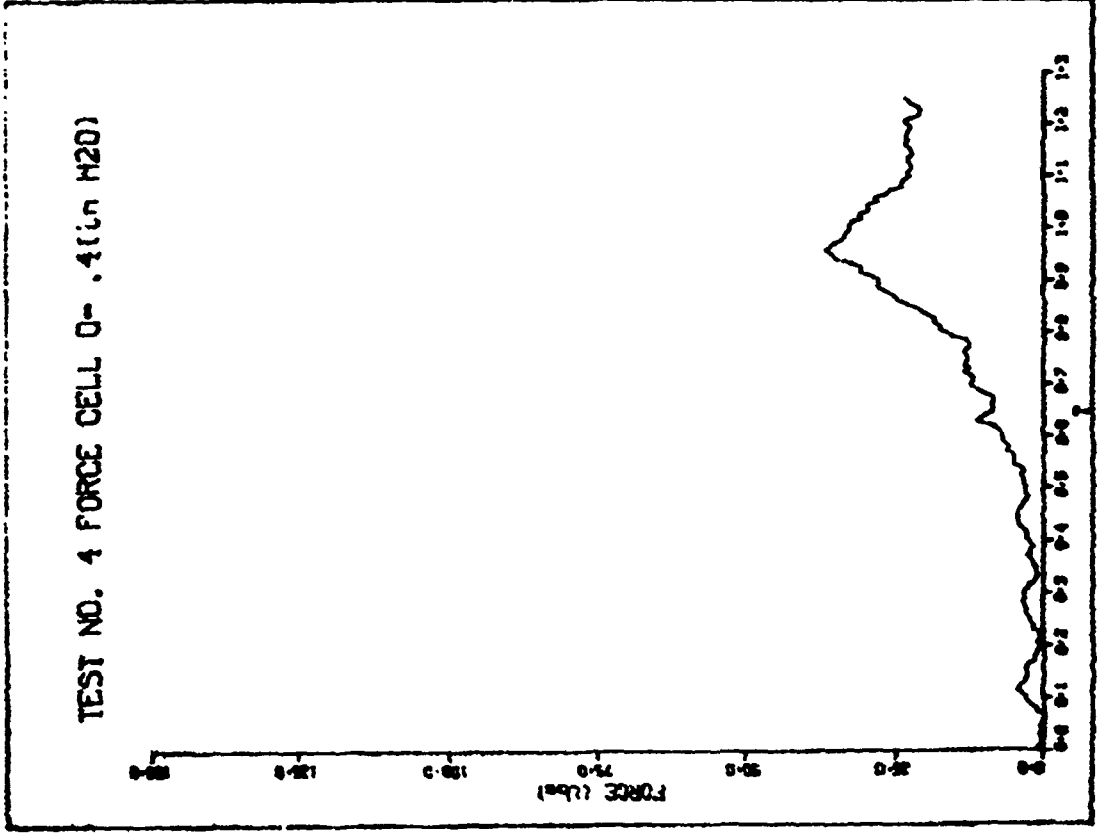
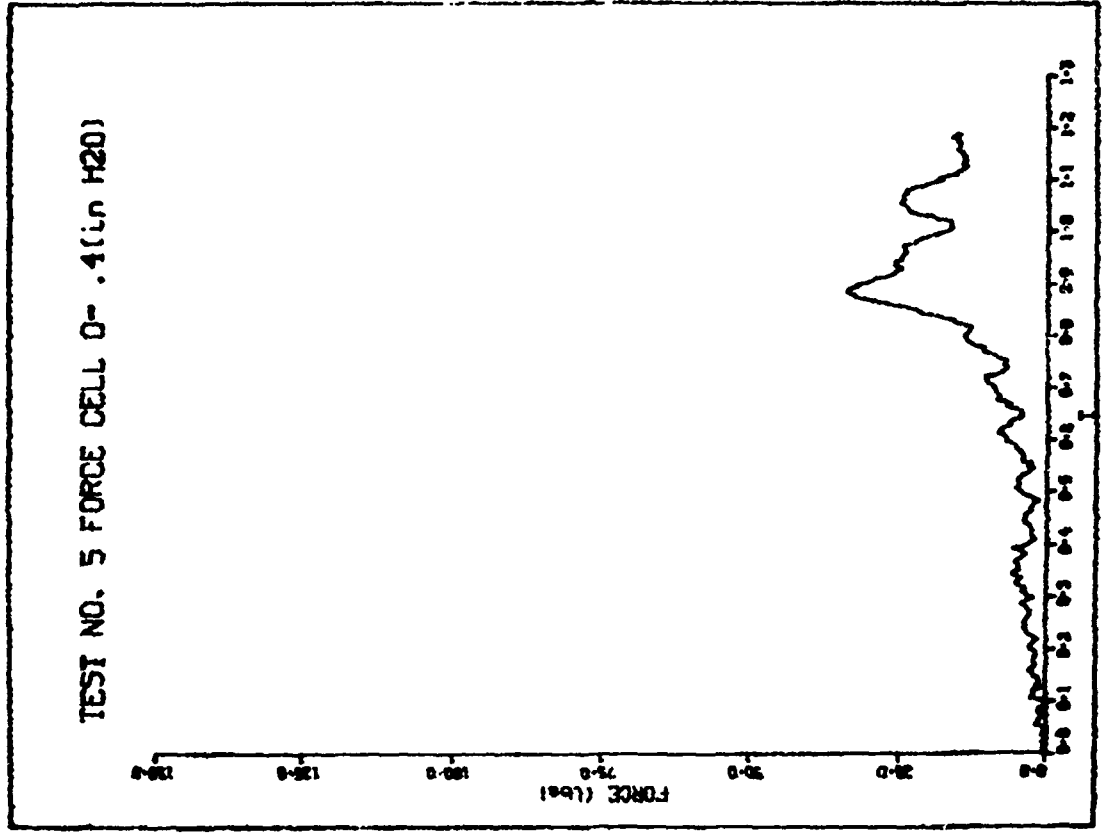
AREA GROWTH 0-2.0



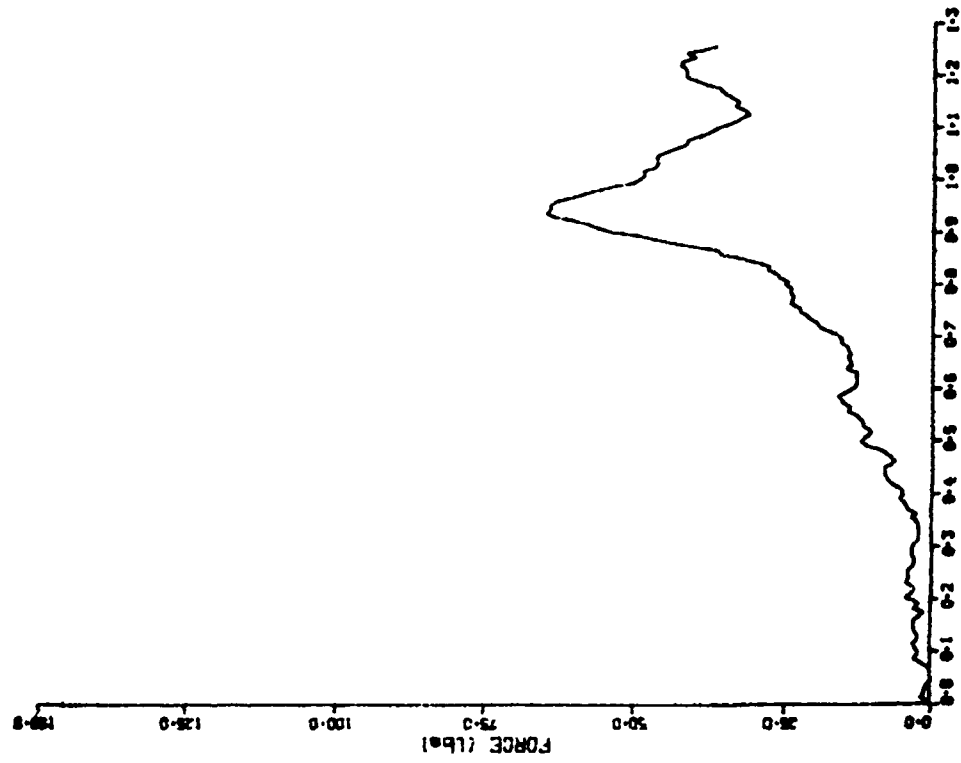
APPENDIX D

FORCE PLOTS

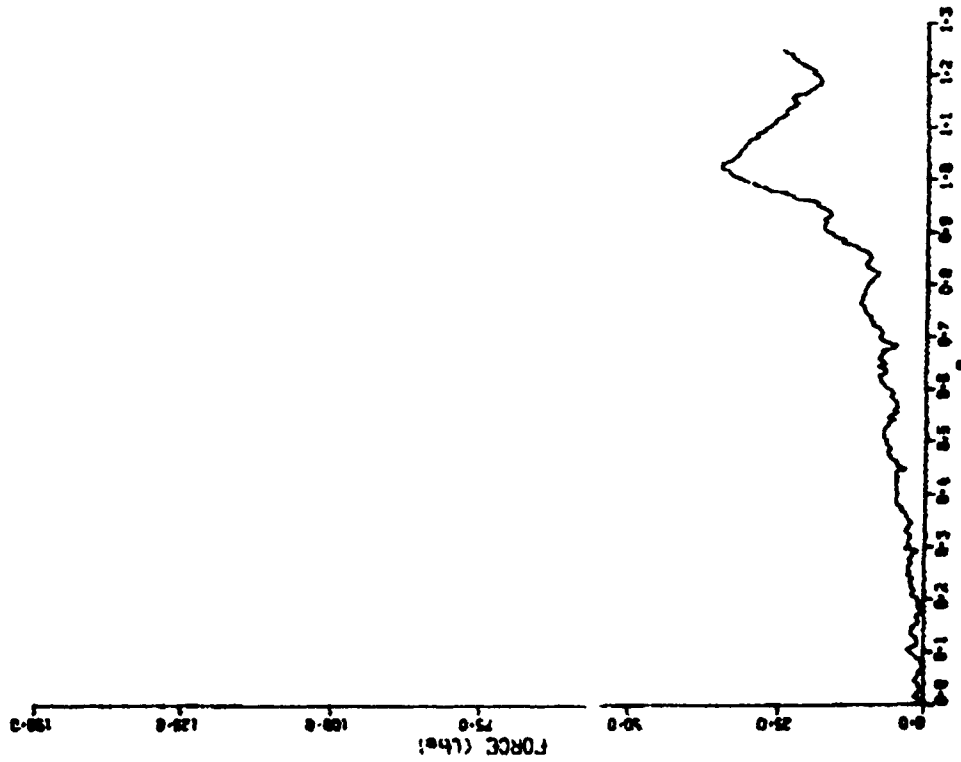




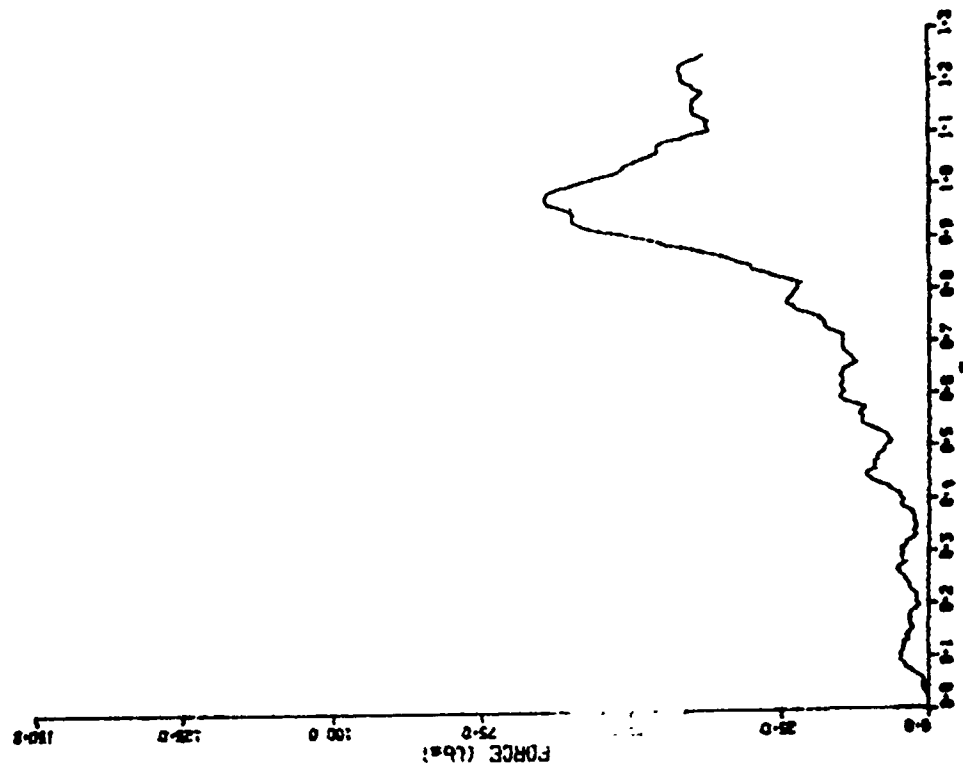
TEST NO. 7 FORCE CELL 0- .8 (in H2O)



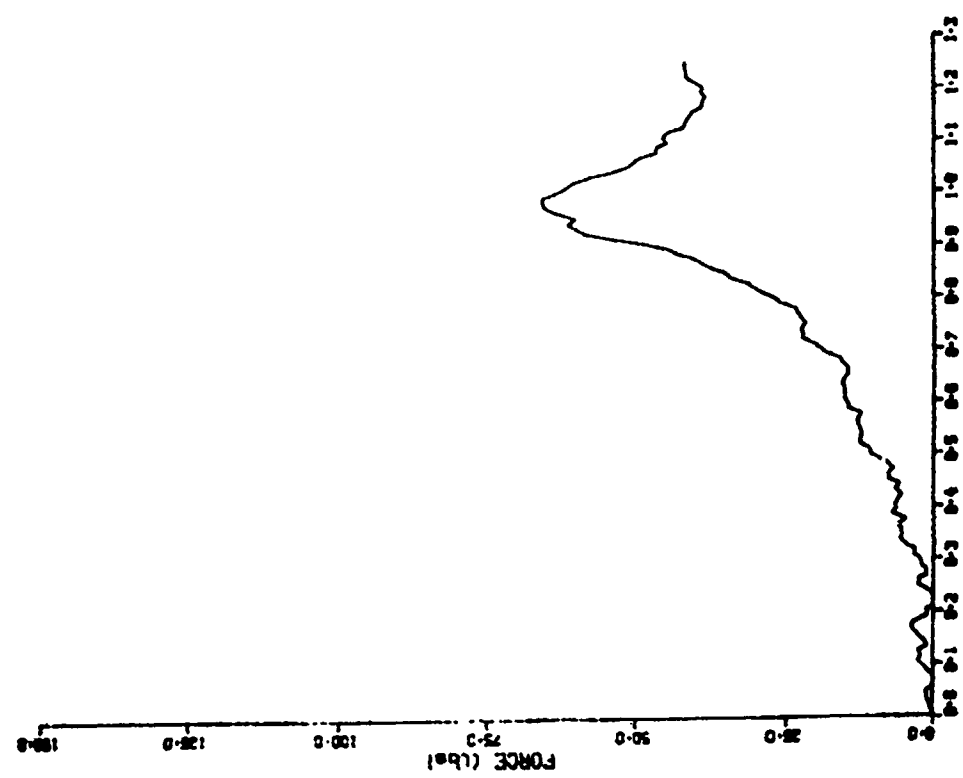
TEST NO. 6 FORCE CELL 0- .4 (in H2O)

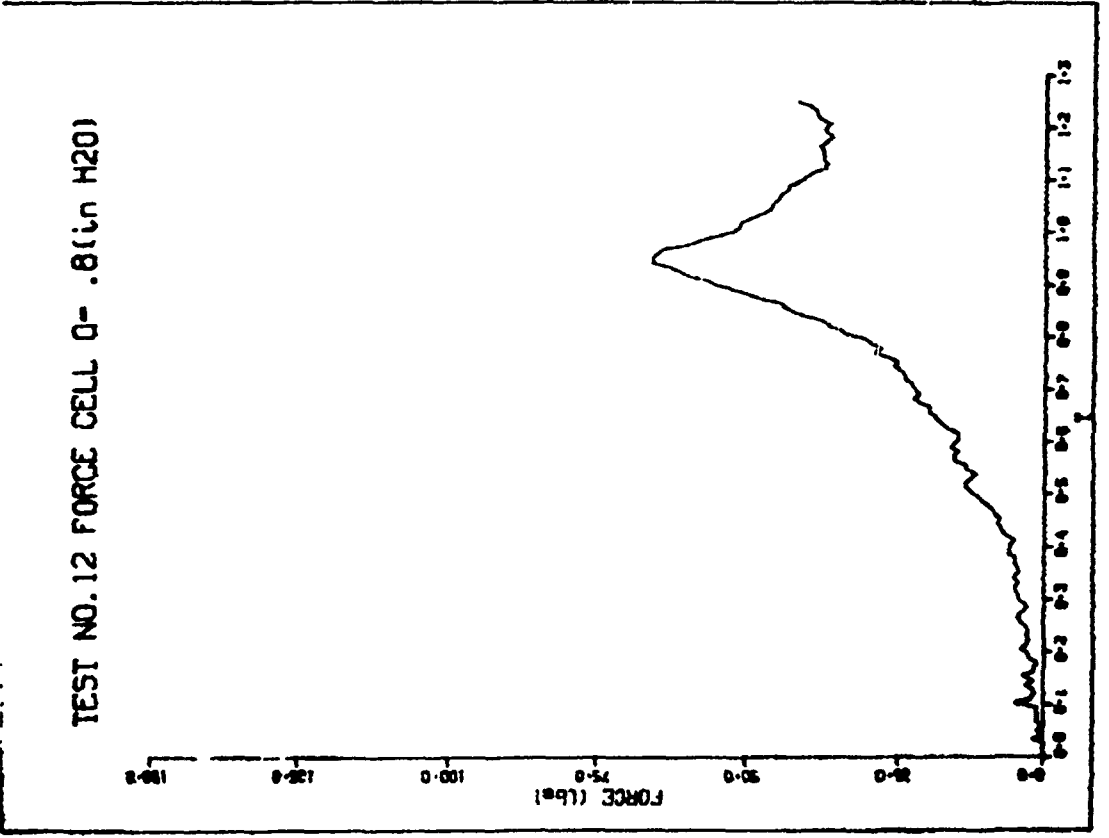
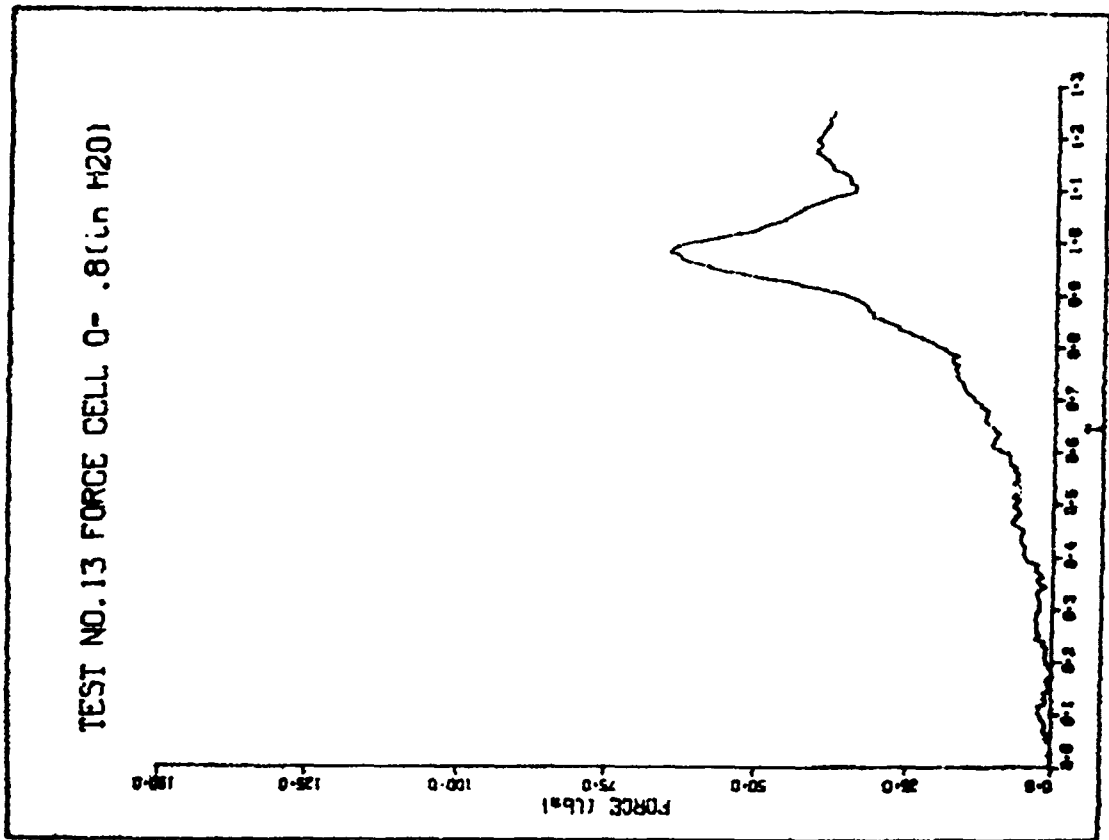


TEST NO. 11 FORCE CELL 0- .8(in H2O)

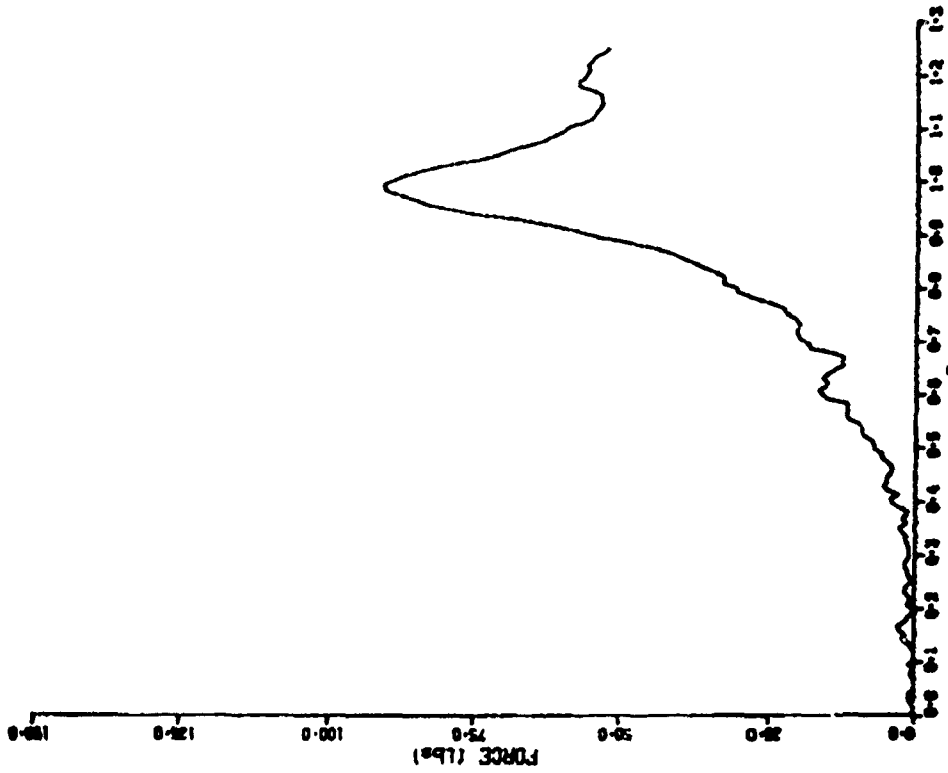


TEST NO. 9 FORCE CELL 0- .8(in H2O)

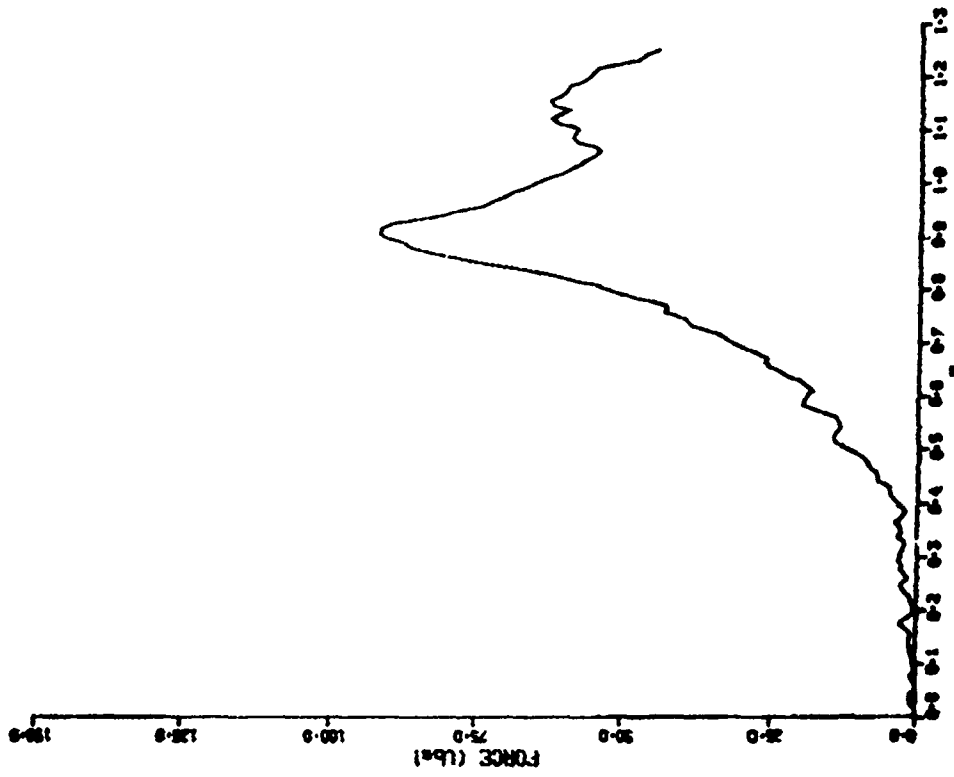


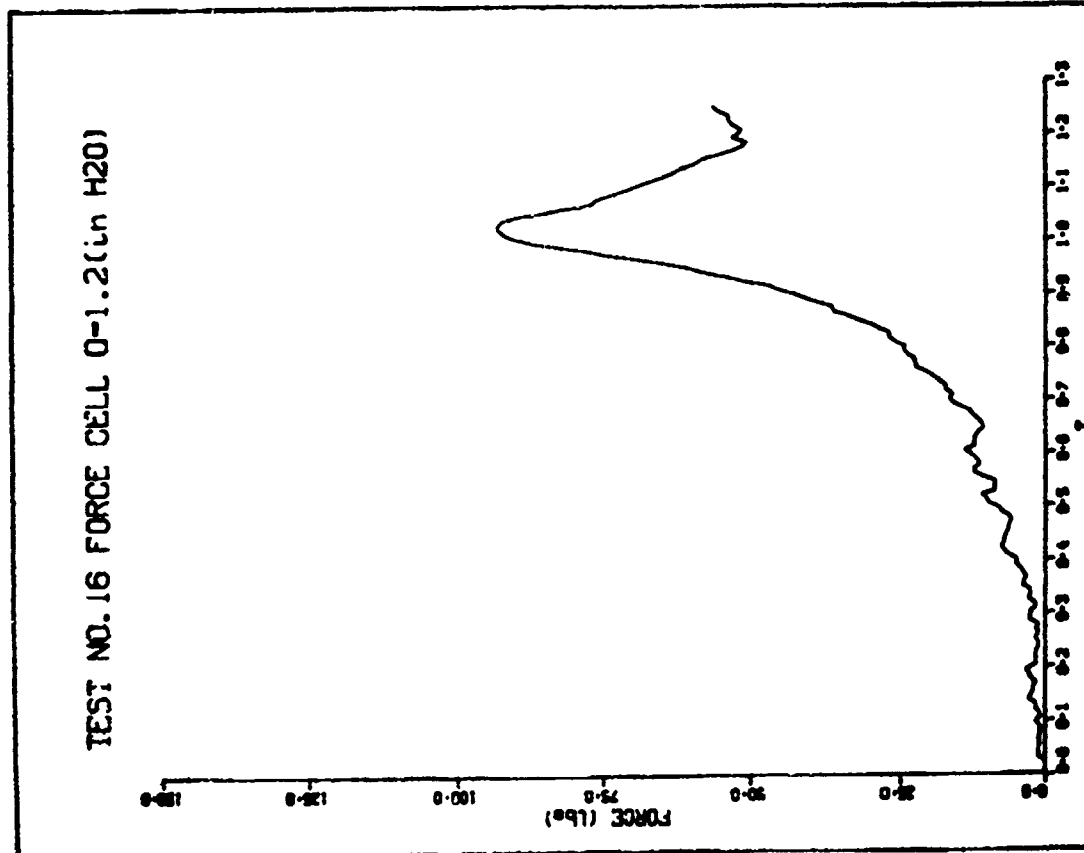
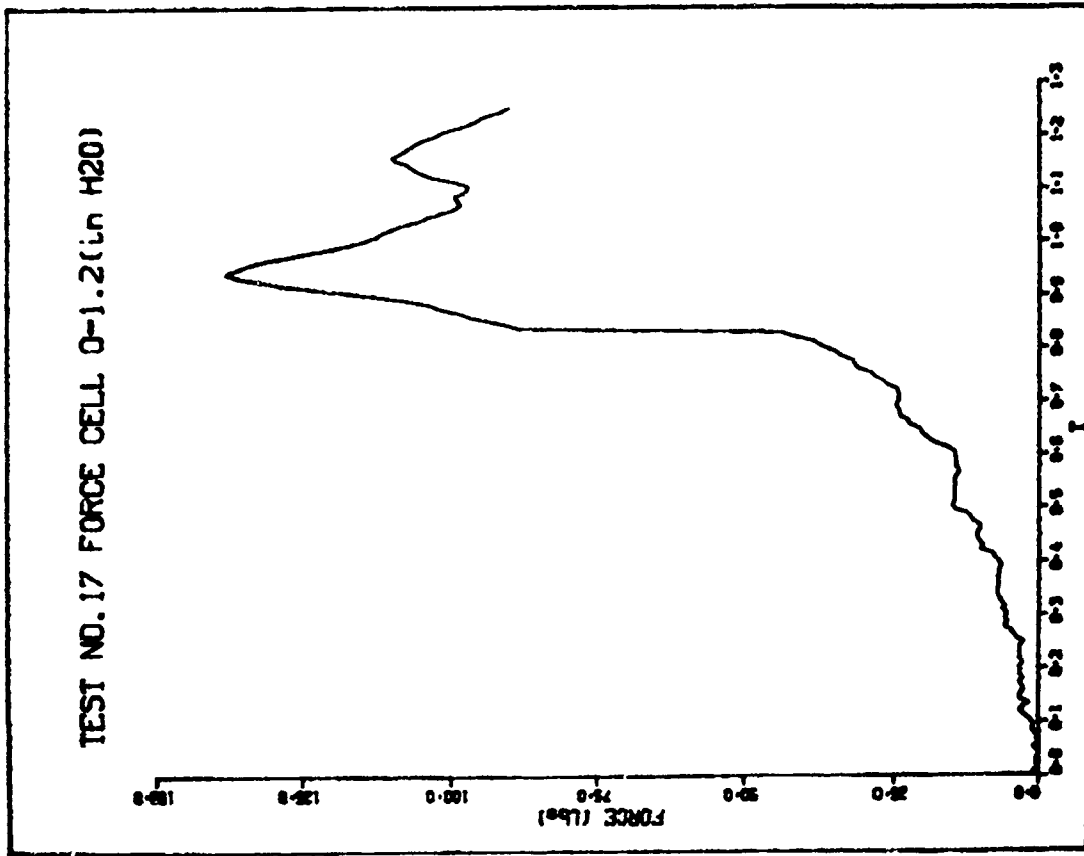


TEST NO.15 FORCE CELL 0-1.2(Ln H20)

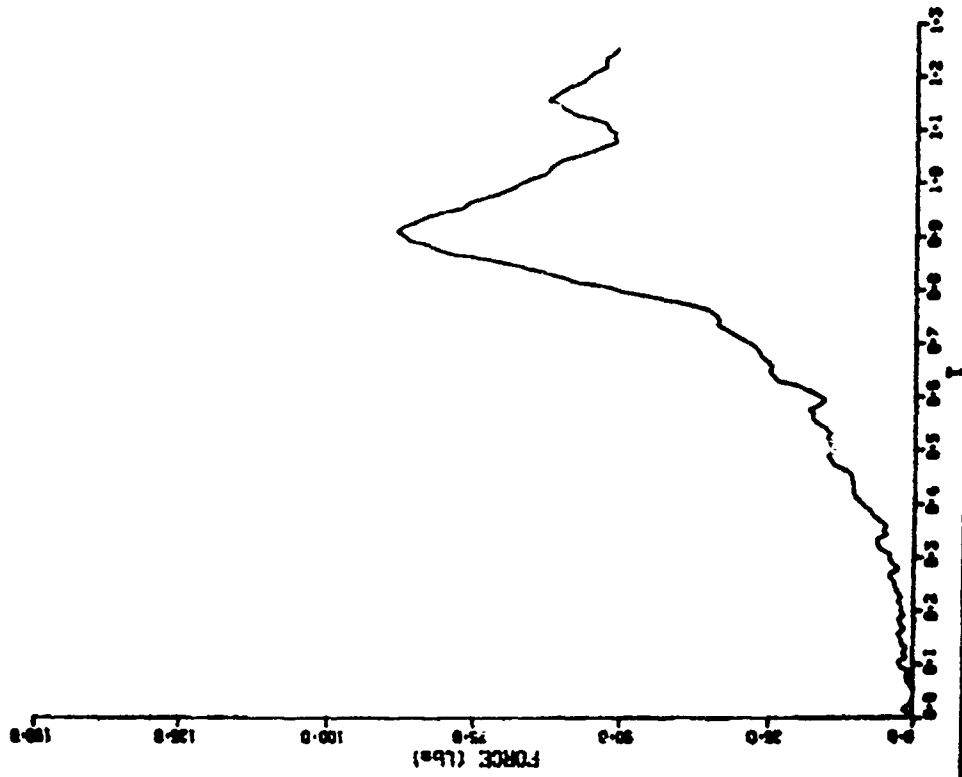


TEST NO.14 FORCE CELL 0-1.2(Ln H20)

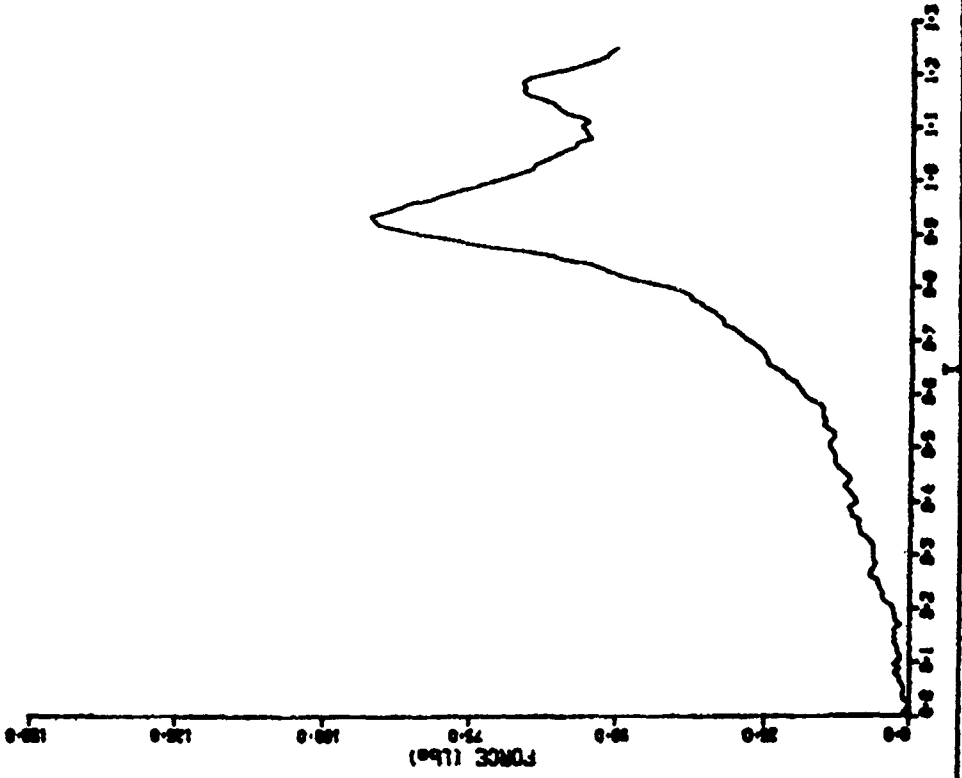


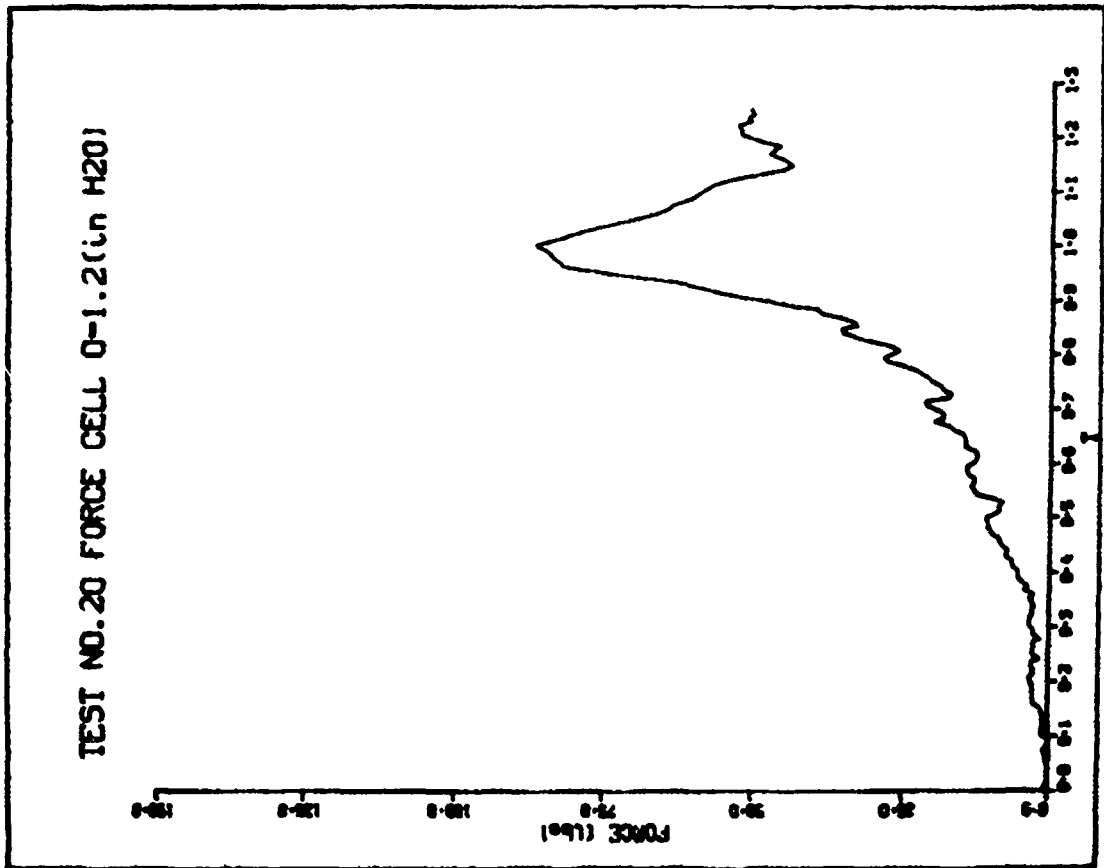
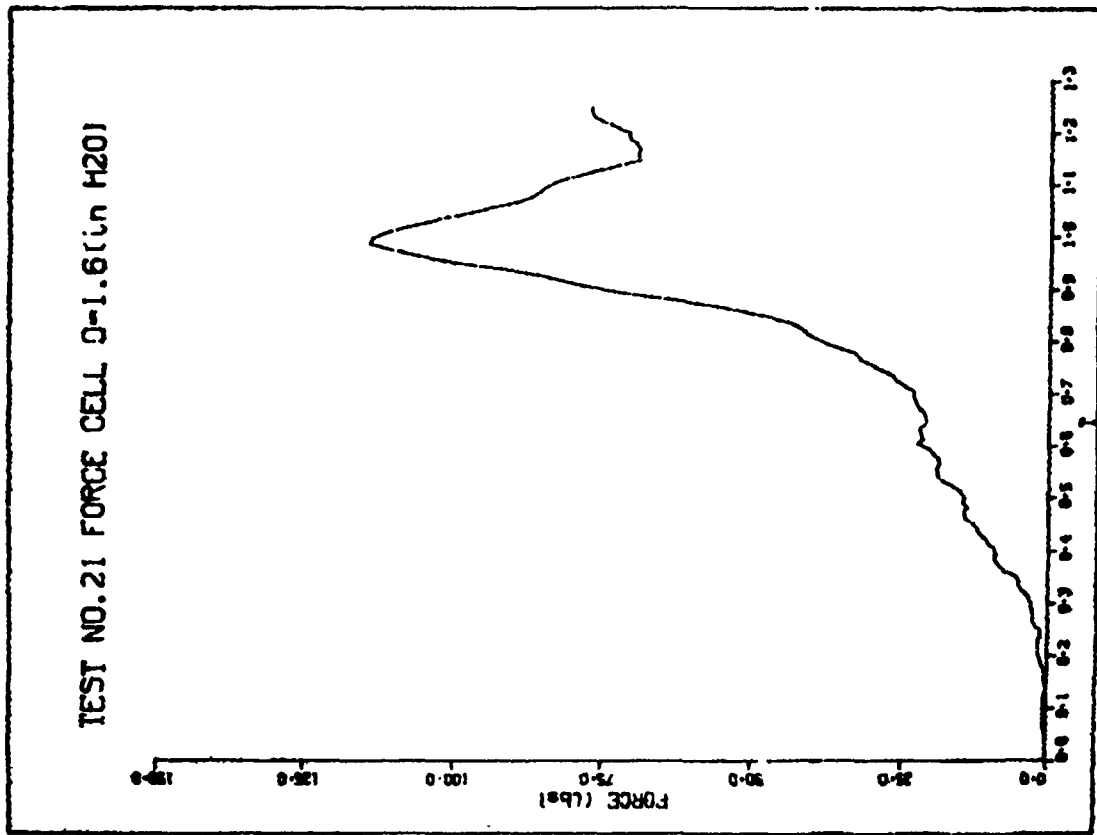


TEST NO. 19 FORCE CELL 0-1.2 (in H2O)

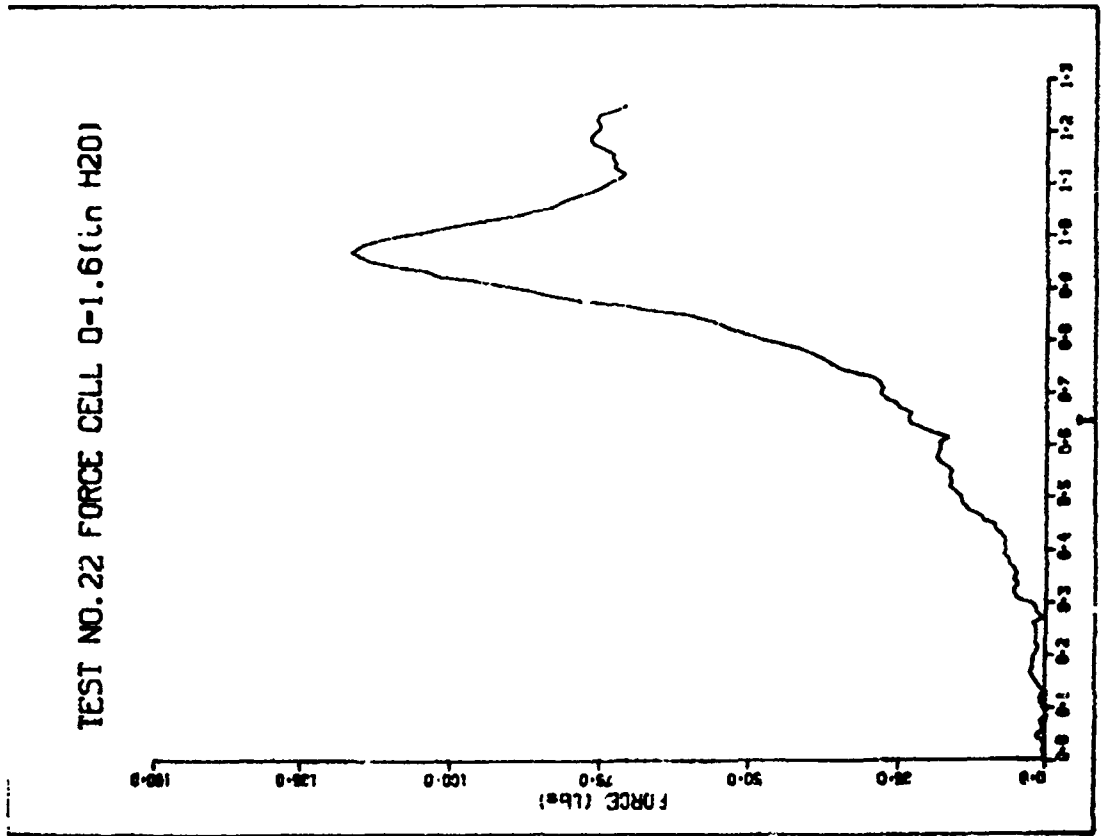
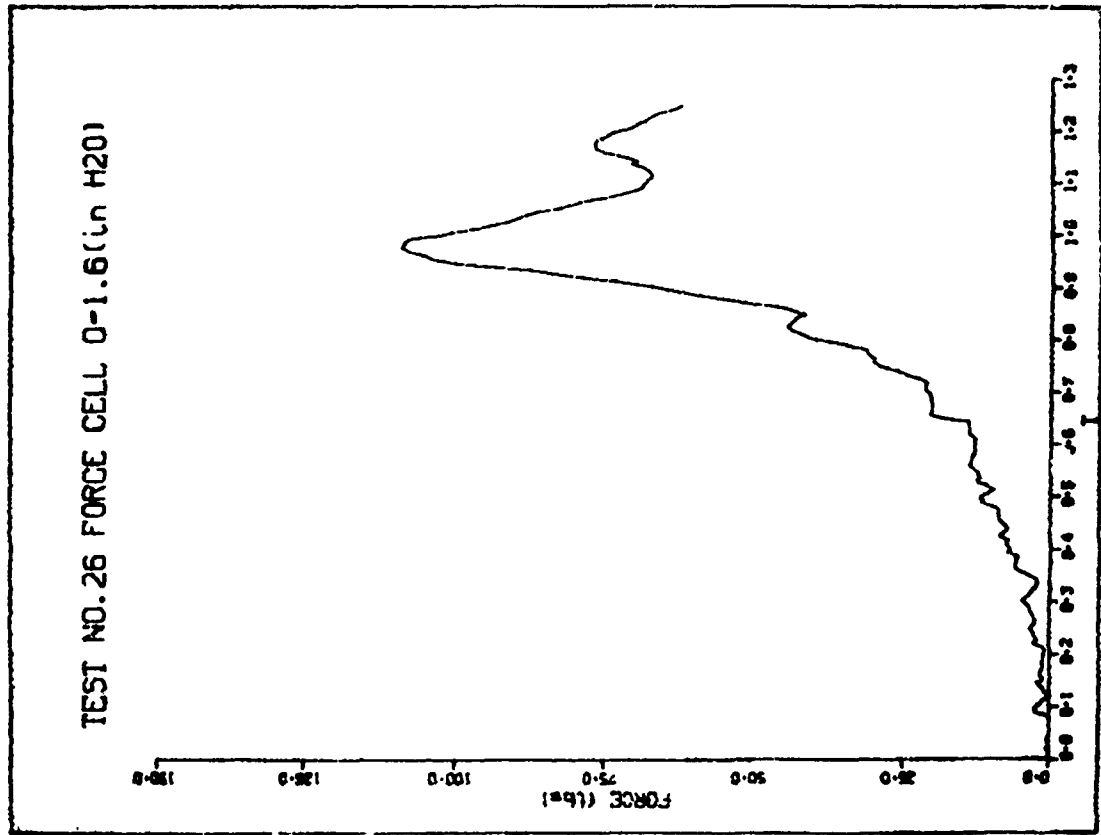


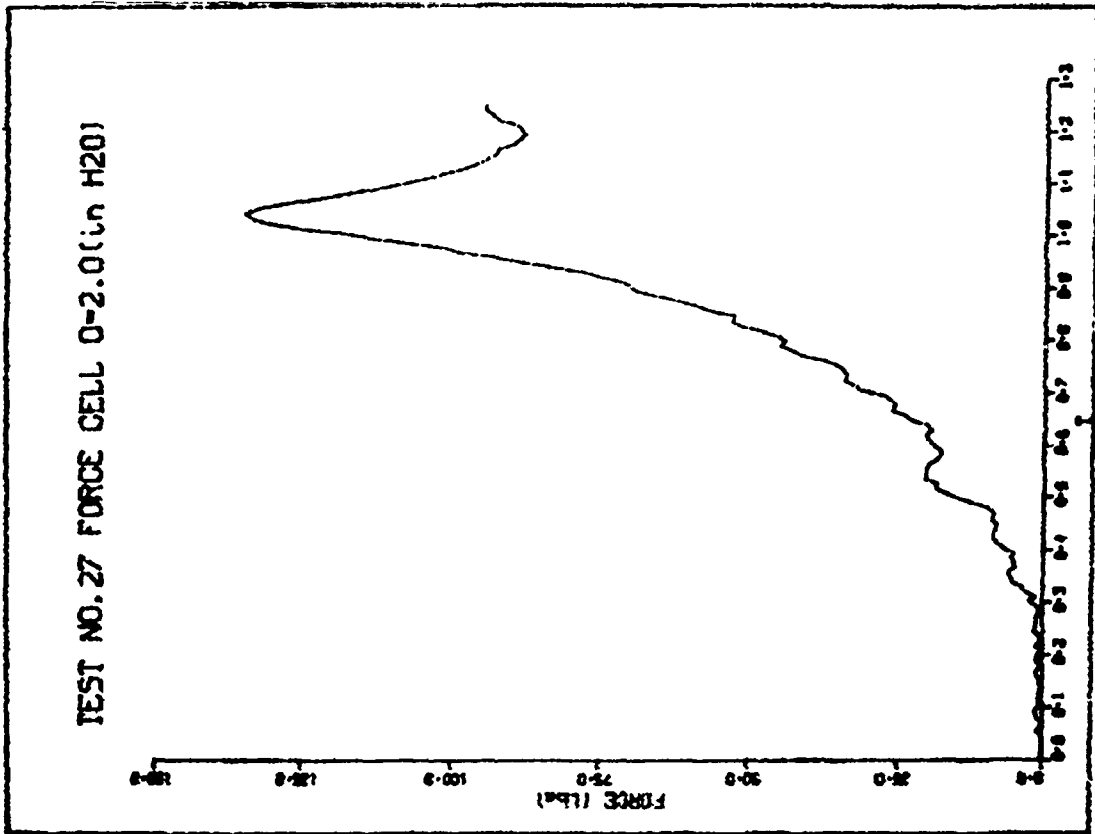
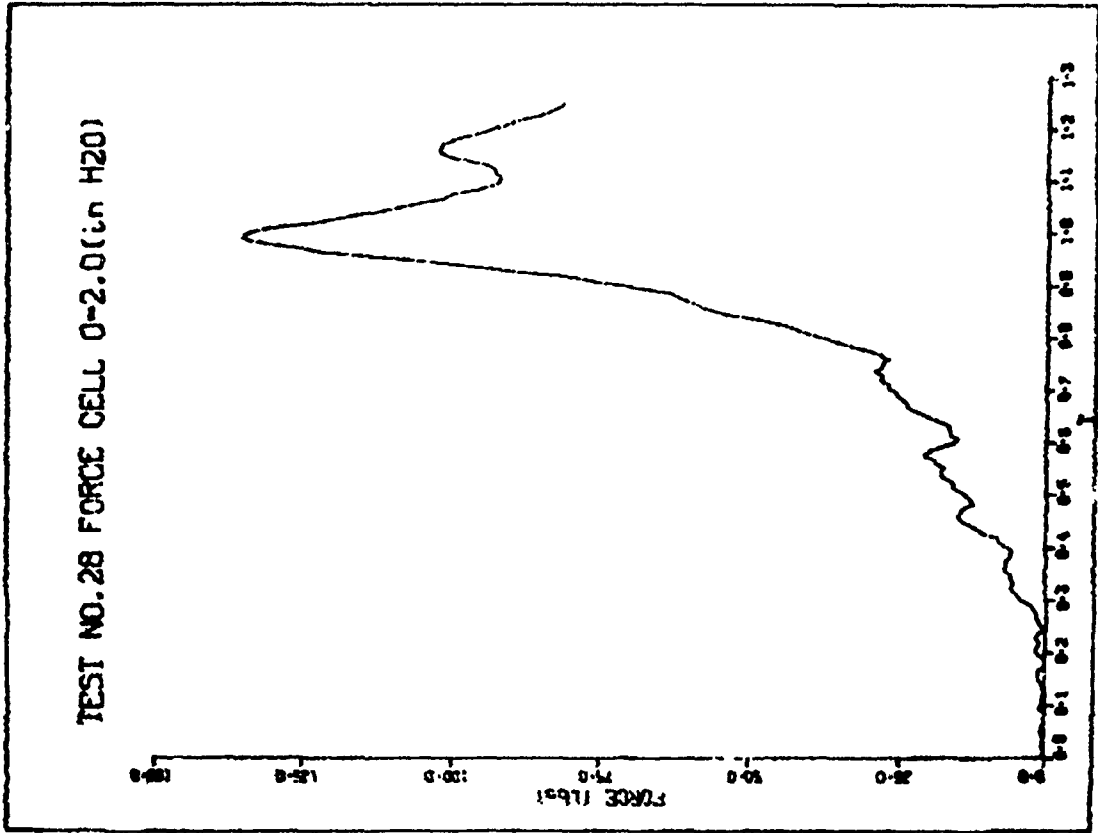
TEST NO. 18 FORCE CELL 0-1.2 (in H2O)

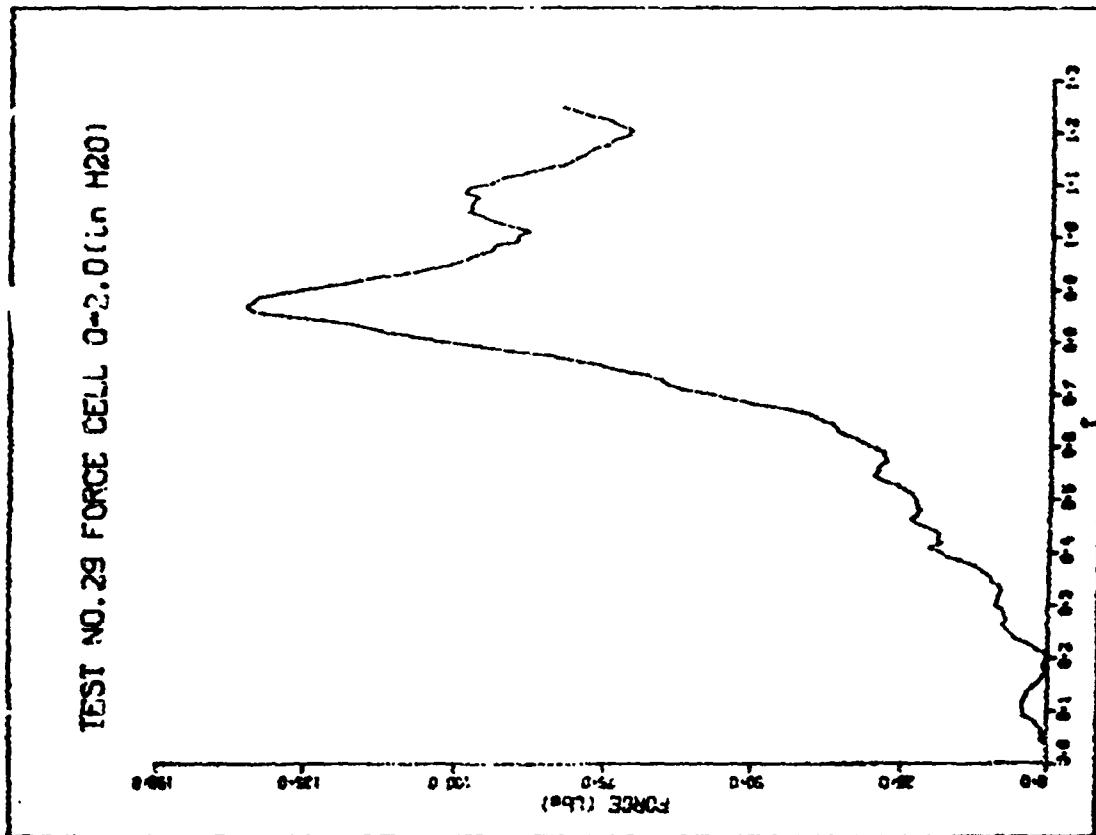
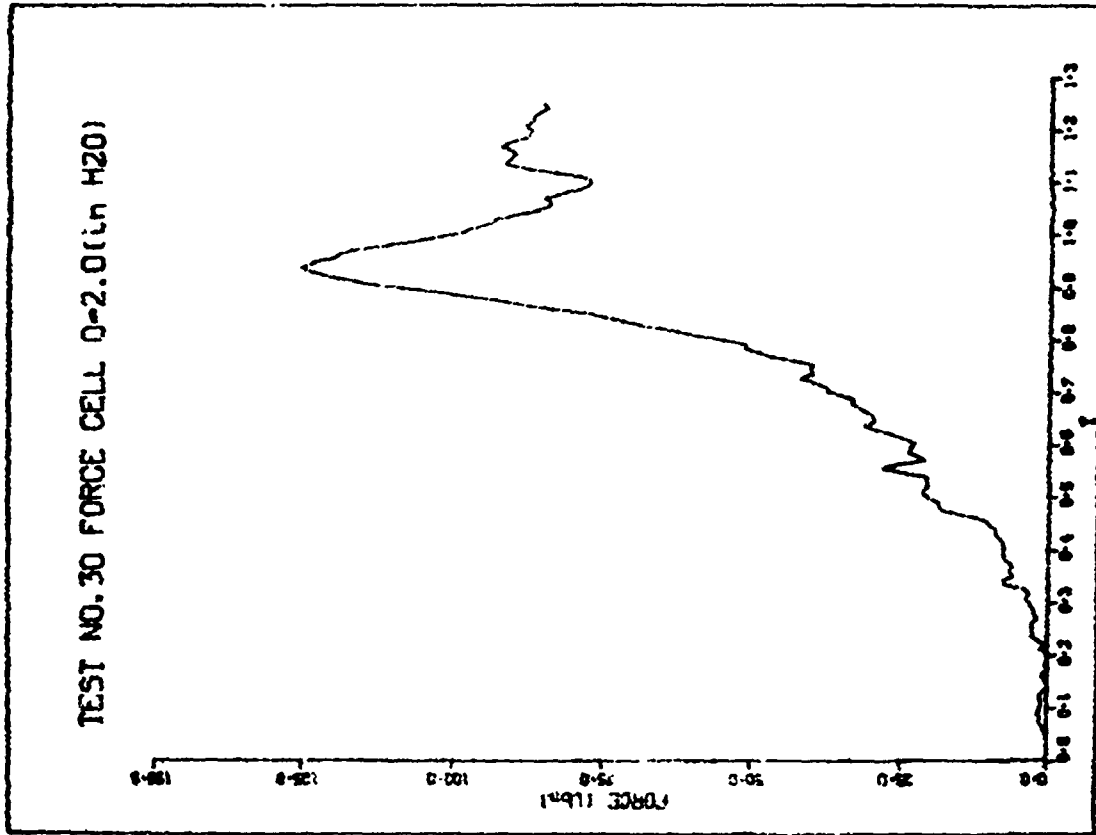


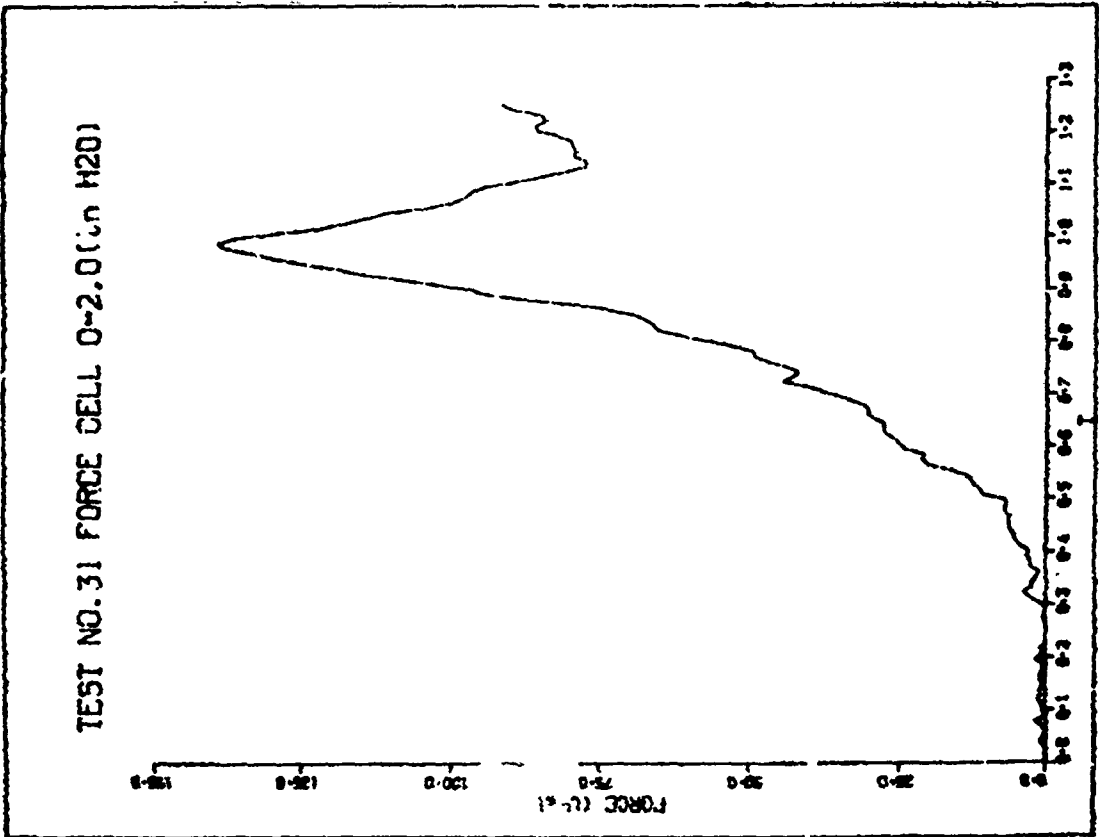
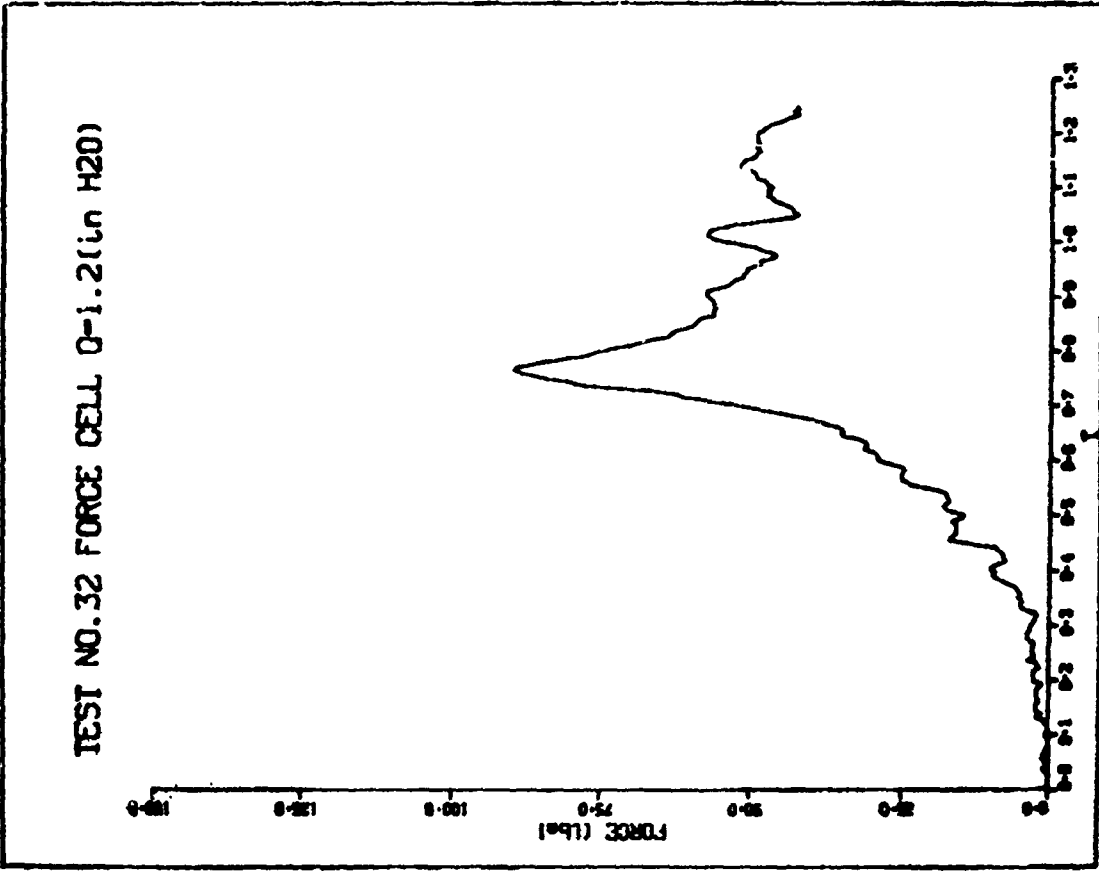


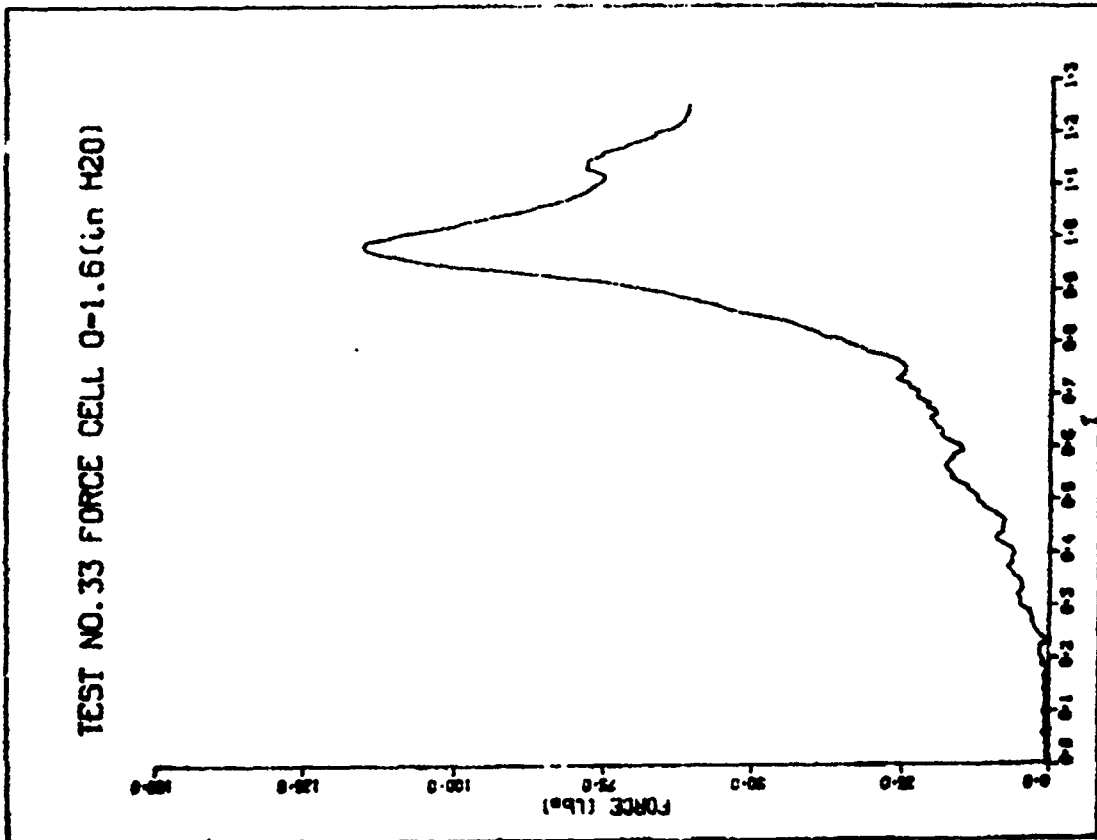
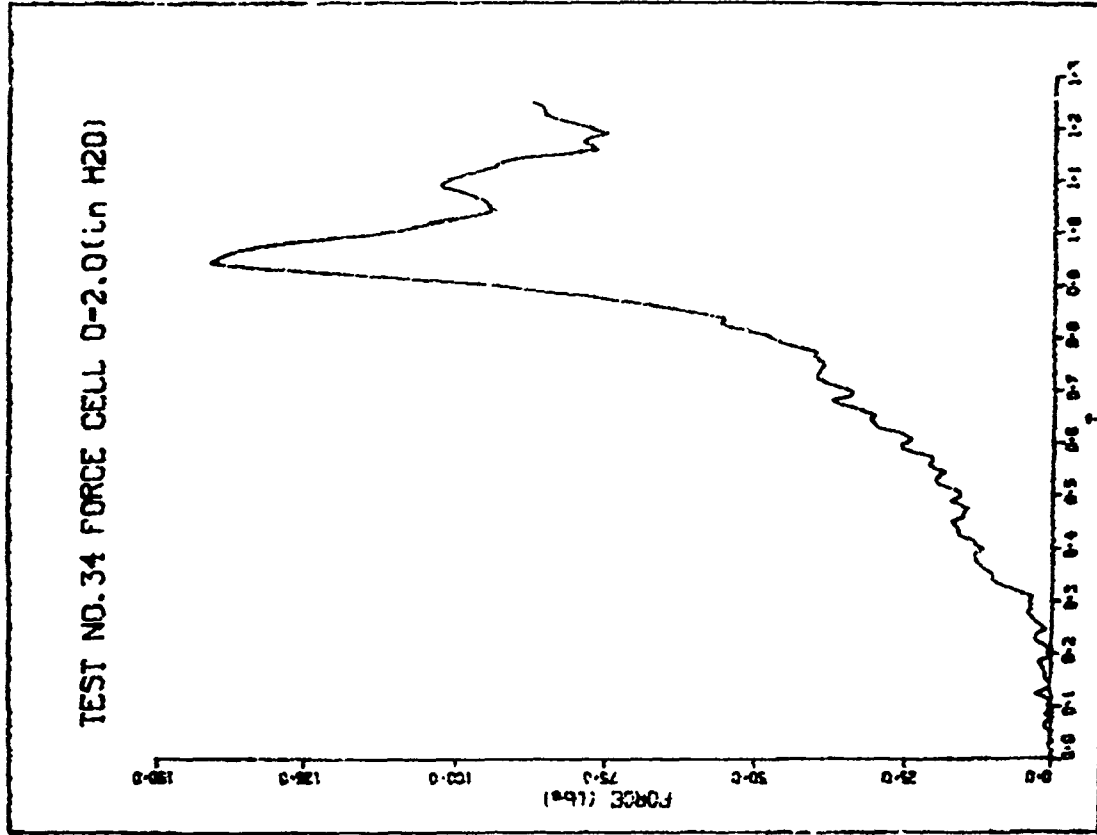




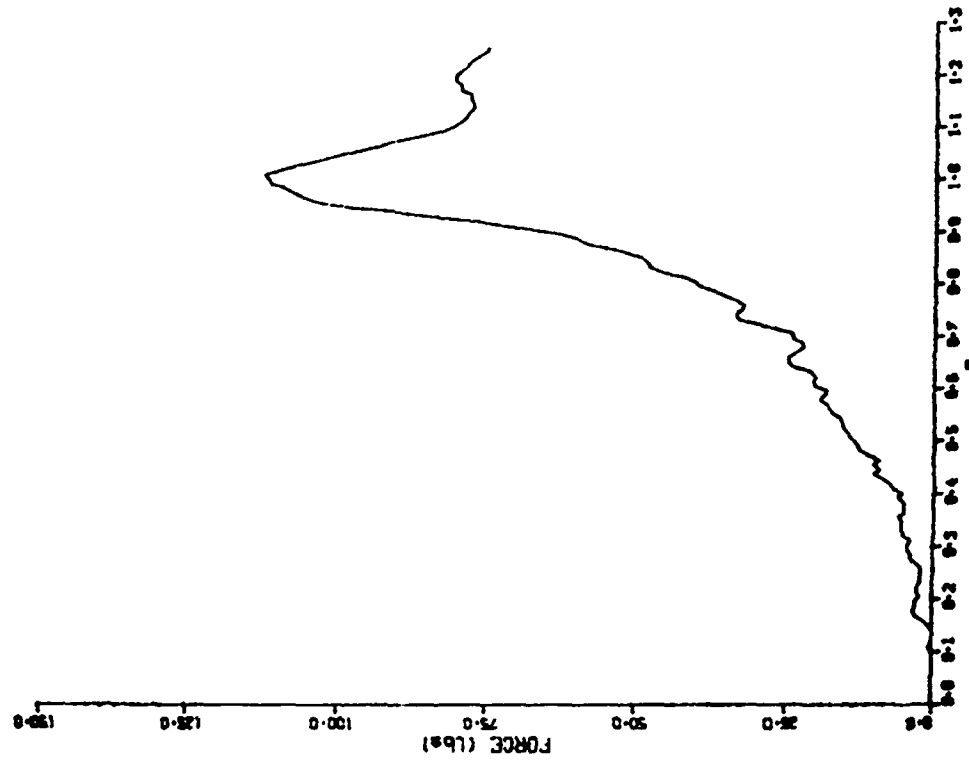




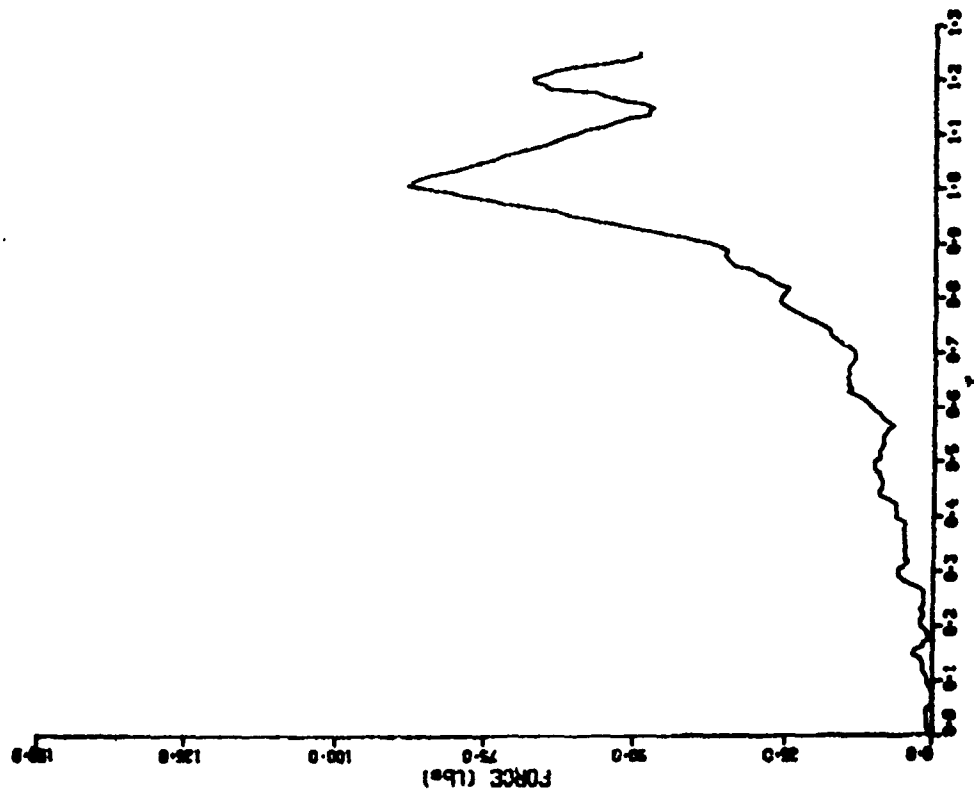




TEST NO. 37 FORCE CELL 0-1.6 (in H2O)



TEST NO. 36 FORCE CELL 0-1.2 (in H2O)



## REFERENCES

1. Jones, R.A., "On the Aerodynamic Characteristics of Parachutes," British ARC Report; R. and N. No. 862, June 1923.
2. Ross, E.W., Jr., "Approximate Analysis of a Flat, Circular Parachute in Steady Descent," Journal of Aircraft, Vol. 7, No. 3, May-June 1970.
3. Heinrich, H.G., and Jamison, L.R., Jr., "Stress Analysis of a Fully Inflated Ribless Guide Surface Parachute, AFFDL-TR-65-111, September 1965.
4. Duncan, W.J., Stevens, G.W.H., and Richards, G.J., "Theory of the Flat Elastic Parachute," R. and M. No. 2118, AERONAUTICAL RESEARCH COUNCIL, March 1942.
5. Jaeger, J.A., "A Study of the Load Distribution in a Conical Ribbon Type Parachute," Report No. 8541, Lockheed Aircraft Corp., August 1952.
6. Reagan, J.F., "A Theoretical Investigation Into the Dynamics and Stress Analysis of Parachutes for the Purpose of Determining the Design Factors," The Daniel Guggenheim Airship Institute, University of Akron, Feb. 1945.
7. Saliaris, C., "Approximate Calculation of the Canopy Shape and the Stresses in Lines and Fabric of a Flat Circular Parachute in Steady Descent," DLR-FB-71-98, DFVLR, Braunschweig, W. Germany, Aug. 1971.
8. Topping, A.D., Marketos, J.D., and Costakos, N.C., "A Study of Canopy Shapes and Stresses for Parachutes in Steady Descent," WADC-TR-55-294, Goodyear Aircraft Corp., October 1955.
9. Mullins, W.M., and Reynolds, D.T., "Stress Analysis of Ribbon Parachutes," AIAA Paper No. 75-1372, Presented at the AIAA Aerodynamic Deceleration Systems Conference, Albuquerque, New Mexico, 17-19 November 1975.
10. Mullins, W.M., and Reynolds, D.T., "Stress Analysis of Spacecraft Parachutes Using Finite Elements and Large Deformation Theory," AIAA Paper No. 70-1195, Presented at the AIAA Aerodynamic Deceleration Systems Conference, Dayton, Ohio, 14-16 September 1970.
11. Heinrich, H.G., and Jamison, L.R., "Stress Analysis of a Parachute During Inflation and at Steady State," FDL-TDR-64-125, University of Minnesota, February 1965.

12. Houmard, J.E., "Stress Analysis of the Viking Parachute," AIAA Paper No. 73-444, presented at the AIAA Aerodynamic Deceleration Systems Conference, Palm Springs, California, 21-23 May 1973.
13. Roberts, B.W., "The Shape and Stresses in an Arbitrarily Shaped Core Parachute Under an Arbitrarily Pressure Distribution," AIAA Paper No. 70-1197, presented at the AIAA Aerodynamic Deceleration Systems Conference, Dayton, Ohio, 14-16 September 1970.
14. Asfour, K.J., "Analysis of Dynamic Stress in an Inflating Parachute," Journal of Aircraft, Vol. 4, Sep-Oct 1967.
15. Saari, D.P., "Parachute Stress Analysis Incorporating a Measured Pressure Distribution," Unpublished M.S. Thesis, University of Minnesota, June 1973.
16. Mullins, W.M., Reynolds, D.T., and Lindh, K.G., "Investigation of Prediction Methods for the Loads and Stresses of APOLLO Type Spacecraft Parachutes," Vol. II Stresses, NASA-CE-134231, Northrop Corp., prepared under Contract NAS 9-8131 for National Aeronautics and Space Administration, June 1970.
17. Kenner, P.M., "Structural Analysis of a Parawig During Deployment," AIAA Paper No. 70-1196, presented at AIAA Aerodynamic Deceleration Systems Conference, Dayton, Ohio, 14-16 September 1970.
18. Alley, V.L., Jr., "A Stress Analysis of the Viking BLDT-1 Parachute Canopy With Emphasis on the Effects of Asymmetries," LWP-1067, Langley Working Paper, National Aeronautics and Space Administration, 25 July 1972.
19. Keck, E.L., "A Computer Simulation of Parachute Opening Dynamics," AIAA Paper No. 75-1379, presented at AIAA Aerodynamic Deceleration Systems Conference, Albuquerque, New Mexico, 17-19 November 1975.
20. Sundberg, W.D., "Finite-Element Modeling of Parachute Deployment and Inflation," AIAA Paper No. 75-1380, presented at AIAA Aerodynamic Deceleration Systems Conference, Albuquerque, New Mexico, 17-19 November 1975.
21. Heinrich, H.G., and Noreen, R.A., "Stress Measurements on Inflated Model Parachutes," AFFDL-TR-72-43, University of Minnesota, Wright-Patterson AFB, Ohio, December 1972.
22. Hoffman, I.S., "Evaluation of a Parachute Load Distribution Measuring System During Low Altitude Drop," NASA-TM-X-1832, Langley AFB, July 1969.



23. Heinrich, H.G., and Saari, D.O., "Exploratory Parachute Canopy Stress Measurements During Inflation and at Steady State," AIAA No. 75-1374, presented at AIAA Aerodynamic Decelerator Systems Conference, Albuquerque, New Mexico, 17-19 November 1975.
24. Raspe, W., "A Method of Experimental Determination of Maximum Cloth Elongation in Parachute Canopies," DLR-MITT-71-17, German Report, July 1971.
25. Melzig, H.D., "The Dynamic Stress-Strain Behavior of Parachute Cloth," NASA-CR-92353, University of Minnesota, December 1967.
26. Melzig, H.D., and Schmidt, P.K., "Pressure Distribution During Parachute Opening Phase I. Infinite Mass Operating Case," AFFDL-TR-66-10, prepared by Deutsche Forschungsanstalt für Luft und Raumfahrt V. (DFL) for Wright-Patterson AFB, Ohio, Contract No. AF61(052)-681, Dayton, Ohio, March 1966.
27. Heinrich, H.G., and Noreen, R.A., "Functioning of the Omega Sensor on Textile Samples Under High Loading Rates," AFFDL-TR-74-78, University of Minnesota, Wright-Patterson AFB, Ohio, September 1974.
28. "Operation and Maintenance Manual for Added Mass Text Fixture." Technical Manual No. TI-402-73-1, prepared under Contract F33615-71-C-1194 for Wright-Patterson AFB, Ohio, July 1973.